



MONASH University

Metabolic engineering of *Saccharomyces cerevisiae* for improved accumulation and storage of standard and high-value lipids and impacts on cellular physiology

Huadong Peng

M. Eng. (Biological Engineering)

B. Eng. (Biological Engineering)

A thesis submitted for the degree of *Doctor of Philosophy*

Department of Chemical Engineering

Monash University, Clayton

Australia

August 2018

Copyright notice

© Huadong Peng (2018).

I certify that I have made all reasonable efforts to secure copyright permissions for third-party content included in this thesis and have not knowingly added copyright content to my work without the owner's permission.

This page is intentionally blank

Table of contents

Copyright notice.....	i
Table of contents.....	iii
List of Figures.....	vii
List of Tables.....	viii
Abbreviations.....	ix
Abstract.....	xi
Publications during enrolment.....	xiii
Thesis including published works declaration.....	xiv
Acknowledgements.....	xv
Chapter 1 Introduction.....	1
1.1 Background.....	3
1.2 Scope of research.....	4
1.3 Research objectives.....	5
1.4 Outline of thesis.....	5
1.5 References.....	8
Chapter 2 Literature review.....	9
2.1. Background.....	11
2.1.1. Host microorganisms.....	11
2.1.2. Lipid synthesis in yeast.....	14
2.2. Metabolic engineering strategies for lipid accumulation and storage of standard FA..	19
2.2.1. Mechanisms to increase FA biosynthesis.....	20
2.2.2. Mechanisms to enhance lipid accumulation.....	23
2.2.3. Mechanisms to improve lipid sequestration.....	25
2.2.4. Lipid pathways engineering approach.....	27
2.3. Fatty acid modification towards high-value lipid production.....	30
2.3.1. Cyclopropane fatty acid.....	30
2.3.2. Other value-added fatty acid.....	31
2.4. Cellular physiological responses to lipid pathway engineering.....	32
2.4.1. Cell growth.....	32
2.4.2. Cell membrane integrity.....	33
2.4.3. Reactive oxygen species.....	34
2.4.4. Mitochondria membrane potential.....	35

2.4.5. Heterogeneity.....	36
2.5. Combination of metabolic engineering and bioprocess strategy	37
2.6. Conclusions	37
References	38
Chapter 3 Functional assessment of plant and microalgal lipid pathway genes in yeast to enhance microbial industrial oil production	55
Chapter 4 Metabolic engineering of lipid pathways in <i>Saccharomyces cerevisiae</i> and staged bioprocess for enhanced lipid production and cellular physiology	67
Chapter 5 Enhanced production of high-value cyclopropane fatty acid in yeast engineered for increased lipid synthesis and accumulation	87
5.1. Abstract	89
5.2. Introduction	90
5.3. Materials and methods	91
5.3.1. Plasmids, strain construction and cell culture	91
5.3.2. Lipid analysis and quantification.....	92
5.4. Results	92
5.5.1 Lipid pathway engineering increased intracellular TAG and CFA content	92
5.5.2 Two-stage bioprocess recovered cell growth with higher CFA yield	94
5.5. Discussion	95
5.6. Conclusions	96
References	96
Chapter 6 Flow cytometry-based physiological characterisation and transcriptome analyses reveal a mechanism for reduced cell viability in yeast engineered for increased lipid content	111
6.1. Abstract	113
6.2. Introduction	114
6.3. Materials and methods	116
6.3.1. Strains	116
6.3.2. Cell culture	116
6.3.3. Antioxidant addition to cell culture	117
6.3.4. RNA-Seq analysis.....	117
6.3.5. Cell physiology characterization	118
6.4. Results and Discussion.....	119

6.4.1. Whole transcriptome view of gene expression among strains engineered for standard lipid production by Degust analysis.....	119
6.4.2. Global transcriptional profiling emphasising central metabolic and mitochondrial pathways	120
6.4.3. Cellular physiological characterisation and corresponding regulated genes/pathways	123
6.4.4. Potential for oxidative stress generation in lipid pathway engineering.....	124
6.5. Conclusions	126
References	126
Chapter 7 Conclusion and outlook.....	145
Appendix I Assessment of effect of additional lipid accumulation genes on cyclopropane fatty acid production	153
Appendix II Single cell assessment of yeast metabolic engineering for enhanced lipid production using Raman and AFM-IR imaging.....	155
Appendix III Raman spectroscopy as a tool for tracking cyclopropane fatty acids in genetically engineered <i>Saccharomyces cerevisiae</i>	175

This page is intentionally blank

List of Figures

Figure 2.1 Four major steps in yeast lipids production.....	15
Figure 2.2 Fatty acid biosynthesis pathway	15
Figure 2.3 Pathways leading to the formation of TAG.....	17
Figure 2.4 Endoplasmic reticulum budding model of lipid droplet formation and expansion (redrawn with modifications from (Walther & Farese Jr, 2012)).....	19
Figure 5.1 Comparison of fatty acid lipid-containing fractions in engineered yeast strains .	103
Figure 5.2 (A) Cell growth and (B) CFA yield of CP1 and CP6 at 72 h post-induction produced via one-stage or two-stage bioprocess	104
Figure 6.1 Schematic of the process flow for transcriptome and physiological response analyses of yeast cells engineered for enhanced lipid production	134
Figure 6.2 Overall view of gene expression among engineered strains for improved standard lipids production generated by the Degust program	135
Figure 6.3 Relative expression levels of heterologously expressed genes among engineered strains by mRNA-seq analysis	136
Figure 6.4 Lipid content and soluble metabolite concentrations of engineered strains at 24 h post-induction	137
Figure 6.5 Overview of transcriptional reprogramming of the strains HBY14, 20, 27 and 31 at 24 h post-induction of gene expression	138
Figure 6.6 Cellular physiological characterisation and related differentially regulated genes in strain HBY31 compared with control after 24 h post-induction of gene expression.....	139
Figure 6.7 Comparison of cellular physiological responses between strain HBY31 and control after antioxidant (vitamin C and resveratrol) treatment.....	140
Figure 6.8 Effect of cyclopropane fatty acid biosynthesis on the cellular physiological performance between control, HBY20 and CBY20	141

List of Tables

Table 2.1 Comparison of different hosts for lipids production.....	14
Table 2.2 Current status of metabolic engineering strategies of <i>S. cerevisiae</i> for improved lipid production.....	14
Table 5.1 Recombinant yeast strains engineered for enhanced CFA production in this study	100
Table 6.1 Details of plasmids and strains used in this study	133

Abbreviations

Ald6, native aldehyde dehydrogenase isoform 6; **AtDGATI**, diacylglycerol acyltransferase from *Arabidopsis thaliana*; **Atclo1**, caleosin, lipid droplet stabilization protein from *Arabidopsis thaliana*; **ACCI**, acetyl-CoA carboxylase; **ACCI****, acetyl-CoA carboxylase carrying two mutations ser659ala, and ser1157ala; **ACS**, acetyl-CoA synthetase; **ADH**, alcohol dehydrogenase; **ALD**, aldehyde dehydrogenase; **ADR**, 1-acyl-DHAP reductase; **CFA**, cyclopropane fatty acid; **CMI**, cell membrane integrity; **DAG**, diacylglycerol; **DGA(T1)**, diacylglycerol acyltransferase; **DHAP**, dihydroxyacetone phosphate; **DHAPAT**, DHAP acyltransferase; **DCW**, dry cell weight; **Ec. CFAS**, cyclopropane fatty acid *synthetase* from *E.coli*; **FA**, fatty acid; **FAS**, fatty acid synthase; **FAEE**, fatty acid ethyl esters; **GAPT**, glycerol-3-phosphate acyltransferase; **GC-FID**, gas chromatography with flame ionisation detection; **HPLC**, High-performance liquid chromatography; **LD**, lipid droplet; **LPAT**, lysophosphatidic acid acyltransferase; **OD**, optical density; **PL**, phospholipid; **PI**, propidium iodine; **PAP**, phosphatidate phosphatase; **RID**, refractive index detector; **RNA-seq**, ribonucleic acid sequencing; **ROS**, reactive oxygen species; **SCFAs**, short chain fatty acids; **SE**, sterol ester; **SEACS^{L641P}**, acetyl-CoA synthetase with an L641P mutation from *Salmonella enterica*; **TAG**, triacylglycerol; **TGL**, triglyceride lipase; **TCA**, tricarboxylic acid cycle; **ATgl3**, triglyceride lipase 3 knock out; **$\Delta\psi_m$** , mitochondria membrane potential.

This page is intentionally blank

Abstract

Triacylglycerols (TAGs) are a significant component of oils found in nature and are also used as essential platform metabolites in nutrition, and for biochemicals and biofuel production. However, TAGs are usually poorly understood at the metabolic level in plants and microorganisms. Yeast *Saccharomyces cerevisiae* is a well-studied model microorganism, which was used in this study because it can store lipid stably as TAG and has a long track record in industrial applications. The novel approach taken in this study brings together four main steps in lipid production in yeast namely fatty acid (FA) biosynthesis, FA modification, lipid accumulation (TAG synthesis), and lipid sequestration (lipid droplet, LD biogenesis) and also studies the impact of these of lipid production both as individual cells and in cultures.

Firstly, five potential candidate genes from plant and microalgae for FA accumulation were studied and compared, and the diacylglycerol acyltransferase from *Arabidopsis thaliana* (*AtDGATI*) was found to be an effective enzyme for lipid accumulation in yeast (1.81-fold than control).

Then, three main steps of lipid production: FA biosynthesis, lipid accumulation and sequestration were studied individually and in combination for their ability to increase lipid production. The engineered strain HBY31 recombinantly expressed additional genes: *Ald6*, *SEACS^{L641P}*, *ACCI***, *AtDGATI*, *AtClo1*, and had *Tgl3* knocked out, and produced the highest lipid content (8.0% DCW basis, 2.6-fold over control) but this impacted yeast growth and viability. To address these drawbacks, a two-stage bioprocess was designed that separated biomass growth and lipid synthesis stages. This strategy convincingly ameliorated the negative effects and resulted in normal cell growth, very high lipid productivity (307 mg/L, 4.6-fold than control) and improved cell viability.

Thirdly, the lipid storage strategy was assessed for the production of unusual FA, cyclopropane fatty acid (CFA), which is a high value saturated fatty acid showing excellent lubricity and low oxidation

potential. Cyclopropane fatty acid synthase from *E. coli* (*Ec.CFAS*) was expressed in yeast engineered for high lipid content. The strain CBY20 achieved the highest CFA content (18.3 mg/g dry cell weight DCW), 2.7-fold higher than *Ec.CFAS*-only cells and it maintained a high TAG content (74.4 mg/g DCW), 10.3-fold higher than *EcCFAS*-only cells.

Finally, transcriptomic analysis and flow cytometry-based physiological characterisations were employed on the above engineered strains to investigate the relationship between lipid engineering and cellular physiological responses, and identify further metabolic engineering targets. The results showed elevated ROS levels are not the primary cause of reduced membrane integrity or low cell growth. Unbalanced energy supplies and redox levels in the cell are promising targets for further lipid pathway engineering.

In conclusion, this thesis has used the yeast *S. cerevisiae* as a model production host to test the effectiveness of different lipid metabolic engineering strategies on the enhancement of standard and unusual lipid production and its impacts on cellular physiology. The concept of construction of a microbial cell factory was exemplified in this project and it can be extended to other industrial microorganisms and valuable biochemicals.

Publications during enrolment

Published or submitted articles (included in this thesis)

- [1] **Huadong Peng**, Lalehvash Moghaddam, Anthony Brinin, Brett Williams, Sagadevan Mundree, Victoria S. Haritos. Functional assessment of plant and microalgal lipid pathway genes in yeast to enhance microbial industrial oil production. **Biotechnology and Applied Biochemistry** 2018; 65 (2), 138-144 (**Chapter 3**)
- [2] **Huadong Peng**, Lizhong He, Victoria S. Haritos. Metabolic engineering of lipid pathways in *Saccharomyces cerevisiae* and staged bioprocess for enhanced lipid production and cellular physiology **Journal of Industrial Microbiology & Biotechnology** 2018; 45(8): 707-717. (**Chapter 4**)
- [3] **Huadong Peng**, Lizhong He, Victoria S. Haritos. Enhanced production of high-value cyclopropane fatty acid in yeast engineered for increased lipid synthesis and accumulation (submitted to **Biotechnology Journal**) (**Chapter 5**)
- [4] **Huadong Peng**, Lizhong He, Victoria S. Haritos. Flow cytometry-based physiological characterisation and transcriptome analyses reveal a mechanism for reduced cell viability in yeast engineered for increased lipid content (submitted to **Biotechnology for Biofuels**) (**Chapter 6**)

Published articles (not included in this thesis)

- [1] Kamila Kochan†, **Huadong Peng**†, Bayden R Wood, Victoria S Haritos Single cell assessment of yeast metabolic engineering for enhanced lipid production using Raman and AFM-IR imaging **Biotechnology for Biofuels** 2018; 11 (1), 106 (†**Co-first author**, related to **Chapter 4**)
- [2] Kamila Kochan, **Huadong Peng**, Shuhui Eunice Gwee, Ekaterina Pas, Victoria Haritos, Bayden R. Wood. Raman spectroscopy as a tool for tracking cyclopropane fatty acids in genetically engineered *Saccharomyces cerevisiae* **Analyst** 2018; DOI: 10.1039/C8AN01477A (related to **Chapter 5**)

Thesis including published works declaration

I hereby declare that this thesis contains no material which has been accepted for the award of any other degree or diploma at any university or equivalent institution and that, to the best of my knowledge and belief, this thesis contains no material previously published or written by another person, except where due reference is made in the text of the thesis.

This thesis includes 2 original papers published in peer reviewed journals and 2 submitted publications. The core theme of the thesis is lipid metabolic engineering in yeast. The ideas, development and writing up of all the papers in the thesis were the principal responsibility of myself, the student, working within the Department of Chemical Engineering under the supervision of Associate Professor Victoria Haritos and Dr. Lizhong He.

The inclusion of co-authors reflects the fact that the work came from active collaboration between researchers and acknowledges input into team-based research.

In the case of *Chapter 3, 4* my contribution to the work involved the following:

Thesis Chapter	Publication Title	Status <i>(published, in press, accepted or returned for revision, submitted)</i>	Nature and % of student contribution	Co-author name(s) Nature and % of Co-author's contribution*	Co-author(s), Monash student Y/N*
3	<i>Functional assessment of plant and microalgal lipid pathway genes in yeast to enhance microbial industrial oil production</i>	Published	60%, experimental design and work, results analysis and write-up	1. Lalehvash Moghaddam, 5%, results discussion 2. Anthony Brinin, 10%, plasmid construct 3. Brett Williams, 5%, results discussion 4. Sagadevan Mundree, 5%, results discussion 5. Victoria S. Haritos, 15%, Idea, data interpretation & editing	No, Academic staff from Queensland University of Technology Yes, Monash staff
4	<i>Metabolic engineering of lipid pathways in Saccharomyces cerevisiae and staged bioprocess for enhanced lipid production and cellular physiology</i>	Published	70%, experimental design and work, results analysis and write-up	1. Lizhong He, 10%, results discussion & editing 2. Victoria S. Haritos, 20% Idea, data interpretation & editing	Yes, Monash staff

*If no co-authors, leave fields blank

I have renumbered sections of submitted or published papers in order to generate a consistent presentation within the thesis.

Student signature: 

Date: 31/8/2018

The undersigned hereby certify that the above declaration correctly reflects the nature and extent of the student's and co-authors' contributions to this work. In instances where I am not the responsible author I have consulted with the responsible author to agree on the respective contributions of the authors.

Main Supervisor signature: 

Date: 31/8/2018

Acknowledgements

This Ph.D. thesis would not have been possible without my dear supervisor Associate Professor Victoria Haritos, who led me into a (new) research field (for me), metabolic engineering. Victoria has multiple hats but she keeps them balanced and seems to have endless energy. Not only does Victoria have a fantastic capacity for engaging her students scientifically, she makes time for a warm smile or chat that will brighten and inspire everyone's spirit. Victoria has supported me throughout my Ph.D. project and at my life's crucial times. What's more, she has encouraged me to be open to new scientific trends, to visit or communicate with researchers outside the campus and participate at conferences. Victoria's consistent lifelong learning habit keeps her knowledge base updated in biology and engineering and allows her to identify the latest scientific questions in the forefront of the field. My journey in addressing hard questions in my thesis with her is memorable, and I am very grateful to have worked with her in the past 3.5 years.

I would like to thank my co-supervisor, Dr. Lizhong He, he is not a co-supervisor only on paper but in fact, he has given me a lot of help and guidance in my project. In particular, I appreciated being part of his group meetings which gave me opportunities to learn from his senior Ph.D. students and make friendships. Although my Ph.D. project is not in his research field, he contributes many valuable and interesting ideas based on his abundant knowledge of biotechnology. Besides, his encouragement and support has also made my Ph.D. life much more confident and comfortable.

I would like to thank the postgraduate scholarships (MGS & MIPRS) from Monash University that have allowed me the chance to study at the Department of Chemical Engineering, and meet amazing colleagues and Professors. I also thank the financial support of the Australia–India Strategic Research Fund Grand Challenge Fund and ARC linkage project (LE160100185) in support of my Ph.D. project. Also, I would like to thank the department general office team who have given me a lot of help in life

and work including Lilyanne Price, Jillian Crisfield, Kim Phu, Harry Bouwmeester and Ross Ellingham.

Also, I would like to thank my colleague, Melissa Jane Mace, she was the first person I met at Monash University. She helped me become familiar with the campus and lab environment and relieved the culture shock of my first time of studying overseas. I enjoyed and appreciated the time we worked together and I wish her all the best at Tatura Milk!

I would like to thank my collaborator, Kamila Kochan, an expert in biospectroscopy. She is an excellent model of a young researcher, totally professional and efficient with a results-oriented manner. Also, I would like to thank Pradeep GC, the previous laboratory manager of the Bioengineering Laboratory. He will always be 'Boss' and I thank him for his optimism and constant smile about life. For a long time we worked together in the lab on our individual projects but we shared many opinions about study and life and this eased the sometime boredom of lab life.

I would like to thank the undergraduate and master students studying Chemical Engineering at Monash University whom I was able to supervise for their final year projects and learn from them. They are: Brandon Lim, Kuan Che Chen, Sheridan Vella, Alastair Katrivessis, Mitchell Drowley, Nguyen Ho, Astrid Ichsan, Benny Nguyen and Amy To Y Cao. Also, there are many prior and current lab members, colleagues and friends to be thanked including Jason Zhao, Huazhen Li, Bhuvana Shanbhag, Craig Osborne, Jamie Joseph Castillo, Negin Amini, Madura Kumar, Lavaraj Devkota, Xueqing Liu, Chang Liu, Tayyaba Younas, Ruihuan Ge, Baiqian Dai, Fanghua Li, Ruosang Qiu, Tao Xu, Zike Wang, Jiushuai Deng, Renyuan Ouyang, Zhenyang Bao, Jianrong Sang and Yao Chen.

Finally, I would like to thank my girlfriend Wei Jiang, although she came later to the lab, her support and understanding during the finalisation of my Ph.D. thesis helped me in a better way. Also, I would

like to offer my sincere thanks to my family members for their understanding of my wish to pursue Ph.D. studies.

This page is intentionally blank

CHAPTER 1

INTRODUCTION

This page is intentionally blank

Chapter 1 Introduction

1.1 Background

Microbial lipids are valuable as sustainable feedstock alternatives to crude oil for the production of chemicals and fuels. Microbes that have been metabolically engineered to improve productivity can produce large quantities of renewable chemicals from simple, readily available, inexpensive starting materials (Keasling, 2010; Markham & Alper, 2015). There are several advantages to using the sustainable approach of metabolically engineered microorganisms to produce biofuel or chemicals: (1) it can avoid competition with food-derived sugars by supplying non-food carbon feedstocks such as cellulosic sugars, (2) it has the flexibility in fatty acid (FA) type produced that are suited to various industrial applications such as biofuels, surfactants, lubricants (Lennen & Pfleger, 2013; Pfleger et al., 2015), (3) production can be scaled up to satisfy growing worldwide oleochemicals demand for renewable non-food sources of FA (Pfleger et al., 2015), (4) the approach reduces deforestation and greenhouse gases emissions caused by widespread land clearing that is required for plant oil production (such as oil palm) (Fargione et al., 2008; OECD/FAO, 2014).

Research into the improvement in productivity of microbial lipids through metabolic engineering is relatively new. Despite excellent recent progress, even the best lipid producing organisms to date in *Saccharomyces cerevisiae* (254 mg TAG/g DCW) (Ferreira et al., 2018) and *Yarrowia lipolytica* (99 g lipid/L in the fed-batch bioreactor by increasing NADPH supply) (Qiao et al., 2017), are insufficient for commercial lipid production. To improve low lipid titres, there are several approaches worth exploring including the development of new metabolic engineering targets, the discovery of high-value lipid-derived products, combination of metabolic engineering and bioprocess approaches and deepening our understanding of cellular physiology of engineered microorganisms.

While microbial lipids from fungi, bacteria, microalgae, and plants are the subject of intensive research, the yeast *S. cerevisiae* was selected as the target organism of this project due to its advantages of being a very well studied organism with a wide range of strains and excellent genetic tools available, it store lipids as stable droplets and has a proven track record in industrial applications. Moreover, successful metabolic engineering strategies developed in *S. cerevisiae* may be easily transferred to other useful industrial organisms such as the oleaginous yeast *Yarrowia lipolytica*.

1.2 Scope of research

This thesis studied lipid pathway metabolic engineering using the yeast *S. cerevisiae* as a host strain. Multiple steps in lipid production were addressed in the research including FA biosynthesis, FA modification, lipid accumulation and sequestration. The main mode of production was intracellular rather than by extracellular secretion because lipid storage as specific triacylglycerol (TAG) compositions is usually poorly understood at the metabolic level and lack available tools (Ferreira et al., 2018). Cyclopropane fatty acids (CFA) was the single example of unusual and modified FA used in the thesis. Bioprocess strategies were investigated for improving the final yield of lipid but the emphasis of this work was on overcoming slow biomass growth rather than investigating novel bioprocess methods. Several methods of investigating cell physiological responses to metabolic engineering were implemented to elucidate the performance of engineered cells and these encompassed cell growth, cell membrane integrity, reactive oxygen species, and mitochondrial membrane potential. Furthermore, transcriptome analysis was used to determine the response of the organism to metabolic pathway engineering and to support the information from cellular physiology measures but restricted to gene expression in the areas of central carbon metabolism, reactive

oxygen species production pathway and cellular energy balance such as NADPH, ATP synthesis.

1.3 Research objectives

The objective of this thesis is to discover fundamental knowledge on the impact of lipid metabolic engineering strategies on the enhancement of standard and unusual lipid stores within yeast and on cell physiology. The metabolic engineering strategies that were examined included combining of FA biosynthesis, FA modification, lipid accumulation and sequestration steps. These were achieved through the systematic study of:

- selection of an effective lipid accumulation gene for yeast
- combination of genes for the individual steps to improved standard lipid storage
- application of the metabolic engineering strategy to improving the intracellular unusual lipid (cyclopropane fatty acid) titre to the highest reported level

The potential mechanisms of impact on cell physiology of lipid metabolic engineering were examined through transcriptomics and functional measurements. The knowledge coming from this project will guide the design of engineered microbes for the production of bulk and fine oleochemicals and fuels in the near future.

1.4 Outline of thesis

The Ph.D. thesis has seven chapters as listed below.

Chapter 1 Introduction

The first chapter provides an overview of this Ph.D. project. It describes four main aspects including background, research scope, project objectives and an outline of the thesis.

Chapter 2 Literature review

Chapter 1 Introduction

This chapter critically reviews current metabolic engineering strategies for enhanced intracellular lipid storage in the yeast *S. cerevisiae*. It begins with the necessity and drivers for microbial lipids production, followed by the metabolic engineering strategies to enhance standard lipid and unusual lipid production. Then, the impacts on cell physiology due to lipid pathway engineering are summarized such as: cell growth, cell membrane integrity, reactive oxygen species and mitochondria membrane potential. Bioprocess strategies are introduced especially two-stage bioprocesses that are implemented to improve lipid production. Finally, the promising approaches for metabolic engineering strategies for enhanced intracellular lipid production and better cell health in yeast are proposed.

Chapter 3 Screen lipid accumulation gene

This chapter evaluated the effectiveness of recombinant expression of 5 fatty acid accumulation genes through establishing a set of valid analytical tools to measure intracellular lipid content in yeast. A diacylglycerol acyltransferase 1 (DGAT) from the plant *Arabidopsis thaliana*, *AtDGAT1* was identified as an effective lipid accumulation gene (lipid yield 1.81-fold higher than control) in yeast and was selected for the subsequent study. A second gene, *AtRODI* led to increased unsaturated fatty acid content of lipid in the yeast.

Chapter 4 Lipid pathway engineering towards standard lipids storage

This chapter examined, stepwise, the effective of introducing up to 6 genes that manipulate FA synthesis, lipid accumulation and sequestration of stored triacylglycerol (TAG). The metabolic engineering strategy significantly improved cellular lipid content (up to 8.0% DCW basis, 2.6-fold over control) but severely reduced yeast growth and cell viability. To address this drawback, a two-stage process was designed to recover cell growth and achieved very high lipid productivity (307 mg/L, 4.6-fold above control) and improved cell viability. The work

has demonstrated that cell viability and other physiological measures are key indicators to guide successful metabolic engineering strategies.

Chapter 5 Lipid pathway engineering towards unusual lipids storage

This chapter investigated the production and storage of a value-added FA, cyclopropane fatty acid within the highly engineered strains developed in Chapter 4. This chapter has demonstrated that the lipid pathway engineering strategy developed for standard fatty acids is effective also for CFA production and accumulation in yeast although further improvement is needed in transferring CFA from phospholipid where it is generated into the storage TAG fraction for greater overall yields.

Chapter 6 Cellular physiological responses and transcriptome analysis

In this chapter, cellular physiological responses and transcriptome analysis were employed to examine the mechanisms of low growth and cell viability in yeast engineered for high lipid content. In addition to the regulated central carbon pathway, the ROS production pathway was upregulated and respiratory pathway (or energy synthesis such as NADPH, ATP) was downregulated. These insights also open up opportunities to ameliorate the side effects of lipid pathway engineering to deliver both high lipid yield and high cell viability.

Chapter 7 Conclusion and outlook

In this chapter, the main conclusions were drawn together, and the potential for further metabolic engineering strategies to increase lipid storage without unbalancing energy supply and to improve unusual FA production and storage are discussed.

1.5 References

Fargione, J., Hill, J., Tilman, D., Polasky, S., Hawthorne, P. 2008. Land clearing and the biofuel carbon debt. *Science*, **319**(5867), 1235-1238.

Ferreira, R., Teixeira, P.G., Gossing, M., David, F., Siewers, V., Nielsen, J. 2018. Metabolic engineering of *Saccharomyces cerevisiae* for overproduction of triacylglycerols. *Metabolic Engineering Communications*, **6**, 22-27.

Keasling, J.D. 2010. Manufacturing molecules through metabolic engineering. *Science*, **330**(6009), 1355-1358.

Lennen, R.M., Pfleger, B.F. 2013. Microbial production of fatty acid-derived fuels and chemicals. *Current opinion in biotechnology*, **24**(6), 1044-1053.

Markham, K., Alper, H.S. 2015. Synthetic Biology for Specialty Chemicals. *Annual Review of Chemical and Biomolecular Engineering*, **6**(1), 1-18.

OECD/FAO. 2014. "Oilseeds and oilseed products", in OECD-FAO Agricultural Outlook 2014, OECD Publishing, Paris., 145-156.

Pfleger, B.F., Gossing, M., Nielsen, J. 2015. Metabolic engineering strategies for microbial synthesis of oleochemicals. *Metabolic engineering* **29**, 1-11.

Qiao, K., Wasylenko, T.M., Zhou, K., Xu, P., Stephanopoulos, G. 2017. Lipid production in *Yarrowia lipolytica* is maximized by engineering cytosolic redox metabolism. *Nat Biotech*, **35**(2), 173-177.

CHAPTER 2

LITERATURE REVIEW

This page is intentionally blank

Chapter 2 Literature review

2.1. Background

Fatty acids (FAs) are hydrocarbon derivatives, they are carboxylic acids with hydrocarbon chains ranging from 4 to 36 carbons long (C4 to C36). In some FAs, this chain is unbranched and fully saturated (without double bonds), such as palmitic acid (C16:0), stearic acid (C18:0); in others, the chain contains one or more double bonds, such as palmitoleic acid (C16:1, Δ^9), oleic acid (C18:1, Δ^9), and linoleic acid (C18:2, $\Delta^{9,12}$), etc. (Nelson & Cox, 2013). Cellular lipids can be classified into two major categories, namely energy storage lipids (neutral) and membrane lipids (polar). Triacylglycerols (TAGs) are the simplest neutral lipids constructed from FAs, also referred to as triglycerides, fats, or neutral fats, which contain three FA molecules esterified to three hydroxyl groups of glycerol. Phospholipids (PLs) and sterols are major structural elements of biological membranes. Membrane lipids are amphipathic, with one end of the lipid molecule being hydrophobic, while the other end being hydrophilic. Among membrane lipids, PLs use a polar head group to join into the hydrophobic moiety through the phosphodiester linkage (Nelson & Cox, 2013; Ratledge, 2008).

2.1.1. Host microorganisms

Fatty acid synthesis is one of the ubiquitous pathways in organisms, including bacteria, fungi, algae and plants, etc. Most bacteria such as *Escherichia coli* (*E. coli*) and Archaea synthesise FAs and use them as membrane components, while storing energy in the form of polyhydroxyalkanoates instead of TAG in lipid droplets (LDs) as seen in Eukaryotes (JanSZen & Steinbuchel, 2014; Rottig et al., 2015). Nevertheless, there are few bacteria having the ability to synthesise TAG. The short generation time and industrial track record of *E. coli* attract the attention of using it as a chassis for lipid engineering. For example, *E.coli* MG1655 *dgkA* mutant strain achieved a very high TAG yield (9%, w/w) by overexpressing *fadD* and two

copies of *atfA*, which encodes the wax synthase (WS)/DGAT from *Acinetobacter baylyi* (Janßen & Steinbüchel, 2014; Rottig et al., 2015). Additionally, a very high yield of medium chain FAs (3.8 g/L) were reached via the reverse beta-oxidation cycle (Wu et al., 2017). However, the lipid yield is still insufficient to reach levels that would meet commercialisation requirements.

Due to the advantages of having high cellular lipid content (> 60%, DCW) and the ability to photosynthesise, microalgae has long been designated for lipid production, including the well-studied model microalgae from among Chlorophyta, Bacillariophyceae (Liang & Jiang, 2013). However, there are also some obstacles such as low biomass concentrations, high dewatering cost, high water demand and high oil recovery costs that limiting the development of microalgae as a lipid production cell factory (Chisti, 2007; Greenwell et al., 2010). Besides, the cultivation of microalgae is also biotechnologically challenging due to the fact that photosynthesis requires illumination, CO₂ (limited by CO₂ content of air) and moderate temperatures (limitation of geographical development). In addition, predators such as protozoa, viruses and disease caused by other algae or even bacteria add the difficulties of algae culture in open ponds (Ratledge, 2008; Ratledge, 1994).

In oil-producing plants such as *Brassica napus*, *Nicotiana tabacum* and palm, several effective metabolic engineering approaches have been undertaken, including the overexpression of acyltransferase genes obtained from model plants like *Arabidopsis thaliana*, tobacco and *Brassica napus* to enhance TAG production in seed oils, fruit, pollen grains or leaves of the transformed hosts (Aznar-Moreno et al., 2015; Bouvier - Navé et al., 2000; Vanhercke et al., 2014). However, plant oil production can result in deforestation because of the widespread land clearing required to establish new oil crops, which may make the process environmentally

unsustainable (Fitzherbert et al., 2008) especially when the product is for non-food purposes. Furthermore, it takes many years or even decades to establish genetically modified organism (GMO) crop plants such as oil-bearing crambe or brassicas, mainly due to the time taken for official approvals then establishing the production and value chain (Lessman, 1990).

There are several species of oleaginous yeasts (25 out of 600) that are able to produce high yields of TAG (more than 20% DCW) (Ratledge C & S.G., 1988), such as *Yarrowia lipolytica*. While the lipid content of most yeasts/fungi is normally low, they are important sources of metabolites such as nutritional and pharmaceutical applications, especially polyunsaturated FAs (PUFAs), eicosapentaenoic acid (20:5 ω -3; EPA), docosahexaenoic acid (22:6 ω -3; DHA) and γ -linolenic acid (18:3 ω -6; GLA) (Davidoff & Korn, 1963; Kendrick & Ratledge, 1992; Ratledge, 2008; Ratledge, 1994). Baker's yeast *Saccharomyces cerevisiae*, despite not being classified as oleaginous, does have many advantages that could be exploited when being used for metabolic engineering for lipid production and has thus been widely studied. For example, it is highly tractable and is available in a wide range of genetic backgrounds; there are abundant molecular tools, large assortment of commercially-available deletion strains, short generation time, easy to culture, and proven track record in various industry applications (Runguphan & Keasling, 2014) (Table 2.1).

Based on the comparison above, Table 2.1 briefly lists the principal pros and cons of different organisms when being used for lipid production. While all four main lipid production sources are the subjects of intensive researches, in this study *S. cerevisiae* was chosen as the target organism owing to some of its attractive advantages, namely its capability of storing lipids stably and its proven track record in industrial applications.

Table 2.1 Comparison of different hosts for lipids production

Sources	Model organism	Pros	Cons	Refs
Fungi	<i>S. cerevisiae</i>	<ul style="list-style-type: none"> • robust • genetically tractable • easy to culture • industrial usage 	<ul style="list-style-type: none"> • low lipid yield (oleaginous – high yield) • not yet commercialised 	(Li et al., 2014; Runguphan & Keasling, 2014)
Bacteria	<i>E. coli</i>	<ul style="list-style-type: none"> • short generation time • genetically tractable • industrial usage 	<ul style="list-style-type: none"> • low lipid yield • no stable lipid body 	(JanSZen & Steinbuchel, 2014)
Microalgae	<i>Chlorella</i>	<ul style="list-style-type: none"> • high oil productivity • CO₂ fixation 	<ul style="list-style-type: none"> • low biomass concentrations • high costs for oil recovery • difficulties in open pond culture 	(Ratledge, 2008; Ratledge, 1994)
Plant	<i>Arabidopsis thaliana</i>	<ul style="list-style-type: none"> • high oil yield • CO₂ fixation 	<ul style="list-style-type: none"> • difficulties to industrialize • deforestation and greenhouse gases emission 	(Lessman, 1990)

2.1.2. Lipid synthesis in yeast

From carbon source to lipid production, there are four major steps in yeast: namely FA synthesis, FA modification, lipid accumulation and sequestration, as shown in Fig. 2.1. FAs represent a suitable storage compound for energy and carbon due to the fact that the degradation of FAs yields a high amount of adenosine triphosphate (ATP) and reducing equivalents (JanSZen & Steinbuchel, 2014). FA modification may occur on the acyl chain while it is attached to Coenzyme A (CoA) or for some unusual FAs such as cyclopropane and ricinoleic acid, it may occur when the FA is attached to another substrate which would be discussed in part 3.2. In multicellular organisms, unicellular eukaryotes and some prokaryotes, FAs are stored in the form of TAG or wax esters, a process described herein as FA accumulation. The surplus neutral lipids such as TAG and sterol ester (SE) can then be sequestered into lipid droplets (LDs). The LD organelles are a stable reservoir of stored lipids within the cell. LDs provide the most efficient form of energy storage due to the package of highly reduced, hydrophobic lipids, such as TAG in a phase without water. LDs can also provide building blocks for cellular membranes or substrates for energy metabolism (Walther & Farese Jr, 2012; Walther & Farese, 2009).

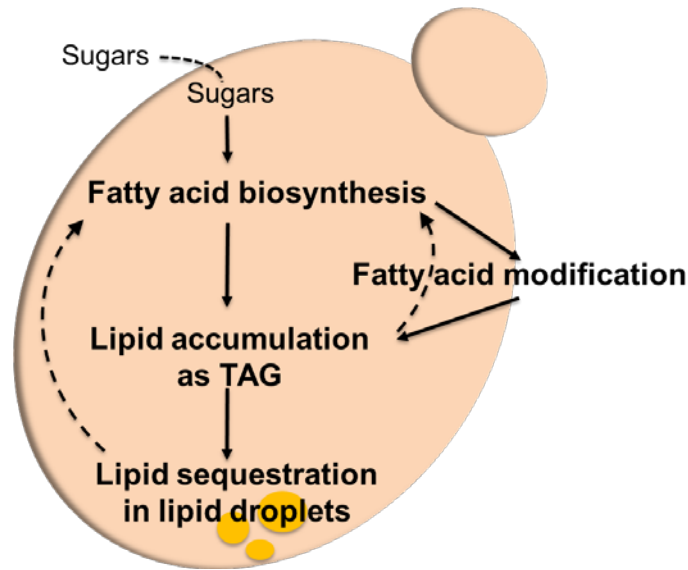


Figure 2.1 Four major steps in yeast lipids production

FA synthesis requires the participation of a three-carbon intermediate, malonyl-CoA, which is formed from acetyl-CoA and bicarbonate. The formation of malonyl-CoA from acetyl-CoA is an irreversible process, catalysed by acetyl-CoA carboxylase (ACC) (Fig. 2.2), which contains a biotin prosthetic group covalently bound in an amide linkage to the ϵ -amino group of a lysine residue in one of the three polypeptides or domains of the enzyme molecule. The carboxyl group, derived from bicarbonate (HCO_3^-), first transfers to biotin in an ATP-dependent reaction. Subsequently, the biotinyl group serves as a temporary carrier of CO_2 , transferring it to acetyl-CoA in the second step to yield malonyl-CoA (Nelson & Cox, 2013).

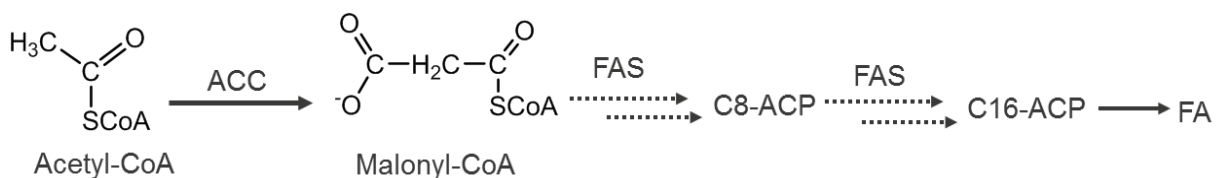
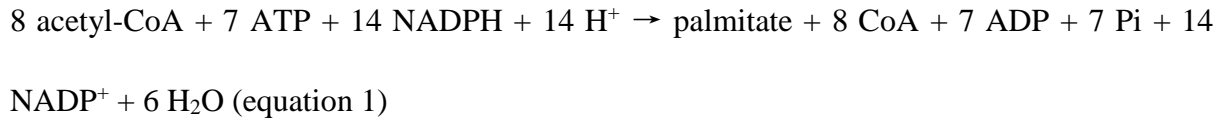


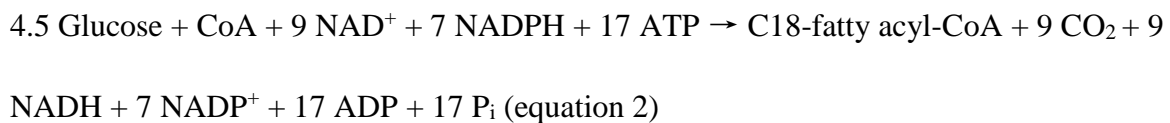
Figure 2.2 Fatty acid biosynthesis pathway

(*ACC, acetyl-CoA carboxylase; FAS, fatty acid synthase; ACP, acyl carrier protein.)

FA are synthesised from acetyl-CoA by a cytosolic complex of six enzyme activities plus acyl carrier protein (ACP), proceeds in a repeating four-step reaction sequence which include condensation, reduction of the carbonyl group, dehydration, and reduction of the double bond. For example, synthesis of palmitate (C16:0), requires seven cycles of condensation and reduction:



The overall stoichiometry of glucose conversion to stearic acid and TAG synthesis is approximated as equations 2 & 3 below. Therefore, if glucose is not used for the synthesis of any other product, the lipid yield is approximately 32 g per 100 g glucose (Ratledge, 2008).



All the reactions in the synthetic process are catalysed by a multienzyme complex, FA synthase (FAS). In some organisms, FAS consists of multifunctional polypeptides which function as carriers of the fatty acyl intermediates. Although the details of enzyme structure differ between prokaryotes (*E. coli*) and eukaryotes (*S. cerevisiae*), the four-step process of FA synthesis is the same (Nelson & Cox, 2013). Synthesis of FA requires acetyl-CoA and the input of chemical energy in two forms: ATP to power the joining of CO₂ to acetyl-CoA to make malonyl-CoA and NADPH to reduce the double bonds. Biosynthesis of FAs is regulated at the level of malonyl-CoA formation (Nelson & Cox, 2013).

Most of the FAs synthesised or ingested by yeast have one of two fates for incorporation: incorporation into triacylglycerols (TAGs) for the storage of metabolic energy or incorporation into the phospholipid components of membranes. TAGs have the highest energy content of all stored nutrients - more than 38 kJ/g (Nelson & Cox, 2013). In yeasts, TAG synthesis occurs via the Kennedy pathway (Kennedy, 1962) in two phases, one is diacylglycerol (DAG) formation; another is the acylation reaction that converts DAG to TAG. There are two different pathways to accomplish *de novo* synthesis of DAG in the yeast, namely the glycerol-3-phosphate (G3P) pathway and the dihydroxyacetone phosphate (DHAP) pathway (Fig. 2.3). In the first step of TAG assembly, lysophosphatidic acid (LPA) can be acylated from G3P in the *sn-1* position by G3P acyltransferase (*SCT1*) directly or formed via DHAP by the combination of G3P acyltransferase, DHAP acyltransferase and 1-acyl DHAP reductase. Then LPA is acylated to phosphatidic acid (PA) in the *sn-2* position by LPA acyltransferase (*SLC1*), followed by dephosphorylation of PA by phosphatidate phosphatase (PAP) to yield MAG. Then, MAG acyltransferase (MGAT) catalyses the addition of a FA-CoA to MAG to form DAG. In the last step, the third acyl group can be added at the *sn-3* position either through the acetyl-CoA dependent pathway (DAG acyltransferase (DGAT), *DGA1* with acyl-CoA as an acyl donor) or through the acyl-CoA-independent pathway (phospholipid DAG acyltransferase (PDAT), *LROI* with glycerophospholipids as an acyl donor) (Beopoulos et al., 2008; Czabany et al., 2007). Furthermore, TAGs can also be produced from FAs on the DAGs in a phospholipase A₂ - dependent deacylation-reacylation mechanism (Sorger & Daum, 2002).

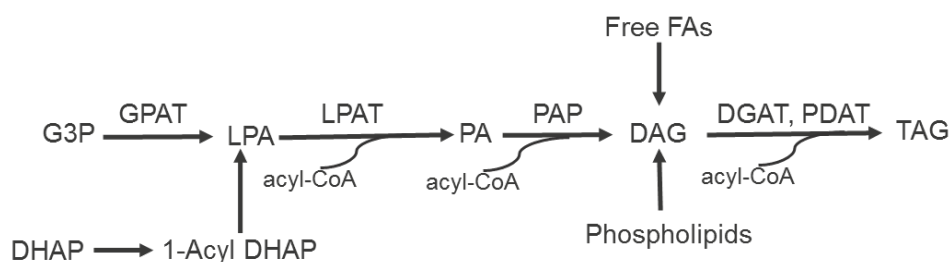


Figure 2.3 Pathways leading to the formation of TAG

Chapter 2 Literature review

(*G3P, glycerol-3-phosphate; GPAT, G3P acyltransferase; DHAP, dihydroxyacetone phosphate; LPA, lysophosphatidate; LPAT, lysophosphatidate acyl-transferase; PA, phosphatidate; PAP, phosphatidate phosphatase; DAG, diacylglycerol; DGAT, acyl-CoA: diacylglycerol acyltransferase; PDAT, phospholipid: diacylglycerol acyltransferase.)

In contrast to FA accumulation, FA degradation occurs via the β -oxidation pathway in the peroxisomes in yeast cells. FA degradation can happen during the exponential phase of cell growth to provide energy for membrane lipid synthesis, cellular growth and division, during the stationary phase to overcome the lack of environment nutrients, and during the phase where cells exit starvation conditions (Kurat et al., 2006).

Surplus neutral lipids such as TAG are sequestered into LDs. In the 19th century, LDs were firstly identified by light microscopy as cellular organelles, and have been referred to as lipid bodies, fat bodies, oil bodies, spherosomes, or adiposomes. LDs have been ignored for a long time as inert lipid globules with little functional relevance before being recognised as metabolically highly active organelles. LDs form the main lipid storage organelles for neutral lipids in eukaryotic cells such as *S. cerevisiae* and even some prokaryote cells such as *Mycobacteria*, *Rhodococcus*, *Streptomyces*, and *Nocardia* (Alvarez & Steinbüchel, 2002; Walther & Farese Jr, 2012). LDs are primarily composed of TAG and sterol ester (SE) (roughly 50% each by weight) with a small amount of phospholipids in the wild type yeast (Leber et al., 1994), and its formation and utilisation is not essential to *S. cerevisiae* (Sandager et al., 2002). These LDs are speculated to be formed in the endoplasmic reticulum (ER) and surrounded by a phospholipid monolayer with a highly hydrophobic core. LDs vary dramatically in size but have an approximate diameter of 0.1 μm in yeast (Walther & Farese Jr, 2012; Walther & Farese, 2009). It is not known precisely how the bi-layered membrane gives rise to LDs enclosed by monolayers, but several models of LD biogenesis have been proposed. For example, (1) ER

budding model (also most widely cited model) where LDs grow from the endoplasmic reticulum (ER) bilayer and remain connected or bud off. (2) Bicelle formation in which an entire lipid lens is excised from the ER (Ploegh, 2007). (3) Vesicular budding in which a bilayer vesicle forms, followed by filling of the bilayer intramembranous space with neutral lipids (Walther & Farese, 2009). (4) An “eggcup” model in which a LD grows within a concave depression of the ER through transport of neutral lipids from the ER (Robenek et al., 2006; Walther & Farese Jr, 2012).

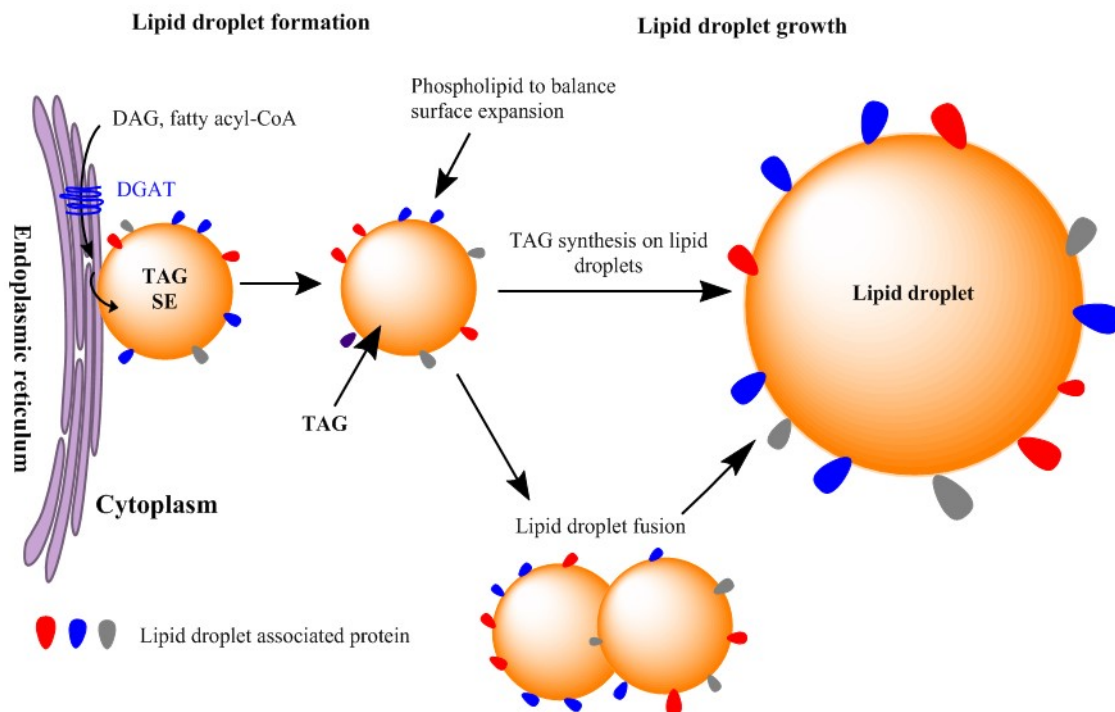


Figure 2.4 Endoplasmic reticulum budding model of lipid droplet formation and expansion (redrawn with modifications from (Walther & Farese Jr, 2012))

2.2. Metabolic engineering strategies for lipid accumulation and storage of standard FA

In general, lipid production is optimised by blocking competing pathways that consume lipids, FFAs and other intermediates, strengthening the lipid synthesis pathway, and keeping a balance between the synthesis of precursors, intermediates and cofactors (Pfleger et al., 2015). To increase lipid production in yeast, there are several approaches using genetic engineering such

as (1) increasing FA biosynthesis via: overexpression of acyl-CoA carboxylase (ACC), Acyl-CoA synthase (ACS), fatty acid synthase (FAS) genes; improving energy supply such as NADPH and ATP via pathway engineering; deleting genes for FA consumption pathways such as β -oxidation pathway (2) Increasing TAG synthesis via overexpressing acyl-transferases including lysophosphatidate acyl-transferase (LPAT), acyl-CoA: diacylglycerol acyl-transferase (DGAT) and other related pathway enzymes. (3) Enhance LD biogenesis and stability through overexpression of LD-associated genes/proteins and deletion of LD consumption-related proteins/genes or precursors. (4) Lipid pathway engineering approach where all the main routes are brought together to enhance lipid production (Courchesne et al., 2009; Hegde et al., 2015).

2.2.1. Mechanisms to increase FA biosynthesis

Acetyl-CoA synthase

Acetyl-CoA synthase (ACS) catalyses the formation of acetyl-CoA from acetate and CoA, which is the starting point of fatty acid biosynthesis. Chen et al. overexpressed both *ACS1* and *ACS2* in *S. cerevisiae* to increase the intracellular acyl-CoA levels about 2 to 5 times (Chen et al., 2010). Shiba et al. (2007) overexpressed *ACS1* gene in *S. cerevisiae*, improved acyl-CoA level with increased amorphadiene production by 8-23% (Shiba et al., 2007), while the Nielsen group optimised an ACS variant (L641P) from *S. enterica* (*SEACS^{L641P}*) to increase α -santalene and polyhydroxybutyrate production in *S. cerevisiae* (Chen et al., 2013; Kocharin et al., 2012). The mutant form *SEACS^{L641P}* was employed to increase production of lipid (Peng et al., 2018a) and in a separate study, resveratrol (Li et al., 2015).

Acetyl-CoA carboxylase

The enzyme acetyl-CoA carboxylase (ACC) catalyses acetyl-CoA to form malonyl-CoA, which is an important rate-limiting step in FAs biosynthesis. The Keasling group showed that plasmid-based overexpression of endogenous *ACCI* increased lipid content by 58% in *S. cerevisiae*, from 4.3% to 6.8% by DCW (Runguphan & Keasling, 2014). However, no significant increase in total FAs content was observed by plasmid based overexpression of wild type *ACCI* in *S. cerevisiae* by Nielsen group (Shi et al., 2014a), the possible reason for limited effects of *ACCI* overexpression maybe the inherently low enzyme activity. In addition, ACC activity can be inactivated by *Snf1*- or other mediated phosphorylation in yeast, so a malonyl-CoA sensor could be used to screen phosphorylation sites to improve malonyl-CoA derived products (Chen et al., 2018). Furthermore, Nielsen group engineered the mutant version *ACCI^{ser659ala,ser1157ala}*, showed a 3-fold improved ACCase activity, and increased the total lipid content by 65% (Shi et al., 2014a). Interestingly, Da Silva group engineered another mutant version *AccI^{ser1157ala}* and demonstrated 3-fold improvement in both polyketide and fatty acid production (Choi & Da Silva, 2014).

Fatty acid synthase

Another important enzyme involved in FA biosynthesis is FA synthase (FAS) complex. It receives acetyl and malonyl groups for subsequent elongation and final formation of acyl-CoAs. In *S. cerevisiae*, the FAS is composed of two non-identical subunits with multiple functions, encoded by the genes *FAS1* and *FAS2*, respectively. Plasmid-based overexpression of both *FAS1* and *FAS2* in yeast led to 30% increase in lipid content (from 42.7 mg/L to 70.6 mg/L) (Runguphan & Keasling, 2014). As FAS is a large molecular weight, multi-enzyme complex with subunits closely related with each other, and multipoint controls differing with species, these together are a challenge for employing this complex in lipid engineering strategies.

β-oxidation pathway

Blocking FAs consumption via the β -oxidation pathway is a logical strategy to provide more FAs. In *S. cerevisiae*, the β -oxidation pathway was engineered (Δ pox1 [pox2+]) to increase total FAs by 29.5%, 2.26-fold higher intracellular FA than wild type (Chen et al., 2014a). Similarly, inhibition of β -oxidation (*POXI* deletion) led to 4-fold increase in FFA content in *S. cerevisiae* (Valle-Rodriguez et al., 2014). However, as the β -oxidation pathway provides the acetyl-CoA, NADPH etc. precursors and energy, a potential disadvantage of deleting the β -oxidation pathway is the result of slow cell growth, which has been reported for deletion of *POXI* in *S. cerevisiae* (Chen et al., 2014a).

NADPH supply

In addition to the precursors acetyl-CoA, chemical energy in the form of ATP and NADPH are also important because fatty acid biosynthesis is a highly energy-consuming process. The pentose phosphate pathway is a main source of generation of NADPH for FA biosynthesis in yeast, which is constrained by the supply of NADPH (Ouyang et al., 2018; Wasylenko et al., 2015) and this suggests FA biosynthesis could be improved by increasing NADPH supply. Engineering the cytosolic redox metabolism to increase the NADPH supply improved lipid content to 90 g/L in *Y. lipolytica* (Qiao et al., 2017). In *S. cerevisiae*, NADPH limitation could be overcome by expression of isocitrate dehydrogenase (Partow et al., 2017) and furthermore, fine-tuning of NADPH and ATP supply, together with other metabolic engineering strategies to replace alcoholic fermentation with lipogenesis in *S. cerevisiae*, achieved the highest 33.4 g/L extracellular free fatty acids (Yu et al., 2018) This approach was not limited to yeast; two examples where NADPH supply was enhanced in microalgae improved the lipid production (Ren et al., 2009; Xue et al., 2017).

2.2.2. Mechanisms to enhance lipid accumulation

Acyltransferases are the key enzymes catalysing the addition of fatty acids to the glycerol backbone of triacylglycerol or phospholipids. There are three important acyltransferases in the lipid accumulation including glycerol-3-phosphate acyltransferase (GPAT), lysophosphatidate acyltransferase (LPAT), and diacylglycerol acyltransferase (DGAT).

Glycerol-3-phosphate acyltransferase

GPAT catalyses the first step in TAG synthesis, the conversion of glycerol 3-phosphate and acyl-CoA to lysophosphatidate (LPA). The overexpression of GPAT from cocoa in *S. cerevisiae* effectively increased the total lipid content 1.3-fold with more cocoa butter like TAG (Wei et al., 2017).

Lysophosphatidate acyltransferase

LPAT can assist lysophosphatidate (LPA) acylate to form phosphatidate (PA), which is an important precursor for TAG synthesis (Fig. 3). The overexpression of LPAT from cocoa in *S. cerevisiae* effectively increased the total lipid content 1.2-fold with more cocoa butter like TAG (Wei et al., 2017). In a further example, Zou et al. (1997) achieved a 6-fold increased oil content on a dry seed weight basis in *A. thaliana* and *Brassica napus* by transforming a putative *sn*-2-acyl-transferase gene *SLC1-1* (encoding LPAT activity) from the yeast *S. cerevisiae* (Zou et al., 1997).

Diacylglycerol acyltransferase

DGAT catalyses the last step of TAG synthesis from DAG and fatty acyl-CoA, which has been shown to be a very effective lipid accumulation enzyme. When an extra copy of the yeast *DGAI*

was expressed in yeast under the control of a strong constitutive promoter, lipid content was increased 1.5-fold (Runguphan & Keasling, 2014) and heterologous expression of DGATs from plants including cocoa, *A. thaliana*, *B. napus*, *Linum usitatissimum* and the fungi *Mortierella ramanniana* in *S. cerevisiae* also increased TAG or lipid content (Bouvier-Navé et al., 2000; Greer et al., 2015; Peng et al., 2018b; Sorger & Daum, 2002; Wickramaratna et al., 2015).

Other potential lipid accumulation enzymes

Phospholipid: diacylglycerol acyltransferase (PDAT) catalyses the acyl-CoA independent formation of TAG using phospholipid and DAG as substrates (Dahlqvist et al., 2000). PDAT was also reported to have overlap functions with DGAT for TAG synthesis in *Arabidopsis* (Zhang et al., 2009). Besides, PDAT overexpression increased 29-47% total fatty acids (Dahlqvist et al., 2000) and rescued oleic acid sensitivity and TAG accumulation in yeast (Boyle et al., 2012).

Additionally, the enzyme PC: DAG phosphocholine transferase (also known as Reduced Oleate Desaturation, ROD1) transfers a phosphocholine headgroup of PC to the *sn*-3-position of a DAG molecule. The ROD1 from *Arabidopsis* was identified by its action in increasing significantly the content of polyunsaturated fatty acid (PUFA) in oil but not overall oil content (Chapman & Ohlrogge, 2012), and similar trend was found after heterologous expression of *AtROD1* in *S. cerevisiae* (Peng et al., 2018b).

2.2.3. Mechanisms to improve lipid sequestration

Increase neutral lipid supply

As described earlier, TAG is synthesised and then sequestered in the form of LDs which contain a hydrophobic core composed of TAG and sterol esters (SE), surrounded by a monolayer of phospholipids. Five enzymes are responsible for the mobilisation of stored lipids in yeast: TAG lipases including Tgl3p, Tgl4p and Tgl5p and SE hydrolases including Yeh1p and Tgl1p. Tgl3p and Tgl4p are the major TAG lipases in yeast; deletion of these genes leads to markedly increased LD size and number whereas Tgl5p only marginally contributes to TAG hydrolysis under standard growth conditions (Kohlwein et al., 2013). Reduction in TAG hydrolysis via the deletion of *tgl3* or *slc1* (*slc1* encodes a 1-acylglycerol-3-phosphate acyltransferase involved in phosphatidic acid biosynthesis), increased LD production (Bozaquel-Morais et al., 2010), which was consistent with previous research findings that the deletion of *tgl3* or *slc1* could increase TAG levels in cells (Athenstaedt & Daum, 1997; Athenstaedt & Daum, 2003). Whereas deletions of sterol synthesis genes (*HMG2*, *ERG4* and *ERG5*), TAG synthesis gene (*DGA1*), and SE synthesis gene (*ARE2*) all showed reduction in LD contents (Bozaquel-Morais et al., 2010).

Lipid droplet stabilisation

On the surface of LDs, the phospholipid monolayer membrane contains a small content of embedded proteins which assist in the formation of LDs and are called lipid droplet-associated proteins (LDAPs) (Kohlwein et al., 2013). Several proteins of yeast LD have putative assignments for involvement in phosphatidic acid biosynthesis, FA activation, TAG and SE metabolism and sterol synthesis. In contrast to other cellular organelles, the monolayer membrane of LDs is distinctive and the LDAP have been poorly characterised (Gidda et al., 2013). The prominent LDAPs in mammalian cells are perilipin, adipophilin, adipose TG lipase

(ATGL) while oleosins are the most prominent proteins of plant oil droplets; these help cover the surface of droplet and prevent them from coalescence (Grillitsch et al., 2011; Huang, 1996). Some LDAPs have been identified in the formation and turnover of LDs such as SNAP23, LDAP1, LDAP2 and At3g0550 in avocado (*Persea americana*) mesocarp and *A. thaliana* (Olofsson et al., 2008) and some proteins have been associated with lipid accumulation in oil-rich fruit tissues (Horn et al., 2013). Since LDAPs are important for covering the droplet in plants, they may also be important in the yeast LD formation mechanism. Interestingly, yeast LDs do not contain proteins related to the perilipin family of proteins in mammals or oleosins in plants raising questions as to the formation and stabilisation of LDs in yeast without associated proteins (Kohlwein et al., 2013).

There are several yeast LDAPs related proteins or factors including Fld1p (encodes seipin), fat-inducing transcript (FIT), Pah1p (yeast lipin orthologue), phosphatase, phospholipid and phosphatidic acid etc. which have showed effect on the formation, morphology, size or number of LDs (Bozaquel-Morais et al., 2010; Fei et al., 2011b; Olofsson et al., 2008). *Fld1*, the functional orthologue of the human *BSC2* gene encoding seipin, is important to LD morphology, subcellular distribution and inheritance, and deletion of *Fld1* in *S. cerevisiae* leads to impaired dynamics of yeast LDs, defective lipolysis and causes abnormal LDs (Walther & Farese Jr, 2012), which might be due to aberrant ER structures (Wolinski et al., 2011). Besides, *Fld1* was identified among ten yeast mutants producing “supersized” LDs that were up to 50 times the volume of those in WT cells (Fei et al., 2011a).

Another two proteins of fat-inducing transcript (*FIT*) and yeast lipin orthologue of Pah1p are reported to help LD formation. FIT are ER proteins that bind TAG and have been implicated in LDs assembly. FIT2 overexpression in yeast achieved more LDs while the deletion of the

genes resulted in fewer LDs and TAG, but there is no evidence that FIT proteins affect DGAT activity (Kadereit et al., 2008). The yeast lipin orthologue of Pah1p was reported to control the formation of cytosolic LDs. Disruption of *Pah1* resulted in 63% decrease in LDs number, so it was concluded that DAG generated by Pah1p is important for LDs biogenesis (Adeyo et al., 2011).

2.2.4. Lipid pathways engineering approach

Well-targeted single gene or pathway modifications in yeast normally leads to increased lipid content though this improvement is limited; for more considerable improvement in lipid production it is necessary to combine strategies such as the “push - pull - block” strategy (Ferreira et al., 2018; Tai & Stephanopoulos, 2013). Several multi-pathway attempts have been undertaken by researchers to enhance (extracellular & intracellular) lipid production in *S. cerevisiae* and here only recent examples with the maximum lipids yield are summarised. For the extracellular lipids, Da Silva group achieved 2.2 g/L extracellular FFAs through disrupted neutral lipid recycle in *S. cerevisiae* including disruption of β -oxidation and FA accumulation Δ *FAA2*, *PXA1*, *POX1*, *FAA1*, *FAA4*, *FAT1* and co-expression of *DGAI* and *TGL3* (Leber et al., 2015). In 2016, the Nielsen group reached 10.4 g/L extracellular FFAs by enhancing acetyl-CoA pathway, malonyl-CoA pathway and reverse pathway and disrupting FA accumulation (Zhou et al., 2016). Furthermore, a recent breakthrough from Nielsen group through reprogramming yeast metabolism from alcoholic fermentation to lipogenesis, constructed a synthetic oil yeast that could produce up to 33.4 g/L FFAs (Yu et al., 2018). In terms of intracellular accumulation, notably the Nielsen group reported the highest TAG content of 254 mg TAG/g DCW in *S. cerevisiae* as per the gene combination shown in Table 2 and reaching 27.4% of the maximum theoretical yield (Ferreira et al., 2018). A summary of the achievements

in lipid production in yeast through combinations of engineering approaches are summarised in Table 2.2.

Table 2.2 Current status of metabolic engineering strategies of *S. cerevisiae* for improved lipid production

Gene/enzyme modification	Remarks/achievements	Refs
↑ <i>ACC1</i>	↑ 58%, 6.8% lipid	(Runguphan & Keasling, 2014)
(1) ↑ <i>ACC1</i> (2) ↑ <i>ACC1</i> ^{ser659ala,ser1157ala}	(1) No significant increase (2) ↑ 65% FA	(Shi et al., 2014a)
<i>ACC1</i> ^{ser1157ala}	↑ 3-fold FA	(Choi & Da Silva, 2014)
<i>ACC1</i> ^{ser659ala,ser1157ala}	No improve	(Peng et al., 2018a)
↑ <i>FAS1</i> , <i>FAS2</i>	↑ 30% lipid, 70.6 mg/L (5.6% DCW)	(Runguphan & Keasling, 2014)
↑ <i>ACS1</i> , <i>ACS2</i>	↑ 2-5 × acetyl-CoA level	(Chen et al., 2010; Chen et al., 2013)
↑ <i>SEACS</i> ^{L641P}	↑ α-santalene	(Chen et al., 2013)
↑ <i>ACS1</i>	↑ acyl-CoA level ↑ 8-23% amorphadiene	(Shiba et al., 2007)
↑ <i>SeACS</i> ^{L641P} , <i>ADH2</i> , <i>ALD6</i> , <i>WS2</i>	↑ 3 × FAEE, 408 ± 270 µg/g DCW	(de Jong et al., 2014)
(1) Δ <i>pox1</i> , ↑ <i>pox2</i> (2) Δ <i>pox1</i> , ↑ <i>pox2</i> , ↑ <i>crot</i>	(1) ↑ 29.5% total FA, 2.26 × intracellular MCFA, 3.29 × extracellular MCFA (2) ↑ 15.6% total FA, 1.87 × intracellular MCFA, 3.34 × extracellular MCFA	(Chen et al., 2014a)
Δ <i>pox1</i>	↑ 4 × FFA	(Valle-Rodriguez et al., 2014)
Δβ-oxidation, Δ <i>ACSs</i> , Δ <i>ADH1</i> , ↑ thioesterases, ↑ <i>ACC1</i> , ↑ acetyl-CoA	↑ 2 ×, 140 mg/L FA	(Li et al., 2014)
(1) Δβ-oxidation, Δ <i>FAA2</i> , <i>PXA1</i> & <i>POX1</i> ; (2) Δ <i>ACSs</i> <i>FAA1</i> , <i>FAA4</i> & <i>FAT1</i> ; (3) Combine (1) & (2)	(1) ↑ intracellular FA up to 55% (2) ↑ extracellular FFA to 490 mg/L (3) 1.3 g/L extracellular FFA	(Leber et al., 2015)
Δ <i>faa1</i> Δ <i>faa4</i> , ↑ acyl-CoA thioesterase <i>ACOT5</i> (<i>Acot5s</i>)	↑ 6.43 × FFA, 500 µg/mL ↑ UFA ratio, <i>ACOT5</i> help restore growth	(Chen et al., 2014b)
(1) Δ <i>are1</i> Δ <i>dgal</i> Δ <i>are2</i> Δ <i>lrol1</i> ; (2) Δ <i>pox1</i> ; (3) Combine (1) & (2)	(1) 3 × FFA (2) 4 × FFA (3) 5 × FFA	(Valle-Rodriguez et al., 2014)
↑ <i>ACC1</i> , ↑ <i>FAS1</i> , ↑ <i>FAS2</i>	>17% DCW lipid, ↑ 4 × than WT	(Runguphan & Keasling, 2014)

↑ <i>DGAT</i>	↑ 3-9 × TAG. (25- 80 nmol TAG/mg DCW)	(Bouvier - Navé et al., 2000)
↑ <i>Dga1p</i> (YOR245c)	↑ 70-90 × <i>DGAT</i> activity in LD ↑ 2-3 × in ER.	(Sorger & Daum, 2002)
↑ <i>DGAT1</i> , ↑ N-terminal tag	↑ 53% × TAG, 28% × total FA, 453 mg FA/L	(Greer et al., 2015)
↑ <i>PDAT</i>	↑ TAG, 2× (log phase), 40% × (stationary phase), identified <i>PDAT</i> gene YNR008w	(Dahlqvist et al., 2000)
↑ <i>LuPDCT1</i> , <i>LuPDCT2</i> , ↑ <i>FAD2</i> , <i>FAD3</i>	↑ PUFA (linoleic acid (18:2 ^{cisΔ9,12}), α-linolenic acid (18:3 ^{cisΔ9,12,15})) levels in phosphatidylcholine, DAG and TAG	(Wickramarathna et al., 2015)
Δ <i>SLC1</i> (YDL052C), or Δ <i>TGL3</i> (YMR313C)	↑ LD content	(Bozaquel-Morais et al., 2010)
Δ <i>HMG2</i> (YLR450W), or Δ <i>DGA1</i> (YOR245C), or Δ <i>ERG4</i> (YGL012W), or Δ <i>ERG5</i> (YMR015C), or Δ <i>ARE</i> (YNR019W), or Δ <i>SIT4</i> (YDL047W), or Δ <i>REG1</i> (YDR028C), or Δ <i>SAP190</i> (YKR028W)	↓ LD content	(Bozaquel-Morais et al., 2010)
Δ <i>Pah1</i>	↓ 63% × LD number, total lipid stable	(Adeyo et al., 2011)
↑ <i>WS2</i> , <i>ACB1</i> , <i>GAPN</i>	↑ 7.7×, 48 mg/L FAEE	(Shi et al., 2014b)
↑ <i>ACC1</i> , <i>FAS1</i> , <i>FAS2</i> , terminal “converting enzymes”	400 mg/L FFA, 100 mg/L fatty alcohol, 5 mg/L FAEE.	(Runguphan & Keasling, 2014)
(1) ↑ <i>ACL</i> , Δ <i>IDH1</i> (2) ↑ <i>ACL</i> , Δ <i>IDH2</i> (3) ↑ <i>ACL</i> , Δ <i>IDH1</i> , 2	(1) ↑ 80% C16:1, ↑60% C18:1 (2) ↑ 60% C16:1, ↑45% C18:1 (3) ↑ 92% C16:1, ↑77% C18:1	(Tang et al., 2013)
(1) ↑ Reversed β-oxidation pathway, <i>SeACS^{L641P}</i> , Δ <i>ADH1</i> , 4, Δ <i>GPD1,2</i> (2) ↑ Reversed β-oxidation pathway, <i>EEB1</i> or <i>ETH1</i>	The first successful reversal of the β-oxidation cycle in <i>S. cerevisiae</i> . (1) ↑ medium-chain FAEE (0.011 g/L FFA, C16, C18) (2) ↑ FAEE (C4-C10, 0.75 g/L)	(Lian & Zhao, 2014)
(1) ↑ <i>WS2</i> , <i>ADH2</i> , <i>ALD6</i> & <i>SeACS^{L641P}</i> , (2) ↑ <i>WS2</i> , <i>xpkA</i> , <i>ack</i> , <i>pta</i>	(1) ↑ 3× FAEE (408 ± 270 μg/g, DCW) (2) ↑ 1.7-fold FAEE (5100 ± 509 μg/g, DCW).	(de Jong et al., 2014)
↑ <i>WS2</i> , Δ <i>FAA2</i> , Δ <i>ACB1</i> , Δ <i>PXA2</i>	↑ 17×, 25 mg/L FAEE	(Thompson & Trinh, 2014)
Δβ-oxidation, Δ <i>FAA2</i> , Δ <i>PXA1</i> & Δ <i>POX1</i> , Δ <i>ACSs</i> , Δ <i>FAA1</i> , 4 & Δ <i>FAT1</i> , ↑ <i>DGA1</i> & ↑ <i>TGL3</i>	2.2 g/L extracellular FFA	(Leber et al., 2015)
(1) Δ <i>SNF2</i> , (2) ↑ <i>Leu2</i> , Δ <i>SNF2</i> , (3) ↑ <i>DGA1</i> , Δ <i>SNF2</i> , (4) ↑ <i>LRO1</i> , Δ <i>SNF2</i> ,	(1) ↑ lipid, (2) ↑ growth and lipid accumulation, (3) ↑ lipid, (4) ↓ lipid;	(Kamisaka et al., 2007)

(5) ↑ <i>FAA3</i> , ↑ <i>DGAI</i> , Δ <i>SNF2</i>	(5) ↑lipid, 30% lipids content, mainly TAG (add exogenous FA).	
↑ <i>ACCI</i> ** , ↑ <i>PAHI</i> , ↑ <i>DGAI</i> , Δ <i>GUT2</i> , Δ <i>ARE1</i> , Δ <i>PXA1</i> , Δ <i>POXI</i> , Δ <i>FAA2</i> , Δ <i>TGL3</i> , 4, 5	254 mg TAG/g DCW, 27.4% of the maxi theoretical yield	(Ferreira et al., 2018)
↑ <i>RtME</i> , ↑ <i>MDH3</i> , ↑ <i>CTPI</i> , ↑ <i>MmACL</i> , ↑ <i>RtFAS</i> , ↑ <i>ACCI</i> , ↑ <i>tesA</i> , Δ <i>POXI</i> , Δ <i>FAA1</i> , 4	10.4 g/L extracellular FFA	(Zhou et al., 2016)
↑ <i>MPC</i> , <i>RtCIT1</i> , <i>ME</i> , <i>PYCI</i> , <i>YHM2</i> , <i>MDH3</i> , <i>RtFAS</i> , <i>ACCI</i> , <i>AnACL</i> , <i>MmACL</i> , <i>IDP2</i> , ↓ <i>PGII</i> , <i>IDH2</i> , ↑ <i>ZWF1</i> , <i>GND1</i> , <i>TKL1</i> , <i>TALI</i> , etc.	33.4 g/L extracellular FFA	(Yu et al., 2018)

(* ‘↑’, overexpression or heterologous expression, increase; ‘↓’: downregulation or reduce; ‘Δ’: deletion or knockout, ‘×’, times by folds. Abbreviations in the table: FFA, free fatty acid; FAEE, fatty acid ethyl ester; FAME, fatty acid methyl ester; LD, lipid droplet; ER, endoplasmic reticulum; WT, wild type; DCW, dry cell weight; MCFA, medium chain fatty acid; DGAT, acyl-CoA: diacylglycerol acyltransferase; ACC, acetyl-CoA carboxylase; ACSs, acyl-CoA synthetases; ADH, alcohol dehydrogenase; PDAT, phospholipid: diacylglycerol acyltransferase; FADs, fatty acid desaturases; *POX*, peroxisomal β-oxidation; ACB1, acyl-CoA binding protein; GAPN, NADP⁺-dependent glyceraldehyde-3-phosphate dehydrogenase; *GUT2*, glycerol-3-phosphate dehydrogenase gene; *tesA*, encode thioesterase I; UFA, unsaturated fatty acid.)

2.3. Fatty acid modification towards high-value lipid production

2.3.1. Cyclopropane fatty acid

Cyclopropane fatty acids (CFAs) are modified fatty acids possessing a unique strained ring structure which conveys oxidative stability and lubricity to lipids where they are incorporated. Such lipids have applications as high value cosmetics and in specialist lubrication. Genetically modified plant seeds and cyanobacteria have been explored as potential biofactories of cyclopropane fatty acids and while progress has been made toward increasing the CFA levels, there are complex metabolic engineering challenges to be overcome in these systems. Multiple attempts from Shanklin group have been made to increase CFA yield in seeds of both crop and model plants such as tobacco, *Camelina sativa* and *Arabidopsis thaliana* through engineering of acyl-CoA dependent and independent routes toward stable triacylglycerol (TAG) formation and by comparing the effectiveness of plant or bacterial-sourced cyclopropane fatty acid synthetases (CFAS) (Shanklin et al., 2016; Yu et al., 2017; Yu et al., 2014; Yu et al., 2011). The latest result from Shanklin group was the 12% of total fatty acids accumulated in TAG by

the CFA form in *Camelina sativa* seed oil after combining *Ec.CFAS* with a lysophosphatidic acyl transferase (Yu et al., 2017). Whereas, in *Synechocystis* cyanobacterium expressing the CFAS sourced from *Escherichia coli* (*Ec.CFAS*) in combination with desaturase engineering (*desA-/desD-/desC2+*) the result was 30% CFA of total fatty acids but growth was severely reduced in these cells when cultured at 26°C (Machida et al., 2016). Moreover, expression of *Ec.CFAS* in heavy engineered *Yarrowia lipolytica* achieved > 32% CFA of total lipids, and titre reached 3.0 g/L in the bioreactor (Markham & Alper, 2018). However, the distribution of CFA between neutral lipids and phospholipid is rarely reported.

2.3.2. Other value-added fatty acid

Ricinoleic acid (RA) is an unsaturated omega-9 fatty acid with a hydroxyl group in the $\Delta 12$ position, and a major fatty acid in triglyceride form of castor oil seed (James et al., 1965). Similar to CFA, RAs have lots of industrial applications such as lubricants, nylon, dyes, ink, etc. and its production has been conducted at commercial scale for many decades. Issues stemming from oilseed castor cultivation and harvest such as dermatitis among field workers and presence of deadly ricin toxin make it necessary to develop the microbial sources to produce RAs (Holic et al., 2012). In the fission yeast *Schizosaccharomyces pombe*, *CpFAH12* was expressed to bring RAs production to 137.4 $\mu\text{g/ml}$ (Holic et al., 2012). Moreover, the Uemura group engineered the *Schizosaccharomyces pombe* to secrete RA and reduce its toxicity to cells (Yazawa et al., 2013; Yazawa et al., 2014). The Nicaud group engineered *Yarrowia lipolytica* by co-expression of *CpFAH12* and *PDAT* to accumulate RA to 43% of total lipids, and over 60 mg/g DCW (Béopoulos et al., 2014). RAs accumulation attempts were also tested in microalgae and plant by expressing castor LPAT or *CpFAH* (Chen et al., 2016; Kajikawa et al., 2016).

Gamma linoleic acid (GLA) is a high value polyunsaturated fatty acid containing 18-carbon chain and three cis double bonds in the $\Delta^{6,9,12}$ positions. GLA is regarded as an essential fatty acid in the diet because mammals lack the ability to synthesise it and it is important to regulate normal physiological functions (Huang et al., 1999). Co-expression of Δ^{12} - and Δ^6 -desaturases from *Mortierella alpina* in *S. cerevisiae* achieved 8% GLA of total fatty acids and GLA was accumulated predominantly in the phospholipid fraction (Huang et al., 1999).

2.4. Cellular physiological responses to lipid pathway engineering

Since lipid can be used for membrane synthesis and energy storage in the yeast cell, lipid pathway engineering inevitably will have some impact on cell growth and replication, intracellular biochemical process and energy balances. These effects can be manifested in cellular physiological differences between wild type and engineered cells, including cell growth, cell membrane integrity, reactive oxygen species, and mitochondria membrane potential.

2.4.1. Cell growth

Cell growth means cell reproduction or growth in cell populations, which is often coupled to cell division and contains three phases including first growth phase, synthesis phase and second growth phase (Johnston & Singer, 1983). Cell growth is routinely measured by optical density at 600 nm in the liquid cell culture or colony forming units on an agar plate (Xu et al., 2014). FA biosynthesis is one of the prerequisites for yeast cell growth and cell division due to its importance for membrane synthesis. Imbalance in synthesis or turnover of lipids affects yeast growth and viability (Natter & Kohlwein, 2013). Many biologically critical functional proteins that control Na^+ , K^+ , and pH homeostasis are housed by lipid and membrane rafts and effects on these could influence cell growth (Mollinedo, 2012). Besides, supplying more malonyl-CoA

by overexpressing *ACCI*^{ser659ala, ser1157ala} to enhance FA biosynthesis severely reduced to two thirds of yeast cell growth (Shi et al., 2014a). Lipotoxicity, a metabolic syndrome, is caused by the accumulation of FFA, leading to cellular dysfunction and death. Thus, the connection of lipids to cell growth and cell death is more complicated than solely the lipotoxic effects of excess free fatty acids. In addition, the saturated FA did not affect cell growth, while shorter chain FA or highly unsaturated FA impaired cell growth, and caused ROS accumulation, activation of the unfolded protein response (Eisenberg & Buttner, 2014). However, neither storage lipids or lipid bodies are essential for yeast cell growth because no apparent growth defects were found in the yeast strain lacks all four genes including *ARE1*, *ARE2*, *DGAI* and *LROI* (Sandager et al., 2002). Moreover, TAG accumulation is reported to protect against fatty acid-induced lipotoxicity (Listenberger et al., 2003).

2.4.2. Cell membrane integrity

Cell membrane integrity means the cell membrane can protect the intracellular organelles such as nucleus, mitochondria, ribosomes, etc., and regulate the entry of substances such as nutrition and toxins passing through the cell. A break in the cell membrane immediately compromises its essential role to protect the cell and may cause cell death (McNeil & Steinhardt, 1997). Besides, cell membrane integrity indicates the 'cell health' (da Silva et al., 2012), is closely related to cell growth and an important response to lipid pathway engineering. Compromised cell membranes cannot generate an electrochemical gradient, or called membrane potential, which is generated by the regular passive and active transport across the intact cell membrane (Boswell et al., 2003) and may not act as a barrier against the loss of essential cellular electrolytes. The cell membrane lipid composition affects its integrity to impact the ethanol tolerance of yeast cell (Henderson & Block, 2014). Also, sphingolipids and sterols in the yeast cell membrane co-ordinately regulate cell membrane integrity (de Almeida, 2018). The

membranes of yeast may also be affected by metabolites secreted into the cell culture medium such as acetic acid and ethanol (Freitas et al., 2012). Furthermore, the fatty acid unsaturation degree and chain length affects cell membrane fluidity of *S. cerevisiae* and hence the organisms resistance to metabolites in the medium (Degreif et al., 2017; Sen et al., 2015). Measurement of cell membrane integrity is routinely detected by flow cytometry with propidium iodide (PI) staining as the dye only penetrates permeable membranes where it binds to DNA and fluoresces (da Silva et al., 2010; Riccardi & Nicoletti, 2006).

2.4.3. Reactive oxygen species

Due to the reactive nature of molecular oxygen, reactive oxygen species (ROS) includes either oxidants such as peroxide, superoxide, or reductants such as hydroxyl radical, superoxide anion (Perrone et al., 2008). Most endogenous ROS production in a yeast cell is generated by the mitochondria (Perrone et al., 2008), which originates from the leakage of electrons from the respiratory transport chain as an ordinary consequence of aerobic respiration (Cadenas et al., 1977). If the ROS levels exceed cellular antioxidant defenses such as specific enzymes and metabolites like glutathione, oxidative damage will be applied to proteins, lipids, and DNA, and these may impair cell membrane integrity (Brookheart et al., 2009). Mitochondria are capable of generating antioxidant enzymes such as glutathione-s-transferase (GSTs) and manganese-dependent superoxide dismutase (Mn-SOD) to reduce or eliminate the presence of ROS (Perrone et al., 2008). ROS generation in the cell may be detected by cell-permeant fluorescent dye CM-H₂DCFDA, which is first cleaved by an intracellular esterase although the technique has not been widely implemented for ROS detection in yeast (Ameziane-El-Hassani & Dupuy, 2013).

While a mechanistic link between enhanced lipid synthesis and oxidative stress in yeast has not, as yet, been identified there are studies drawn from yeast and mammalian systems to support the existence of such relationship. The FFA metabolite, ceramide, can activate NADPH oxidase and disrupt mitochondrial respiration, or FFAs can cause endoplasmic reticulum stress and indirectly lead to oxidative stress (Brookheart et al., 2009). Drawing on human and experimental animal research, oxidative stress is involved in the response to lipid overload in both organisms *in vivo*, while a palmitate feeding test induced ROS production which was inhibited by antioxidant treatments in Chinese hamster ovary cell culture (Listenberger et al., 2001). In studies involving human liver cells, the population with high lipid content also showed high ROS level and metabolic dysfunction as determined through microscopy and flow cytometry (Herms et al., 2013). In yeast engineered for elevated lipid content, high acyl-CoA or toxic fatty acid (oleic acid) accumulation was associated with increased expression of transcripts for genes that are protective to oxidative stress (de Jong et al., 2016) and in separate research, these effects were accompanied by reduced cell viability (cell membrane integrity) (Trancikova et al., 2004). Additionally, engineering of cellular redox or oxidative stress defence pathways to alleviate the ROS and enhance NADPH supply was found to significantly improve yields of both standard lipid and PUFA in yeast (Qiao et al., 2017; Xu et al., 2017; Zhang et al., 2018).

2.4.4. Mitochondria membrane potential

The mitochondria membrane potential ($\Delta\psi_m$) generated by proton pumps from complexes I, III and IV is an important index for functional mitochondria (Zorova et al., 2018). Moreover, mitochondria are the major organelle to produce ROS and mitochondrial function is found to be required for resistance to oxidative stress in the yeast *S. cerevisiae* (Grant et al., 1997). The adaptive responses to oxidative stress may involve opening of mitochondrial channels such as

the mitochondrial permeability transition pore and the inner membrane anion channels. As these channels get activated, this causes a change in intra and inter-mitochondrial oxidative environment and results in the release of ROS (Westermann, 2014). Mitochondrial membrane potential is closely related to ROS, cell membrane integrity and growth, which is also crucial to lipid pathway engineering. Lipotoxicity can disrupt mitochondrial respiration, either by inducing the release of cytochrome c or through interaction with mitochondrial respiratory chain complex III (Brookheart et al., 2009). Flow cytometry is a useful technique to measure cellular mitochondria membrane mass or potential and employs fluorescence dyes including Rhodamine123, Rhodamine B hexyl ester, MitoTracker® Green, SYTO 18, DiOC6 and TMRE.

2.4.5. Heterogeneity

Microbial life is most often described by average population behaviours, but cell-to-cell heterogeneity in gene expression state or phenotypic heterogeneity is a widespread phenomenon and may affect the robustness of cells and result in below optimal yields in bioprocesses (Delvigne & Goffin, 2014; Martins & Locke, 2015). Heterogeneity among isogenic cells arises through both intrinsic (differences at all stages of metabolic processes of the cell) and extrinsic (external to the cell such as oxygen and nutrient availability, temperature gradients etc.) factors. The understanding that heterogeneity in cell-to-cell productivity occurs within cultures and that strategies are needed to overcome potential issues with subpopulations before transferring these cells into large-scale bioprocesses has been discussed (Binder et al., 2017; Schuster et al., 2000). Heterogeneity in lipid droplet size and occurrence was indicated as a mechanism to reduce lipotoxicity in human liver cells, resulting in a population of high-lipid cells that protected not only the population of low-lipid cells but, importantly, reduced ROS levels of the entire cell population (Herms et al., 2013). Whether this is occurring to any degree in populations of yeast cells engineered for high lipid production is not known nor has

it been tested to date. Multiple analytical approaches such as flow cytometry, biospectroscopy, and microfluidic single-cell cultivation exist to assist in the understanding of microbial populations at the single cell level.

2.5. Combination of metabolic engineering and bioprocess strategy

While metabolic lipid pathway engineering of an organism is the primary step towards creating a lipid production biofactory, apart from lipid yield and titre, volumetric productivity is a key performance indicator for successful lipid production. For intracellular production of lipid, volumetric productivity is limited by biomass yield due to the inherent trade-off between the production of biomass and lipid, and biomass growth is easily impaired during the lipid pathway modification. To improve lipid productivity, bioprocess strategies are commonly employed especially the two-stage strategy which uncouples lipid production and biomass growth. This can be achieved through inducible expression of genes coding for enhanced lipid productivity being turned on after the biomass growth stage has been achieved. However, the productivity in the two-stage bioprocess is not automatically better than a single stage bioprocess but it is dependent on substrate uptake rate and utilisation rate (Klamt et al., 2018). Other strategies that are employed to improve yeast biomass and lipid productivity include the use of altered C: N ratio in a second stage of the bioprocess (Slininger et al., 2016).

2.6. Conclusions

This literature review summarises the mechanisms of lipid production and current efforts of metabolic engineering to increase lipid storage in the yeast *S. cerevisiae*. Except the standard lipids, it also covers the value-added FAs such as cyclopropane fatty acid, ricinoleic acid and gamma linoleic acid. To be specific, it discusses the mechanisms of four individual and combinational major steps in the lipid production including FA biosynthesis, lipid

accumulation and sequestration, and FA modification. Moreover, the potential relationships between lipid pathway engineering and cellular physiological responses in cell growth, membrane integrity, intracellular reactive oxygen species, mitochondrial membrane potential and cell populational heterogeneity are reviewed and discussed. In addition, the attempts of the combination of metabolic engineering and bioprocess strategy are reviewed. To further engineering *S. cerevisiae* for a higher production of standard or unusual lipids, it will be a challenge to raise novel metabolic engineering strategies to address the lipid droplet formation mechanism. Furthermore, intensifying and employing the understandings of cellular physiological responses to lipid pathway modification will be a promising alternative approach to strive for a higher lipid content in engineered yeast.

References

- Adeyo, O., Horn, P.J., Lee, S., Binns, D.D., Chandrabhas, A., Chapman, K.D., Goodman, J.M. 2011. The yeast lipin orthologue Pah1p is important for biogenesis of lipid droplets. *J Cell Biol*, **192**(6), 1043-55.
- Alvarez, H., Steinbüchel, A. 2002. Triacylglycerols in prokaryotic microorganisms. *Applied microbiology and biotechnology*, **60**(4), 367-376.
- Ameziane-El-Hassani, R., Dupuy, C. 2013. Detection of intracellular reactive oxygen species (CM-H2DCFDA). *Bio-protocol*, **3**, e313.
- Athenstaedt, K., Daum, G. 1997. Biosynthesis of phosphatidic acid in lipid particles and endoplasmic reticulum of *Saccharomyces cerevisiae*. *Journal of bacteriology*, **179**(24), 7611-7616.
- Athenstaedt, K., Daum, G. 2003. YMR313c/TGL3 encodes a novel triacylglycerol lipase located in lipid particles of *Saccharomyces cerevisiae*. *Journal of Biological Chemistry*, **278**(26), 23317-23323.

- Aznar-Moreno, J., Denolf, P., Van Audenhove, K., De Bodt, S., Engelen, S., Fahy, D., Wallis, J.G. 2015. Type 1 diacylglycerol acyltransferases of *Brassica napus* preferentially incorporate oleic acid into triacylglycerol. *Journal of experimental botany*, **66**(20), 6497-6506.
- Beopoulos, A., Mrozova, Z., Thevenieau, F., Le Dall, M.-T., Hapala, I., Papanikolaou, S., Chardot, T., Nicaud, J.-M. 2008. Control of lipid accumulation in the yeast *Yarrowia lipolytica*. *Applied and environmental microbiology*, **74**(24), 7779-7789.
- Béopoulos, A., Verbeke, J., Bordes, F., Guicherd, M., Bressy, M., Marty, A., Nicaud, J.-M. 2014. Metabolic engineering for ricinoleic acid production in the oleaginous yeast *Yarrowia lipolytica*. *Applied microbiology and biotechnology*, **98**(1), 251-262.
- Binder, D., Drepper, T., Jaeger, K.-E., Delvigne, F., Wiechert, W., Kohlheyer, D., Grünberger, A. 2017. Homogenizing bacterial cell factories: Analysis and engineering of phenotypic heterogeneity. *Metabolic Engineering*, **42**, 145-156.
- Boswell, C., Nienow, A., Gill, N., Kocharunchitt, S., Hewitt, C. 2003. The impact of fluid mechanical stress on *Saccharomyces cerevisiae* cells during continuous cultivation in an agitated, aerated bioreactor; its implication for mixing in the brewing process and aerobic fermentations. *Food and bioproducts processing*, **81**(1), 23-32.
- Bouvier-Navé, P., Benveniste, P., Oelkers, P., Sturley, S.L., Schaller, H. 2000. Expression in yeast and tobacco of plant cDNAs encoding acyl CoA:diacylglycerol acyltransferase. *European Journal of Biochemistry*, **267**(1), 85-96.
- Bouvier-Navé, P., Benveniste, P., Oelkers, P., Sturley, S.L., Schaller, H. 2000. Expression in yeast and tobacco of plant cDNAs encoding acyl CoA: diacylglycerol acyltransferase. *European Journal of Biochemistry*, **267**(1), 85-96.
- Boyle, N.R., Page, M.D., Liu, B., Blaby, I.K., Casero, D., Kropat, J., Cokus, S.J., Hong-Hermesdorf, A., Shaw, J., Karpowicz, S.J. 2012. Three acyltransferases and nitrogen-

responsive regulator are implicated in nitrogen starvation-induced triacylglycerol accumulation in *Chlamydomonas*. *Journal of Biological Chemistry*, **287**(19), 15811-15825.

Bozaquel-Morais, B.L., Madeira, J.B., Maya-Monteiro, C.M., Masuda, C.A., Montero-Lomeli, M. 2010. A new fluorescence-based method identifies protein phosphatases regulating lipid droplet metabolism. *PLoS One*, **5**(10), e13692: 1-14.

Brookheart, R.T., Michel, C.I., Schaffer, J.E. 2009. As a Matter of Fat. *Cell Metabolism*, **10**(1), 9-12.

Cadenas, E., Boveris, A., Ragan, C.I., Stoppani, A.O. 1977. Production of superoxide radicals and hydrogen peroxide by NADH-ubiquinone reductase and ubiquinol-cytochrome c reductase from beef-heart mitochondria. *Archives of biochemistry and biophysics*, **180**(2), 248-257.

Chapman, K.D., Ohlrogge, J.B. 2012. Compartmentation of triacylglycerol accumulation in plants. *Journal of Biological Chemistry*, **287**(4), 2288-2294.

Chen, F., Zhou, J., Shi, Z., Liu, L., Du, G., Chen, J. 2010. Effect of acetyl-CoA synthase gene overexpression on physiological function of *Saccharomyces cerevisiae*. *Wei sheng wu xue bao = Acta microbiologica Sinica*, **50**(9), 1172-1179.

Chen, G.Q., Van Erp, H., Martin-Moreno, J., Johnson, K., Morales, E., Eastmond, P.J., Lin, J.-T. 2016. Expression of castor LPAT2 enhances ricinoleic acid content at the sn-2 position of triacylglycerols in lesquerella seed. *International journal of molecular sciences*, **17**(4), 507.

Chen, L., Zhang, J., Chen, W.N. 2014a. Engineering the *Saccharomyces cerevisiae* β -oxidation pathway to increase medium chain fatty acid production as potential biofuel. *PloS one*, **9**(1), e84853: 1-10.

Chen, L., Zhang, J., Lee, J., Chen, W.N. 2014b. Enhancement of free fatty acid production in *Saccharomyces cerevisiae* by control of fatty acyl-CoA metabolism. *Applied microbiology and biotechnology*, **98**(15), 6739-6750.

- Chen, X., Yang, X., Shen, Y., Hou, J., Bao, X. 2018. Screening Phosphorylation Site Mutations in Yeast Acetyl-CoA Carboxylase Using Malonyl-CoA Sensor to Improve Malonyl-CoA-Derived Product. *Frontiers in microbiology*, **9**, 47.
- Chen, Y., Daviet, L., Schalk, M., Siewers, V., Nielsen, J. 2013. Establishing a platform cell factory through engineering of yeast acetyl-CoA metabolism. *Metabolic engineering*, **15**, 48-54.
- Chisti, Y. 2007. Biodiesel from microalgae. *Biotechnology advances*, **25**(3), 294-306.
- Choi, J.W., Da Silva, N.A. 2014. Improving polyketide and fatty acid synthesis by engineering of the yeast acetyl-CoA carboxylase. *Journal of biotechnology*, **187**, 56-59.
- Courchesne, N.M.D., Parisien, A., Wang, B., Lan, C.Q. 2009. Enhancement of lipid production using biochemical, genetic and transcription factor engineering approaches. *Journal of biotechnology*, **141**(1), 31-41.
- Czabany, T., Athenstaedt, K., Daum, G. 2007. Synthesis, storage and degradation of neutral lipids in yeast. *Biochimica et Biophysica Acta (BBA)-Molecular and Cell Biology of Lipids*, **1771**(3), 299-309.
- da Silva, T.L., Feijão, D., Reis, A. 2010. Using Multi-parameter Flow Cytometry to Monitor the Yeast *Rhodotorula glutinis* CCMI 145 Batch Growth and Oil Production Towards Biodiesel. *Applied Biochemistry and Biotechnology*, **162**(8), 2166-2176.
- da Silva, T.L., Roseiro, J.C., Reis, A. 2012. Applications and perspectives of multi-parameter flow cytometry to microbial biofuels production processes. *Trends in biotechnology*, **30**(4), 225-232.
- Dahlqvist, A., Stahl, U., Lenman, M., Banas, A., Lee, M., Sandager, L., Ronne, H., Stymne, H. 2000. Phospholipid : diacylglycerol acyltransferase: An enzyme that catalyzes the acyl-CoA-independent formation of triacylglycerol in yeast and plants. *Proceedings of the National Academy of Sciences of the United States of America*, **97**(12), 6487-6492.

Davidoff, F., Korn, E. 1963. Fatty acid and phospholipid composition of the cellular slime mold, *Dictyostelium discoideum*. *J. biol. Chem*, **238**, 3199-3209.

de Almeida, R.F.M. 2018. A route to understanding yeast cellular envelope - plasma membrane lipids interplaying in cell wall integrity. *Febs j*, **285**(13), 2402-2404.

de Jong, B.W., Shi, S., Siewers, V., Nielsen, J. 2014. Improved production of fatty acid ethyl esters in *Saccharomyces cerevisiae* through up-regulation of the ethanol degradation pathway and expression of the heterologous phosphoketolase pathway. *Microb. Cell Fact*, **13**(39), 1-10.

de Jong, B.W., Siewers, V., Nielsen, J. 2016. Physiological and transcriptional characterization of *Saccharomyces cerevisiae* engineered for production of fatty acid ethyl esters. *FEMS yeast research*, **16**(1), 1-9.

Degreif, D., de Rond, T., Bertl, A., Keasling, J.D., Budin, I. 2017. Lipid engineering reveals regulatory roles for membrane fluidity in yeast flocculation and oxygen-limited growth. *Metabolic Engineering*, **41**, 46-56.

Delvigne, F., Goffin, P. 2014. Microbial heterogeneity affects bioprocess robustness: Dynamic single-cell analysis contributes to understanding of microbial populations. *Biotechnology Journal*, **9**(1), 61-72.

Eisenberg, T., Buttner, S. 2014. Lipids and cell death in yeast. *Fems Yeast Research*, **14**(1), 179-197.

Fei, W., Shui, G., Zhang, Y., Krahmer, N., Ferguson, C., Kapterian, T.S., Lin, R.C., Dawes, I.W., Brown, A.J., Li, P. 2011a. A role for phosphatidic acid in the formation of "supersized" lipid droplets. *PLoS Genet*, **7**(7), e1002201: 1-11.

Fei, W., Shui, G., Zhang, Y., Krahmer, N., Ferguson, C., Kapterian, T.S., Lin, R.C., Dawes, I.W., Brown, A.J., Li, P., Huang, X., Parton, R.G., Wenk, M.R., Walther, T.C., Yang, H. 2011b. A role for phosphatidic acid in the formation of "supersized" lipid droplets. *PLoS Genet*, **7**(7), e1002201-e1002201.

Ferreira, R., Teixeira, P.G., Gossing, M., David, F., Siewers, V., Nielsen, J. 2018. Metabolic engineering of *Saccharomyces cerevisiae* for overproduction of triacylglycerols. *Metabolic Engineering Communications*, **6**, 22-27.

Fitzherbert, E.B., Struebig, M.J., Morel, A., Danielsen, F., Brühl, C.A., Donald, P.F., Phalan, B. 2008. How will oil palm expansion affect biodiversity? *Trends in Ecology & Evolution*, **23**(10), 538-545.

Freitas, C., Neves, E., Reis, A., Passarinho, P.C., da Silva, T.L. 2012. Effect of acetic acid on *Saccharomyces carlsbergensis* ATCC 6269 batch ethanol production monitored by flow cytometry. *Appl Biochem Biotechnol*, **168**(6), 1501-15.

Gidda, S.K., Watt, S.C., Collins-Silva, J., Kilaru, A., Arondel, V., Yurchenko, O., Horn, P.J., James, C.N., Shintani, D., Ohlrogge, J.B. 2013. Lipid droplet-associated proteins (LDAPs) are involved in the compartmentalization of lipophilic compounds in plant cells. *Plant signaling & behavior*, **8**(11), e27141: 1-4.

Grant, C.M., MacIver, F.H., Dawes, I.W. 1997. Mitochondrial function is required for resistance to oxidative stress in the yeast *Saccharomyces cerevisiae*. *FEBS Letters*, **410**(2), 219-222.

Greenwell, H.C., Laurens, L.M.L., Shields, R.J., Lovitt, R.W., Flynn, K.J. 2010. Placing microalgae on the biofuels priority list: a review of the technological challenges. *Journal of The Royal Society Interface*, **7**, 703-726.

Greer, M.S., Truksa, M., Deng, W., Lung, S.C., Chen, G.Q., Weselake, R.J. 2015. Engineering increased triacylglycerol accumulation in *Saccharomyces cerevisiae* using a modified type 1 plant diacylglycerol acyltransferase. *Applied Microbiology and Biotechnology*, **99**(5), 2243-2253.

Grillitsch, K., Connerth, M., Köfeler, H., Arrey, T.N., Rietschel, B., Wagner, B., Karas, M., Daum, G. 2011. Lipid particles/droplets of the yeast *Saccharomyces cerevisiae* revisited:

Lipidome meets Proteome. *Biochimica et Biophysica Acta (BBA) - Molecular and Cell Biology of Lipids*, **1811**(12), 1165-1176.

Hegde, K., Chandra, N., Sarma, S.J., Brar, S.K., Veeranki, V.D. 2015. Genetic Engineering Strategies for Enhanced Biodiesel Production. *Molecular Biotechnology*, **57**(7), 606-624.

Henderson, C.M., Block, D.E. 2014. Examining the Role of Membrane Lipid Composition in Determining the Ethanol Tolerance of *Saccharomyces cerevisiae*. *Applied and Environmental Microbiology*, **80**(10), 2966-2972.

Herms, A., Bosch, M., Ariotti, N., Reddy, B.J.N., Fajardo, A., Fernandez-Vidal, A., Alvarez-Guaita, A., Fernandez-Rojo, M.A., Rentero, C., Tebar, F., Enrich, C., Geli, M.I., Parton, R.G., Gross, S.P., Pol, A. 2013. Cell-to-Cell Heterogeneity in Lipid Droplets Suggests a Mechanism to Reduce Lipotoxicity. *Current Biology*, **23**(15), 1489-1496.

Holic, R., Yazawa, H., Kumagai, H., Uemura, H. 2012. Engineered high content of ricinoleic acid in fission yeast *Schizosaccharomyces pombe*. *Applied microbiology and biotechnology*, **95**(1), 179-187.

Horn, P.J., James, C.N., Gidda, S.K., Kilaru, A., Dyer, J.M., Mullen, R.T., Ohlrogge, J.B., Chapman, K.D. 2013. Identification of a new class of lipid droplet-associated proteins in plants. *Plant physiology*, **162**(4), 1926-1936.

Huang, A. 1996. Oleosins and oil bodies in seeds and other organs. *Plant Physiology*, **110**(4), 1055-1061.

Huang, Y.-S., Chaudhary, S., Thurmond, J.M., Bobik, E.G., Yuan, L., Chan, G.M., Kirchner, S.J., Mukerji, P., Knutzon, D.S. 1999. Cloning of $\Delta 12$ - and $\Delta 6$ -desaturases from *Mortierella alpina* and recombinant production of γ -linolenic acid in *Saccharomyces cerevisiae*. *Lipids*, **34**(7), 649-659.

James, A., Hadaway, H., Webb, J.P. 1965. The biosynthesis of ricinoleic acid. *Biochemical Journal*, **95**(2), 448.

- Janßen, H., Steinbüchel, A. 2014. Production of triacylglycerols in *Escherichia coli* by deletion of the diacylglycerol kinase gene and heterologous overexpression of *atfA* from *Acinetobacter baylyi* ADP1. *Applied Microbiology and Biotechnology*, **98**(4), 1913-1924.
- Janßen, H., Steinbüchel, A. 2014. Fatty acid synthesis in *Escherichia coli* and its applications towards the production of fatty acid based biofuels. *Biotechnology for Biofuels*, **7**(1), 7: 1-26.
- Johnston, G.C., Singer, R.A. 1983. Growth and the cell cycle of the yeast *Saccharomyces cerevisiae*: I. Slowing S phase or nuclear division decreases the G1 cell cycle period. *Experimental Cell Research*, **149**(1), 1-13.
- Kadereit, B., Kumar, P., Wang, W.-J., Miranda, D., Snapp, E.L., Severina, N., Torregroza, I., Evans, T., Silver, D.L. 2008. Evolutionarily conserved gene family important for fat storage. *Proceedings of the National Academy of Sciences*, **105**(1), 94-99.
- Kajikawa, M., Abe, T., Ifuku, K., Furutani, K.-i., Yan, D., Okuda, T., Ando, A., Kishino, S., Ogawa, J., Fukuzawa, H. 2016. Production of ricinoleic acid-containing monoester diacylglycerides in an oleaginous diatom, *Chaetoceros gracilis*. *Scientific reports*, **6**, 36809.
- Kamisaka, Y., Tomita, N., Kimura, K., Kainou, K., Uemura, H. 2007. DGA1 (diacylglycerol acyltransferase gene) overexpression and leucine biosynthesis significantly increase lipid accumulation in the *Delta snf2* disruptant of *Saccharomyces cerevisiae*. *Biochemical Journal*, **408**, 61-68.
- Kendrick, A., Ratledge, C. 1992. Lipids of selected molds grown for production of n-3 and n-6 polyunsaturated fatty acids. *Lipids*, **27**(1), 15-20.
- Kennedy, E. 1962. The biosynthesis of phosphatides and triglycerides. *Deutsche medizinische Wochenschrift*, **87**, 99-102.
- Klamt, S., Mahadevan, R., Hadicke, O. 2018. When Do Two-Stage Processes Outperform One-Stage Processes? *Biotechnol J*, **13**(2).

Kocharin, K., Chen, Y., Siewers, V., Nielsen, J. 2012. Engineering of acetyl-CoA metabolism for the improved production of polyhydroxybutyrate in *Saccharomyces cerevisiae*. *Amb Express*, **2**.

Kohlwein, S.D., Veenhuis, M., van der Klei, I.J. 2013. Lipid droplets and peroxisomes: Key players in cellular lipid homeostasis or a matter of fat—store'em up or burn'em down. *Genetics*, **193**(1), 1-50.

Kurat, C.F., Natter, K., Petschnigg, J., Wolinski, H., Scheuringer, K., Scholz, H., Zimmermann, R., Leber, R., Zechner, R., Kohlwein, S.D. 2006. Obese yeast: triglyceride lipolysis is functionally conserved from mammals to yeast. *Journal of Biological Chemistry*, **281**(1), 491-500.

Leber, C., Polson, B., Fernandez-Moya, R., Da Silva, N.A. 2015. Overproduction and secretion of free fatty acids through disrupted neutral lipid recycle in *Saccharomyces cerevisiae*. *Metabolic engineering*, **28**, 54-62.

Leber, R., Zinser, E., Paltauf, F., Daum, G., Zellnig, G. 1994. Characterization of lipid particles of the yeast, *Saccharomyces cerevisiae*. *Yeast*, **10**(11), 1421-1428.

Lessman, K.J. 1990. Crambe: A new industrial crop in limbo. In: J. Janick and J.E. Simon (eds.), *Advances in new crops*. Timber Press, Portland, OR. . 217-222.

Li, M., Kildegaard, K.R., Chen, Y., Rodriguez, A., Borodina, I., Nielsen, J. 2015. De novo production of resveratrol from glucose or ethanol by engineered *Saccharomyces cerevisiae*. *Metabolic Engineering*, **32**, 1-11.

Li, X.W., Guo, D.Y., Cheng, Y.B., Zhu, F.Y., Deng, Z.X., Liu, T.G. 2014. Overproduction of Fatty Acids in Engineered *Saccharomyces cerevisiae*. *Biotechnology and Bioengineering*, **111**(9), 1841-1852.

Lian, J., Zhao, H. 2014. Reversal of the β -oxidation cycle in *Saccharomyces cerevisiae* for production of fuels and chemicals. *ACS synthetic biology*, **4**(3), 332-341.

- Liang, M.-H., Jiang, J.-G. 2013. Advancing oleaginous microorganisms to produce lipid via metabolic engineering technology. *Progress in Lipid Research*, **52**(4), 395-408.
- Listenberger, L.L., Han, X.L., Lewis, S.E., Cases, S., Farese, R.V., Ory, D.S., Schaffer, J.E. 2003. Triglyceride accumulation protects against fatty acid-induced lipotoxicity. *Proceedings of the National Academy of Sciences of the United States of America*, **100**(6), 3077-3082.
- Listenberger, L.L., Ory, D.S., Schaffer, J.E. 2001. Palmitate-induced Apoptosis Can Occur through a Ceramide-independent Pathway. *Journal of Biological Chemistry*, **276**(18), 14890-14895.
- Machida, S., Shiraiwa, Y., Suzuki, I. 2016. Construction of a cyanobacterium synthesizing cyclopropane fatty acids. *Biochimica et Biophysica Acta (BBA)-Molecular and Cell Biology of Lipids*, **1861**(9), 980-987.
- Markham, K.A., Alper, H.S. 2018. Engineering *Yarrowia lipolytica* for the production of cyclopropanated fatty acids. *J Ind Microbiol Biotechnol* doi: 10.1007/s10295-018-2067-8
- Martins, B.M., Locke, J.C. 2015. Microbial individuality: how single-cell heterogeneity enables population level strategies. *Current opinion in microbiology*, **24**, 104-112.
- McNeil, P.L., Steinhardt, R.A. 1997. Loss, Restoration, and Maintenance of Plasma Membrane Integrity. *The Journal of Cell Biology*, **137**(1), 1-4.
- Mollinedo, F. 2012. Lipid raft involvement in yeast cell growth and death. *Frontiers in Oncology*, **2**(140).
- Natter, K., Kohlwein, S.D. 2013. Yeast and cancer cells – common principles in lipid metabolism. *Biochimica et Biophysica Acta*, **1831**(2), 314-326.
- Nelson, D.L., Cox, M.M. 2013. *Lehninger principles of biochemistry*. Freeman press. *Chapter 10 lipids, p. 343-368.*

- Olofsson, S.-O., Boström, P., Andersson, L., Rutberg, M., Levin, M., Perman, J., Borén, J. 2008. Triglyceride containing lipid droplets and lipid droplet-associated proteins. *Current opinion in lipidology*, **19**(5), 441-447.
- Ouyang, L., Holland, P., Lu, H., Bergenholm, D., Nielsen, J. 2018. Integrated analysis of the yeast NADPH-regulator Stb5 reveals distinct differences in NADPH requirements and regulation in different states of yeast metabolism. *FEMS Yeast Research*, foy091-foy091.
- Partow, S., Hyland, P.B., Mahadevan, R. 2017. Synthetic rescue couples NADPH generation to metabolite overproduction in *Saccharomyces cerevisiae*. *Metabolic Engineering*, **43**(Pt A), 64-70.
- Peng, H., He, L., Haritos, V.S. 2018a. Metabolic engineering of lipid pathways in *Saccharomyces cerevisiae* and staged bioprocess for enhanced lipid production and cellular physiology. *Journal of Industrial Microbiology & Biotechnology*, **45**(8), 707-717.
- Peng, H., Moghaddam, L., Brinin, A., Williams, B., Mundree, S., Haritos, V.S. 2018b. Functional assessment of plant and microalgal lipid pathway genes in yeast to enhance microbial industrial oil production. *Biotechnol Appl Biochem*, **65**(2), 138-144.
- Perrone, G.G., Tan, S.-X., Dawes, I.W. 2008. Reactive oxygen species and yeast apoptosis. *Biochimica et Biophysica Acta (BBA) - Molecular Cell Research*, **1783**(7), 1354-1368.
- Pfleger, B.F., Gossing, M., Nielsen, J. 2015. Metabolic engineering strategies for microbial synthesis of oleochemicals. *Metabolic engineering* **29**, 1-11.
- Ploegh, H.L. 2007. A lipid-based model for the creation of an escape hatch from the endoplasmic reticulum. *Nature*, **448**(7152), 435-438.
- Qiao, K., Wasylenko, T.M., Zhou, K., Xu, P., Stephanopoulos, G. 2017. Lipid production in *Yarrowia lipolytica* is maximized by engineering cytosolic redox metabolism. *Nat Biotech*, **35**(2), 173-177.

- Ratledge, C. 2008. Microbial Lipids. in: *Biotechnology*, Wiley-VCH Verlag GmbH, pp. 133-197.
- Ratledge, C. 1994. Yeasts, moulds, algae and bacteria as sources of lipids. in: *Technological Advances in Improved and Alternative Sources of Lipids*, (Eds.) B.S. Kamel, Y. Kakuda, Springer US, pp. 235-291.
- Ratledge C, S.G., W. 1988. Microbial Lipids, Academic Press, London. 567-668.
- Ren, L.J., Huang, H., Xiao, A.H., Lian, M., Jin, L.J., Ji, X.J. 2009. Enhanced docosahexaenoic acid production by reinforcing acetyl-CoA and NADPH supply in *Schizochytrium* sp HX-308. *Bioprocess and Biosystems Engineering*, **32**(6), 837-843.
- Riccardi, C., Nicoletti, I. 2006. Analysis of apoptosis by propidium iodide staining and flow cytometry. *Nat Protoc*, **1**(3), 1458-61.
- Robenek, H., Hofnagel, O., Buers, I., Robenek, M.J., Troyer, D., Severs, N.J. 2006. Adipophilin-enriched domains in the ER membrane are sites of lipid droplet biogenesis. *Journal of Cell Science*, **119**(20), 4215-4224.
- Rottig, A., Zurek, P.J., Steinbuchel, A. 2015. Assessment of bacterial acyltransferases for an efficient lipid production in metabolically engineered strains of *E. coli*. *Metabolic Engineering*, **32**, 195-206.
- Runguphan, W., Keasling, J.D. 2014. Metabolic engineering of *Saccharomyces cerevisiae* for production of fatty acid-derived biofuels and chemicals. *Metabolic Engineering*, **21**, 103-113.
- Sandager, L., Gustavsson, M.H., Stahl, U., Dahlqvist, A., Wiberg, E., Banas, A., Lenman, M., Ronne, H., Stymne, S. 2002. Storage lipid synthesis is non-essential in yeast. *Journal of Biological Chemistry*, **277**(8), 6478-6482.
- Schuster, K.C., Urlaub, E., Gapes, J.R. 2000. Single-cell analysis of bacteria by Raman microscopy: spectral information on the chemical composition of cells and on the heterogeneity in a culture. *Journal of Microbiological Methods*, **42**(1), 29-38.

- Sen, S., Sirobhusanam, S., Hantak, M.P., Lawrence, P., Brenna, J.T., Gatto, C., Wilkinson, B.J. 2015. Short Branched- Chain C6 Carboxylic Acids Result in Increased Growth, Novel 'Unnatural' Fatty Acids and Increased Membrane Fluidity in a *Listeria monocytogenes* Branched- Chain Fatty Acid-Deficient Mutant. *Biochimica et biophysica acta*, **1851**(10), 1406-1415.
- Shanklin, J., Yu, X.-H., Prakash, R.R. 2016. Engineering Cyclopropane Fatty Acid Accumulation in Plants. *Patent*, 1-20.
- Shi, S., Chen, Y., Siewers, V., Nielsen, J. 2014a. Improving Production of Malonyl Coenzyme A-Derived Metabolites by Abolishing Snf1-Dependent Regulation of Acc1. *mBio*, **5**(3), e01130-14.
- Shi, S., Valle-Rodríguez, J.O., Siewers, V., Nielsen, J. 2014b. Engineering of chromosomal wax ester synthase integrated *Saccharomyces cerevisiae* mutants for improved biosynthesis of fatty acid ethyl esters. *Biotechnology and bioengineering*, **111**(9), 1740-1747.
- Shiba, Y., Paradise, E.M., Kirby, J., Ro, D.-K., Keasling, J.D. 2007. Engineering of the pyruvate dehydrogenase bypass in *Saccharomyces cerevisiae* for high-level production of isoprenoids. *Metabolic Engineering*, **9**(2), 160-168.
- Slininger, P.J., Dien, B.S., Kurtzman, C.P., Moser, B.R., Bakota, E.L., Thompson, S.R., O'Bryan, P.J., Cotta, M.A., Balan, V., Jin, M., Sousa, L.d.C., Dale, B.E. 2016. Comparative lipid production by oleaginous yeasts in hydrolyzates of lignocellulosic biomass and process strategy for high titers. *Biotechnology and Bioengineering*, **113**(8), 1676-1690.
- Sorger, D., Daum, G. 2002. Synthesis of triacylglycerols by the acyl-coenzyme A: diacylglycerol acyltransferase Dgalp in lipid particles of the yeast *Saccharomyces cerevisiae*. *Journal of bacteriology*, **184**(2), 519-524.
- Tai, M., Stephanopoulos, G. 2013. Engineering the push and pull of lipid biosynthesis in oleaginous yeast *Yarrowia lipolytica* for biofuel production. *Metabolic Engineering*, **15**, 1-9.

- Tang, X., Feng, H., Chen, W.N. 2013. Metabolic engineering for enhanced fatty acids synthesis in *Saccharomyces cerevisiae*. *Metabolic Engineering*, **16**, 95-102.
- Thompson, R.A., Trinh, C.T. 2014. Enhancing fatty acid ethyl ester production in *Saccharomyces cerevisiae* through metabolic engineering and medium optimization. *Biotechnology and bioengineering*, **111**(11), 2200-2208.
- Trancikova, A., Weisova, P., Kissova, I., Zeman, I., Kolarov, J. 2004. Production of reactive oxygen species and loss of viability in yeast mitochondrial mutants: protective effect of Bcl-xL. *FEMS Yeast Res*, **5**(2), 149-56.
- Valle-Rodriguez, J.O., Shi, S.B., Siewers, V., Nielsen, J. 2014. Metabolic engineering of *Saccharomyces cerevisiae* for production of fatty acid ethyl esters, an advanced biofuel, by eliminating non-essential fatty acid utilization pathways. *Applied Energy*, **115**, 226-232.
- Vanhercke, T., El Tahchy, A., Liu, Q., Zhou, X.-R., Shrestha, P., Divi, U.K., Ral, J.-P., Mansour, M.P., Nichols, P.D., James, C.N., Horn, P.J., Chapman, K.D., Beaudoin, F., Ruiz-López, N., Larkin, P.J., de Feyter, R.C., Singh, S.P., Petrie, J.R. 2014. Metabolic engineering of biomass for high energy density: oilseed-like triacylglycerol yields from plant leaves. *Plant Biotechnology Journal*, **12**(2), 231-239.
- Walther, T.C., Farese Jr, R.V. 2012. Lipid droplets and cellular lipid metabolism. *Annual review of biochemistry*, **81**, 687-714.
- Walther, T.C., Farese, R.V. 2009. The life of lipid droplets. *Biochimica Et Biophysica Acta-Molecular and Cell Biology of Lipids*, **1791**(6), 459-466.
- Wasylenko, T.M., Ahn, W.S., Stephanopoulos, G. 2015. The oxidative pentose phosphate pathway is the primary source of NADPH for lipid overproduction from glucose in *Yarrowia lipolytica*. *Metabolic Engineering*, **30**, 27-39.

- Wei, Y., Gossing, M., Bergenholm, D., Siewers, V., Nielsen, J. 2017. Increasing cocoa butter-like lipid production of *Saccharomyces cerevisiae* by expression of selected cocoa genes. *AMB Express*, **7**(1), 34.
- Westermann, B. 2014. Mitochondrial inheritance in yeast. *Biochimica et Biophysica Acta (BBA)-Bioenergetics*, **1837**(7), 1039-1046.
- Wickramaratna, A.D., Siloto, R.M.P., Mietkiewska, E., Singer, S.D., Pan, X., Weselake, R.J. 2015. Heterologous expression of flax phospholipid:diacylglycerol cholinephosphotransferase (PDCT) increases polyunsaturated fatty acid content in yeast and *Arabidopsis* seeds. *Bmc Biotechnology*, **15**(63), 1-15.
- Wolinski, H., Kolb, D., Hermann, S., Koning, R.I., Kohlwein, S.D. 2011. A role for seipin in lipid droplet dynamics and inheritance in yeast. *Journal of cell science*, **124**(22), 3894-3904.
- Wu, J., Zhang, X., Xia, X., Dong, M. 2017. A systematic optimization of medium chain fatty acid biosynthesis via the reverse beta-oxidation cycle in *Escherichia coli*. *Metabolic Engineering*, **41**, 115-124.
- Xu, P., Qiao, K., Stephanopoulos, G. 2017. Engineering oxidative stress defense pathways to build a robust lipid production platform in *Yarrowia lipolytica*. *Biotechnology and Bioengineering*, **114**(7), 1521-1530.
- Xu, X., Lambrecht, A.D., Xiao, W. 2014. Yeast survival and growth assays. in: *Yeast Protocols*, Springer, pp. 183-191.
- Xue, J., Balamurugan, S., Li, D.W., Liu, Y.H., Zeng, H., Wang, L., Yang, W.D., Liu, J.S., Li, H.Y. 2017. Glucose-6-phosphate dehydrogenase as a target for highly efficient fatty acid biosynthesis in microalgae by enhancing NADPH supply. *Metabolic Engineering*, **41**, 212-221.
- Yazawa, H., Kumagai, H., Uemura, H. 2013. Secretory production of ricinoleic acid in fission yeast *Schizosaccharomyces pombe*. *Applied Microbiology and Biotechnology*, **97**(19), 8663-8671.

Yazawa, H., Ogiso, M., Kumagai, H., Uemura, H. 2014. Suppression of ricinoleic acid toxicity by *ptl2* overexpression in fission yeast *Schizosaccharomyces pombe*. *Appl Microbiol Biotechnol*, **98**(22), 9325-37.

Yu, T., Zhou, Y.J., Huang, M., Liu, Q., Pereira, R., David, F., Nielsen, J. 2018. Reprogramming Yeast Metabolism from Alcoholic Fermentation to Lipogenesis. *Cell*.

Yu, X.-H., Cahoon, R.E., Horn, P.J., Shi, H., Prakash, R.R., Cai, Y., Hearney, M., Chapman, K.D., Cahoon, E.B., Schwender, J., Shanklin, J. 2017. Identification of bottlenecks in the accumulation of cyclic fatty acids in camelina seed oil. *Plant Biotechnology Journal*, **16**(4), 926-938.

Yu, X.-H., Prakash, R.R., Sweet, M., Shanklin, J. 2014. Coexpressing *Escherichia coli* cyclopropane synthase with *Sterculia foetida* lysophosphatidic acid acyltransferase enhances cyclopropane fatty acid accumulation. *Plant physiology*, **164**(1), 455-465.

Yu, X.-H., Rawat, R., Shanklin, J. 2011. Characterization and analysis of the cotton cyclopropane fatty acid synthase family and their contribution to cyclopropane fatty acid synthesis. *BMC Plant Biology*, **11**(1), 97.

Zhang, M., Fan, J., Taylor, D.C., Ohlrogge, J.B. 2009. DGAT1 and PDAT1 acyltransferases have overlapping functions in *Arabidopsis* triacylglycerol biosynthesis and are essential for normal pollen and seed development. *The Plant Cell*, **21**(12), 3885-3901.

Zhang, S., He, Y., Sen, B., Chen, X., Xie, Y., Keasling, J.D., Wang, G. 2018. Alleviation of reactive oxygen species enhances PUFA accumulation in *Schizochytrium* sp. through regulating genes involved in lipid metabolism. *Metabolic Engineering Communications*, **6**, 39-48.

Zhou, Y.J., Buijs, N.A., Zhu, Z., Qin, J., Siewers, V., Nielsen, J. 2016. Production of fatty acid-derived oleochemicals and biofuels by synthetic yeast cell factories. *Nature Communications*, **7**.

Zorova, L.D., Popkov, V.A., Plotnikov, E.Y., Silachev, D.N., Pevzner, I.B., Jankauskas, S.S., Babenko, V.A., Zorov, S.D., Balakireva, A.V., Juhaszova, M., Sollott, S.J., Zorov, D.B. 2018. Mitochondrial membrane potential. *Analytical Biochemistry*, **552**, 50-59.

Zou, J., Katavic, V., Giblin, E.M., Barton, D.L., MacKenzie, S.L., Keller, W.A., Hu, X., Taylor, D.C. 1997. Modification of seed oil content and acyl composition in the brassicaceae by expression of a yeast sn-2 acyltransferase gene. *The Plant Cell*, **9**(6), 909-923.

CHAPTER 3

**FUNCTIONAL ASSESSMENT OF
PLANT AND MICROALGAL LIPID
PATHWAY GENES IN YEAST TO
ENHANCE MICROBIAL INDUSTRIAL
OIL PRODUCTION**

**: This chapter has been published in Biotechnology and Applied Biochemistry*

Peng, H., Moghaddam, L., Brinin, A., Williams, B., et al., Functional assessment of plant and microalgal lipid pathway genes in yeast to enhance microbial industrial oil production. Biotechnol Appl Biochem 2018, 65, 138-144.

This page is intentionally blank

Functional assessment of plant and microalgal lipid pathway genes in yeast to enhance microbial industrial oil production

Huadong Peng¹
Lalehvash Moghaddam²
Anthony Brinin²
Brett Williams²
Sagadevan Mundree²
Victoria S. Haritos ^{1*}

¹Department of Chemical Engineering, Monash University, Clayton, Australia

²Centre for Tropical Crops and Biocommodities, Queensland University of Technology, Brisbane, Australia

Abstract

As promising alternatives to fossil-derived oils, microbial lipids are important as industrial feedstocks for biofuels and oleochemicals. Our broad aim is to increase lipid content in oleaginous yeast through expression of lipid accumulation genes and use *Saccharomyces cerevisiae* to functionally assess genes obtained from oil-producing plants and microalgae. Lipid accumulation genes *DGAT* (diacylglycerol acyltransferase), *PDAT* (phospholipid: diacylglycerol acyltransferase), and *ROD1* (phosphatidylcholine: diacylglycerol choline-phosphotransferase) were separately expressed in yeast and lipid production measured by

fluorescence, solvent extraction, thin layer chromatography, and gas chromatography (GC) of fatty acid methyl esters. Expression of *DGAT1* from *Arabidopsis thaliana* effectively increased total fatty acids by 1.81-fold above control, and *ROD1* led to increased unsaturated fatty acid content of yeast lipid. The functional assessment approach enabled the fast selection of candidate genes for metabolic engineering of yeast for production of lipid feedstocks. © 2017 International Union of Biochemistry and Molecular Biology, Inc. Volume 65, Number 2, Pages 138–144, 2018

Keywords: acyltransferase, biofuel, fatty acid accumulation, triacylglycerol

1. Introduction

Microbial lipids are a promising replacement for fossil-derived oil as they are nonfood feedstocks that can be converted into biodiesel and oleochemicals like surfactants and lubricants [1]. Furthermore, microbial lipids are a renewable resource whose use can result in greenhouse gas reductions especially when grown on cellulosic feedstocks [2]. Although current yields of lipid from microbial sources are not sufficient to be commercially viable, research to date by overexpression

or knockout of key genes in lipid metabolic pathways has been very promising [3, 4]. Thus, there is an opportunity for discovery and assessment of highly effective genes for lipid accumulation in microbes.

Triacylglycerol (TAG) biosynthesis has been intensively studied in yeast and plants and forms via both acyl CoA-dependent and -independent routes, which are governed by diacylglycerol acyltransferase (DGAT) or phospholipid: diacylglycerol acyltransferase (PDAT) enzymes, respectively (Fig 1) [5]. The heterologous expression of the plant *Arabidopsis thaliana* *DGAT1* (*AtDGAT1*) was first studied in yeast [6], then followed by other studies showing increased lipid or oil production in different organisms including insect cells [7], yeast [8], *A. thaliana* [9, 10], and canola [11]. Various microalgal *DGAT* genes from *Chlamydomonas reinhardtii* were partially characterized by functional complementation in TAG-deficient yeast strains [12–16] with mixed results: *DGTT1* generally gave a positive effect on TAG quantity, but *DGTT4* did not improve or slightly reduced oil content in yeast [12, 15, 16] and *C. reinhardtii* [13, 14].

Two further plant genes from *A. thaliana*, *PDAT1*, coding for phospholipid: diacylglycerol acyltransferase [5, 10] and *ROD1* for phosphatidylcholine: diacylglycerol

Abbreviation: *DGAT*, diacylglycerol acyltransferase; *FAME*, fatty acid methyl ester; *GC*, gas chromatography; *PDAT*, phospholipid: diacylglycerol acyltransferase; *ROD1*, phosphatidylcholine: diacylglycerol choline-phosphotransferase; *TAG*, triacylglycerol; *TLC*, thin layer chromatography.

*Address for correspondence: Victoria S. Haritos, Ph.D, Department of Chemical Engineering, Monash University, Clayton, Victoria, 3800, Australia. Tel: +61 3 9905 6873; e-mail: victoria.haritos@monash.edu.

Supporting Information is available in the online issue at wileyonlinelibrary.com.

Received 22 May 2017; accepted 18 June 2017

DOI: 10.1002/bab.1573

Published online 11 July 2017 in Wiley Online Library (wileyonlinelibrary.com)

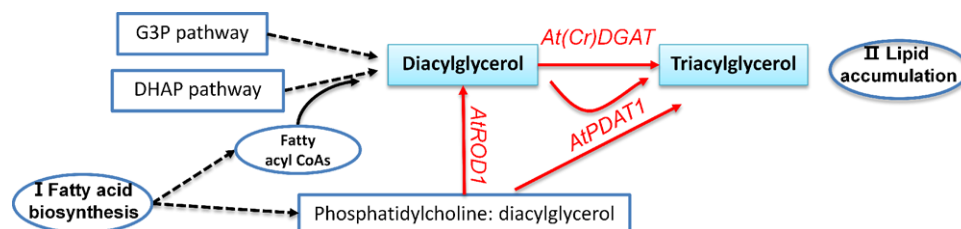


FIG. 1

Simplified acyl-CoA-dependent and acyl-CoA-independent pathways for triacylglycerol biosynthesis in yeast. Two important steps in lipid production include I Fatty acid biosynthesis and II lipid accumulation also known as triacylglycerol (TAG) biosynthesis. Two pathways feed into diacylglycerol (DAG) formation, which is the immediate precursor to TAG: the glycerol-3-phosphate (G3P) and dihydroxyacetone phosphate (DHAP) pathways. In terms of DAG conversion to TAG, there are acyl CoA-dependent and -independent routes, which are catalyzed by diacylglycerol acyltransferase (DGAT) or phospholipid: diacylglycerol acyltransferase (PDAT) enzymes, respectively. AtROD1 catalyzes the conversion of phosphatidylcholine diacylglycerol to DAG. G3P, glycerol-3-phosphate; DHAP, dihydroxyacetone phosphate; AtROD1, Phosphatidylcholine: diacylglycerol cholinephosphotransferase 1 from *A. thaliana*; At(Cr)DAGT1, diacylglycerol acyltransferase from *A. thaliana* or *C. reinhardtii*; AtPDAT1, phospholipid: diacylglycerol acyltransferase from *A. thaliana*. Dashed lines means multiple steps, genes in red color were expressed individually in this study.

choline-phosphotransferase [5, 17] also show potential to enhance lipid accumulation (Fig 1). While *AtDGAT1* [18] and *AtROD1* [17] have been biochemically assessed in plants, they have not yet been expressed in yeast and assessed for their capacity to increase and alter lipid profiles.

While the activities of the lipid pathway genes described above have been previously characterized in either plant, microalgae, or yeast in separate studies and showed some potential for increasing lipid in microbial systems, we aimed to compare their function in yeast under the same conditions to enable the selection of the best candidate (s) for further metabolic engineering research. A range of fast and more detailed analysis techniques including Nile Red fluorescence, lipid droplet visualization, fatty acid, and lipid quantification were employed to determine the best performing gene in yeast; a procedure which could be applied to a wide range of gene candidates for lipid pathway modification.

2. Materials and Methods

2.1. Yeast strains, plasmids, transformation, and culture conditions

The following genes from *A. thaliana*: *AtDGAT1* (AJ238008), *AtPDAT1* (AY052715), *AtROD1* (AY086160) and *C. reinhardtii*: *CrDGATA* (JN815266), *CrDGATB* (XM001693137) were codon

optimized and cloned into pYES2-DEST52 with the addition of a yeast consensus sequence upstream of the gene. The final plasmids and an empty pYES2-DEST52 vector were transformed into NEB® Turbo Competent *E. coli* and sequences confirmed, then transformed into yeast strains: INVSc1 (*MATa his3Δ1 leu2 trp1-289 ura3-52/MATα his3Δ1 leu2 trp1-289 ura3-52*), TAG-deficient quadruple mutant H1246 (*MATα are1-Δ::HIS3 are2-Δ::LEU2 dga1-Δ::KanMX4 lro1-Δ::TRP1 ADE*), and its parent strain SCY62 (*MAT a ADE2 can 1-100 his3-11, 15 leu2-3 trp1-1 ura3-1*) [19] using the Sigma transformation kit following the manufacturer's instructions. Yeast were inoculated into growth media and recombinant expression induced with 2% (w/v) galactose and 1% (w/v) raffinose as previously described [20]. Yeasts were maintained at 30 °C and 250 rpm until harvested. All chemicals used in this study were from Sigma-Aldrich, St. Louis, USA if without special statement.

2.2. Fast intracellular neutral lipid assay and visualization of yeast lipid droplets

Staining and estimation of intracellular neutral lipids was undertaken using a Tecan: Infinite 200 PRO (TECAN, Tecan Austria) fluorescence spectrophotometer. The method was modified from published methods [21, 22] where Nile Red (5 μg/mL) was added to washed yeast cells (200 μL) with OD_{600nm} adjusted to 1 in 10 mM potassium phosphate buffer pH 7.4 containing 0.15 M KCl and fluorescence measured excitation/emission of 530/590 nm. In addition, unfixed yeast cells in stationary phase were dyed with Nile Red and lipid droplets imaged using a Leica Microsystems SP5 confocal microscope coupled with HCX PL APO 63 × /1.4 OIL CS oil-immersion objective (Leica, Wetzlar, Germany).

2.3. Oleic acid sensitivity assay

A complementation assay [12, 15] using the TAG-deficient yeast H1246 was performed to test the activities of the five candidate lipid pathway genes. Briefly, yeast carrying one of the five lipid accumulation genes or empty vector were induced and plated on selection plates containing 1% yeast extract, 2% peptone, 2% raffinose, 1% galactose) in the absence or presence of oleic acid at final concentrations of 0, 0.009%, or 0.027% (w/v). The concentration of cells was adjusted in all samples and diluted to 0.1, 0.01, 0.001, and 0.0001 and 5 μL of each was spotted onto selection plates. The plates were incubated for 2 days at 30 °C.

2.4. Lipid extraction and thin layer chromatography separation

H1246 yeast cells were harvested 72 H postinduction, centrifuged (1500g × 5 Min), and the cell pellets were frozen

at -20°C followed by freeze drying overnight. Lipids were extracted from dry yeast cells using the Bligh–Dyer method with minor modifications [23, 24]. Dry yeast cells (ca. 20 mg) were mixed with 0.4 mL glass beads in 10 mL Pyrex glass test tubes, and 1.5 mL of methanol: chloroform (2:1) was added with vortexing for 6 Min, then 0.5 mL chloroform was added and vortex an additional 1.5 Min, followed by 0.5 mL ddH₂O and vortexed again for 1.5 Min. The cells were filtered through a $0.45\text{-}\mu\text{m}$ polytetrafluoroethylene (PTFE) filter into a clean test tube, centrifuged at 1500 g for 5 Min at room temperature to separate the two phases. The lower chloroform layer containing the lipids was removed via glass syringe and transferred to clean GC vials. The recovered volume was ca. 0.5 mL, and this was reduced 30 μL in a gentle nitrogen stream. The final chloroform extract was applied to thin layer chromatography (TLC) silica gel plates ($L \times W$ 20 cm \times 20 cm; Sigma-Aldrich) and components separated with hexane/diethyl ether/acetic acid (70:30:1, v/v/v). Dried TLC plates were developed by exposure to iodine vapor for 2–3 Min.

2.5. Total fatty acid methyl ester quantification by gas chromatography

Freeze-dried INVSc1 yeast cells (~ 20 mg) were treated with 2 mL methanol/ hydrochloric acid/ chloroform (10:1:1, v/v/v) and heated at 90°C for 1 H in sealed test tubes to convert lipids to fatty acid methyl ester (FAME). FAME was washed with 0.9% NaCl solution (1 mL) and extracted with hexane after mixing. FAME samples (1 μL) were analyzed by Agilent 7890A GC fitted with a DB-5MS capillary column (Agilent J&W 30 m \times 0.25 mm \times 0.25 μm) in splitless mode using helium as the carrier gas. Initial column temperature of 80°C was held for 1 Min then temperature increased at $15^{\circ}\text{C}/\text{Min}$ until 180°C , then $5^{\circ}\text{C}/\text{Min}$ to 220°C , then $10^{\circ}\text{C}/\text{Min}$ until 250°C and held for 10 Min. Inlet and flame ionization detector were both set to 250°C . FAME Mix (Supelco[®] 37 Component, Sigma-Aldrich) was used to prepare the standard curve (oleic acid concentrations ranged from 0.001 to 0.04 mg/mL).

3. Results and Discussion

3.1. Assessment of candidate genes expressed in TAG-deficient yeast H1246

Direct biochemical assay of DGAT activity requires the preparation of microsomal fractions and synthesis of radiolabeled precursors, which are highly specialized and time consuming. Therefore, a range of alternative assays have been developed for high throughput functional comparisons of candidate genes for enhanced lipid production. The TAG-deficient strain H1246 [19] proved very useful for the fast assessment of genes from diverse sources to produce neutral lipid when expressed in yeast. H1246 lacks functional DGAT and PDAT activity as the genes encoding these activities, *dga1* and *lro1* in addition to two sterol ester synthesis genes *are1* and *are2* have been knocked out. Genes that can functionally replace the absent *dga1* and *lro1* in

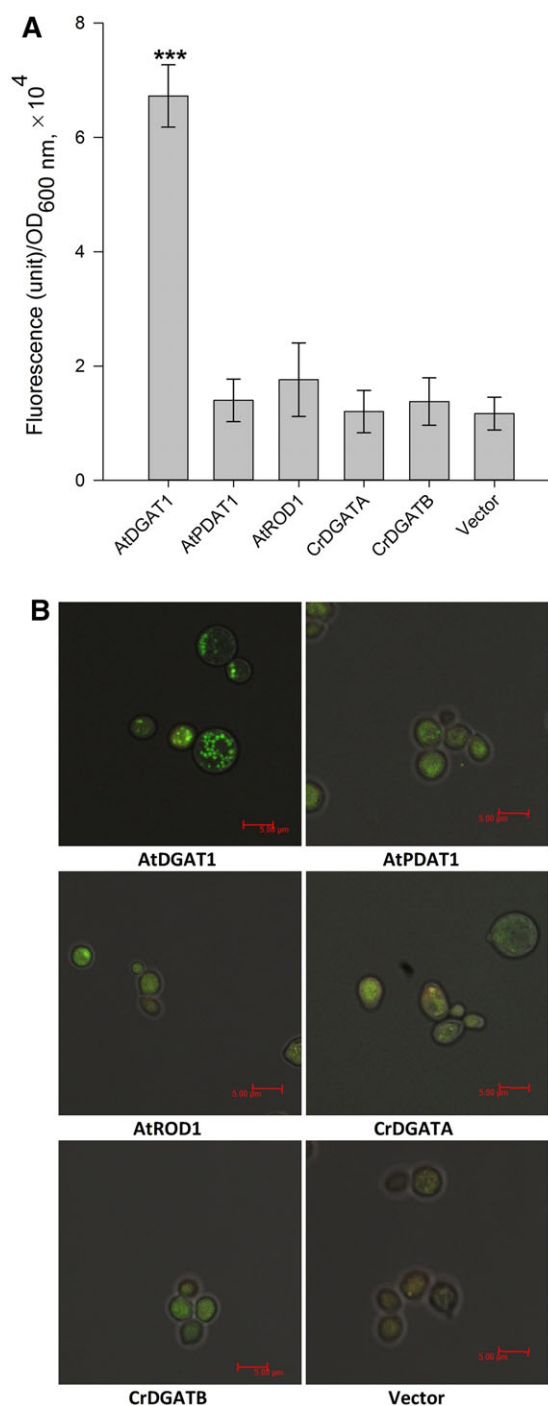
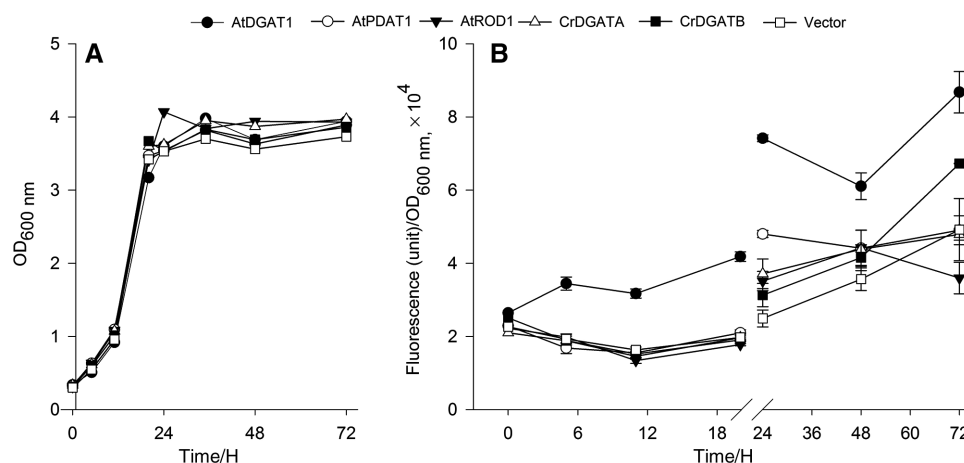


FIG. 2

Estimation of intracellular neutral lipids in TAG-deficient H1246 yeast expressing lipid-handling genes or vector control at 72 H postinduction. (A) Nile Red lipid-binding fluorescence in yeast cells. Asterisks (***) indicate significant difference (one-way analysis of variance, ANOVA, test) at $P < 0.001$, $\alpha = 0.05$ post hoc Holm–Sidak test for AtDGAT1 compared to other four candidate genes and vector control. (B) Imaging of lipid droplets following Nile Red staining with scale bar shown in red text (scale: 5 μm).

**FIG. 3**

Assessment of *INVSc1* yeast cells expressing lipid-handling genes at time periods up to 72 H for (A) growth by optical density at 600 nm and (B) intracellular lipids by Nile Red fluorescence. *AtDGAT1*, filled circles; *AtPDAT1*, open circles; *AtROD1*, filled triangles down; *CrDGATA*, open triangles up; *CrDGATB*, filled squares; Empty vector, open squares.

H1246 will be demonstrated via the production of TAG during recombinant expression in this strain. Relative fluorescence values from intracellular lipids in yeast cells following Nile red staining were compared, and the cells expressing *AtDGAT1* showed highest intensity at 5.7-fold above the vector-only control after 72 H (Fig. 2A). By contrast, expression of *AtPDAT1*, *AtROD1*, *CrDGATA*, or *CrDGATB* did not significantly change lipid-fluorescence values compared with yeast expressing an empty vector. Furthermore, distinct lipid droplets were observed within the *AtDGAT1*-expressing cells stained with Nile Red, but no similar structures were observed within the vector control or other transformed cells as shown in Fig. 2B. Thus, the TAG-free background of the H1246 strain provided a clear contrast for cells expressing an enzyme such as *AtDGAT1* that could effectively complement the activity lacking in this yeast strain. A negative result in this assay did not necessarily mean the gene was ineffective at increasing lipid production in yeast; the result may have been due to weak activity or activity in a different pathway that cannot complement the knocked-out genes.

Oleic acid sensitivity and TAG synthesis were two further tests applied to H1246 yeast expressing candidate genes to compare their potential to increase lipid production. H1246 yeast expressing an empty vector was sensitive to oleic acid as they lack TAG synthesis capability, which can mitigate the toxicity of the fatty acid. Yeast expressing *AtDGAT1* grew well on selection plates with oleic acid (Fig. S1 in the Supporting Information) and extraction of cellular lipids showed obvious TAG formation by TLC (Fig. S2 in the Supporting Information), whereas *AtPDAT1*, *AtROD1*, and *CrDGATA*-expressing yeast showed weak growth and *CrDGATB*-yeast failed to grow on selection plates (Fig. S1 in the Supporting

Information). Furthermore, there was no obvious TAG product extracted from these yeast samples when examined by TLC (Fig. S2 in the Supporting Information). Together the results showed that only *AtDGAT1* among the five candidates tested could effectively complement the TAG-deficiency of H1246.

3.2. Functional characterisation of candidate genes in yeast and TAG production

While the TAG-deficient strain H1246 was useful for fast assessment of candidate genes for enhanced lipid production, wild-type yeasts are more suitable hosts for examining the performance of recombinant genes whose biochemical activities are not known or are unclear. Therefore, the *INVSc1* strain was selected for further assessment of the lipid-handling genes. Yeast expressing one of the five candidate genes or an empty vector produced similar growth curves (Fig. 3A), but the Nile Red fluorescence assay indicated a significantly higher level of TAG production in *AtDGAT1*-expressing yeast from at least 5 H postinduction, a trend that continued up to the final measurement at 72 H (Fig. 3B). Two of the candidate genes produced contrary results in the Nile Red fluorescence assay; *AtROD1*-expressing yeast produced slightly lower and *CrDGATB*-yeast higher than control values for lipid at 72 H (Fig. 3B), whereas the remaining recombinant yeast samples had similar fluorescence to empty vector controls. The estimated lipid increase for yeast expressing *AtDGAT1* over empty vector was highest at 72 H by ~1.8-fold, and this time point was chosen for harvesting yeast cells for fatty acid analysis.

Dry cell weight was not significantly different between yeast expressing lipid-handling genes or empty vector at 72 H (Table 1), but it was noted that *AtROD1*-yeast cell weight was more variable among replicates. *AtDGAT1*-yeast had significantly higher total fatty acid content on a dry cell weight basis compared with all other yeast samples, being 1.8-fold higher than the control sample of yeast (Fig. 4A, Table 1). Similarly, enhanced lipid production in cells expressing *AtDGAT1* was observed in other hosts such as insect cells [7], *A. thaliana* [9], and canola [11]. Furthermore, *DGAT* genes from other sources such

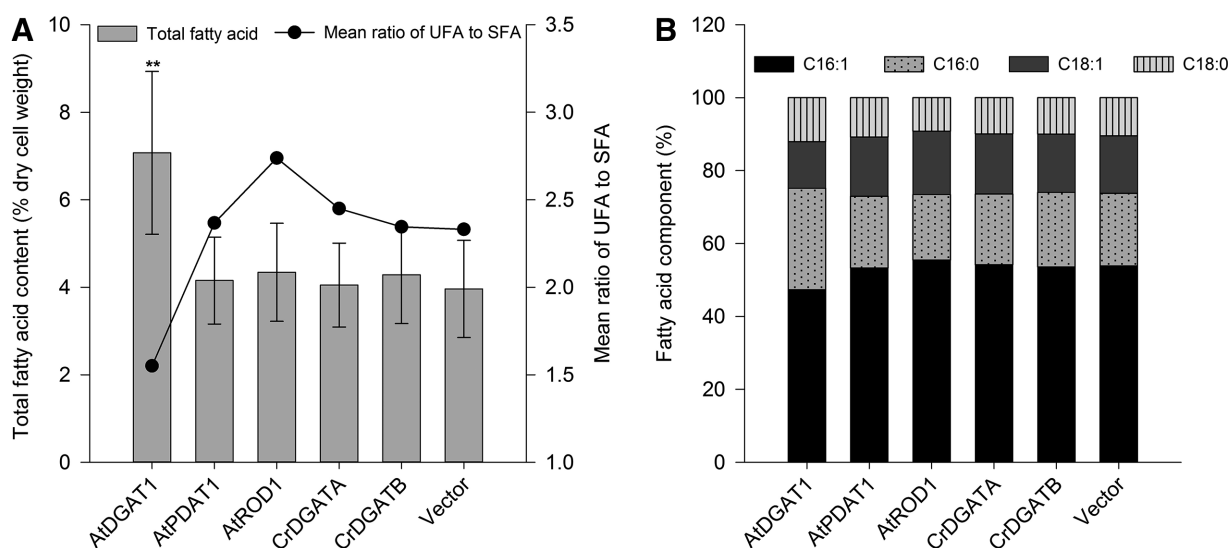
TABLE 1

Dry cell weight and fatty acid content of INVSc1 yeast transformed with lipid handling genes or empty vector harvested 72 H postinduction

Genes	Dry cell weight (mg) ^a		Total fatty acid (mg)/g dry cell weight	
	Average	SD	Average	SD
<i>AtDGAT1</i>	180.5	1.7	70.7 ^b	19.0
<i>AtPDAT1</i>	162.5	2.1	41.5	9.9
<i>AtROD1</i>	168.9	12.9	43.4	11.2
<i>CrDGATA</i>	181.4	7.3	40.5	9.6
<i>CrDGATB</i>	176.7	6.7	42.8	11.1
Vector	177.5	7.8	39.6	11.1

^aHarvested from 100 mL culture.

^bIndicate significant difference (one-way ANOVA test) at $P < 0.01$, $\alpha = 0.05$ post hoc Holm–Sidak test for *AtDGAT1* compared to other four candidate genes and vector control. Each value represents means \pm SD ($n > 3$).

**FIG. 4**

Measurement of FAME from *INVSc1* yeast cells expressing lipid-handling genes at 72 H postinduction. (A) Total fatty acid content as a percentage of dry cell weight (gray bars) where asterisks (**) indicate significant difference (one-way ANOVA test) at $P < 0.01$, $\alpha = 0.05$ post hoc Holm–Sidak test for *AtDGAT1* compared to other four candidate genes and vector control, and ratio of unsaturated fatty acid (UFA) to saturated fatty acid (SFA) by filled circles. (B) Fatty acid composition of the total: C16:1, palmitoleic acid, black bars; C16:0, palmitic acid, dotted bars; C18:1, oleic acid, gray bars; C18:0, stearic acid, striped bars. Each value represents means \pm SD ($n > 3$).

as fungi *Saccharomyces cerevisiae* [4] and *Yarrowia lipolytica* [25], plants such as *Macadamia tetraphylla* [26], and *Brassica napus* [27] showed enhanced TAG or oil production but to varying degrees. The variable performance of the different *DGAT* genes may be caused by inherent differences in enzyme

activities or host interactions. No difference was seen in fatty acid content in yeast expressing the other lipid-handling genes, but unsaturated to saturated fatty acid ratio was clearly higher in *AtROD1* yeast and lower in *AtDGAT1* yeast (Fig. 4A). This result was consistent with an alteration in fatty acid profile where *AtROD1*-expressing yeast cells had a higher proportion of unsaturated hexadecenoic (C16:1) and octadecenoic (C18:1) acids, and *AtDGAT1* cells, a higher proportion of palmitic (C16:0) and stearic (C18:0) acids than yeast expressing vector only (Fig. 4B). The variation of unsaturation in fatty acids in *AtDGAT1* and *AtROD1*-yeast cells was due to the differences in substrate specificities between these two acyl transferases. *AtROD1* was previously demonstrated to transfer oleic acid into the phosphatidyl choline pool of phospholipid which supplied additional unsaturated fatty acids for TAG synthesis, whereas *AtDGAT1* has a substrate preference for saturated acyl-CoA, especially palmitoyl-CoA, for incorporation into TAG [17].

The lipid-enhancing effect of *AtDGAT1* expression in yeast and its preference for increasing saturated fatty acid content noted in this study was consistent with prior research [6, 8]. In plants, *AtPDAT1* was reported to have a role in TAG synthesis which overlaps that of *DGAT1* [5], though in our study, it showed very weak DGAT activity. *AtPDAT1*-expression partially protected the H1246 yeast from oleic acid sensitivity (Fig. S1 in the Supporting Information) but did not produce measurable TAG. In our study, *AtROD1*-expression changed the fatty acid profile in yeast which was comparable to earlier findings [5] but did not increase fatty acid content in INVSc1 or produce TAG in H1246 yeast.

Expression of either of the two *DGAT-like* genes obtained from the microalga *C. reinhardtii* in yeast did not increase lipid production in this study. While the function of *DGAT-like* gene *DGTT1* has been investigated by recombinant expression in both yeast and microalga, the conclusions drawn from these studies are complicated by the existence of two versions of the gene; Boyle et al. [14] assessed the activity of *DGTT1* with accession number JN815266.1, exactly matching our version *CrDGATA*, but others including Hung et al. [15] have expressed and characterized a longer version of the gene (accession KC788199.1). In functional assessment of the shorter *DGTT1* in yeast, Boyle et al. [14] found oleic acid sensitivity of H1246 yeast was rescued at 0.009% and a small quantity of lipid was seen in Nile Red fluorescence imaging. While the Boyle et al.'s result showed a stronger effect than we observed with *DGTT1* in H1246 yeast, neither study found the gene to be highly effective at increasing lipid in yeast cells. Our result for *CrDGATB* was consistent with other studies conducted in yeast that failed to show a significant difference in lipid accumulation under expression of the gene which is also known as *DGTT4* [12–16].

4. Conclusion

Microbial oils could be a convenient source of future feedstocks for biofuels and bioproducts, but improvements in lipid synthesis and accumulation rates will be required for this source to be cost-effective. Improved lipid production levels can be achieved with recombinant expression of appropriate genes, and there are large genomic and transcriptomic data sets of potentially useful genes available for selection of candidates. We have examined the performance of five genes sourced from oil-producing plants and microalgae in yeast using a variety of fast and more detailed analysis techniques including fluorescence, solvent extraction, TLC, and GC of fatty acid methyl esters. It is imperative that when assessing genes from promising sources for heterologous expression that these are directly compared for relative performance in the expression organism. It is concluded that *AtDGAT1* significantly improved lipid yield by 1.8-fold and *AtROD1* could modify lipid composition toward improving unsaturation degree over control yeast, whereas *CrDGATA*, *CrDGATB*, and *AtPDAT1* failed to change the lipid content or fatty acid profile significantly. These two

promising genes can be further studied and used in the further yeast lipid production-related research. Furthermore, Nile red fluorescence measurement of whole cells was confirmed to be a reliable and fast analysis method for yeast genetically engineered to produce high lipid levels and as the method requires fewer cells for analysis compared with total fatty acid measurement, cells can be removed at many stages during the experiment.

5. Acknowledgements

We acknowledge the Australia–India Strategic Research Fund Grand Challenge Fund and Monash University for the Graduate and International Postgraduate Research Scholarships awarded to HP. We thank Dr. Jenny Lindberg Yilmaz and Prof. Sten Stymne for the strain SCY62. We thank Dr. Judy Callaghan and Monash Micro Imaging Facility for support on lipid droplet imaging and Dr. Irnayuli Sitepu for discussions on the fast Nile Red assay.

6. References

- [1] Pfeleger, B. F., Gossing, M., and Nielsen, J. (2015) *Metab. Eng.* 29, 1–11.
- [2] Tai, M., and Stephanopoulos, G. (2013) *Metab. Eng.* 15, 1–9.
- [3] Zhou, Y. J., Buijs, N. A., Zhu, Z., Qin, J., Siewers, V., and Nielsen, J. (2016) *Nat. Commun.* 7, 1–9.
- [4] Runguphan, W., and Keasling, J. D. (2014) *Metab. Eng.* 21, 103–113.
- [5] Chapman, K. D., and Ohlrogge, J. B. (2012) *J. Biol. Chem.* 287, 2288–2294.
- [6] Zou, J., Wei, Y., Jako, C., Kumar, A., Selvaraj, G., and Taylor, D. C. (1999) *Plant J.* 19, 645–653.
- [7] Hobbs, D. H., Lu, C., and Hills, M. J. (1999) *FEBS Lett.* 452, 145–149.
- [8] Bouvier-Navé, P., Benveniste, P., Oelkers, P., Sturley, S. L., and Schaller, H. (2000) *Eur. J. Biochem.* 267, 85–96.
- [9] Jako, C., Kumar, A., Wei, Y., Zou, J., Barton, D. L., Giblin, E. M., Covello, P. S., and Taylor, D. C. (2001) *Plant Physiol.* 126, 861–874.
- [10] Zhang, M., Fan, J., Taylor, D. C., and Ohlrogge, J. B. (2009) *Plant Cell* 21, 3885–3901.
- [11] Taylor, D. C., Zhang, Y., Kumar, A., Francis, T., Giblin, E. M., Barton, D. L., Ferrie, J. R., Laroche, A., Shah, S., and Zhu, W. (2009) *Botany* 87, 533–543.
- [12] Boyle, N. R., Page, M. D., Liu, B., Blaby, I. K., Casero, D., Kropat, J., Cokus, S. J., Hong-Hermesdorf, A., Shaw, J., and Karpowicz, S. J. (2012) *J. Biol. Chem.* 287, 15811–15825.
- [13] Deng, X.-D., Gu, B., Li, Y.-J., Hu, X.-W., Guo, J.-C., and Fei, X.-W. (2012) *Mol. Plant.* 5, 945–947.
- [14] La Russa, M., Bogen, C., Uhmeyer, A., Doebbe, A., Filippone, E., Kruse, O., and Mussgnug, J. H. (2012) *J. Biotechnol.* 162, 13–20.
- [15] Hung, C.-H., Ho, M.-Y., Kanehara, K., and Nakamura, Y. (2013) *FEBS Lett.* 587, 2364–2370.
- [16] Liu, J., Han, D., Yoon, K., Hu, Q., and Li, Y. (2016) *Plant J.* 86, 3–19.
- [17] Lu, C., Xin, Z., Ren, Z., Miquel, M., and Browse, J. (2009) *Proc. Natl. Acad. Sci. U. S. A.* 106, 18837–18842.
- [18] Dahlqvist, A., Stahl, U., Lenman, M., Banas, A., Lee, M., Sandager, L., Ronne, H., and Stymne, H. (2000) *Proc. Natl. Acad. Sci. U. S. A.* 97, 6487–6492.
- [19] Sandager, L., Gustavsson, M. H., Stahl, U., Dahlqvist, A., Wiberg, E., Banas, A., Lenman, M., Ronne, H., and Stymne, S. (2002) *J. Biol. Chem.* 277, 6478–6482.
- [20] Horne, I., Gibb, N., Damcevski, K., Glover, K., and Haritos, V. S. (2010) *Gene* 468, 41–47.



- [21] Sitepu, I., Ignatia, L., Franz, A., Wong, D., Faulina, S., Tsui, M., Kanti, A., and Boundy-Mills, K. (2012) *J. Microbiol. Methods* 91, 321–328.
- [22] Kimura, K., Yamaoka, M., and Kamisaka, Y. (2004) *J. Microbiol. Methods* 56, 331–338.
- [23] Bligh, E. G., and Dyer, W. J. (1959) *Canadian J. Biochem. Physiol.* 37, 911–917.
- [24] Dupont, C. M., and Kremer, L. (2014) *Bio-protocol* 4, 1–7.
- [25] Gajdos, P., Ledesma-Amaro, R., Nicaud, J. M., Certik, M., and Rossignol, T. (2016) *FEMS Yeast Res.* 16, 8.
- [26] Arroyo-Caro, J. M., Mañas-Fernández, A., Alonso, D. L., and García-Maroto, F. (2016) *J. Agric. Food Chem.* 64, 277–285.
- [27] Greer, M. S., Truksa, M., Deng, W., Lung, S. C., Chen, G. Q., and Weselake, R. J. (2015) *Appl. Microbiol. Biotechnol.* 99, 2243–2253.

1 **Supplemental Material for**

2 **Functional assessment of plant and microalgal lipid pathway genes in yeast to enhance microbial**

3 **industrial oil production**

4 Huadong Peng¹, Lalehvash Moghaddam², Anthony Brinin², Brett Williams², Sagadevan Mundree², Victoria S.

5 Haritos^{1*}

6 ¹Department of Chemical Engineering, Monash University, Clayton, Victoria, Australia

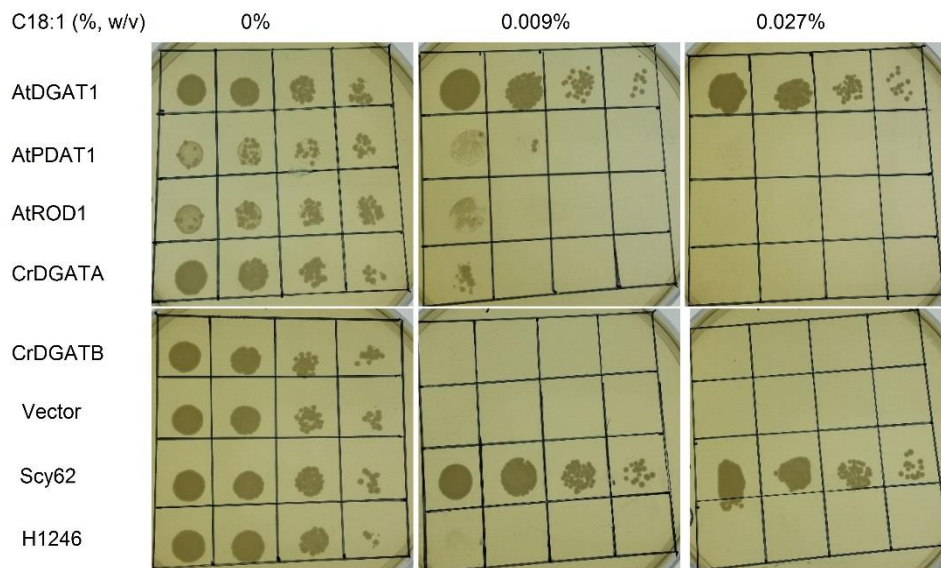
7 ²Centre for Tropical Crops and Biocommodities, Queensland University of Technology, Brisbane, Australia

8 *Corresponding author: Victoria S. Haritos, victoria.haritos@monash.edu

9

10 **Figure S1** Oleic acid sensitivity to TAG-deficient H1246 yeast expressing empty vector or one of 5 candidate

11 lipid handling genes and compared with the sensitivity of parental yeast strain Scy62.

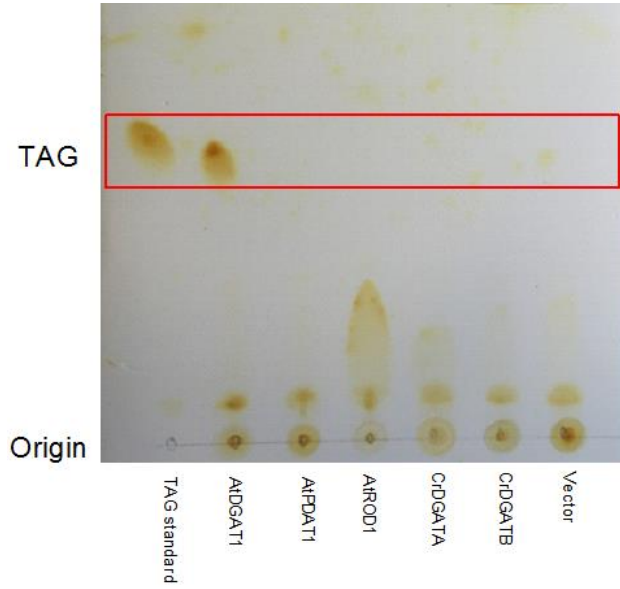


12

13

14

15 **Figure S2** TLC analysis of extracted lipids from H1246 yeast expressing empty vector or one of 5 candidate
16 lipid handling genes. Triolein (TAG standard) is shown on the left hand side of the plate and the expected region
17 for TAG is indicated by the red rectangle.



18

19

This page is intentionally blank

CHAPTER 4

METABOLIC ENGINEERING OF LIPID

PATHWAYS IN SACCHAROMYCES

CEREVISIAE AND STAGED

BIOPROCESS FOR ENHANCED LIPID

PRODUCTION AND CELLULAR

PHYSIOLOGY

**: This chapter has been published in Journal of Industrial Microbiology & Biotechnology.*

Peng, H., He, L., Haritos, V. S., Metabolic engineering of lipid pathways in Saccharomyces cerevisiae and staged bioprocess for enhanced lipid production and cellular physiology. Journal of Industrial Microbiology & Biotechnology 2018, 45, 707-717.

This page is intentionally blank



Metabolic engineering of lipid pathways in *Saccharomyces cerevisiae* and staged bioprocess for enhanced lipid production and cellular physiology

 Huadong Peng¹  · Lizhong He¹ · Victoria S. Haritos¹

 Received: 18 February 2018 / Accepted: 17 May 2018 / Published online: 26 May 2018
 © Society for Industrial Microbiology and Biotechnology 2018

Abstract

Microbially produced lipids have attracted attention for their environmental benefits and commercial value. We have combined lipid pathway engineering in *Saccharomyces cerevisiae* yeast with bioprocess design to improve productivity and explore barriers to enhanced lipid production. Initially, individual gene expression was tested for impact on yeast growth and lipid production. Then, two base strains were prepared for enhanced lipid accumulation and stabilization steps by combining *DGAT1*, $\Delta Tgl3$ with or without *Atclo1*, which increased lipid content ~ 1.8-fold but reduced cell viability. Next, fatty acid (FA) biosynthesis genes *Ald6-SEACS^{L641P}* alone or with *ACCI*** were co-expressed in base strains, which significantly improved lipid content (8.0% DCW, 2.6-fold than control), but severely reduced yeast growth and cell viability. Finally, a designed two-stage process convincingly ameliorated the negative effects, resulting in normal cell growth, very high lipid productivity (307 mg/L, 4.6-fold above control) and improved cell viability.

Keywords Fatty acid · Triacylglycerol · Cell viability · RNA-Seq analysis · Two-stage bioprocess

Abbreviations

<i>Ald6</i>	Native aldehyde dehydrogenase isoform 6	B2	BY4741- <i>AtDGAT1-ΔTgl3-Atclo1</i>
<i>AtDGAT1</i>	Diacylglycerol acyltransferase from <i>Arabidopsis thaliana</i>	B2AS	B2- <i>Ald6-SEACS^{L641P}</i>
<i>Atclo1</i>	Caleosin, lipid droplet stabilization protein from <i>Arabidopsis thaliana</i>	B2ASA	B2- <i>Ald6-SEACS^{L641P}-ACCI**</i>
<i>ACCI</i>	Acetyl-CoA carboxylase	DAG	Diacylglycerol
<i>ACCI**</i>	Acetyl-CoA carboxylase carrying two mutations ser659ala, and ser1157ala	DGA(T1)	Diacylglycerol acyltransferase
ACS	Acetyl-CoA synthetase	DHAP	Dihydroxyacetone phosphate
ADH	Alcohol dehydrogenase	DHAPAT	DHAP acyltransferase
ALD	Aldehyde dehydrogenase	DCW	Dry cell weight
ADR	1-acyl-DHAP reductase	FA	Fatty acid
B1	BY4741- <i>AtDGAT1-ΔTgl3</i>	FAS	Fatty acid synthase
B1AS	B1- <i>Ald6-SEACS^{L641P}</i>	FAEE	Fatty acid ethyl esters
B1ASA	B1- <i>Ald6-SEACS^{L641P}-ACCI**</i>	GAPT	Glycerol-3-phosphate acyltransferase
		GC-FID	Gas chromatography with flame ionization detection
		HPLC	High-performance liquid chromatography
		LD	Lipid droplet
		LPAT	Lysophosphatidic acid acyltransferase
		OD	Optical density
		PI	Propidium iodine
		PAP	Phosphatidate phosphatase
		RID	Refractive index detector
		RNA-seq	Ribonucleic acid sequencing
		SCFAs	Short chain fatty acids
		SE	Sterol ester

Electronic supplementary material The online version of this article (<https://doi.org/10.1007/s10295-018-2046-0>) contains supplementary material, which is available to authorized users.

✉ Victoria S. Haritos
victoria.haritos@monash.edu

¹ Department of Chemical Engineering, Monash University, Wellington Road, Clayton, VIC 3800, Australia

<i>SEACS</i> ^{L641P}	Acetyl-CoA synthetase with L641P mutation, derived from <i>Salmonella enterica</i>
TAG	Triacylglycerol
TGL	Triglyceride lipase
TCA	Tricarboxylic acid cycle
$\Delta Tgl3$	Triglyceride lipase 3 knockout

Introduction

Lipids are produced within single-celled microorganisms such as yeasts and algae both for energy storage and to provide a source of fatty acids (FAs) for the production of metabolic intermediates and cellular precursors of membranes [10]. The neutral lipid triacylglycerol (TAG), composed of three fatty acids attached to a backbone glycerol molecule via ester linkages, is one of the most plentiful forms found within cells. Depending on the microorganism source and any genetic engineering strategies applied to them, lipid can be useful for industrial applications such as biofuels, surfactants and lubricants [18, 21]. In contrast to plant-derived oils and animal fats, production of microbial lipids can avoid competition with the food supplies especially where they are cultivated using non-food carbon feedstocks such as lignocellulosic biomass [14].

The pathways of lipid production in yeast have been heavily studied and among these *S. cerevisiae* is an attractive model organism with many genetic and metabolomic tools readily available and it also has a long history of use in industrial applications [22]. Lipid production and accumulation in yeast can be considered as the metabolic sequence that incorporates acetyl-CoA and malonyl-CoA into FA biosynthesis, followed by accumulation of the lipids as TAG and its stabilization within lipid droplets (Fig. 1). Lipid storage can also be mobilized through the lipolytic release of FA from TAG. Previous metabolic engineering strategies for increased lipid in yeast have manipulated one or more of these steps through lipid pathway genes including *ALD6*, *ACS*, *ACC1*, *FAS*, *DGATI*, *TGL*, *POX1*, etc. [16, 17, 22, 26, 27], but rarely have combined these in a comprehensive strategy.

Increasing FA biosynthesis requires an increase in the pool of acetyl-CoA and this can be achieved through increasing acetaldehyde flux derived from pyruvate, catalyzed by cytosolic aldehyde dehydrogenase (*Ald6*) and acetyl-CoA synthetase (*ACS*) (Fig. 1, step 1 fatty acid biosynthesis). Recombinant expression of a combination of *ACS*^{L641P} derived from *Salmonella enterica* and overexpression of native *Ald6* in *S. cerevisiae* directed carbon flux into end products when combined with six other genes for improved production of α -santalene [4] and amorphadiene [24] by improving the acetyl-CoA level. In the subsequent reaction in the pathway, acetyl-CoA carboxylase (*ACC1*) catalyzes

the extension of acetyl-CoA to form malonyl-CoA, which is the first reaction in building a nascent FA chain. Overexpression of *ACC1* increased yeast lipid content by 58% [22], and heterologous expression of an *ACC1*** (*ACC1* carrying ser658ala, ser1157ala mutations) to remove regulatory control on the enzyme via posttranslational phosphorylation was also found to increase lipid content by 67% when combined with wax synthase in *S. cerevisiae* [23].

Within the yeast cell, FA is accumulated as TAG formed via CoA-independent and -dependent pathways (Fig. 1, step 2 lipid accumulation). For the latter route, the terminal step of the reaction for the formation of TAG is catalyzed by diacylglycerol acyltransferase (*DGA*). Heterologous expression of an analogous enzyme, *DGATI* derived from *Arabidopsis thaliana*, improved TAG levels more than threefold in yeast [3] and increased lipid accumulation in our prior study [20]. Stabilization of lipid stores within cells can be achieved through several mechanisms such as expression of lipid droplet (LD)-associated proteins that stabilize the LDs or prevention of lipolysis of stored lipid (Fig. 1, step 3 lipid stabilization). Heterologous expression of LD-associated proteins, caleosin (*AtClo1*) from *A. thaliana*, in yeast led to an increase in total FAs by 46–74% [9, 12], while deletion of one of the main triglyceride lipase genes of yeast, *Tgl3*, was demonstrated to release FA from LDs, and increased TAG by 2.38-fold [1, 2].

Most metabolic engineering research in microbial lipids in yeast has targeted FA synthesis and to a lesser extent lipid accumulation pathways. Few studies in yeast have included genes to enhance lipid stabilization in lipid droplets, although this is key to building stable lipid pools. Here, we have investigated a distinctive and comprehensive metabolic engineering approach that increases FA synthesis and enhances accumulation and stabilization of TAG. Further, in recognizing that TAG provides both energy and a source of FA for membrane and other essential components, we have assessed the potential impacts of metabolic engineering on cell growth and membrane integrity. The effect of introduction of five genes and one deleted gene to enhance FA synthesis through stabilization was investigated systematically. The yeast with all six gene interventions had the highest individual lipid content, but also the lowest growth rate and cell viability. A two-stage bioprocess successfully ameliorated the negative impacts of metabolic engineering in the highly engineered strain.

Materials and methods

Yeast strains, media and transformation

The wild-type yeast strain BY4741 [ATCC 4040002] (Genotype: MATa his3 Δ 1 leu2 Δ 0 met15 Δ 0 ura3 Δ 0) and its *Tgl3*

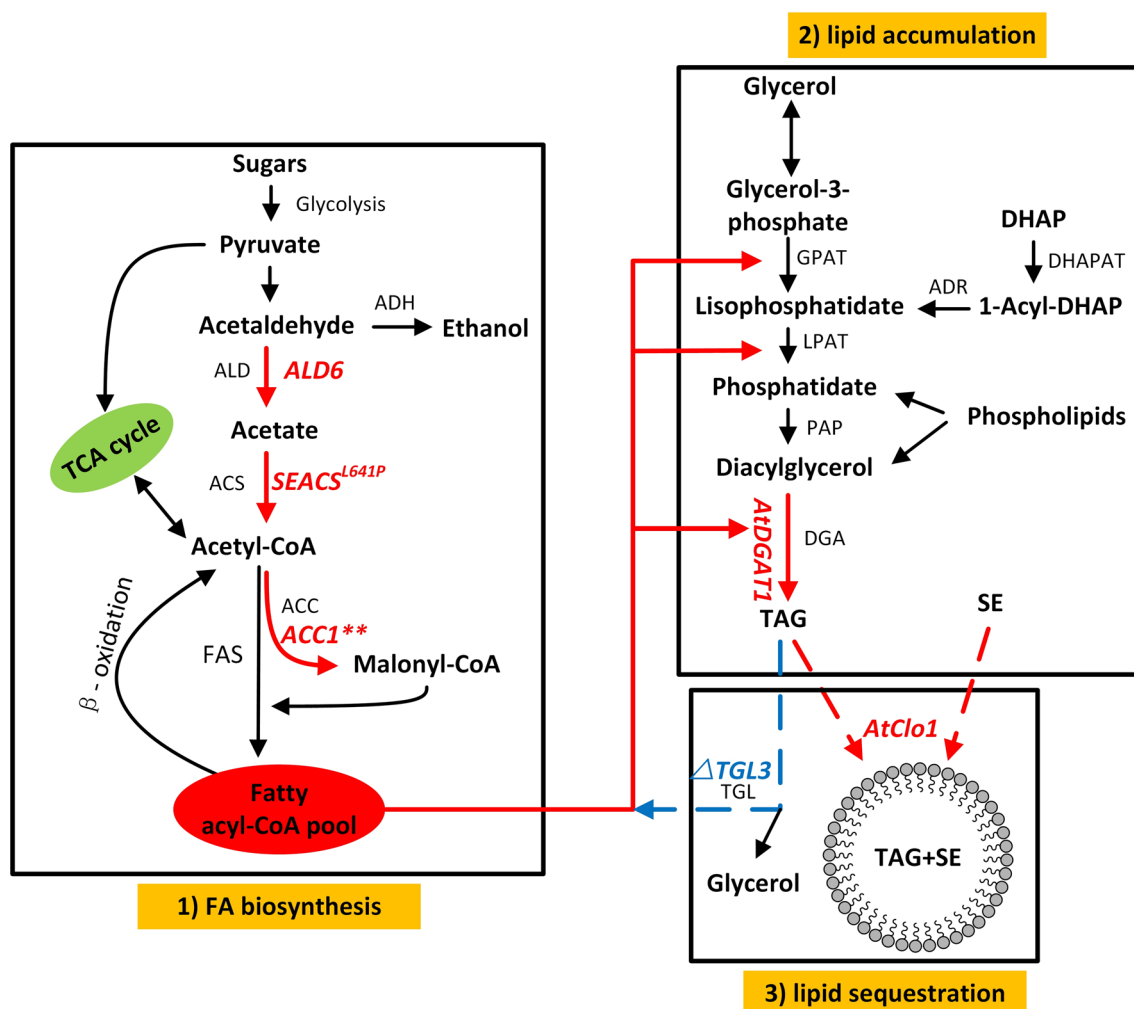


Fig. 1 Lipid production pathway in yeast. The three major steps in yeast lipid production involve 1 FA biosynthesis, 2 lipid accumulation and 3 lipid stabilization. The six genes manipulated in this study are: overexpression of native aldehyde dehydrogenase isoform 6, *Ald6*; heterologous expression of *S. enterica* acetyl-CoA synthetase with L641P mutation, *SEACS*^{L641P}; acetyl-CoA carboxylase carrying two mutations ser659ala and ser1157ala, *ACCI***^{*}; diacylglycerol acyltransferase and LD-associated protein caleosin, both from *A. thaliana*, *AtDGAT1* and *AtClo1*, respectively, are shown in red text.

knockout (Δ) strain were kindly provided by Prof. Hongyuan Yang, University of New South Wales [8]. The wild-type BY4741 was maintained with yeast extract peptone dextrose (YPD) medium (10 g/L yeast extract, 20 g/L Bacto Peptone and 20 g/L glucose), and the BY4741 $\Delta Tgl3$ strain was maintained with YPD plus 200 mg/mL Geneticin. Yeast transformation was conducted using the Sigma Transformation Kit as per the manufacturer's instructions. Selection of yeast transformants was carried out and maintained based on their auxotrophy using yeast synthetic complete (SC) minimal medium, which contains 6.7 g/L of yeast nitrogen base, 20 g/L glucose plus a mixture containing appropriate

Gene knockout triglyceride lipase isoform 3, *Tgl3*, is shown in blue typeface. *TCA* tricarboxylic acid cycle, *ADH* alcohol dehydrogenase, *ALD* aldehyde dehydrogenase, *ACS* acetyl-CoA synthetase, *FAS* fatty acid synthase, *ACC* acetyl-CoA carboxylase, *GPAT* glycerol-3-phosphate acyltransferase, *LPAT* lysophosphatidic acid acyltransferase, *PAP* phosphatidate phosphatase, *DGA* diacylglycerol acyltransferase, *DHAP* dihydroxyacetone phosphate, *DHAPAT* DHAP acyltransferase, *ADR* 1-acyl-DHAP reductase, *DAG* diacylglycerol, *TAG* triacylglycerol, *SE* sterol ester, *TGL* triglyceride lipase

nucleotide bases and amino acids for the various dropout options (SC-His, SC-Ura, SC-Leu, SC-His-Ura, SC-His-Leu, SC-Ura-Leu, SC-His-Leu-Ura).

Plasmid construction

All plasmids, inserts and promoters used in this study are listed in Table 1. The genes caleosin *Atclo1* (At4g26740) and *AtDGAT1* (At2g19450), originally from the plant *A. thaliana*, were synthesized as codon optimized for *S. cerevisiae* expression by GenScript and inserted into pESC vectors (Agilent, USA). *AtDGAT1* and *AtClo1* genes, each

Table 1 Details of genes, promoters and plasmids used in this study

Plasmid name	Description	References
pIYC05	<i>P_{PGKI}-ALD6/P_{TEFI}-SEACS^{L641P}</i> , Addgene plasmid # 64742	Chen et al. [4] and Shi et al. [23]
pIYC04	Vector backbone, derived from pESC-HIS, Addgene plasmid # 64741	Chen et al. [4]
pAD	<i>P_{PGKI}-ACCI</i> (ser659ala, ser1157ala), Addgene plasmid # 64747	Chen et al. [4] and Shi et al. [23]
p-SP-GM2	Vector backbone, derived from pESC-URA, Addgene plasmid # 64740	Chen et al. [4]
pESC-Leu- <i>AtDGAT1</i>	<i>pESC-leu-P_{GALI}-AtDGAT1</i>	This study
pESC-Leu- <i>AtClo1</i>	<i>pESC-leu-P_{GALI0}-AtClo1</i>	This study
pESC-Leu- <i>AtDGAT1-AtClo1</i>	<i>pESC-leu-P_{GALI}-AtDGAT1/P_{GALI0}-AtClo1</i>	This study
pESC-leu2d	Vector backbone, Addgene plasmid # 20120.	

with the Kozak sequence AAACA inserted to the 5' end of the start codon to enhance expression, were ligated into BamHI-XhoI, SpeI-BglIII, and BamHI-XhoI, SpeI-BglIII, respectively, to generate expression plasmids *pESC-Leu-AtDGAT1*, *pESC-Leu-AtClo1* and *pESC-Leu-AtDGAT1-AtClo1*. The remaining plasmids: pAD (*ACCI****, *ACCI* with ser659ala, ser1157ala mutations) and empty backbone pSP-GM2; pIYC05 (*Ald6-SEACS^{L641P}*) and empty backbone pIYC04 and empty backbone pESC-leu2d were shared by Addgene. The specific gene sequences can be obtained via the NCBI or Addgene website.

Lipid production by one-stage and two-stage processes

For standard one-stage bioprocess, seed culture was prepared by inoculating a single transformed colony into 50 mL Falcon tube containing 5 mL yeast SC minimal medium and incubating at 30 °C, 250 rpm, overnight. The culture was diluted into 50 mL SC induction medium containing 2% (w/v) galactose and 1% (w/v) raffinose in 250 mL flasks, with a final OD₆₀₀ nm value of approximately 0.4. The flasks were covered with two layers of aluminum foil and incubated at 30 °C and 250 rpm until harvesting at 72 h. For the two-stage bioprocess, the same procedure was followed to generate the seed culture, but an additional step was included prior to the induction step with galactose. Seed culture was diluted at OD₆₀₀ nm of 0.4 into 50 mL SC minimal medium in 250 mL flask and incubated at 30 °C and 250 rpm for 12 h. Yeast cells were collected by centrifugation (3000 rpm, 5 min), the medium was removed and the cell pellets were suspended in fresh 50 mL SC induction medium containing 2% (w/v) galactose and 1% (w/v) raffinose and cultured at 30 °C and 250 rpm for 60 h before harvesting. The lipid yield in cells produced by one-stage and two-stage processes was further analyzed as below.

Measurement of cell growth and cell viability

The cell growth was measured by optical density (OD) at 600 nm using DR 5000™ UV–Vis spectrophotometer and cell viability was determined by flow cytometry after yeasts were stained with propidium iodide (PI) (ThermoFisher, USA) and individual cell fluorescence measured using the violet laser 488 nm on a CytoFlex (Beckman Coulter, USA). More than 10,000 cells were measured for each sample and the data acquired was analyzed further by the software Cyt-Expert Ver.2.0.

Total fatty acid analysis of yeast cells

After 72 h post-induction, cells were harvested and pelleted by centrifugation at 3000 rpm for 5 min, frozen at –80 °C for ~1 h, then freeze dried overnight using a FreeZone® 4.5 Liter Freeze Dry Systems (Labconco Corporation, USA) to obtain the dry cell weight (DCW) of each culture. Dry cells (~20 mg) were treated with 2 mL methanol/hydrochloric acid/chloroform (10:1:1, v/v/v) and heated at 90 °C for 1 h in sealed test tubes to convert lipids to fatty acid methyl ester (FAME). FAME was washed with 0.9% NaCl solution (1 mL) and extracted with hexane after mixing. FAME samples (1 µL) were analyzed by Agilent 7890A gas chromatography with flame ionization detection (GC–FID) as described previously [20].

Quantification of gene expression levels by RNA-Seq analysis

Yeast cells were cultured as described earlier and harvested at 24 h in one-/two-stage bioprocess after induction for RNA-Seq analysis. Culture samples (20 mL) were collected using pre-chilled 50 mL Falcon tubes and centrifuged at 5000 rpm, 5 min at 4 °C to obtain cell pellets. The cell pellets were washed quickly with autoclaved PBS buffer once and then centrifuged again under the same conditions. Cells

were flash frozen in liquid nitrogen, stored at -80°C before shipping for RNA-Seq analysis and stored on dry ice. The RNA extraction, library preparation (250–300 bp insert cDNA library), RNA sequence analysis and assembly were conducted by Novogene, Hong Kong.

Results and discussion

Effect of expression of individual gene on lipid yield and cell physiology

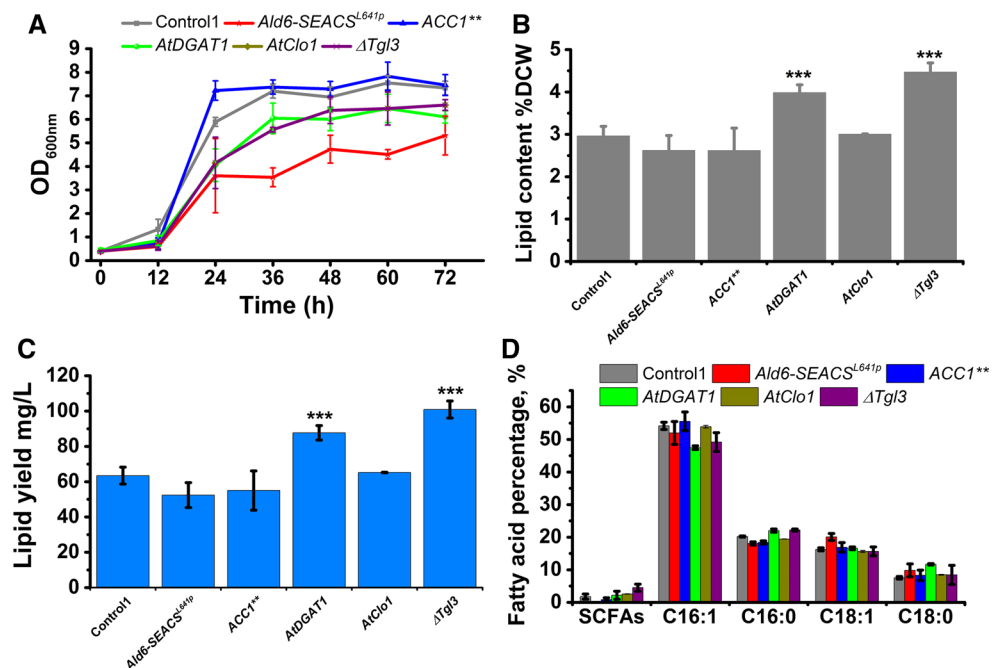
As an initial step in this study, each of the six genes under investigation for yeast lipid engineering was individually expressed to gauge any impact on cell growth and lipid production. The effect on biomass growth of expression or gene deletion was obvious at 24 h post-induction for *ACC1*** (*ACC1* that carries two mutations, ser659ala, and ser1157ala)-expressing strain showing comparable growth to Control1, but the other strains had slightly reduced growth over the culture period (Fig. 2a). Reduction in growth was shown in strains expressing the dual *Ald6-SEACS^{L641P}* genes, which significantly reduced the growth over the entire culture period that may be attributed to toxicity from high levels of intermediate acetate or acetyl-CoA [4] caused by increasing carbon flux through this pathway.

With regard to lipid content, yeast cells with a key lipase knocked out ($\Delta Tgl3$) or expressing *AtDGAT1* had increased lipid content from 3.0 to 4.5% and 4.0%, corresponding to a relative increase of 40 and 25% (Fig. 2b), respectively, performances that matched previous reports [2, 3, 20]. The

same strains also had improved lipid production based on the whole culture compared with Control 1 (Fig. 2c). However, no significant improvement in lipid content was observed for cells expressing *Ald6-SEACS^{L641P}* or *ACC1*** or *Atclo1* on either a dry cell weight (DCW) or whole culture basis (Fig. 2b, c), which was not fully consistent with earlier reports [4, 9, 12, 22]. A higher *K_m* (Michaelis constant) of *SEACS^{L641P}* for its substrates than the yeast *Acs1p* and unbalanced enzyme activities [24] could help to explain the unimproved lipid content of these strains. Furthermore, host strains and medium compositions used here differed from earlier reports, which could contribute to lower than expected lipid values. In terms of substantial changes to FA profiles, *Ald6-SEACS^{L641P}* expression slightly increased C18 and reduced C16 FAs, whereas *AtDGAT1* expression reduced C16:1 but increased C16:0 and C18:0 as shown in Fig. 2d. *Tgl3* knockout led to a reduction in C16:1 and increases in short chain FAs (SCFAs).

While the six genes under examination showed promise for enhancing lipid production when expressed individually in previous reports [2–4, 12, 20, 23], it was clear from our study that altering a single gene either did not increase lipid, or, if it did, it also reduced cell growth. Therefore, it was necessary to examine the impact of the expression of additional genes in a stepwise manner. We have thus constructed two base strains for this purpose. The first base strain (B1) combines two genes with clear positive effects on lipid production in our initial analysis, *AtDGAT1* expression and $\Delta Tgl3$ to explore the effect of addition of further genes coding for enzymes for FA biosynthesis. In parallel, a second base strain, B2, was prepared that included all genes

Fig. 2 Effect of expression or deletion of a single gene on yeast growth and lipid production after 72 h culture period. **a** Biomass production measured using OD_{600nm} at 12 h time points during the culturing, **b** lipid content (measured as total fatty acids) as a percentage of dry cell weight (DCW), **c** lipid yield based on the total culture volume and **d** fatty acid profile in each sample. [*Control1 is the wild-type BY4741 containing the empty pESC-Leu2d vector. SCFAs, short chain fatty acids, include C10:0, C12:0 and C14:0. Asterisks (***) indicate significant difference (one-way analysis of variance, ANOVA, test) at $P < 0.001$, $\alpha = 0.05$ post hoc Holm–Sidak test for engineered strains compared to Control1.]



that enhanced lipid accumulation (*AtDGAT1*) and supported lipid stabilization (*Atclo1* and $\Delta Tgl3$).

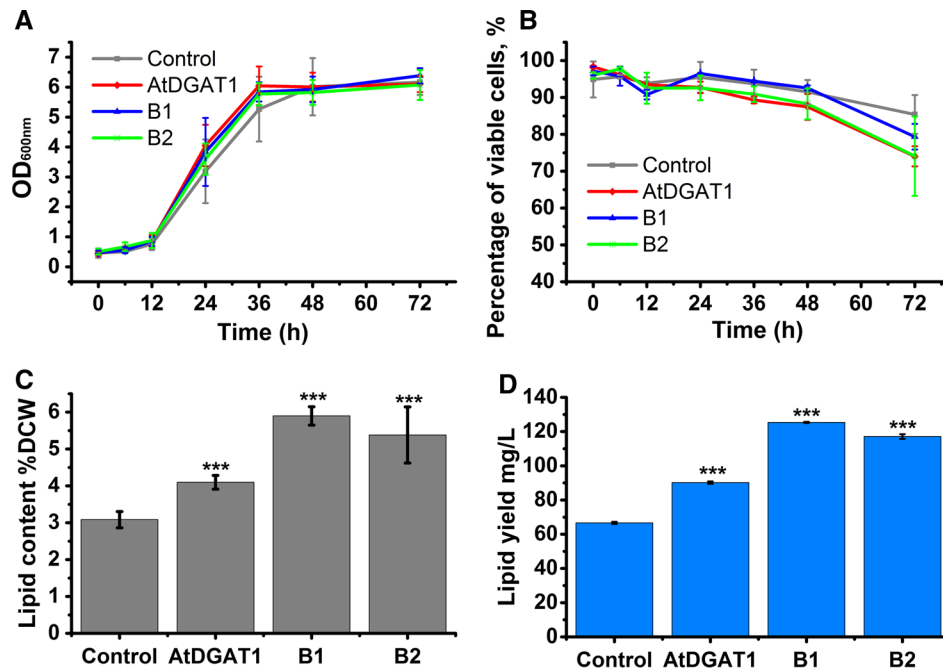
Construction of base strains engineered for enhanced lipid accumulation and stabilization

Expression of the selected genes for lipid accumulation and stabilization had no significant impact on yeast cell growth over the culture period compared to control (Fig. 3a), but resulted in reduced cell viability in the final culture period after 48 h (Fig. S2. A-B, Fig. 3b). Strain B2 in particular showed substantially lower cell viability at 72 h with a mean of 75% versus 88% viability in control cells (Fig. 3b). However, the B1 and B2 strains also showed increased uptake of carbon sources galactose and raffinose, faster ethanol and glycerol production and consumption compared with the control yeast (Fig. S3. A-D). As a consequence, the engineered strains are expected to have experienced longer periods of starvation than the control yeast, especially in the late culture period. The slight instead of serious effects on cell viability resulting from enhanced lipid accumulation could also be explained by the fact that neutral lipid pathways are not essential for yeast; the quadruple knockout

yeast mutant that is devoid of TAG and SE did not show obviously impaired growth in a prior study [11].

Strain B1 having its major TAG lipase gene (*Tgl3*) knocked out and expressing *AtDGAT1* showed improved lipid content from 3.1 to 5.9% (corresponding to a relative increase by 92%) on a DCW basis above control (Fig. 3c), while no additional increase was found for B2 which also expressed *AtClo1*. Similar increases were obtained for total lipid yield in B1 and B2 above controls, as comparable growth and biomass were achieved for these strains (Fig. 3d). Overall, B1 increased total lipid by 1.9-fold higher than that of control (66.6 mg/L), followed by B2 with 1.8-fold improvement above the control.

Lipid accumulation and stabilization genes *AtDGAT1*, *Tgl3* deletion and *Atclo1* were combined in one strain for the first time in this study. *AtDGAT1* and *Tgl3* knockout combination (B1 strain) improved total lipid yield by 88% above the control, without impact on growth or cell viability for most of the culture period. A similar strategy of combining fatty acid synthesis (*WRI1*) and lipid accumulation (*DGAT1*) genes has shown significantly increased lipid content in leaves of *Nicotiana benthamiana* under transient expression [28].



* Control, BY4741-empty vectors; **AtDGAT1**, BY4741-*AtDGAT1*; **B1**, BY4741-*AtDGAT1*- $\Delta Tgl3$; **B2**, BY4741-*AtDGAT1*- $\Delta Tgl3$ -*Atclo1*.

Fig. 3 Effect of expression or deletion of a single gene and multiple gene combinations on yeast growth, cell viability and lipid production over a 72 h culture period. **a** Biomass production measured using OD_{600 nm}, **b** percentage of viable cells in the culture measured in PI-stained cells by flow cytometry, **c** lipid content (measured as total fatty acids) as a percentage of dry cell weight (DCW), **d** lipid yield based on the total culture volume. [*Control is the wild-type BY4741

containing appropriate empty vectors. Base strain 1=B1 expressing *AtDGAT1* in the *Tgl3* knockout. Base strain 2=B2 expressing *AtClo1* and *AtDGAT1* in the *Tgl3* knockout. Asterisks (***) indicate significant difference (one-way analysis of variance, ANOVA, test) at $P < 0.001$, $\alpha = 0.05$ post hoc Holm–Sidak test for engineered strains compared to the control.]

The proposed structure of the lipid droplet-stabilizing protein caleosin supports membrane formation [13] and thus enhances lipid stabilization. The combined expression of a modified oleosin, stabilized through the incorporation of a cysteine–cysteine bond and *AtDGAT1*, increased fatty acids in yeast by 1% DCW compared with *AtDGAT1* expression alone [29], and a combination of yeast *DGAT* (*ScDGAT1*) and *A. thaliana* oleosin (*AtOLEO3*) was found to enhance TAG accumulation in a marine diatom [30]. In our study, *Atclo1* was added to a base strain which already had the *Tgl3* deleted and thus the requirement for an LD-stabilizing protein was reduced.

Physiological effects of expression of enhanced fatty acid biosynthesis genes in base strains

Firstly, *Ald6-SEACS^{L641P}* was introduced into strains B1 and B2 to form B1AS and B2AS, respectively, to test the effect of increasing fatty acid biosynthesis on lipid production. *Ald6-SEACS^{L641P}* expression reduced cell growth to half

that of their respective base strains (B1 and B2) (Fig. 4a, e). Cell viabilities of B1AS and B2AS strains were also lower than the base strains at all culture time points, suggesting that the effect of the expression of *Ald6-SEACS^{L641P}* on the cells was immediate and sustained (Fig. 4B&F). While *Ald6-SEACS^{L641P}* expression significantly increased lipid content on a DCW basis (Fig. 4c, g), it decreased the total lipid yield compared with the lipid production of base strains B1 and B2 (Fig. 4d, h). Specifically, B1AS had increased lipid content by 21% but reduced lipid yield by 17% compared with B1 (5.9% DCW, 125.4 mg/L), while B2AS had increased lipid content by 30% but reduced lipid yield by 38% compared with B2 (5.4% DCW, 117.1 mg/L). B1AS had higher expression of *AtDGAT1* than B1 and, similarly, B2AS had higher expression of *AtDGAT1* and *AtClo1* at 24 h than B2, which likely explains the improvement of cellular lipid content for B1AS and B2AS (Fig. S1. D&F).

In prior research, the inclusion of the genes *Ald6-SEACS^{L641P}* into metabolically engineered yeast has resulted in either improved productivity [4, 5, 15, 24] or negative effects

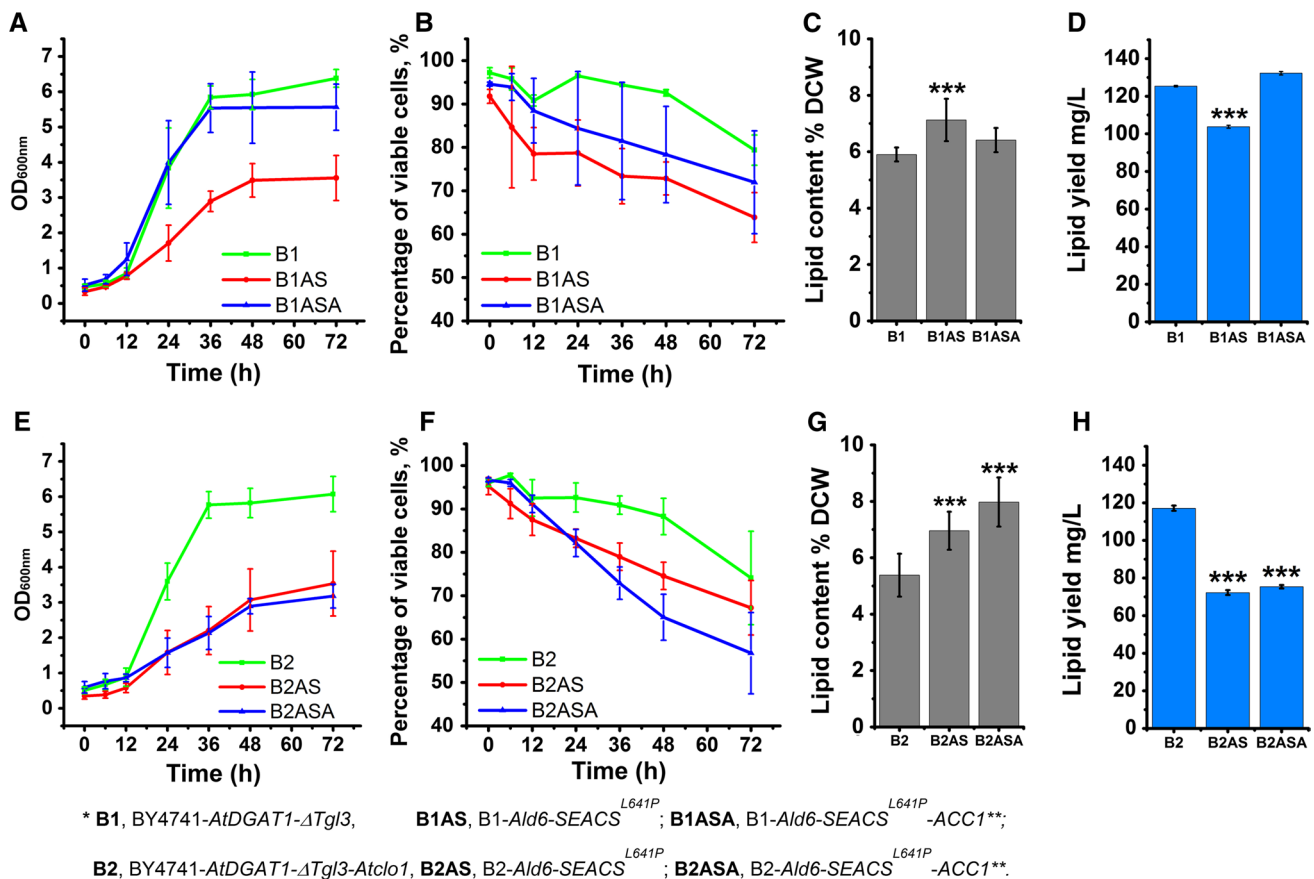


Fig. 4 Comparison of the effects of enhanced fatty acid biosynthesis steps on yeast growth, cell viability and lipid production over 72 h culture period between two base strains. **a, e** Biomass production measured using OD_{600 nm}, **b, f** percentage of viable cells in the culture measured in PI-stained cells by flow cytometry, **c, g** lipid con-

tent (measured as total fatty acids) as a percentage of dry cell weight (DCW), **d, h** lipid yield based on the total culture volume. [Asterisks (***) indicate significant difference (one-way analysis of variance, ANOVA, test) at $P < 0.001$, $\alpha = 0.05$ post hoc Holm–Sidak test for engineered strains compared to B1 and B2.]

such as on resveratrol production [19]. In our case, inclusion of *Ald6-SEACS^{L641p}* impaired yeast growth and cell viability. The cause may be abnormally high levels of cytosolic acetate and acetyl-CoA, due to higher expression of acetaldehyde dehydrogenase (*Ald6*) and acetyl-CoA synthetase (*ACS*) or possible disparity between their products [24].

To alleviate the potential buildup of acetate and acetyl-CoA intermediates in the base strains as a consequence of expressing *Ald6-SEACS^{L641p}*, an additional gene *ACCI*** was brought into the highly engineered strains. Firstly, *ACCI*** was introduced into base strains B1 and B2 resulting in mixed effects on cell growth and lipid production. Specifically, *ACCI*** expression in B1 and B2 severely reduced cell growth but improved lipid content by 24% in B1 strain, while causing no change to lipid content of the B2 strain (Fig. S4. A&B). This result is similar to earlier studies where *ACCI*** expression in yeast CEN.PK 113-5D increased total fatty acids by 65% (11.7% DCW), but with a lower growth rate and a reduced final biomass [23].

To further understand the effect of gene *ACCI*** on our engineered strains, *ACCI*** was introduced into strains B1AS and B2AS (forming B1ASA and B2ASA, respectively) and its impact on cell physiology and lipid production was determined. The growth rate of B1ASA was improved above B1AS and comparable to B1 (Fig. 4a), while the growth of B2ASA was very similar to B2AS and both were considerably lower than B2 (Fig. 4e). Concomitantly, cell viability was improved for B1ASA compared with B1AS, whereas the viability of B2ASA dropped further than B2AS to reach a mean of 55% by 72 h (Fig. 4b, f). There were also mixed results in lipid production in the strains due to *ACCI*** addition: neither lipid content nor yield improved significantly in B1ASA over B1 and B1AS (Fig. 4c, d), but the lipid content of B2ASA increased over both B2 and B2AS to 8.0% DCW (a relative increase of 64 and 15%, respectively), while its lipid yield was below that of B2 (Fig. 4d, h).

The difference in cell physiology response and lipid production in the engineered strains following introduction of *ACCI*** can be explained, at least in part, by the expression levels of the introduced genes. The B1ASA strain showed high relative expression of *Ald6*, *SEACS^{L641p}* and, more importantly, very high *ACCI* levels, compared with the B1AS strain at 24 h; the latter strain displayed negative growth and cell viability and displayed only modest *ACCI* expression (Fig. S1. C). The primary effect of enhanced *ACCI* expression may be to balance metabolic intermediates and alleviate toxicity from the increased levels of acetate and acetyl-CoA, leading to recovery of cell growth and viability observed in B1ASA. Despite more precursors being available for fatty acid synthesis due to higher pathway gene expression in the B1ASA strain, there was slightly reduced lipid content in this strain compared with B1AS.

AtDGAT1 expression was similar between B1AS and B1ASA, suggesting that the lipid accumulation step may be saturated. Higher lipid content can only be achieved with higher DGAT activity to draw fatty acid into TAG. Indeed, B2ASA showed 4.1-fold higher *AtDGAT1* and 4.8-fold higher *AtC1o1* expression levels above those of B2AS and this strain also had the highest lipid level (8%) of any of the engineered strains tested. This observation supports the notion that higher expression of genes for lipid accumulation leads to higher cellular lipid content.

Inclusion of the gene coding for the lipid droplet stabilizing protein, *Atc1o1*, differentiated the B2 engineered strains from the B1 series. Taken as a whole, the B2 series of engineered cells performed slightly worse than their B1 counterparts in terms of growth, cell viability and lipid yield, but these cells had the highest lipid content (DCW).

Upregulated glycerol production pathway in cells engineered for lipid production

The base strains B1 and B2 had slightly reduced growth rate (μ) than the control, but the addition of *Ald6-SEACS^{L641p}* expression clearly reduced the growth rate of B1AS and B2AS to around half that of B1 and B2, respectively (Table 2). Addition of *ACCI*** to the B1AS and B2AS strains recovered the growth rate of B1ASA, but not of B2ASA.

The production of two by-products, ethanol and glycerol, was also compared among the engineered strains. The ethanol biosynthesis pathway was not significantly affected in most engineered strains where ethanol production rate was slightly lower than control (0.179 h^{-1}), except B2ASA which was reduced to 0.083 h^{-1} (Table S1). The final ethanol concentration of most of the engineered strains at 72 h post-induction was maintained around 7–8 mg/mL, slightly lower than that of the control, 8.5 mg/mL (Table S1). Interestingly, glycerol production rate was 4–6 fold higher in the engineered strains compared with the control, including the strain expressing *AtDGAT1* only (Table 2), suggesting that the glycerol biosynthesis pathway was upregulated with the introduction of this gene. A similar phenomenon was observed in strains engineered for improved production of fatty acid ethyl esters (FAEE) [6]. There could be several causes for the upregulated glycerol biosynthesis pathway, including the availability of more precursors for glycerol biosynthesis such as glycerol-3-phosphate (G3P) from the heavily modified lipid production pathway or due to a generalized stress response of the cells to genetic engineering.

Two-stage bioprocess recovers cell growth and improves lipid yield

Strain B2ASA gave the highest cellular lipid content of 8.0% (259% above control), but low growth compared with control

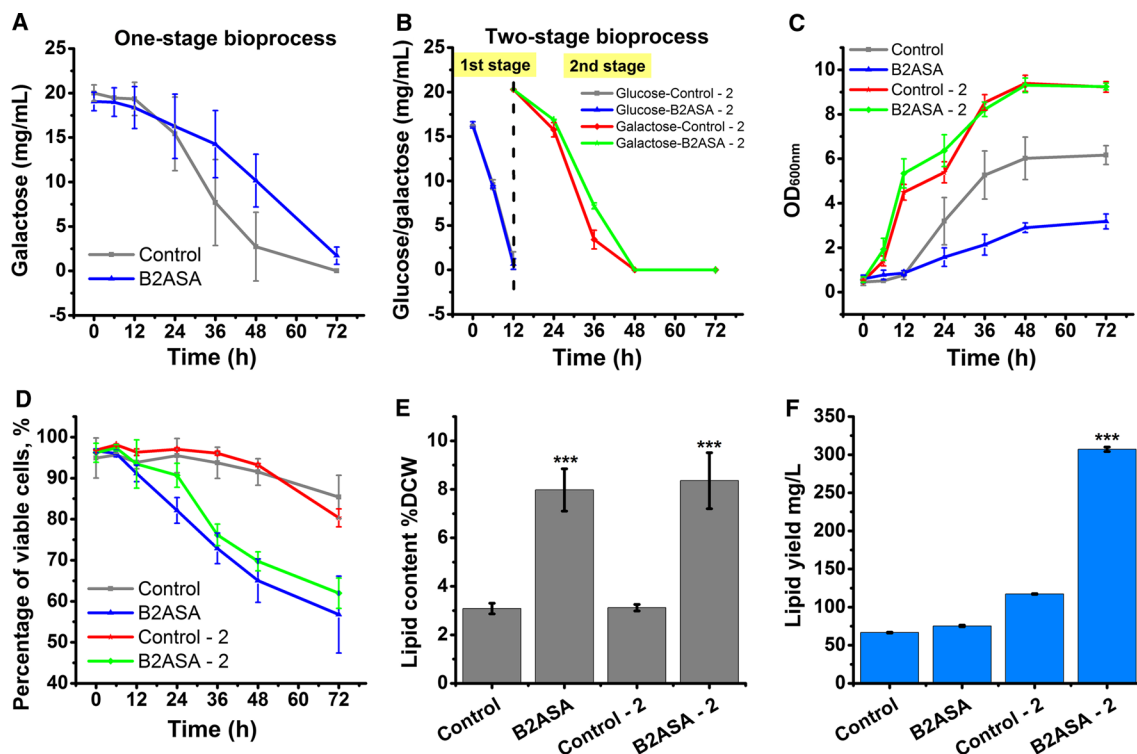
Table 2 Physiological parameters of engineered yeast strains during exponential phase in flasks

Strain name	Growth rate μ (h ⁻¹)		Galactose uptake rate (h ⁻¹)		Raffinose uptake rate (h ⁻¹)		Ethanol production rate (h ⁻¹)		Glycerol production rate (h ⁻¹)	
	AVG	SD	AVG	SD	AVG	SD	AVG	SD	AVG	SD
Control	0.082	0.007	-0.278	0.016	-0.155	0.077	0.179	0.091	0.005	0.003
<i>AtDGATI</i>	0.084	0.001	-0.394	0.031	-0.100	0.010	0.164	0.094	0.021	0.004
B1	0.072	0.001	-0.375	0.009	-0.076	0.002	0.159	0.003	0.025	0.001
B1AS	0.041	0.004	-0.345	0.079	-0.069	0.016	0.157	0.035	0.026	0.005
B1ASA	0.068	0.007	-0.322	0.070	-0.083	0.003	0.134	0.040	0.026	0.010
B2	0.071	0.008	-0.343	0.005	-0.097	0.038	0.145	0.011	0.020	0.003
B2AS	0.041	0.001	-0.321	0.031	-0.102	0.058	0.147	0.055	0.030	0.010
B2ASA	0.034	0.001	-0.220	0.063	-0.168	0.002	0.083	0.056	0.018	0.003

AVG average, SD standard deviation

(Fig. 5a) led to a poor overall lipid yield. Consideration was given to a culturing process that separated biomass and lipid production stages. This was achieved by placing lipid accumulation genes *DGATI* and *AtClo1* under control of the

GAL1/10 promoters, where expression was suppressed in the presence of glucose. During the first stage of growth in glucose, B2ASA utilized glucose and produced biomass at a similar rate to the control (Fig. 5b, c). *Ald6-SEACS*^{L641P} and



* Control, BY4741-empty vectors, in one-stage bioprocess; Control-2, control in two-stage bioprocess;
 B2ASA, B2-*Ald6-SEACS*^{L641P}-*ACC1*^{**}, in one-stage bioprocess, B2ASA-2, B2ASA in two-stage bioprocess.

Fig. 5 Comparison of the performances of engineered strain B2ASA and control over a 72 h culture period between one-stage and two-stage bioprocesses. **a** Galactose consumption in one-stage bioprocess, **b** sugar consumption in two-stage bioprocess, **c** biomass production measured using OD_{600nm}, **d** percentage of viable cells in the culture measured in PI-stained cells by flow cytometry, **e** lipid content (meas-

ured as total fatty acids) as a percentage of dry cell weight (DCW), **f** lipid yield based on the total culture volume. [Asterisks (***) indicate significant difference (one-way analysis of variance, ANOVA, test) at $P < 0.001$, $\alpha = 0.05$ post hoc Holm-Sidak test for engineered strains compared to control and Control2, respectively.]

*ACC1*** were expressed at this stage, as these genes were under control of constitutive promoters. During the second stage of incubation under galactose, where all recombinant genes in strain B2ASA were expressed (Fig. S1. A–F), both sugar uptake and growth rate were highly similar to the control (Fig. 5b, c).

In terms of cell viability, B2ASA had significantly reduced cell viability levels at both stages (Fig. 5d), with a faster rate of decline for cells in the two-stage process when fed with galactose (where all recombinant genes are turned on) than when fed with glucose. Conversely, the growth of B2ASA as measured by OD600 nm in the two-stage process was the same as the control. Stressed cells may have delayed growth and be unable to divide [7], but membrane-damaged cells with poor cell viability could also contribute to growth measures by OD600 nm. While cell viability and cell growth are not always positively correlated, viability should be considered as an important index to assess the fitness of engineered cells.

In comparison with B2ASA in one-stage bioprocess, the two-stage bioprocess achieved significantly higher lipid content (8.36% DCW), 2.7-fold over the control (Fig. 5e), and more striking was the improvement in lipid yield to > 300 mg/L (Fig. 5f). Two-stage bioprocesses are known for increasing product yields in metabolic engineered organisms, such as the altered C:N ratio for yeast production of lipids [25]. Here, we demonstrated that the combination of yeast lipid pathway engineering and bioprocess strategy can simultaneously achieve high lipid content and lipid yield.

Conclusions

Metabolic engineering for increased production of lipid in yeast was achieved through the combined expression of genes for fatty acid biosynthesis (*Ald6-SEACS^{L641P}*, *ACC1***), lipid accumulation (*AtDGAT1*) and stabilization (*ΔTgl3*, *Atclo1*). Lipid content and yield and cell viability were shown to be important indicators of productivity of the engineered strains. The final engineered strain had the highest cellular lipid content but lowest growth, a hurdle which was overcome by separating the growth and lipid accumulation stages of the bioprocess. Thus, a combination of metabolic engineering and bioprocess strategies was shown to be a powerful approach to achieve high end-product yield; this can also be extended to high lipid production microorganisms such as *Y. lipolytica*.

Acknowledgements We acknowledge the financial support from the ARC linkage project (LE160100185) and Monash University for the graduate and international postgraduate research scholarships awarded to HP. We thank the undergraduates Mr. Alastair Katrivessis and Mr. Mitchell Drowley for assistance with experiments and useful discussion

on the results. We are grateful to Ms. Yanqin Xu and Prof. Hongyuan Yang for the strains BY4741 and BY4741 *ΔTgl3*.

Compliance with ethical standards

Conflict of interest The authors declare no financial or commercial conflict of interest.

References

1. Athenstaedt K, Daum G (2003) YMR313c/TGL3 encodes a novel triacylglycerol lipase located in lipid particles of *Saccharomyces cerevisiae*. *J Biol Chem* 278:23317–23323
2. Athenstaedt K, Daum G (2005) Tgl4p and Tgl5p, two triacylglycerol lipases of the yeast *Saccharomyces cerevisiae* are localized to lipid particles. *J Biol Chem* 280:37301–37309
3. Bouvier-Navé P, Benveniste P, Oelkers P, Sturley SL, Schaller H (2000) Expression in yeast and tobacco of plant cDNAs encoding acyl CoA: diacylglycerol acyltransferase. *Eur J Biochem* 267:85–96
4. Chen Y, Daviet L, Schalk M, Siewers V, Nielsen J (2013) Establishing a platform cell factory through engineering of yeast acetyl-CoA metabolism. *Metab Eng* 15:48–54
5. de Jong BW, Shi S, Siewers V, Nielsen J (2014) Improved production of fatty acid ethyl esters in *Saccharomyces cerevisiae* through up-regulation of the ethanol degradation pathway and expression of the heterologous phosphoketolase pathway. *Microb Cell Fact* 13:1–10
6. de Jong BW, Siewers V, Nielsen J (2016) Physiological and transcriptional characterization of *Saccharomyces cerevisiae* engineered for production of fatty acid ethyl esters. *FEMS Yeast Res* 16:1–9
7. Eisenberg T, Buttner S (2014) Lipids and cell death in yeast. *FEMS Yeast Res* 14:179–197
8. Fei W, Shui G, Zhang Y, Krahmer N, Ferguson C, Kapterian TS, Lin RC, Dawes IW, Brown AJ, Li P, Huang X, Parton RG, Wenk MR, Walther TC, Yang H (2011) A role for phosphatidic acid in the formation of “supersized” lipid droplets. *PLoS Genet* 7:e1002201
9. Froissard M, D’Andrea S, Boulard C, Chardot T (2009) Heterologous expression of AtClo1, a plant oil body protein, induces lipid accumulation in yeast. *FEMS Yeast Res* 9:428–438
10. Garay LA, Boundy-Mills KL, German JB (2014) Accumulation of high-value lipids in single-cell microorganisms: a mechanistic approach and future perspectives. *J Agric Food Chem* 62:2709–2727
11. Garbarino J, Padamsee M, Wilcox L, Oelkers PM, D’Ambrosio D, Ruggles KV, Ramsey N, Jabado O, Turkish A, Sturley SL (2009) Sterol and diacylglycerol acyltransferase deficiency triggers fatty acid-mediated cell death. *J Biol Chem* 284:30994–31005
12. Jamme F, Vindigni J-D, Méchin V, Cherifi T, Chardot T, Froissard M (2013) Single cell synchrotron FT-IR microspectroscopy reveals a link between neutral lipid and storage carbohydrate fluxes in *S. cerevisiae*. *PLoS One* 8:e74421
13. Jiang P-L, Tzen JT (2010) Caleosin serves as the major structural protein as efficient as oleosin on the surface of seed oil bodies. *Plant Signal Behav* 5:447–449
14. Jin M, Slininger PJ, Dien BS, Waghmode S, Moser BR, Orjuela A, da Costa Sousa L, Balan V (2015) Microbial lipid-based lignocellulosic biorefinery: feasibility and challenges. *Trends Biotechnol* 33:43–54
15. Kocharin K, Chen Y, Siewers V, Nielsen J (2012) Engineering of acetyl-CoA metabolism for the improved production of

- polyhydroxybutyrate in *Saccharomyces cerevisiae*. *Amb Express* 2:1–11
16. Leber C, Polson B, Fernandez-Moya R, Da Silva NA (2015) Overproduction and secretion of free fatty acids through disrupted neutral lipid recycle in *Saccharomyces cerevisiae*. *Metab Eng* 28:54–62
 17. Ledesma-Amaro R, Dulermo R, Niehus X, Nicaud J-M (2016) Combining metabolic engineering and process optimization to improve production and secretion of fatty acids. *Metab Eng* 38:38–46
 18. Lennen RM, Pfleger BF (2013) Microbial production of fatty acid-derived fuels and chemicals. *Curr Opin Biotechnol* 24:1044–1053
 19. Li M, Kildegaard KR, Chen Y, Rodriguez A, Borodina I, Nielsen J (2015) De novo production of resveratrol from glucose or ethanol by engineered *Saccharomyces cerevisiae*. *Metab Eng* 32:1–11
 20. Peng H, Moghaddam L, Brinin A, Williams B, Mundree S, Haritos VS (2017) Functional assessment of plant and microalgal lipid pathway genes in yeast to enhance microbial industrial oil production. *Biotechnol Appl Biochem*. <https://doi.org/10.1002/bab.1573>
 21. Pfleger BF, Gossing M, Nielsen J (2015) Metabolic engineering strategies for microbial synthesis of oleochemicals. *Metab Eng* 29:1–11
 22. Runguphan W, Keasling JD (2014) Metabolic engineering of *Saccharomyces cerevisiae* for production of fatty acid-derived biofuels and chemicals. *Metab Eng* 21:103–113
 23. Shi S, Chen Y, Siewers V, Nielsen J (2014) Improving production of malonyl coenzyme a-derived metabolites by abolishing Snf1-dependent regulation of Acc1. *mBio* 5:e01130–e01214
 24. Shiba Y, Paradise EM, Kirby J, Ro D-K, Keasling JD (2007) Engineering of the pyruvate dehydrogenase bypass in *Saccharomyces cerevisiae* for high-level production of isoprenoids. *Metab Eng* 9:160–168
 25. Slininger PJ, Dien BS, Kurtzman CP, Moser BR, Bakota EL, Thompson SR, O'Bryan PJ, Cotta MA, Balan V, Jin M, Sousa LdC, Dale BE (2016) Comparative lipid production by oleaginous yeasts in hydrolyzates of lignocellulosic biomass and process strategy for high titers. *Biotechnol Bioeng* 113:1676–1690
 26. Valle-Rodriguez JO, Shi SB, Siewers V, Nielsen J (2014) Metabolic engineering of *Saccharomyces cerevisiae* for production of fatty acid ethyl esters, an advanced biofuel, by eliminating non-essential fatty acid utilization pathways. *Appl Energy* 115:226–232
 27. Vanhercke T, El Tahchy A, Liu Q, Zhou X-R, Shrestha P, Divi UK, Ral J-P, Mansour MP, Nichols PD, James CN, Horn PJ, Chapman KD, Beaudoin F, Ruiz-López N, Larkin PJ, de Feyter RC, Singh SP, Petrie JR (2014) Metabolic engineering of biomass for high energy density: oilseed-like triacylglycerol yields from plant leaves. *Plant Biotechnol J* 12:231–239
 28. Vanhercke T, El Tahchy A, Shrestha P, Zhou X-R, Singh SP, Petrie JR (2013) Synergistic effect of WRI1 and DGAT1 coexpression on triacylglycerol biosynthesis in plants. *FEBS Lett* 587:364–369
 29. Winichayakul S, Scott RW, Roldan M, Hatier JH, Livingston S, Cookson R, Curran AC, Roberts NJ (2013) In vivo packaging of triacylglycerols enhances *Arabidopsis* leaf biomass and energy density. *Plant Physiol* 162:626–639
 30. Zulu NN, Popko J, Zienkiewicz K, Tarazona P, Herrfurth C, Feussner I (2017) Heterologous co-expression of a yeast diacylglycerol acyltransferase (ScDGA1) and a plant oleosin (AtOLEO3) as an efficient tool for enhancing triacylglycerol accumulation in the marine diatom *Phaeodactylum tricornutum*. *Biotechnol Biofuels* 10:187

1 **Supplemental Material for**

2

3 **Metabolic engineering of lipid pathways in *Saccharomyces cerevisiae* and staged bioprocess for**

4 **enhanced lipid production and cellular physiology**

5

6 Huadong Peng, Lizhong He, Victoria S. Haritos*

7 Department of Chemical Engineering, Monash University, Clayton, Victoria, Australia

8 *Corresponding author: Victoria S. Haritos, victoria.haritos@monash.edu

9

10

11

12

13

14

15

16

17

18

19

20

21

22

23

24

25

26 *Supplemental methods*

27 *Sugar and metabolite analysis*

28 The analysis of sugars: glucose, galactose and raffinose and extracellular metabolic byproducts
29 such as ethanol and glycerol were determined by HPLC. Culture broth sample (1 mL) was
30 filtered through a 0.2 mm syringe filter before analysis using an Agilent 1260 Infinity HPLC
31 and refractive index detector (RID) fitted with a Rezex™ RHM-Monosaccharide H+ (8%)
32 column (300 x 7.8um, Phenomenex). The column was eluted with deionized water at a flow
33 rate of 0.5 mL/min at 65 °C for 35 min [2,1].

34

35

36

37

38

39

40

41

42

43

44

45

46

47

48

49 **Table S1 Lipid content, lipid yield, lipid profile and by-products of engineered strains**
 50 **after 72h post-induction**

Strains	Lipid	Lipid	UFAs	Average of fatty acid component %					Ethanol	Glycerol
	content % DCW	yield mg/L	%	SCFAs	C16:1	C16:0	C18:1	C18:0	mg/mL	mg/mL
Control1	3.2%	63.4	70.4%	1.8%	54.1%	20.2%	16.3%	7.6%	ND	ND
<i>Ald6-</i>	2.60%	52.4	72.1%	0.0%	52.0%	18.1%	20.1%	9.8%	ND	ND
<i>SEACS^{L641P}</i>										
<i>ACC1**</i>	2.6%	55.0	72.5%	0.8%	55.6%	18.4%	16.9%	8.3%	ND	ND
<i>AtDGAT1</i>	4.1%	87.7	64.1%	2.2%	47.5%	22.0%	16.6%	11.7%	7.9	1.0
<i>Atclo1</i>	3.0%	65.2	69.5%	2.6%	53.9%	19.4%	15.6%	8.5%	ND	ND
<i>ΔTgl3</i>	4.5%	100.9	64.8%	4.5%	49.2%	22.2%	15.7%	8.4%	ND	ND
Control	3.1%	66.6	71.8%	0.6%	54.7%	19.1%	17.1%	8.5%	8.6	0.5
B1	5.9%	125.4	61.5%	4.5%	45.2%	23.6%	16.3%	10.4%	7.4	1.1
B1AS	7.1%	103.8	52.4%	5.9%	38.3%	29.0%	14.1%	12.7%	7.2	1.2
B1ASA	6.4%	132.2	58.6%	4.7%	39.7%	23.1%	18.9%	13.6%	7.2	1.5
B2	5.4%	117.1	60.1%	5.3%	44.6%	24.5%	15.5%	10.0%	7.5	0.9
B2AS	7.0%	72.3	51.6%	6.3%	38.3%	30.5%	13.4%	11.6%	7.8	1.8
B2ASA	8.0%	75.4	51.2%	6.4%	37.7%	29.6%	13.5%	12.8%	7.3	1.2
Control-2	3.1%	117.2	73.0%	0.6%	56.2%	18.6%	16.9%	7.8%	9.6	0.5
B2ASA-2	8.4%	307.1	59.8%	6.1%	43.7%	23.6%	16.1%	10.5%	8.4	0.92

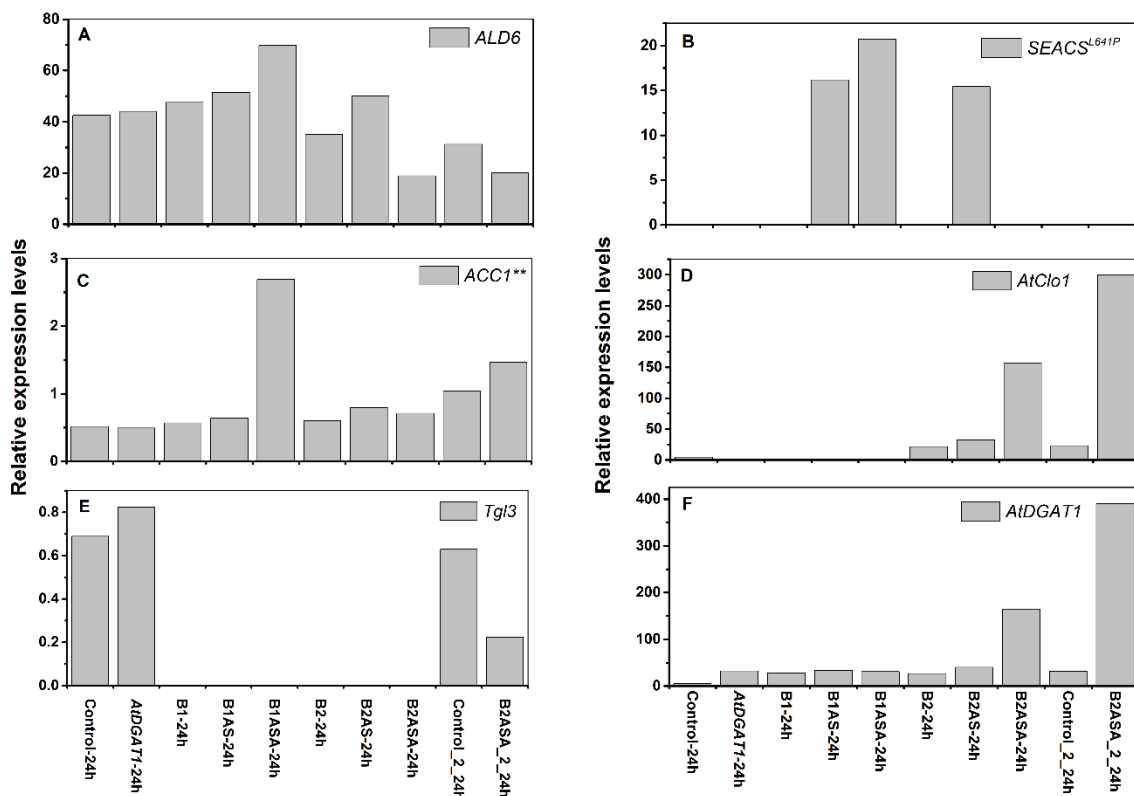
51 *UFAs%: percentage of unsaturated fatty acids; SCFAs, short chain fatty acids include C10:0,
 52 C12:0 and C14:0; ND, not detected; Control1, wild type BY4741 with empty pESC-Leu2d
 53 vector; Control, wild type BY4741 with three empty vectors of pSP-GM2, pIYC04, pESC-
 54 leu2d.

55

56

57 **Fig. S1**

58 Expression levels quantification of target genes of interest of engineered strains by mRNA-seq
 59 analysis including (A) *ALD6*, (B) *SEACS^{L641p}*, (C) *ACC1***, (D) *AtClo1*, (E) *Tgl3*, (F)
 60 *AtDGAT1*. The samples in one-stage and two-stage bioprocess were taken for mRNA-Seq
 61 analysis after 24h post-induction including Control-24h, AtDGAT1-24h, B1-24h, B1AS-24h,
 62 B1ASA-24h, B2-24h, B2AS-24h, B2ASA-24h, Control_2_24h, B2ASA_2_24h. *TAF10*, a
 63 gene that encodes a subunit of transcription factor IID (TFIID), was popularly regarded as a
 64 housekeeping gene, used to normalize the amount of the total mRNA in all samples.



65

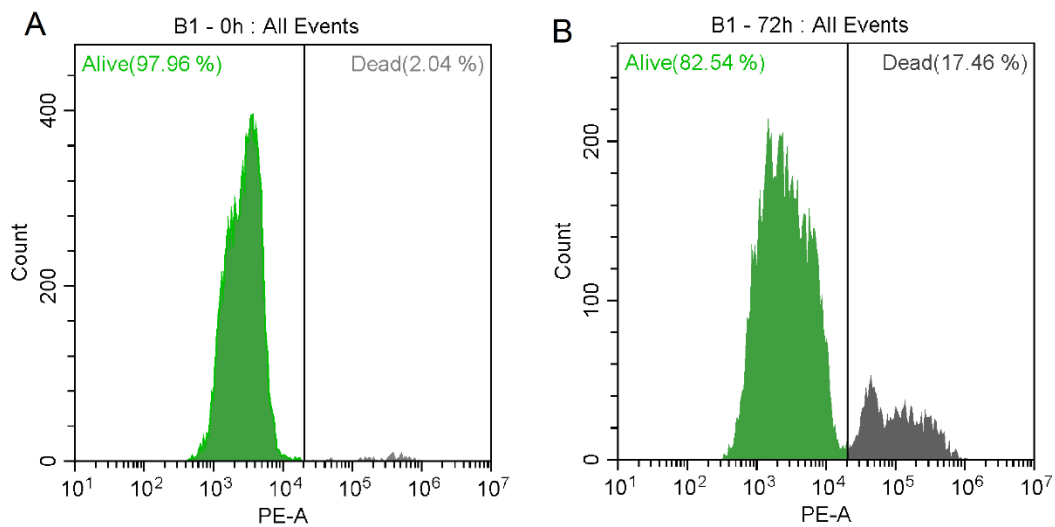
66

67

68

69 **Fig. S2**

70 Example of cell viability measurement of the base strain B1 after propidium iodide (PI) staining
71 by flow cytometry. (A) The cell population distribution and percentage of viable cells in the
72 culture of B1 strain at 0 h (before induction), (B) The cell population distribution and
73 percentage of viable cells in the culture of B1 strain at 72 h post-induction.



74

75

76

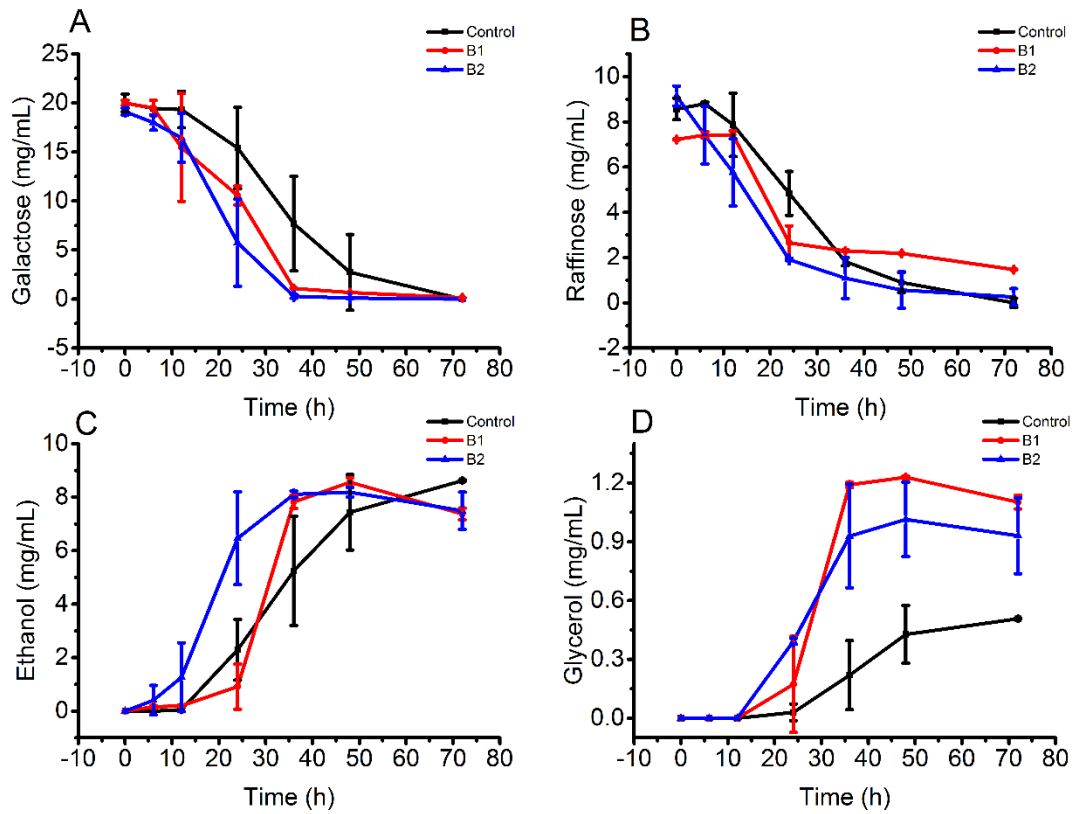
77

78

79

80 **Fig. S3**

81 Comparison of sugar consumption and metabolite production rates between base strains and
 82 control yeast over 72 h culture period. (A) galactose consumption curve, (B) raffinose
 83 consumption curve, (C) ethanol production curve, (D) glycerol production curve.



84

85

86

87

88

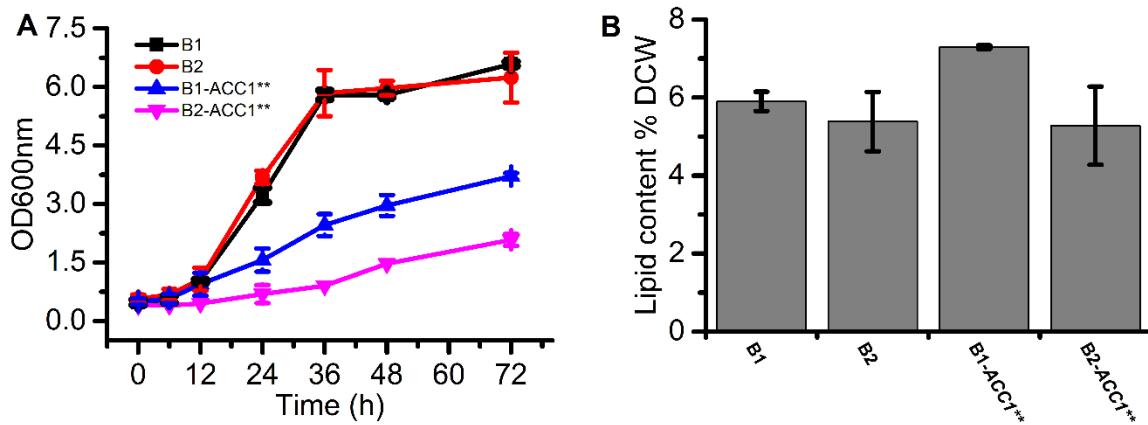
89

90

91

92 **Fig. S4**

93 Comparison of the effect of *ACC1*** expression on the cell growth and lipid content among
 94 two base strains expressing lipid accumulation and sequestration genes. (A) biomass
 95 production measured using OD600 nm, (B) lipid content (measured as total fatty acids) as a
 96 percentage of dry cell weight (DCW).



97

98

99

100 **References**

- 101 1. Peng H, Li H, Luo H, Xu J (2013) A novel combined pretreatment of ball milling and
 102 microwave irradiation for enhancing enzymatic hydrolysis of microcrystalline cellulose.
 103 *Bioresource Technology* 130:81-87.
- 104 2. Sluiter A, Hames B, Ruiz R, Scarlata C, Sluiter J, Templeton D (2006) Determination of
 105 sugars, byproducts, and degradation products in liquid fraction process samples. Golden, CO:
 106 National Renewable Energy Laboratory:1-14

107

CHAPTER 5

**ENHANCED PRODUCTION OF HIGH-
VALUE CYCLOPROPANE FATTY ACID
IN YEAST ENGINEERED FOR
INCREASED LIPID SYNTHESIS AND
ACCUMULATION**

**: This chapter has been submitted to Biotechnology Journal.*

Peng, H., He, L., Haritos, V. S., Enhanced production of high-value cyclopropane fatty acid in yeast engineered for increased lipid synthesis and accumulation. Biotechnology Journal (submitted)

This page is intentionally blank

Chapter 5 Enhanced production of high-value cyclopropane fatty acid in yeast engineered for increased lipid synthesis and accumulation

5.1. Abstract

The unique strained ring structure in cyclopropane fatty acids (CFA) conveys oxidative stability and lubricity to lipids. These attributes are highly valuable for industrial applications such as cosmetics and specialist lubrication but there is currently no commercial source of the lipid. Here, built on recently engineered strains of *Saccharomyces cerevisiae*, we have developed an efficient strategy for CFA production. Expression of the *Escherichia coli* cyclopropane fatty acid synthetase (*Ec.CFAS*) in the engineered yeast resulted in formation of *cis*-9,10-methylene-hexadecanoic and octadecanoic acids in both the phospholipid (PL) and triacylglycerol (TAG) fractions. CFA concentration in TAG of engineered yeast was 12 mg CFA/g DCW (4-fold above the strain expressing CFAS only). The yield of CFA increased from 13.2 to 68.3 mg/L, the highest reported in yeast, using a two-stage bioprocess strategy that separated cell growth from the lipid modification stage. Strategies for further improvement of this valuable lipid are proposed.

5.2. Introduction

The oxidative stability and lubricity of cyclopropane fatty acids (CFA) make them valuable for industrial applications such as cosmetics and in specialist lubrication [1]. CFA are naturally produced in seeds of plants including gymnosperms, *Litchi chinensis* and many representatives of the Malvales order and also by many bacteria, whose production of CFA in cell membranes in response to stress is considered to be protective towards the effects of acidic media, in particular [2, 3]. While cyclopropane fatty acids oils offer good prospects for industrial applications, there are currently no commercial sources of the product.

Genetically modified plant seeds and cyanobacteria have been explored as potential biofactories of cyclopropane fatty acids and while progress has been made toward increasing the CFA levels, there are complex lipid pathway engineering challenges to be overcome in these systems. Multiple attempts have been made to increase CFA yield in seeds of both crop and model plants such as tobacco, *Camelina sativa* and *Arabidopsis thaliana* through engineering of acyl-CoA dependent and independent routes toward stable triacylglycerol (TAG) formation and by comparing the effectiveness of plant or bacterial-sourced cyclopropane fatty acid synthetases (CFAS) [1, 4-6]. Whereas, in *Synechocystis* cyanobacterium expressing the CFAS sourced from *Escherichia coli* (Ec.CFAS) in combination with desaturase engineering (*desA*-/*desD*-/*desC2*+), the result was 30% CFA of total fatty acids but growth was severely reduced in these cells when cultured at 26°C [7]. No measure of CFA productivity or presence in neutral lipids was reported.

Saccharomyces cerevisiae is both a widely-used yeast in biotechnology and model for eukaryotic lipid metabolism. There have been many achievements in engineering *S. cerevisiae* yeast for enhanced lipid production where either standard fatty acids [8-10] or unusual fatty

acids [11-13] have been synthesised and stored in TAG. On this basis we hypothesize that yeast may also be a useful biofactory for CFA and that yeast engineered for enhanced fatty acid synthesis and/or accumulation and/or storage [9] maybe additionally beneficial for elevated CFA production.

In this study, a series of yeast strains engineered for increased lipid content (Table 1) were transformed with *Ec.CFAS*. Importantly, CFA was found accumulated in PL and TAG fractions with up to 42% of TAG fatty acids present as CFA. Moreover, the CFA yield of the yeast strain that produced the most CFA on a dry cell weight (DCW) basis was 5-fold increased by adopting a two-stage bioprocess strategy, that is to our best knowledge the highest yield to date.

5.3. Materials and methods

5.3.1. Plasmids, strain construction and cell culture

Cyclopropane fatty acid synthase gene from *E. coli* (*Ec.CFAS*) (Accession No.: NC_000913.3) was synthesized and inserted by GeneArt Gene Synthesis into pYES2 (Invitrogen) vector under Gal1 promoter. The details of other genes and vectors used in this study including *Ald6*, *SEACS^{L641P}*, *AtDGATI*, were as previously described [9]. *S. cerevisiae* BY4741 (genotype: MATa his3 Δ 1 leu2 Δ 0 met15 Δ 0 ura3 Δ 0) cells were transformed with the prepared plasmids using the Sigma Transformation Kit to form strains listed in Table 1. According to the requirements to maintain auxotrophy (SC-Leu, SC-His-Ura, SC-His-Leu-Ura), the engineered yeast strains were maintained using the appropriate synthetic complete (SC) minimal medium. Gene expression (for genes linked to the GAL1 promoter) was induced by the addition of galactose and the cells were incubated at 30 °C, 250 rpm for 72 h before harvest. A two-stage bioprocess was adopted for the strains CP1 and CP6 (see summary of strains in Table 1), to separate the biomass growth and lipid production stages as described previously [8, 9]. Cell

culturing was initiated with an initial OD 0.4 in SC minimal medium with glucose for 24 h to generate high biomass levels, cells were pelleted by centrifugation then suspended in fresh 50 mL SC induction medium containing 2% (w/v) galactose and 1% (w/v) raffinose and incubated for a further 48 h before sampling.

5.3.2. Lipid analysis and quantification

Freeze-dried cell pellets were extracted using a modified Bligh Dyer procedure [14] where both neutral and polar lipids are extracted from the cell mass into a solvent fraction. The solvent extract was loaded onto silica coated thin layer chromatography (TLC) [15] plates to separate PL and TAG. Fatty acid methyl esters (FAME) were prepared from the lipids in the scraped regions of the TLC plates and analysed by gas chromatography (GC) with a Flame Ionization Detector [16].

Neutral lipid content of cells was also measured by flow cytometry using a CytoFlex (Beckman Coulter, USA) instrument after staining with BODIPY 493/503 (1 μ M final concentration). Detailed procedures of lipid extraction, separation, GC and Flow cytometry analysis are given in the Supplementary Information.

5.4. Results

5.5.1 Lipid pathway engineering increased intracellular TAG and CFA content

Neutral lipid content of yeast cells from each engineered strain were measured by flow cytometry with Bodipy 493/503 staining; average fluorescence intensity of engineered strains CP5 and CP6 were 7-10 fold higher than control cells, confirming the strategy is effective to increase cell TAG content through lipid pathway engineering. Total PL and TAG content in each of the engineered strains was also assessed by quantification of methylated FA by GC as

shown in Fig. 1 (A and B, respectively). There was strong concordance between the quantification of TAG in control and engineered yeast strains by flow cytometry and by GC-FID (linear regression $R^2 = 0.97$, see supplementary information) suggesting the flow cytometry method can be used to rapidly screen recombinant cells for high TAG content.

As expected, PL amount was relatively stable among the different engineered strains but the TAG content increased significantly, especially in strains CP5 and CP6 (Fig. 1A &B). Both strains have *AtDGAT1* recombinantly expressed and *Tgl3* knocked out; this combination is very effective for increasing lipid content in TAG well above levels in strains where just one of the two genes is included (Fig. 1B). Furthermore, the 7-10 fold improvement in TAG content in CP5 and CP6 strains above the strain expressing *Ec.CFAS* only (CP1), suggesting the lipid accumulation and storage strategy developed for standard fatty acids [9] plays an important role to make *Ec.CFAS* work effectively.

Ec.CFAS expression in yeast strains CP1-CP6 produced two CFA, *cis*-9,10-methylenehexadecanoic acid (C17:0, cyclo9) and *cis*-9,10-methyleneoctadecanoic acid (C19:0, cyclo9) (supplementary information) due to the action of the enzyme on the only $\Delta 9$ unsaturated fatty acids of *Saccharomyces* yeast: palmitoleic and oleic acids. As expected, CFA were absent in control yeast as there is no natural production of CFA in these organisms (supplementary information). CFA amount in the PL fraction (DCW basis) showed a slight increase from the base strain that expressed only *Ec.CFAS* (CP1) to CP6 which has had substantial lipid pathway modification (Fig. 1C). Conversely, CFA content of the TAG fraction (DCW basis) showed a substantial increase with greater lipid engineering especially for CP6 where there was a 4-fold increase in CFA in TAG above that of CP1 (Fig. 1D). The increase in CFA in TAG was restricted to CP4 - 6 which have in common the expression of *AtDGAT1*.

Therefore, to increase CFA content in TAG in yeast requires an acyltransferase with stronger activity than that of the native yeast enzyme.

The proportions of CFA to the total fatty acid in the PL of engineered strains CP1 – 6 were roughly similar, varying from ~30 – 40% across all strains (Fig. 1D). However, the proportion of CFA to total fatty acid in TAG changed dramatically in the engineered strains; the highest proportion was measured in CP1 at 42.4% but then the fraction reduced substantially down to ~16.1% in CP3 and 6 (Fig. 1E). When taken together, CP6 TAG content increased by 10-fold above CP1 while the proportion of that lipid that was due to CFA was 4-fold increased. Therefore, a majority of the increase in TAG in CP6 was due to increase in standard fatty acid-containing TAG while 40% of that was attributable to CFA-containing TAG.

5.5.2 Two-stage bioprocess recovered cell growth with higher CFA yield

The growth rate of strains CP4-6 over 72 h was lower at all time points compared with strains CP1-3, as shown in the supplementary information. This resulted in a low overall yield of CFA from CP6 despite its high CFA percentage due to low biomass production. As such, CP6 has a similar yield as CP1 which has higher biomass (~14 mg/L, Fig. 2A). A two-stage bioprocess controlled by differential gene expression (via galactose induction of lipid accumulation genes controlled by the GAL1 promoter) was employed to favour cell biomass production in the first stage and lipid pathway engineering in the second stage. Strikingly, the two-stage bioprocess improved CFA yield in CP6 by a 5-fold. Although overall cell growth of CP6 was only increased by two-stage bioprocess to approximately 70% of the biomass productivity of CP1 which expressed *Ec.CFAS* only, the final yield of CFA in CP6 was 2.1-fold higher than CP1. Therefore, selective and staged gene expression succeeded in recovering most of the cell growth of CP6 and produced the highest reported CFA yield in yeast of 68.3 mg/L.

5.5. Discussion

Built on our previous approach of lipid pathway engineering for enhanced lipid accumulation and storage that was successful for standard fatty acids in yeast [9], we have successfully developed an effective strategy to produce unusual fatty acids such as CFA. Here, we introduced *Ec.CFAS* into a range of strains engineered to increase lipid accumulation and sequestration. Note that strains CP5 and CP6 showed a promising neutral lipid content of CFA. Furthermore, we demonstrated that the yield could be improved through straightforward bioprocess manipulation [9, 17] achieving the highest CFA yield (68.3 mg/L) in yeast reported to date. Prior to this work, the highest report of CFA content in TAG was 12% of total fatty acids in *Camelina sativa* seed oil after combining *Ec.CFAS* with a lysophosphatidic acyl transferase [6]. Earlier attempts at producing CFA in *Arabidopsis thaliana* seed oil resulted in unviable seed in lines with higher percentage CFA [5].

In *Saccharomyces*, the strains with highest CFA content (CP4-6) all expressed *AtDGATI* whereas strains CP1-3 lacked this gene, confirming the benefit of including an acyl transferase in the lipid pathway engineering strategy. Also, it was observed that CP3 and CP6 having enhanced fatty acid synthesis (expressing *Ald6* and *SEACS^{L641P}*) had the lowest proportions of CFA in TAG. This suggests that new fatty acids added to the pool are not modified to CFA but instead move unchanged into TAG. Of further note from this work, is the potential substrate competition between *AtDGATI* and *Ec.CFAS* as both enzymes have a preference for unsaturated FAs palmitoleic acid and oleic acid for TAG or CFA biosynthesis [7, 18, 19] . Therefore, an acyl transferase in place of *AtDGAT1* with selectivity for CFA over unsaturated fatty acids should improve the concentration of CFA in TAG. Another benefit from the use of

a more specific acyl transferase would be the increased availability of unsaturated fatty acids for cell homeostasis.

CFA is known to be synthesized in PL of *E. coli* [20], cyanobacterium [7] and plants and much engineering effort has focussed on increasing the transfer CFA from membrane into storage lipids in plants [1, 4-6]. Prior to this study, the lipid location of CFA produced in yeast was not known but here we have clearly shown that CFA does migrate from the PL where it is presumably synthesized, into TAG, suggesting yeast as a suitable biofactory for this product. There is, however, great potential to improve CFA concentration in TAG further as the proportion in our best performing strain (CP6) was still quite low (16.1%) with 40% CFA left in PL fraction. This may be achieved through a combination of increasing the PL CFA turnover to TAG and introducing fatty acid transferases with greater specificity for CFA.

5.6. Conclusions

While production of valuable fatty acids such as CFA have been explored in plants and cyanobacteria, whether yeast such as *Saccharomyces cerevisiae* could be a useful biofactory was not known. Here, we demonstrate that yeast engineered for enhanced lipid production when combined with *Ec.CFAS*, is very promising for production and stable storage of CFA. The unusual fatty acid was found at higher amounts in TAG than PL fractions of engineered strains and our engineering strategy combining engineering strains and two-stage processes delivered the highest yield yet reported of 68.3 mg/L to date.

References

- [1] Shanklin, J., Yu, X.-H., Prakash, R. R., Engineering Cyclopropane Fatty Acid Accumulation in Plants. *Patent* 2016, 1-20.

- [2] Chang, Y. Y., Cronan, J. E., Membrane cyclopropane fatty acid content is a major factor in acid resistance of *Escherichia coli*. *Molecular microbiology* 1999, 33, 249-259.
- [3] Chen, Y. Y., Gänzle, M. G., Influence of cyclopropane fatty acids on heat, high pressure, acid and oxidative resistance in *Escherichia coli*. *International journal of food microbiology* 2016, 222, 16-22.
- [4] Yu, X.-H., Rawat, R., Shanklin, J., Characterization and analysis of the cotton cyclopropane fatty acid synthase family and their contribution to cyclopropane fatty acid synthesis. *BMC Plant Biology* 2011, 11, 97.
- [5] Yu, X.-H., Prakash, R. R., Sweet, M., Shanklin, J., Coexpressing *Escherichia coli* cyclopropane synthase with *Sterculia foetida* Lysophosphatidic acid acyltransferase enhances cyclopropane fatty acid accumulation. *Plant physiology* 2014, 164, 455-465.
- [6] Yu, X.-H., Cahoon, R. E., Horn, P. J., Shi, H., *et al.*, Identification of bottlenecks in the accumulation of cyclic fatty acids in camelina seed oil. *Plant Biotechnology Journal* 2017, 16, 926-938.
- [7] Machida, S., Shiraiwa, Y., Suzuki, I., Construction of a cyanobacterium synthesizing cyclopropane fatty acids. *Biochimica et Biophysica Acta (BBA)-Molecular and Cell Biology of Lipids* 2016, 1861, 980-987.
- [8] Kochan, K., Peng, H., Wood, B. R., Haritos, V. S., Single cell assessment of yeast metabolic engineering for enhanced lipid production using Raman and AFM-IR imaging. *Biotechnology for Biofuels* 2018, 11, 106.
- [9] Peng, H., He, L., Haritos, V. S., Metabolic engineering of lipid pathways in *Saccharomyces cerevisiae* and staged bioprocess for enhanced lipid production and cellular physiology. *Journal of Industrial Microbiology & Biotechnology* 2018, 45, 707-717.

- [10] Ferreira, R., Teixeira, P. G., Gossing, M., David, F., *et al.*, Metabolic engineering of *Saccharomyces cerevisiae* for overproduction of triacylglycerols. *Metabolic Engineering Communications* 2018, 6, 22-27.
- [11] Huang, Y.-S., Chaudhary, S., Thurmond, J. M., Bobik, E. G., *et al.*, Cloning of $\Delta 12$ - and $\Delta 6$ -desaturases from *Mortierella alpina* and recombinant production of γ -linolenic acid in *Saccharomyces cerevisiae*. *Lipids* 1999, 34, 649-659.
- [12] Kainou, K., Kamisaka, Y., Kimura, K., Uemura, H., Isolation of $\Delta 12$ and $\omega 3$ -fatty acid desaturase genes from the yeast *Kluyveromyces lactis* and their heterologous expression to produce linoleic and α -linolenic acids in *Saccharomyces cerevisiae*. *Yeast* 2006, 23, 605-612.
- [13] Kajiwara, S., Shirai, A., Fujii, T., Toguri, T., *et al.*, Polyunsaturated fatty acid biosynthesis in *Saccharomyces cerevisiae*: expression of ethanol tolerance and the FAD2 gene from *Arabidopsis thaliana*. *Applied and environmental microbiology* 1996, 62, 4309-4313.
- [14] Bligh, E. G., Dyer, W. J., A rapid method of total lipid extraction and purification. *Canadian Journal of Biochemistry and Physiology* 1959, 37, 911-917.
- [15] Knittelfelder, O. L., Kohlwein, S. D., Thin-layer chromatography to separate phospholipids and neutral lipids from yeast. *Cold Spring Harbor Protocols* 2017, 2017, pdb. prot085456.
- [16] Peng, H., Moghaddam, L., Brinin, A., Williams, B., *et al.*, Functional assessment of plant and microalgal lipid pathway genes in yeast to enhance microbial industrial oil production. *Biotechnol Appl Biochem* 2018, 65, 138-144.
- [17] Slininger, P. J., Dien, B. S., Kurtzman, C. P., Moser, B. R., *et al.*, Comparative lipid production by oleaginous yeasts in hydrolyzates of lignocellulosic biomass and process strategy for high titers. *Biotechnology and Bioengineering* 2016, 113, 1676-1690.

- [18] Czabany, T., Wagner, A., Zweytick, D., Lohner, K., *et al.*, Structural and biochemical properties of lipid particles from the yeast *Saccharomyces cerevisiae*. *J Biol Chem* 2008, 283, 17065-17074.
- [19] Grillitsch, K., Connerth, M., Kofeler, H., Arrey, T. N., *et al.*, Lipid particles/droplets of the yeast *Saccharomyces cerevisiae* revisited: lipidome meets proteome. *Biochim Biophys Acta* 2011, 1811, 1165-1176.
- [20] Kaneshiro, T., Marr, A. G., cis-9, 10-Methylene hexadecanoic acid from the phospholipids of *Escherichia coli*. *J. biol. Chem* 1961, 236, 2615-2619.
- [21] Chen, Y., Partow, S., Scalcinati, G., Siewers, V., Nielsen, J., Enhancing the copy number of episomal plasmids in *Saccharomyces cerevisiae* for improved protein production. *FEMS Yeast Res* 2012, 12, 598-607.
- [22] Ro, D.-K., Paradise, E. M., Ouellet, M., Fisher, K. J., *et al.*, Production of the antimalarial drug precursor artemisinic acid in engineered yeast. *Nature* 2006, 440, 940-943.
- [23] Chen, Y., Daviet, L., Schalk, M., Siewers, V., Nielsen, J., Establishing a platform cell factory through engineering of yeast acetyl-CoA metabolism. *Metabolic engineering* 2013, 15, 48-54.

Table 5.1 Recombinant yeast strains engineered for enhanced CFA production in this study

Strain	Description	Promoters (respectively)
Control	BY4741 - empty vectors ^a	None
CP1	BY4741 - <i>Ec.CFAS</i>	GAL1
CP2	BY4741 - <i>Ec.CFAS</i> - $\Delta Tgl3$	GAL1
CP3	BY4741 - <i>Ec.CFAS</i> - $\Delta Tgl3$ - <i>Ald6</i> - <i>SeACS</i> ^{L641P}	GAL1, PGK1, TEF1
CP4	BY4741 - <i>Ec.CFAS</i> - <i>AtDGAT1</i>	GAL1, GAL10
CP5	BY4741 - <i>Ec.CFAS</i> - <i>AtDGAT1</i> - $\Delta Tgl3$	GAL1, GAL10
CP6	BY4741 - <i>Ec.CFAS</i> - <i>AtDGAT1</i> - $\Delta Tgl3$ - <i>Ald6</i> - <i>SeACS</i> ^{L641P}	GAL1, GAL10, PGK1, TEF1

^apSP-GM2, pIYC04, pESC-leu2d [21-23]

Tgl3, yeast triglyceride lipase 3

Ald6 - *SEACS*^{L641P}, Addgene plasmid # 64742 [23]

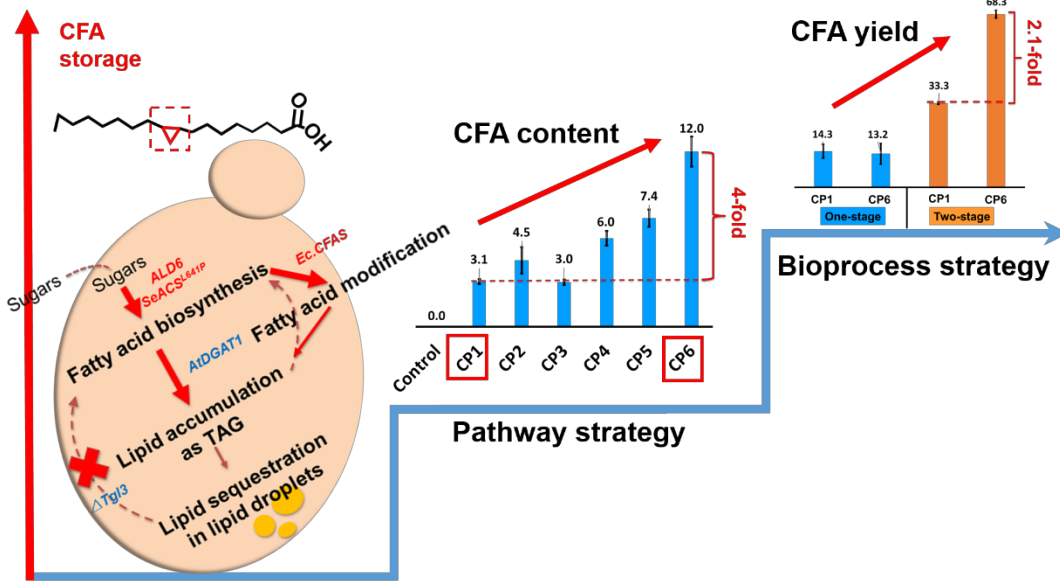
AtDGAT1, *A. thaliana* diacylglycerol acyl transferase 1

Δ indicates endogenous gene was knocked out.

Figure captions

Figure 5.1 Comparison of fatty acid lipid-containing fractions in engineered yeast strains (A) total phospholipid (PL) content by dry cell weight (DCW), (B) total triacylglycerol (TAG) content by DCW, (C) CFA content in PL by DCW, (D) CFA content in TAG by DCW, (E) CFA percentage of total FA within PL fraction, (F) CFA percentage of total FA within TAG fraction. The error bars represent the standard deviation of three biological replicates for each sample.

Figure 5.2 (A) Cell growth and (B) CFA yield of CP1 and CP6 at 72 h post-induction produced via one-stage or two-stage bioprocess. The error bars represent the standard deviation of three biological replicates for each sample.



TOC Graphic

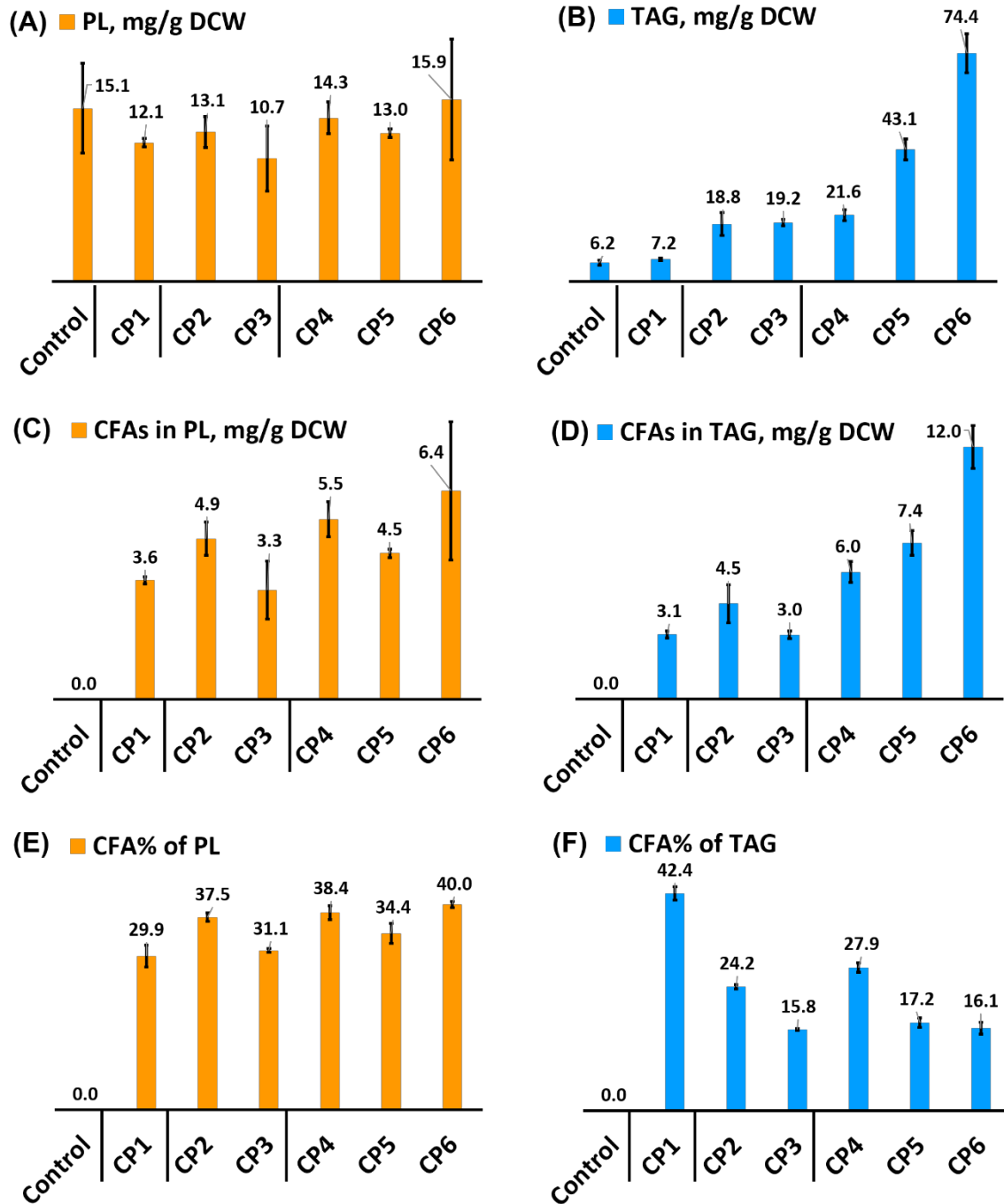


Figure 5.1

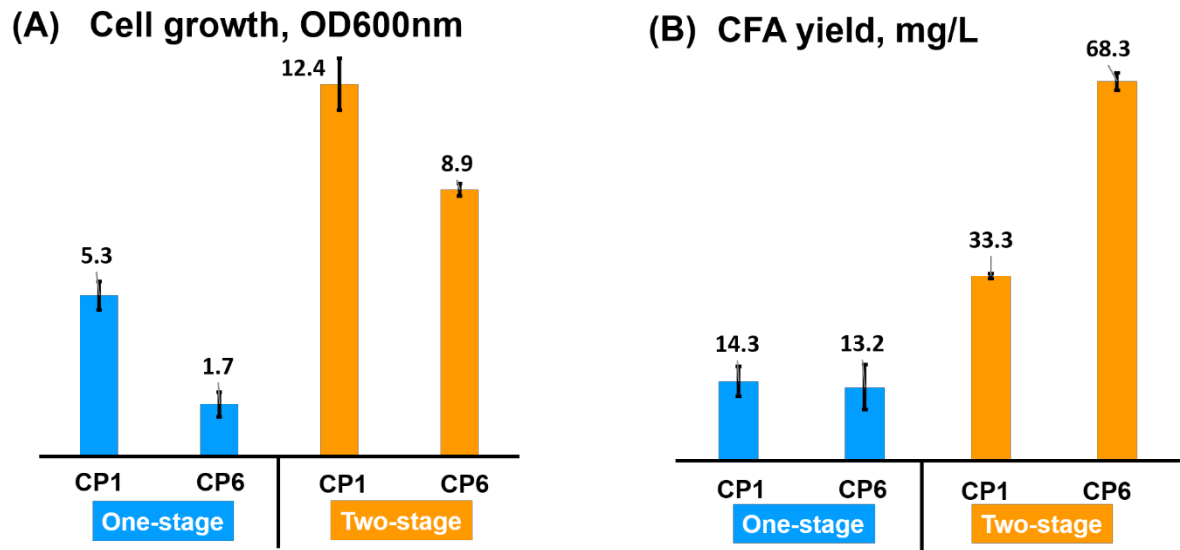


Figure 5.2

Supplementary materials for

Enhanced production of high-value cyclopropane fatty acid in yeast engineered for increased lipid synthesis and accumulation

Huadong Peng, Lizhong He, Victoria S. Haritos*

Department of Chemical Engineering, Monash University, Clayton, Vic 3800, Australia

Correspondence: Victoria S. Haritos, Department of Chemical Engineering, Monash University, Clayton, Vic 3800, Australia

Email: victoria.haritos@monash.edu

Materials and methods

1. Neutral lipid content by Bodipy 493/503 staining by flow cytometry

Cell growth was monitored by optical density (OD) at 600 nm using DR 5000™ UV-Vis Spectrophotometer. Harvested cells were adjusted into 10^6 /mL (OD ~ 0.2), washed twice using $1\times$ PBS buffer (pH 7.4), and resuspended in 1 mL fresh PBS buffer. BODIPY 493/503 (final concentration 1 μ M) was added to cells and incubated in the dark at room temperature for 5 min. Individual cell fluorescence was measured after excitation via the violet laser 488 nm and emission via the FITC filter using a CytoFlex (Beckman Coulter, USA). More than 10,000 cells were measured for each sample and the data acquired was analyzed further by the software CytExpert Ver.2.0.

2. Lipid extraction and separation

Harvested cells were pelleted by centrifugation at 3000 rpm for 5 min, frozen at -80°C for ~ 1 h and subsequently freeze-dried overnight using a FreeZone® 4.5 Liter Freeze Dry Systems (Labconco Corporation, USA) to obtain the dry cell weight (DCW) of each culture. Bligh

Dyer extraction with slight modification was used to extract the lipids as follows [1]. ~20 mg dry cells, 20 μL of 10 mg/mL glyceryl tritridecanoate (internal standard), 400 μL glass beads, and 1.5 mL of methanol: chloroform (2: 1) were added into a test tube, vortexed 6 min, then 500 μL chloroform was added and vortexed for an additional 1.5 min. Millipore H_2O (500 μL) was added and the mixture vortexed again for 1.5 min then filtered through a 0.45 μm PTFE filter into a clean test tube, centrifuged at 5000 rpm for 5 min at room temperature to separate into two phases. The lower chloroform layer containing the lipids was recovered with glass syringe and transferred to a fresh, clean test tube (keep glass syringe with gentle positive pressure) and the recovered volume (~500 μL) recorded.

After the chloroform layer was removed in a gentle N_2 stream, the extracted lipids (dissolved in ~30 μL chloroform) were separated by thin layer chromatography (TLC) [2], into phospholipid and triacylglycerol (TAG) as below. 10 μL solvent sample was applied to activated aluminium TLC plate (25 x 75 mm) using 10 μL capillary tubes and the TLC was developed with the solvent mixture: hexane/diethyl ether/acetic acid (70/30/1, v/v/v). Once the plate was developed, the plate was air dried.

3. Lipid quantification by GC

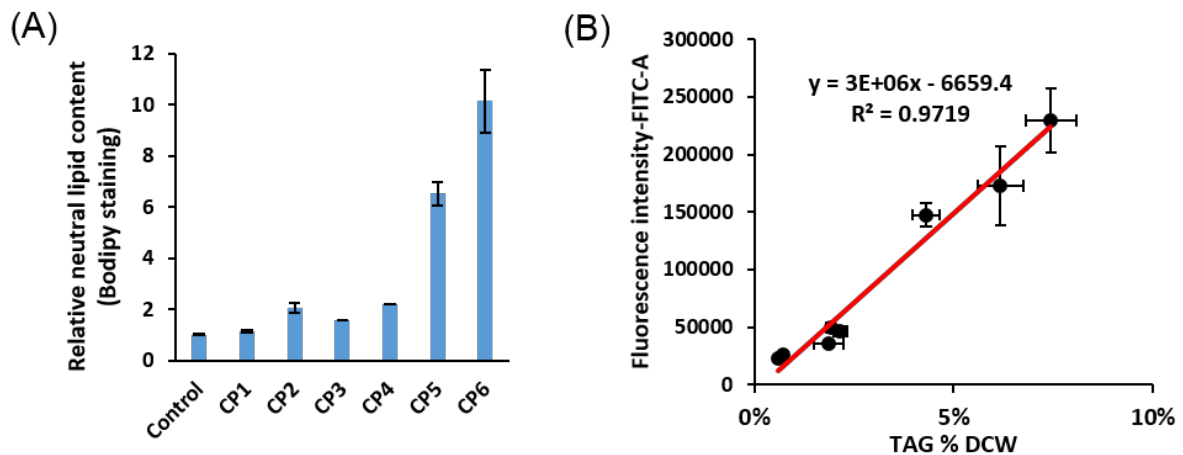
Bands on the TLC plate equating to TAG and PL were scraped from the plate and treated with 2 mL methanol/hydrochloric acid/chloroform (10:1:1, v/v/v) and heated at 80°C for 1 h in sealed test tubes to convert lipids to fatty acid methyl ester (FAME). FAME was washed with 0.9% NaCl solution (1 mL) and extracted with hexane after mixing. FAME samples (1 μL) were analyzed by Agilent 7890A gas chromatography with flame ionization detection (GC-FID) as described previously [3].

Figure Captions

Figure S1 (A) Relative neutral lipid content measured by flow cytometry and averaged from cells stained with Bodipy 493/503, control response was normalized to 1. (B) Linear regression of neutral lipid content measured by GC analysis of FAME and average fluorescence intensity measured via Bodipy 493/503 staining. The error bars represent the standard deviation, three biological replicates for each sample.

Figure S2 Examples of GC-FID chromatograms of fatty acid methyl ester derivatives of yeast lipids extracted from TAG portion of (A) control and (B) CP1 strain yeast.

Figure S3 Comparison of cell growth (measured by OD600 nm) after 72 h for control and yeast strains (CP1 - 6) engineered to produce CFA. The error bars represent the standard deviation, three biological replicates for each sample.

**Figure S1**

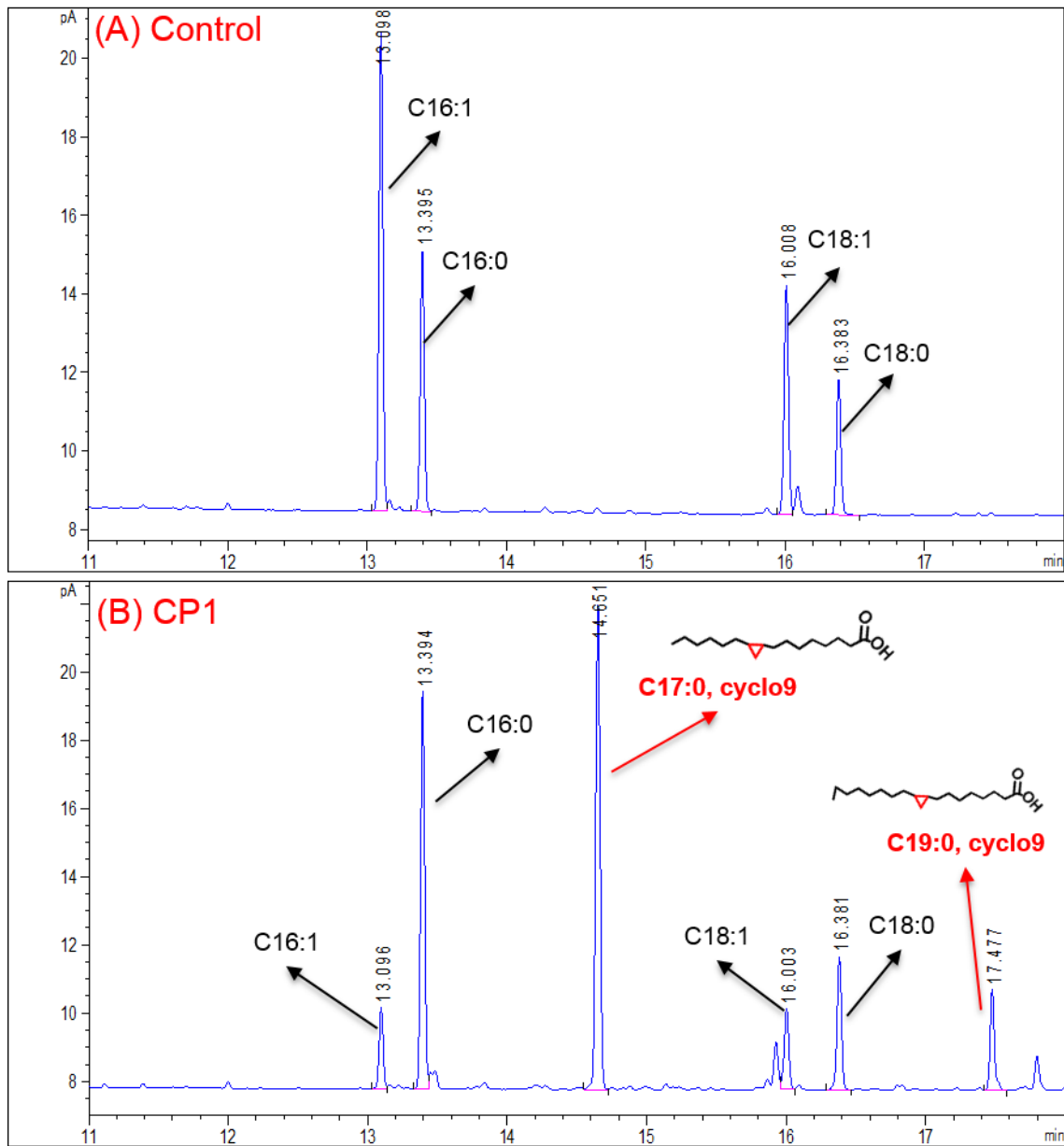


Figure S2

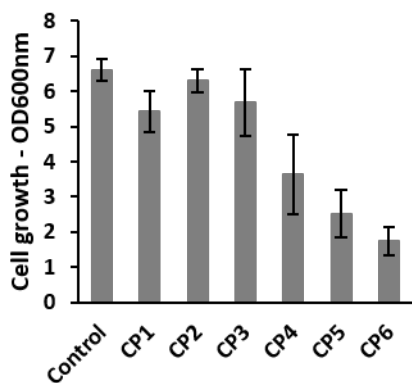


Figure S3

References

- [1] Bligh, E. G., Dyer, W. J., A rapid method of total lipid extraction and purification. *Canadian Journal of Biochemistry and Physiology* 1959, 37, 911-917.
- [2] Knittelfelder, O. L., Kohlwein, S. D., Thin-layer chromatography to separate phospholipids and neutral lipids from yeast. *Cold Spring Harbor Protocols* 2017, 2017, pdb. prot085456.
- [3] Peng, H., Moghaddam, L., Brinin, A., Williams, B., *et al.*, Functional assessment of plant and microalgal lipid pathway genes in yeast to enhance microbial industrial oil production. *Biotechnol Appl Biochem* 2018, 65, 138-144.

This page is intentionally blank

CHAPTER 6

FLOW CYTOMETRY-BASED

PHYSIOLOGICAL CHARACTERISATION

AND TRANSCRIPTOME ANALYSES

REVEAL A MECHANISM FOR REDUCED

CELL VIABILITY IN YEAST ENGINEERED

FOR INCREASED LIPID CONTENT

**: This chapter has been submitted to Biotechnology for Biofuels.*

Peng, H., He, L., Haritos, V. S., Enhanced production of high-value cyclopropane fatty acid in yeast engineered for increased lipid synthesis and accumulation. Biotechnology for Biofuels (submitted)

This page is intentionally blank

Chapter 6 Flow cytometry-based physiological characterisation and transcriptome analyses reveal a mechanism for reduced cell viability in yeast engineered for increased lipid content

6.1. Abstract

Yeast has been the focus of development of cell biofactories for the production of lipids and interest in the field has been driven by the need for sustainably sourced lipids for use in a broad range of industrial applications. Previously we reported a metabolic engineering strategy for enhanced lipid production in yeast which delivered high per-cell lipid but with low cell growth and compromised physiology. To investigate the relationship between lipid engineering and cellular physiological responses and to identify further metabolic engineering targets, we analysed transcriptomes and measured cell physiology parameters in engineered strains. In the engineering strategy, central carbon pathway was reprogrammed to provide more precursors for lipid production and the steps of accumulation and sequestration were enhanced through the expression of additional genes. Flow cytometry analysis of fluorescent-dye stained cells showed highest radical oxygen species (ROS) levels and mitochondrial membrane potential ($\Delta\psi_m$) in cells with highest lipid content supporting the known relationship between mitochondrial activity and ROS generation. The downregulated pentose phosphate and beta-oxidation pathways and downregulated genes for ATP and NADPH biosynthesis, indicated that the intracellular energy supplies were limited and the redox environment was unbalanced, which could be regarded as targets for further lipid engineering. Thus, lipid pathway engineering has an important effect on the central carbon pathway, directing these towards lipid production and sacrificing the precursors, energy and cofactor supply to satisfy homeostatic metabolic requirements.

Keywords: metabolic engineering, triacylglycerol, reactive oxygen species, mitochondria membrane potential, transcriptome

6.2. Introduction

Increasing market demand and broad applications of oleochemicals have made novel and sustainable routes to their production targets for research over the last decade (Pfleger et al., 2015). Compared with the traditional conversion of plant oils and animal fats, the approach of using a microbial chassis presents a lot of advantages, such as feedstock availability and feedstock-product flexibility (Marella et al., 2018). Much progress in improving microbial lipid production levels has been made, which brings them closer to commercialization (Qiao et al., 2017; Xu et al., 2017). Yeast, *Saccharomyces cerevisiae*, as a popular model and industrial microbe, has been widely investigated for lipid production and more broadly as a model for lipid engineering of oleaginous yeasts. Yeast engineered for enhanced standard and unusual lipids production have been constructed by a selective combination of genes supporting the steps of fatty acid biosynthesis and modification, lipid accumulation and sequestration (Béopoulos et al., 2014; Markham & Alper, 2018; Peng et al., 2018b). In our prior research we observed that lipid pathway modification markedly increased the intracellular lipid content but also led to reduced cell growth and membrane integrity which affected the volumetric lipid yield (Peng et al., 2018b).

Investigation of the basis of productivity loss and physiological impacts to cells subject to lipid pathway engineering may reveal mechanisms that could be addressed through further genetic modification or culture conditions, as examples. Two powerful approaches for revealing the responses of cells to metabolic engineering include transcriptome and physiological parameter analysis. While there have been few prior reports of transcriptomic analyses of yeast engineered for enhanced lipid production (de Jong et al., 2016), analysis has revealed likely oxidative stress impacts on cell growth and additional demand for NADPH in yeast engineered

for high production of fatty acid esters. Technologies that have been used for transcriptome analysis include Sanger, microarray and RNA-seq, the latter shows advantages such as higher resolution, identification of novel transcripts and avoids background noise associated with fluorescence quantification and has become the dominant technology in research (Nookaew et al., 2012). Regardless of the technology used, transcriptomics has been broadly applied to great effect in the study of cell metabolism (Nookaew et al., 2012).

Cell physiological measurements such as cell growth, soluble metabolite production and lipid yields are commonly reported in yeast metabolic engineering research. However, these measures are limited by two aspects: they report an averaged response of the culture, and physiological states are inferred from metabolite profiles. Flow cytometry, when coupled with validated fluorescent dyes, can address these deficiencies as the technique measures cells individually and suitable dyes can be selected to measure intracellular functions. Flow cytometry has been widely used for the measurement of cell membrane integrity (CMI) of cells treated with the fluorescent dye propidium iodide, as a key measure of general cell health, and detection of reactive oxygen species (ROS) is often used to evaluate the cellular redox environment and oxidative stress. ROS is harmful to cells as it could damage DNA or RNA, oxidize polyunsaturated fatty acids, amino acids and co-factors. Mitochondria are critical organelles implicated in the production of ROS in the cell as a normal consequence of aerobic metabolism (Cadenas et al., 1977) and their function can also be probed using flow cytometry with the addition of appropriate dyes. Mitochondrial membrane potential ($\Delta\psi_m$) generated by proton pumps (Complexes I, III and IV) is an important index for functional mitochondria (Zorova et al., 2018).

Here we employed complementary technologies of RNA-seq transcriptomic analysis and flow-cytometry-based physiological characterisation to investigate the performance and viability of yeast at different stages of lipid pathway engineering (Fig. 6.1). In this study, engineered strains of *S. cerevisiae* were compared by genome-wide transcription analysis and functional assessment of cell membrane integrity and mitochondria and these were supported by selected metabolite analyses. The purpose of the study was to identify the impacts of lipid pathway engineering on cell physiology and to identify potential further engineering targets for enhanced lipid production plus cell health, for the ultimate goal of improving production to economically competitive levels.

6.3. Materials and methods

6.3.1. Strains

In this study, strains from two engineered series (HBY and CBY) described in Chapter 4 and 5 (Peng et al., 2018a; Peng et al., 2018b), that were engineered for improved standard lipids and cyclopropane fatty acid production were selected for analysis. All the engineered strains were constructed based on the parent strain BY4741 (MATa his3 Δ 1 leu2 Δ 0 met15 Δ 0 ura3 Δ 0), and the details of plasmids and strains are listed in Table 1.

6.3.2. Cell culture

Detailed culture conditions have been described earlier (Peng et al., 2018b) and given in brief below. The engineered yeast strains were maintained based on their auxotrophy using yeast synthetic complete (SC) minimal medium, which contains 6.7 g/L of yeast nitrogen base, 20 g/L glucose plus a mixture containing appropriate nucleotide bases and amino acids for the various dropout options (SC-Leu, SC-His-Leu, SC-His-Leu-Ura). For the induction medium, glucose was replaced with 2% (w/v) galactose and 1% (w/v) raffinose. The seed culture was

prepared by inoculating a single transformed colony into five mL yeast SC minimal medium and incubating at 30°C, 250 rpm, overnight. The culture was diluted using SC induction medium to make the initial OD_{600 nm} value of approximately 0.4, incubated at 30°C and 250 rpm.

6.3.3. Antioxidant addition to cell culture

Two antioxidants (vitamin C and resveratrol) were selected to test their effects on the cell physiology of strain HBY31. Cell growth was evaluated in the absence and presence of vitamin C or resveratrol (0.5 μ M and 2.5 mM, respectively) added to media in 48-well plates. Seed cultures of control and HBY31 cells were dispensed into each well and diluted to an initial OD_{600nm} of 0.2. The microplates were incubated at 30°C, and OD_{600nm} was measured every 30 min using the Tecan microplate reader (Vázquez et al., 2017). Cell samples were taken at 24 h for flow cytometry analysis.

6.3.4. RNA-Seq analysis

Samples for transcriptome analysis were taken at 24 h post-induction during late exponential phase growth. ~ 20 ml cell culture for each strain was directly cold (-4°C) centrifuged to obtain the cell pellets, which were washed quickly with autoclaved PBS buffer once and then centrifuged again. Then the cell pellets were directly frozen in liquid nitrogen and stored at -80°C before shipping for RNA-Seq analysis and stored on dry ice. The RNA extraction, library preparation (250–300 bp insert cDNA library), RNA sequence analysis and assembly were conducted by Novogene, Hong Kong. The detailed method is provided in the supplementary material.

6.3.5. Cell physiology characterization

Cell growth was monitored by optical density (OD) at 600 nm using DR 5000™ UV-Vis Spectrophotometer. Harvested cells were adjusted into 10^6 /mL (OD ~ 0.2), washed twice using 1× PBS buffer (pH 7.4), and resuspended in 1 mL fresh PBS buffer, then the cells were ready for flow cytometry analysis for neutral lipid content, cell membrane integrity (CMI) , reactive oxygen species (ROS) level, and mitochondria membrane potential ($\Delta\psi_m$). In the following analyses, following staining cells were kept in the dark to avoid photobleaching. Individual cell fluorescence measured using the violet laser 488 nm on a CytoFlex (Beckman Coulter, USA) under PE or FITC filter. More than 10,000 cells were measured for each sample and the data acquired was analyzed further by the software CytExpert Ver.2.0.

For neutral lipid content analysis, BODIPY 493/503 was used to stain the cells with a final conc. of 1 μ M and incubated at room temperature for 5 min before reading under FITC filter. The stained cells were also used for lipid droplet visualization by a Leica Microsystems SP5 confocal microscope coupled with HCX PL APO 63 \times /1.4 OIL CS oil immersion objective (Leica, Wetzlar, Germany) (Peng et al., 2018c).

For CMI and ROS analysis, the cell samples were firstly stained with CM-H₂DCFDA (Thermo Fisher Scientific, USA) with a final conc. of 5 μ M and incubated at 30 °C, 250 rpm for 30 min, then stained with propidium iodine (PI) (ThermoFisher, USA) with a final conc. of 5 μ g/mL, and run immediately through flow cytometry under both FITC and PE filter, which could reflect the ROS level and cell membrane integrity, respectively.

TMRE (tetramethylrhodamine, ethyl ester) (Abcam, UK) was used to analyse the mitochondrial membrane potential ($\Delta\psi_m$). Freshly washed cells were treated with TMRE with a final conc. of 0.5 nM, and incubated at 30°C, 250 rpm for 20 min before flow cytometry

analysis using the PE filter. The depolarization (negative) control was prepared by treating the cells with 20 μ M FCCP (carbonyl cyanide 4-(trifluoromethoxy) phenylhydrazone) 10 min before adding TMRE.

6.4. Results and Discussion

6.4.1. Whole transcriptome view of gene expression among strains engineered for standard lipid production by Degust analysis

The transcriptome-wide view of gene expression among engineered strains was analysed using the Degust program (<http://degust.erc.monash.edu/>) which has an element of principal component-like analysis (PCA) analysis developed specifically for transcriptomics data. HBY series strains including control, HBY03, 14, 20, 24, 25, 27, 28 and 31 were distributed based on the distance between MDS dimensions 1 vs 2 (Fig. 6.2A). The sum percentage of Dimension 1 and 2 was > 60% (Fig. 6.2B), which indicated these were the major components that represent the whole gene expression situation.

The number of differential expressed (DE) genes in the engineered strains VS control was compared and are summarized in Fig. 6.2C, including the number of total DE genes, upregulated genes and downregulated genes. Based on the number of total DE genes, the 8 strains could be divided into three groups, one group with total DE genes ~150 including strain HBY03, 14 and 27, one group with total DE genes ~200 including strain HBY20, 24, 25, another group with total DE genes ~300 including strain HBY28, 31. In the Venn diagram (Fig. 6.2D), there were 42 DE genes among the four engineered strains HBY14, 20, 27 and 31, and 111 DE genes between HBY14 and HBY20, 204 DE genes between HBY27 and HBY31. Of interest was that the expression of *Ald6*, *SeACS^{L641P}* and/or *AtClo1* caused more DE genes in strains HBY20, 28 and 31.

The distance between two strains in the MDS plot determines the similarity of overall gene expression between the two strains. Taken together the distance in the MDS plot and the DE genes numbers, four representative engineered strains HBY14, 20, 27 and 31 were selected for detailed transcriptome analysis to explore relationships between DE genes and lipid pathway modification.

6.4.2. Global transcriptional profiling emphasising central metabolic and mitochondrial pathways

Lipid pathway modification with target genes of interest

Lipid pathway modification in yeast incorporated three steps including FA biosynthesis, lipid accumulation and sequestration. Strain HBY14 was constructed with enhanced lipid accumulation and sequestration through heterologous expression of *AtDGATI* and knock out of the major TAG lipase knockout (*Tgl3Δ*). Strain HBY20 was built on HBY14 by additional expression of genes for FA biosynthesis *Ald6* and an acetyl-CoA synthetase variant from *Salmonella enterica* (*SeACS^{L641P}*). Strain HBY27 further enhanced HBY20 by increasing malonyl-CoA supply by the expression of *ACCI***. Strain HBY31 extended HBY27 through the addition of *AtClo1*, a lipid droplet-stabilising protein from *Arabidopsis thaliana*.

Regarding the expression levels of introduced genes (Fig. 6.3), *Ald6* was generally higher and *ACCI*** lower than other target genes. Of further note, the *ACCI*** expression level was almost 5-fold higher in strain HBY27 than other strains. Moreover, *AtDGATI*, *AtClo1* in strain HBY31 showed almost 9-fold higher expression levels than other strains. Considering the neutral lipid content (Bodipy and Nile red staining, Fig. 6.4A-B) among the four engineered strains, HBY20 showed the highest, followed by strains HBY31, 27 and 14. The lipid levels of these strains supported the effectiveness of the engineering strategy.

Heterologous expression of *AtDGAT1* did not change the transcription level of the endogenous *DGA1*, except a slight upregulation on HBY27 (data not shown); similarly knockout of *Tgl3* did not alter expression of other TAG lipases genes *Tgl1-2* and *Tgl4-5* in engineered strains except the downregulation of these in HBY31 (Fig. 6.5). Interestingly, *LRO1* and *ARE1*, responsible for triglyceride and sterol synthesis respectively, were upregulated in strains HBY20, 27 and 31 which suggests that the current lipid accumulation and sequestration strategy was insufficient for demand and there was a requirement for additional lipid accumulation activity for lipid droplet formation. *ARE1*, *LRO1* were more highly upregulated in HBY31 and TAG lipases more downregulated than in strain HBY27; these two strains differ only by the addition of *AtClo1*. Caleosin was proposed to modify lipid droplet membrane function and increase size by impairing lipase accessibility to lipid bodies, inhibiting storage lipid degradation (Froissard et al., 2009). This is due to the special non-canonical structure of caleosin, with a long central hydrophobic region surrounded by two hydrophilic C- and N-terminal regions (Chen & Tzen, 2001).

Effect of lipid engineering on other metabolic enzymes

The engineered strains showed up-regulated genes for pathways for lipid precursor production such as: acetyl-CoA, malonyl-CoA, acyl-CoA, and down-regulated lipid degradation pathways (Fig. 6.4). Expression profiles of orthologues of the introduced genes for FA biosynthesis such as *Ald5*, *ACS1*, *ACS2*, *ACC1* were also upregulated (Fig 6.5) which likely contributed to overall fatty acid synthesis. Lipid pathway engineering resulted in upregulation of related enzymes including fatty acid synthetases (*FAS1*, *FAS2*), acyl-CoA-binding protein (*ACB1*) and fatty acyl-CoA synthetases (*FAA1-4*, *FAT1*) which may have enhanced fatty acid biosynthesis and activation to form fatty acyl-CoA. This agreed, in part, with a previous report (de Jong et al.,

2016), however, in our study the fatty acid consumption process via β -oxidation was also upregulated, as encoded by *TES1*, *POX1*, *FOX2*. In many cases of the expression profile, HBY31 was an exception, such as, downregulation of expression of β -oxidation genes and many of the central carbon pathway and TAG lipase genes whereas these genes were majorly upregulated in the other engineered strains.

Effect of lipid pathway modification on redox pathways

The pentose phosphate pathway (PPP) is considered to be the primary source of NADPH supply in the cell (Wasylenko et al., 2015) which is highly consumed during the reduction steps of fatty acid synthesis. The engineered strains showed overall downregulation of key genes involved in the PPP including *ZWF1*, *GND2*, *TKL2* and *RKII* which suggests NADPH supply was impaired in these strains. Similar expression responses were reported for yeast cells engineered for fatty esters production (de Jong et al., 2016).

Compared to control yeast, the glycerol production pathway encoded by *GDP1*, *GDP2*, *GPP1*, *GPP2* was upregulated and the glycerol catabolism pathway encoded by *YIG1*, *DAK2*, *GUT1* was downregulated in the engineered strains (Fig. 6.5). This agreed with higher media glycerol concentrations in these strains compared with than control (Fig. 6.4D). An upregulated glycerol biosynthesis pathway may have been required to balance NADH and osmotic stress (Modig et al., 2007). Gene expression for the ethanol biosynthesis pathway e.g. alcohol dehydrogenase (*ADH1*) was downregulated in engineered strains together with upregulation of ethanol catabolism genes (e.g. *ADH2*); this result agreed with lower ethanol production in engineered strains except for strain HBY27 (Fig. 6.4C). In the case of strain HBY27, additional alcohol dehydrogenase genes (*ADH2*, *ADH5*, *ADH6*) were upregulated and this may have caused an increase in ethanol production.

Overall, lipid pathway engineering impaired redox pathways and redirected carbon flux from ethanol biosynthesis to lipid and glycerol production. As lipid biosynthesis and derived products require a large quantity of NADPH (synthesis of one palmitate requires 14 NADPH), increasing NADPH supply has been the focus of several studies to improve the production of ethanol and fatty esters (Bro et al., 2006; Shi et al., 2014). Thus, downregulation of the PPP and β -oxidation may explain the slow growth of the more engineered strains HBY20 and HBY31.

6.4.3. Cellular physiological characterisation and corresponding regulated genes/pathways

Effect of lipid pathway modification on ROS production and mitochondrial function

The relationship between cellular physiological responses and differential gene expression was examined in detail using strain HBY31 in comparison to control. Cell growth and CMI were much lower for strain HBY31, accompanied with higher ROS (Fig. 6.6A-C). We speculated that lower CMI may be due to higher ROS level in the cell (Trancikova et al., 2004), and that higher ROS may be due to greater mitochondrial activity as the mitochondria is the major organelle to produce ROS in the cell. However, while there was higher mitochondrial membrane potential measured in the HBY31 cells (Fig 6.6D), more genes coding for mitochondria and mitochondrial membrane were downregulated in this strain compared with control (Fig. 6.6E). This contradiction between physiological and transcriptomic analyses may reflect dynamic changes occurring at the specific time point of sampling (24 h) and warrants further investigation over a broader timeframe.

ROS species including hydrogen peroxide (H_2O_2), superoxide radical (O_2^-) and hydroxyl radical ($\cdot\text{OH}$) cause damage to cells and are metabolised via multiple pathways (indicated in

Fig. 6.6F). In HBY31, genes involved in the respiratory chain and ATP synthesis were downregulated and in the conversion of H_2O_2 from O_2^- may have been affected by *Sod2p* downregulation. Furthermore, genes coding for catalases (*Ctt1p* and *Cta1p*), glutathione-dependent enzymes (*GPX1*, *Grx1*, 3) and glutathione transferases (*GSH1*) which protect the cell from ROS damage were all downregulated. This loss of protection may explain the higher ROS level measured in HBY31 compared with control (Fig 6.6 C).

Energy balance

Most genes responsible for ATP and NADPH synthesis were downregulated in the respiratory chain of HBY31, which indicated the energy and reducing agent or cofactor were limited in these cells. As examples, *Ndi1p*, the internal mitochondrial NADH dehydrogenase that transfers electrons to complex III of the respiratory chain and two aldehyde dehydrogenases (*Ald4*, 6) that contribute to NADPH synthesis, were downregulated. Therefore, unbalanced energy and reducing equivalents supply in strain HBY31 could lower cell growth and reduce CMI.

6.4.4. Potential for oxidative stress generation in lipid pathway engineering

Effect of antioxidants

As HBY31 consistently measured elevated intracellular ROS levels (Fig. 6.6), it is reasonable to suggest that the addition of antioxidants to the culture medium may reduce or eliminate ROS. As previously reported, engineering oxidative stress defense pathways in yeast alleviated ROS and improved standard lipid and PUFA production (Qiao et al., 2017; Xu et al., 2017; Zhang et al., 2018). Two well-studied antioxidants, vitamin C and resveratrol, had previously demonstrated ability to moderate intracellular ROS level in yeast (Dani et al., 2008; Nikolić et al., 2006), and these were applied, separately, to yeast expression induction medium of control

and strain HBY31 and the effects monitored for 24 h. Antioxidant addition did not affect cell growth of control (Fig. 6.7A), while resveratrol slightly improved the cell growth of strain HBY31, and vitamin C slightly reduced growth (Fig. 6.7B). Opposite to expectations, the antioxidants had a negative effect on control cells: membrane integrity was reduced, and ROS and mitochondrial membrane potential were increased. Whereas, these parameters were mostly unaffected in HBY31 and ROS levels remained high (Fig. 6.7C-E). Therefore, employing vitamin C or resveratrol to reduce ROS and improve membrane integrity in HBY31 was not successful suggesting that supplementation of the culture media will not reverse the growth and cell health issues with the strain.

Cell membrane modification by cyclopropane fatty acid biosynthesis

Cyclopropane fatty acid (CFA) incorporation into cellular phospholipid membranes has been reported to increase stress tolerance in organisms such as *E. coli* in response to an acidic environment (Chang & Cronan, 1999). The higher oxidative stability of CFA compared with unsaturated fatty acids may also be an advantage in the protection of membranes. We hypothesised that CFA in membranes might improve membrane integrity and cell growth in compromised engineered yeast strains. To test this, two strains were directly compared: HBY20 expressing *AtDGAT1*, *Ald6-SeACS^{L641P}*; $\Delta Tgl3$ and CBY20 which contained the same genes plus an additional *Ec.CFAS*. CFA concentration in the phospholipid fraction of CBY20 was measured at ~40% and unsaturated FA percentage was reduced from 64 to 25% (Fig. 6.8A). This result verified the inclusion of CFA into phospholipid membranes in the CBY20 strain.

Cell growth of CBY20 was lower (Fig. 6.8B), and ROS levels were unchanged from that for HBY20 (Fig. 6.8C) whereas mitochondrial membrane potential ($\Delta\psi_m$) was similar between CBY20 and control and did not show the large increase that HBY20 exhibited at 72 h (Fig.

8D). These outcomes could be explained by the requirement for unsaturated FAs in maintaining membrane fluidity and cell growth in *S. cerevisiae* which is not satisfied by incorporation of CFA (Doi et al., 1978; Henderson & Block, 2014) and that ROS generated internally may not be targeting membrane phospholipids to damage membrane integrity.

6.5. Conclusions

This study investigated the relationships between transcriptomic profile and cellular physiological responses of yeast engineered for increased lipid production. The transcriptomic analysis showed the lipid engineering strategy redirected the global metabolic pathway towards lipid production, such as upregulated pathways for the production of precursors including acetyl-CoA, malonyl-CoA and acyl-CoA, etc. Glycerol biosynthesis pathway was also upregulated and ethanol biosynthesis and the PPP were downregulated. ROS levels were consistently high in engineered strains but so also was mitochondrial membrane potential; as mitochondria are the main source of ROS in the cell, high ROS is likely a result of the high mitochondrial activity. The high ROS and low membrane integrity of the engineered strain HBY31 were not reversed by addition of antioxidants to the culture media or by altering the membrane lipids to include high concentrations of saturated CFA. These results suggest elevated ROS levels are not the primary cause of reduced membrane integrity or low cell growth. Moreover, the downregulated ATP and NADPH synthesis pathways suggested the intracellular energy supply was limited and redox levels were unbalanced in the engineered cells, which are promising targets for further lipid pathway engineering.

References

Anders, S., Huber, W. 2010. Differential expression analysis for sequence count data. *Genome biology*, **11**(10), R106.

- Béopoulos, A., Verbeke, J., Bordes, F., Guicherd, M., Bressy, M., Marty, A., Nicaud, J.-M. 2014. Metabolic engineering for ricinoleic acid production in the oleaginous yeast *Yarrowia lipolytica*. *Applied microbiology and biotechnology*, **98**(1), 251-262.
- Bro, C., Regenber, B., Förster, J., Nielsen, J. 2006. In silico aided metabolic engineering of *Saccharomyces cerevisiae* for improved bioethanol production. *Metabolic engineering*, **8**(2), 102-111.
- Cadenas, E., Boveris, A., Ragan, C.I., Stoppani, A.O. 1977. Production of superoxide radicals and hydrogen peroxide by NADH-ubiquinone reductase and ubiquinol-cytochrome c reductase from beef-heart mitochondria. *Archives of biochemistry and biophysics*, **180**(2), 248-257.
- Chang, Y.Y., Cronan, J.E. 1999. Membrane cyclopropane fatty acid content is a major factor in acid resistance of *Escherichia coli*. *Molecular microbiology*, **33**(2), 249-259.
- Chen, J.C., Tzen, J.T. 2001. An in vitro system to examine the effective phospholipids and structural domain for protein targeting to seed oil bodies. *Plant and Cell Physiology*, **42**(11), 1245-1252.
- Dani, C., Bonatto, D., Salvador, M., Pereira, M.D., Henriques, J.A.P., Eleutherio, E. 2008. Antioxidant Protection of Resveratrol and Catechin in *Saccharomyces cerevisiae*. *Journal of Agricultural and Food Chemistry*, **56**(11), 4268-4272.
- de Jong, B.W., Siewers, V., Nielsen, J. 2016. Physiological and transcriptional characterization of *Saccharomyces cerevisiae* engineered for production of fatty acid ethyl esters. *FEMS yeast research*, **16**(1), 1-9.
- Doi, O., Doi, F., Schroeder, F., Alberts, A.W., Vagelos, P.R. 1978. Manipulation of fatty acid composition of membrane phospholipid and its effects on cell growth in mouse LM cells. *Biochim Biophys Acta*, **509**(2), 239-50.
- Froissard, M., D'Andrea, S., Boulard, C., Chardot, T. 2009. Heterologous expression of AtClo1, a plant oil body protein, induces lipid accumulation in yeast. *FEMS Yeast Res*, **9**(3), 428-38.

- Henderson, C.M., Block, D.E. 2014. Examining the Role of Membrane Lipid Composition in Determining the Ethanol Tolerance of *Saccharomyces cerevisiae*. *Applied and Environmental Microbiology*, **80**(10), 2966-2972.
- Marella, E.R., Holkenbrink, C., Siewers, V., Borodina, I. 2018. Engineering microbial fatty acid metabolism for biofuels and biochemicals. *Current Opinion in Biotechnology*, **50**, 39-46.
- Markham, K.A., Alper, H.S. 2018. Engineering *Yarrowia lipolytica* for the production of cyclopropanated fatty acids. *Journal of Industrial Microbiology & Biotechnology*.
- Modig, T., Granath, K., Adler, L., Liden, G. 2007. Anaerobic glycerol production by *Saccharomyces cerevisiae* strains under hyperosmotic stress. *Appl Microbiol Biotechnol*, **75**(2), 289-96.
- Mortazavi, A., Williams, B.A., McCue, K., Schaeffer, L., Wold, B. 2008. Mapping and quantifying mammalian transcriptomes by RNA-Seq. *Nature methods*, **5**(7), 621.
- Nikolić, B., Stanojević, J., Vuković-Gačić, B., Simić, D., Knežević-Vukčević, J. 2006. The effects of vitamin C on oxidative DNA damage and mutagenesis. *Food Technology and Biotechnology*, **44**(4), 449-456.
- Nookaew, I., Papini, M., Pornputtpong, N., Scalcinati, G., Fagerberg, L., Uhlen, M., Nielsen, J. 2012. A comprehensive comparison of RNA-Seq-based transcriptome analysis from reads to differential gene expression and cross-comparison with microarrays: a case study in *Saccharomyces cerevisiae*. *Nucleic Acids Res*, **40**(20), 10084-97.
- Peng, H., He, L., Haritos, V.S. 2018a. Enhanced production of high-value cyclopropane fatty acid in yeast engineered for increased lipid synthesis and accumulation. *submitted*.
- Peng, H., He, L., Haritos, V.S. 2018b. Metabolic engineering of lipid pathways in *Saccharomyces cerevisiae* and staged bioprocess for enhanced lipid production and cellular physiology. *Journal of Industrial Microbiology & Biotechnology*, **45**(8), 707-717.

- Peng, H., Moghaddam, L., Brinin, A., Williams, B., Mundree, S., Haritos, V.S. 2018c. Functional assessment of plant and microalgal lipid pathway genes in yeast to enhance microbial industrial oil production. *Biotechnol Appl Biochem*, **65**(2), 138-144.
- Pfleger, B.F., Gossing, M., Nielsen, J. 2015. Metabolic engineering strategies for microbial synthesis of oleochemicals. *Metabolic engineering* **29**, 1-11.
- Qiao, K., Wasylenko, T.M., Zhou, K., Xu, P., Stephanopoulos, G. 2017. Lipid production in *Yarrowia lipolytica* is maximized by engineering cytosolic redox metabolism. *Nat Biotech*, **35**(2), 173-177.
- Robinson, M.D., McCarthy, D.J., Smyth, G.K. 2010. edgeR: a Bioconductor package for differential expression analysis of digital gene expression data. *Bioinformatics*, **26**(1), 139-140.
- Shi, S., Valle - Rodríguez, J.O., Siewers, V., Nielsen, J. 2014. Engineering of chromosomal wax ester synthase integrated *Saccharomyces cerevisiae* mutants for improved biosynthesis of fatty acid ethyl esters. *Biotechnology and bioengineering*, **111**(9), 1740-1747.
- Trancikova, A., Weisova, P., Kissova, I., Zeman, I., Kolarov, J. 2004. Production of reactive oxygen species and loss of viability in yeast mitochondrial mutants: protective effect of Bcl-xL. *FEMS Yeast Res*, **5**(2), 149-56.
- Trapnell, C., Williams, B.A., Pertea, G., Mortazavi, A., Kwan, G., Van Baren, M.J., Salzberg, S.L., Wold, B.J., Pachter, L. 2010. Transcript assembly and quantification by RNA-Seq reveals unannotated transcripts and isoform switching during cell differentiation. *Nature biotechnology*, **28**(5), 511.
- Vázquez, J., González, B., Sempere, V., Mas, A., Torija, M.J., Beltran, G. 2017. Melatonin Reduces Oxidative Stress Damage Induced by Hydrogen Peroxide in *Saccharomyces cerevisiae*. *Frontiers in Microbiology*, **8**, 1066.

Wasylenko, T.M., Ahn, W.S., Stephanopoulos, G. 2015. The oxidative pentose phosphate pathway is the primary source of NADPH for lipid overproduction from glucose in *Yarrowia lipolytica*. *Metabolic Engineering*, **30**, 27-39.

Xie, C., Mao, X., Huang, J., Ding, Y., Wu, J., Dong, S., Kong, L., Gao, G., Li, C.-Y., Wei, L. 2011. KOBAS 2.0: a web server for annotation and identification of enriched pathways and diseases. *Nucleic acids research*, **39**(suppl_2), W316-W322.

Xu, P., Qiao, K., Stephanopoulos, G. 2017. Engineering oxidative stress defense pathways to build a robust lipid production platform in *Yarrowia lipolytica*. *Biotechnology and Bioengineering*, **114**(7), 1521-1530.

Zhang, S., He, Y., Sen, B., Chen, X., Xie, Y., Keasling, J.D., Wang, G. 2018. Alleviation of reactive oxygen species enhances PUFA accumulation in *Schizochytrium* sp. through regulating genes involved in lipid metabolism. *Metabolic Engineering Communications*, **6**, 39-48.

Zhao, H., Chen, J., Liu, J., Han, B. 2015. Transcriptome analysis reveals the oxidative stress response in *Saccharomyces cerevisiae*. *RSC Advances*, **5**(29), 22923-22934.

Zorova, L.D., Popkov, V.A., Plotnikov, E.Y., Silachev, D.N., Pevzner, I.B., Jankauskas, S.S., Babenko, V.A., Zorov, S.D., Balakireva, A.V., Juhaszova, M., Sollott, S.J., Zorov, D.B. 2018. Mitochondrial membrane potential. *Analytical Biochemistry*, **552**, 50-59.

Figure Captions

Figure 6.1 Schematic of the process flow for transcriptome and physiological response analyses of yeast cells engineered for enhanced lipid (*DEG, differential gene expression, ROS, reactive oxygen species, $\Delta\psi_m$, Mitochondrial membrane potential.)

Figure 6.2 Overall view of gene expression among engineered strains for improved standard lipids production generated by the Degust program. (A) Multidimensional scaling (MDS) plot of gene expressions among different strains, (B) Variance percentage of different dimensions, (C) Number of differentially expressed (DE, including up- & down-regulated) genes, (D) Venn diagram of DE between different groups. (HBY strains were named after ‘H’ plus ‘number (and_24h)’ in the RNA-seq data, such as HBY03 is named after H03 or H03_24h.)

Figure 6.3 Relative expression levels of heterologously expressed genes among engineered strains by mRNA-seq analysis including *ALD6*, *SEACS^{L641p}*, *ACC1***, *AtClo1*, *Tgl3* and *AtDGAT1*. Yeast strains were sampled for mRNA-Seq analysis at 24 h post-induction including Control, HBY14, 20, 27, 31. The gene expression levels of *ACC1*** and *Tgl3* were enhanced separately due to their low levels. Expression levels of genes of interest were normalized against the expression level of *TAF10*, a gene that encodes a subunit of transcription factor IID (TFIID) and regarded as a housekeeping gene

Figure 6.4 Lipid content and soluble metabolite concentrations of engineered strains at 24 h post-induction (A) neutral lipid content using Bodipy 493/503 staining by flow cytometry, (B) neutral lipid content using Nile red staining by flow cytometry, (C) ethanol concentration, mg/L, (D) glycerol concentration, mg/mL.

Figure 6.5 Overview of transcriptional reprogramming of the strains HBY14, 20, 27 and 31 at 24 h post-induction of gene expression. The heatmaps show the transcriptional differences in $\log_2(\text{fold change})$ in engineered strains compared with control strain.

Figure 6.6 Cellular physiological characterisation and related differentially regulated genes in strain HBY31 compared with control after 24 h post-induction of gene expression: (A) Cell growth by OD600 nm, (B) CMI (cell membrane integrity), (C) ROS (reactive oxygen species), (D) $\Delta\psi_m$ (Mitochondrial membrane potential), (E) Number of differentially regulated genes as per Gene Ontology including Mito (Mitochondrion), Mito M (Mitochondrial membrane), ATP and NADPH synthesis. (F) ROS production-related pathways/genes

Figure 6.7 Comparison of cellular physiological responses between strain HBY31 and control after antioxidant (vitamin C and resveratrol) treatment (A) Cell growth of control over 24 h using 48-well plate, (B) Cell growth of HBY31 over 24 h using 48-well plate, (C) Cell membrane integrity, (D) Reactive oxygen species and (E) Mitochondria membrane potential at 24 h post-induction. Cell growth curves in A&B were representatives of three independent experiments, error bars in C-E represents the standard deviation of three biological experiments.

Figure 6.8 Effect of cyclopropane fatty acid biosynthesis on the cellular physiological performance between control, HBY20 and CBY20. (A) Comparison of cell growth by OD600nm and fatty acid profile of the cell membrane (phospholipid) at 72 h post-induction, UFAs, unsaturated fatty acids, (B) comparison of time course of percentage of CMI (cell membrane integrity) using propidium iodide (PI) staining, (C) relative ROS level at 24 h and 72 h after cells stained with CM-H2DCFDA, the ROS level of control at 24 h was normalized to 1, (D) relative $\Delta\psi_m$ level at 24 h and 72 h after cells stained with TMRE, the $\Delta\psi_m$ level of control at 24 h was normalized to 1.

Table 6.1 Details of plasmids and strains used in this study

Plasmid or strain	Description	Reference
pYES2-Ura- <i>Ec.CFAS</i>	P _{GALI} - <i>Ec.CFAS</i>	This study
pIYC05	P _{PGK1} - <i>Ald6</i> /P _{TEF1} - <i>SeACS</i> ^{L641P} , Addgene plasmid # 64742	Chen et al., 2013
pAD	P _{PGK1} - <i>ACC1</i> ** (ser659ala, ser1157ala), Addgene plasmid #64747	Chen et al., 2013
pESC-Leu- <i>AtDGAT1</i>	pESC-leu-P _{GALI} - <i>AtDGAT1</i>	Peng et al., 2018
pESC-Leu- <i>AtDGAT1</i> - <i>AtClo1</i>	pESC-leu-P _{GALI} - <i>AtDGAT1</i> /P _{GALI10} - <i>AtClo1</i>	Peng et al., 2018
pESC-leu2d	Vector backbone, Addgene plasmid # 20120	Ro et al., 2006
pIYC04	Vector backbone, derived from pESC-His, Addgene plasmid # 64741	Chen et al., 2013
pSP-GM2	Vector backbone, derived from pESC-Ura, Addgene plasmid # 64740	Chen et al., 2012
Control	BY4741-pESC-leu2d-pIYC04-pSP-GM2	Peng et al., 2018
HBY03	BY4741 - <i>AtDGAT1</i>	Peng et al., 2018
HBY14	BY4741Δ <i>Tgl3</i> - <i>AtDGAT1</i>	Peng et al., 2018
HBY20	BY4741Δ <i>Tgl3</i> - <i>AtDGAT1</i> - <i>Ald6</i> - <i>SeACS</i> ^{L641P}	Peng et al., 2018
HBY24	BY4741Δ <i>Tgl3</i> - <i>AtDGAT1</i> - <i>ACC1</i> **	Peng et al., 2018
HBY25	BY4741Δ <i>Tgl3</i> - <i>AtDGAT1</i> - <i>AtClo1</i>	Peng et al., 2018
HBY27	BY4741Δ <i>Tgl3</i> - <i>AtDGAT1</i> - <i>ACC1</i> ** - <i>Ald6</i> - <i>SeACS</i> ^{L641P}	Peng et al., 2018
HBY28	BY4741Δ <i>Tgl3</i> - <i>AtDGAT1</i> - <i>AtClo1</i> - <i>Ald6</i> - <i>SeACS</i> ^{L641P}	Peng et al., 2018
HBY31	BY4741Δ <i>Tgl3</i> - <i>AtDGAT1</i> - <i>AtClo1</i> - <i>ACC1</i> ** - <i>Ald6</i> - <i>SeACS</i> ^{L641P}	Peng et al., 2018
CBY20	BY4741Δ <i>Tgl3</i> - <i>Ec.CFAS</i> - <i>AtDGAT1</i> - <i>Ald6</i> - <i>SeACS</i> ^{L641P}	This study

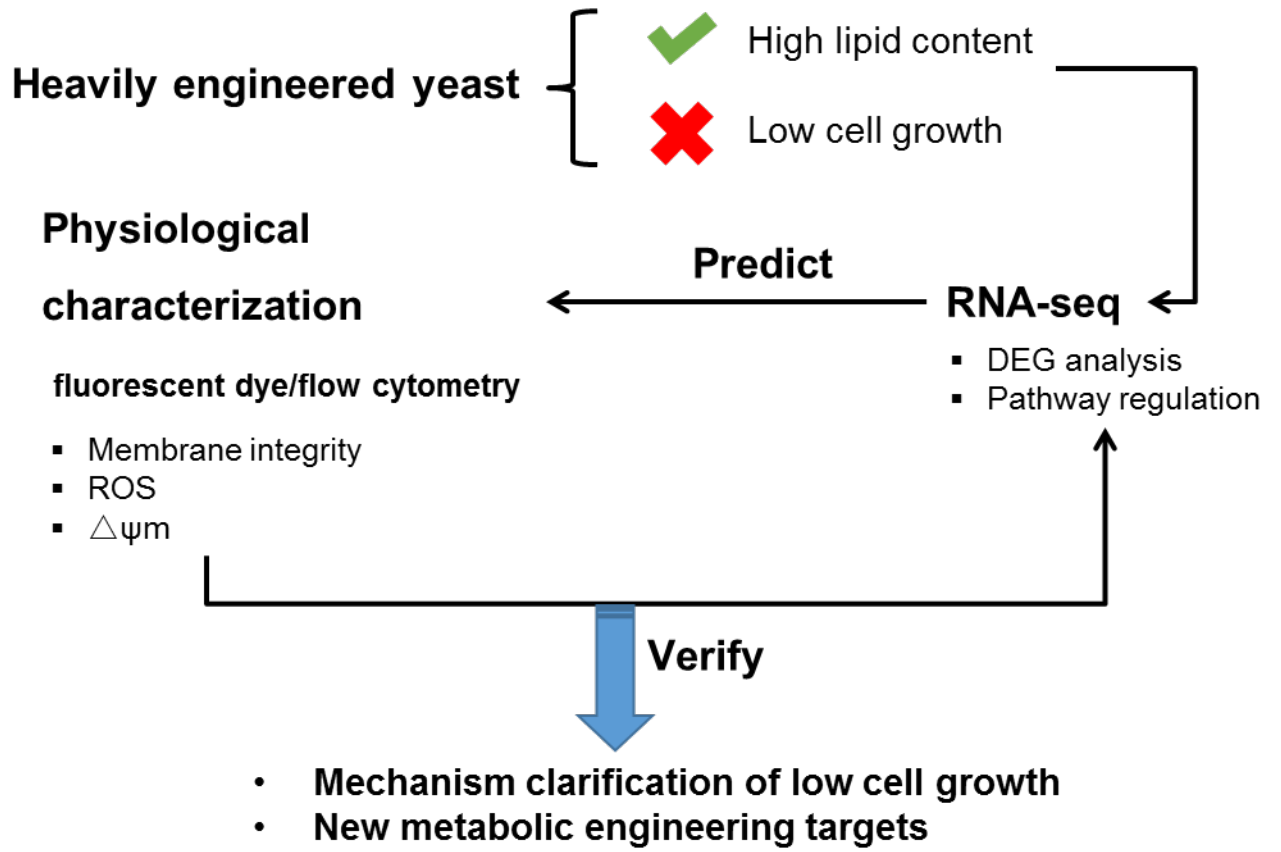


Figure 6.1

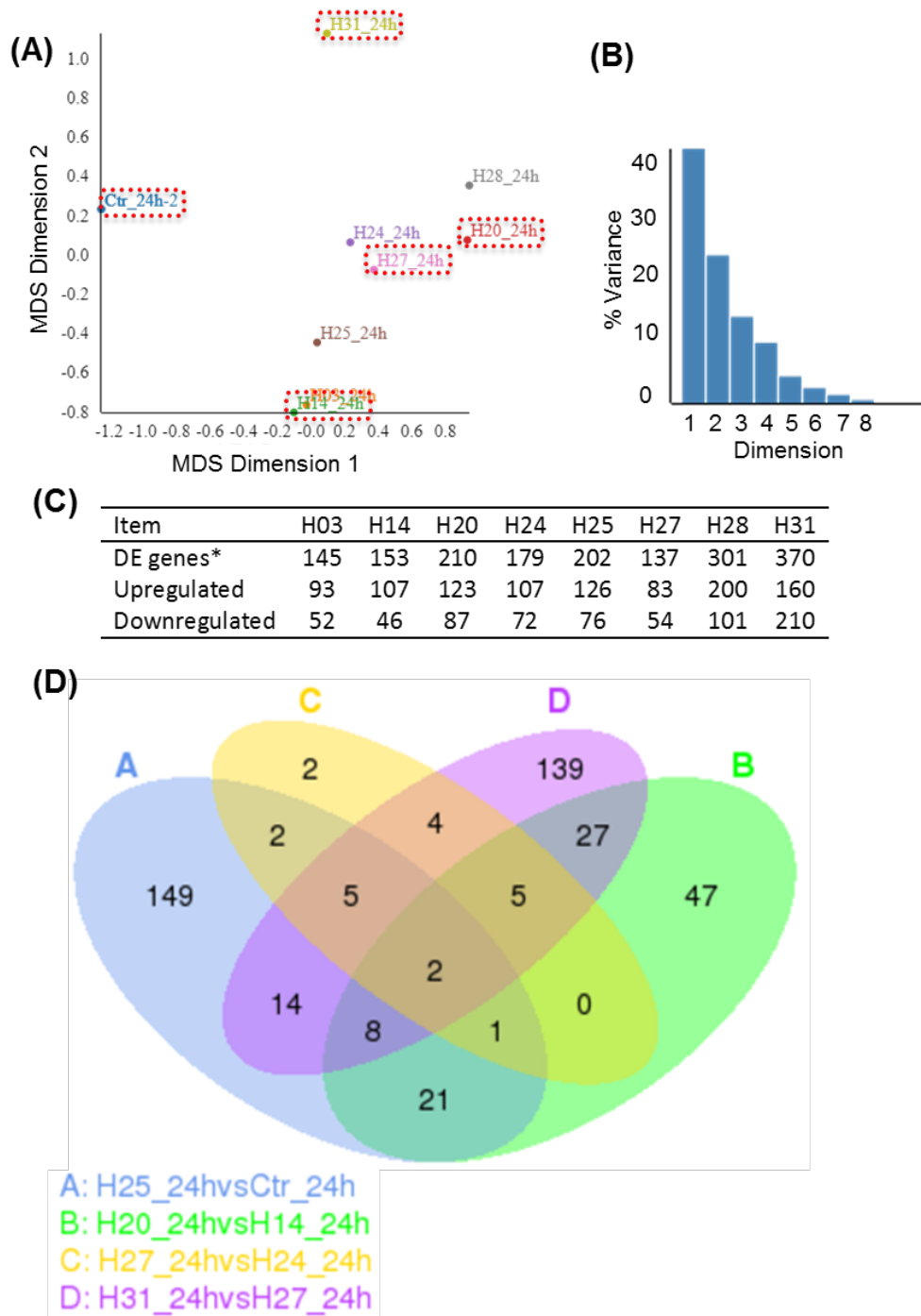


Figure 6.2

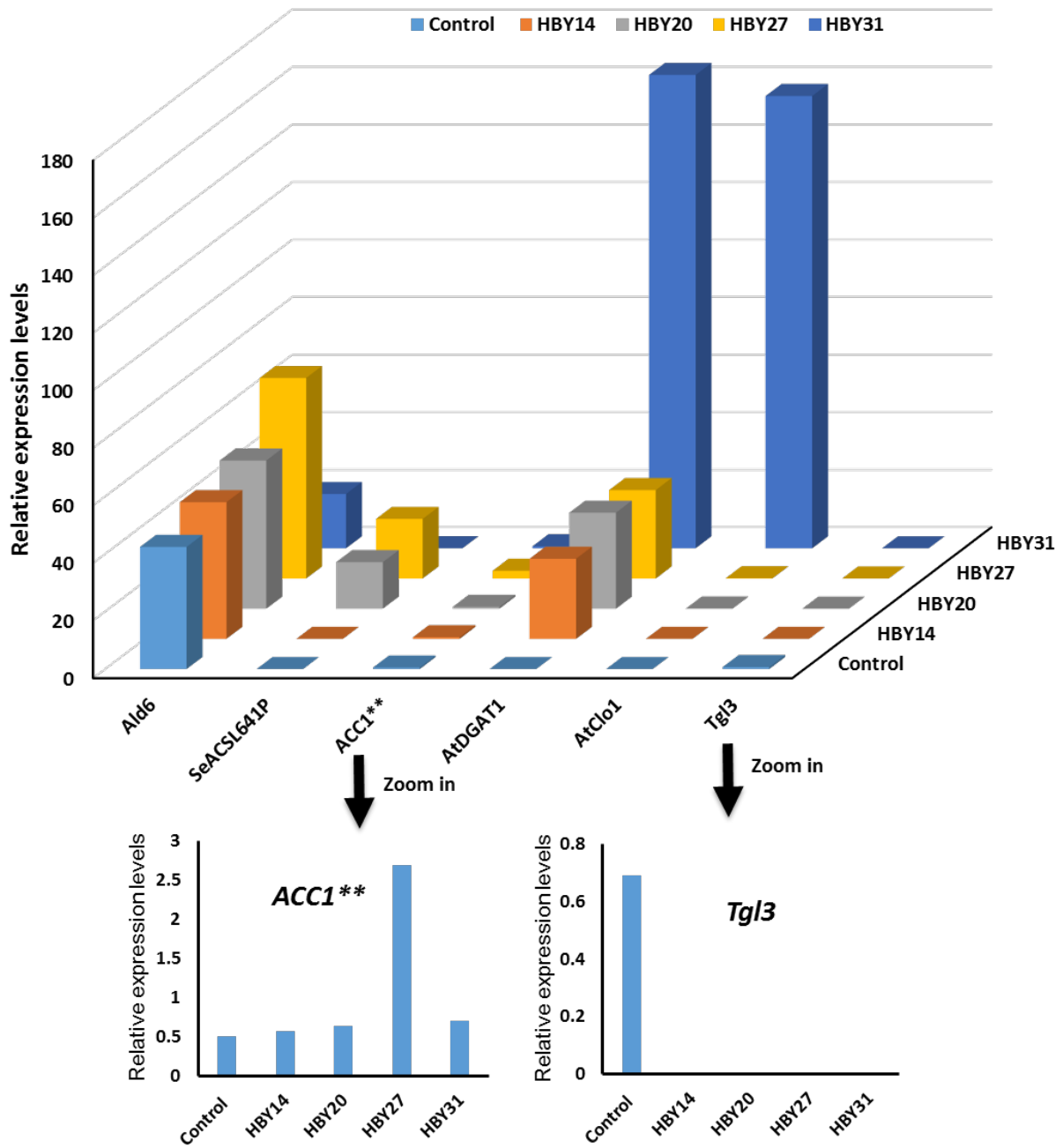


Figure 6.3

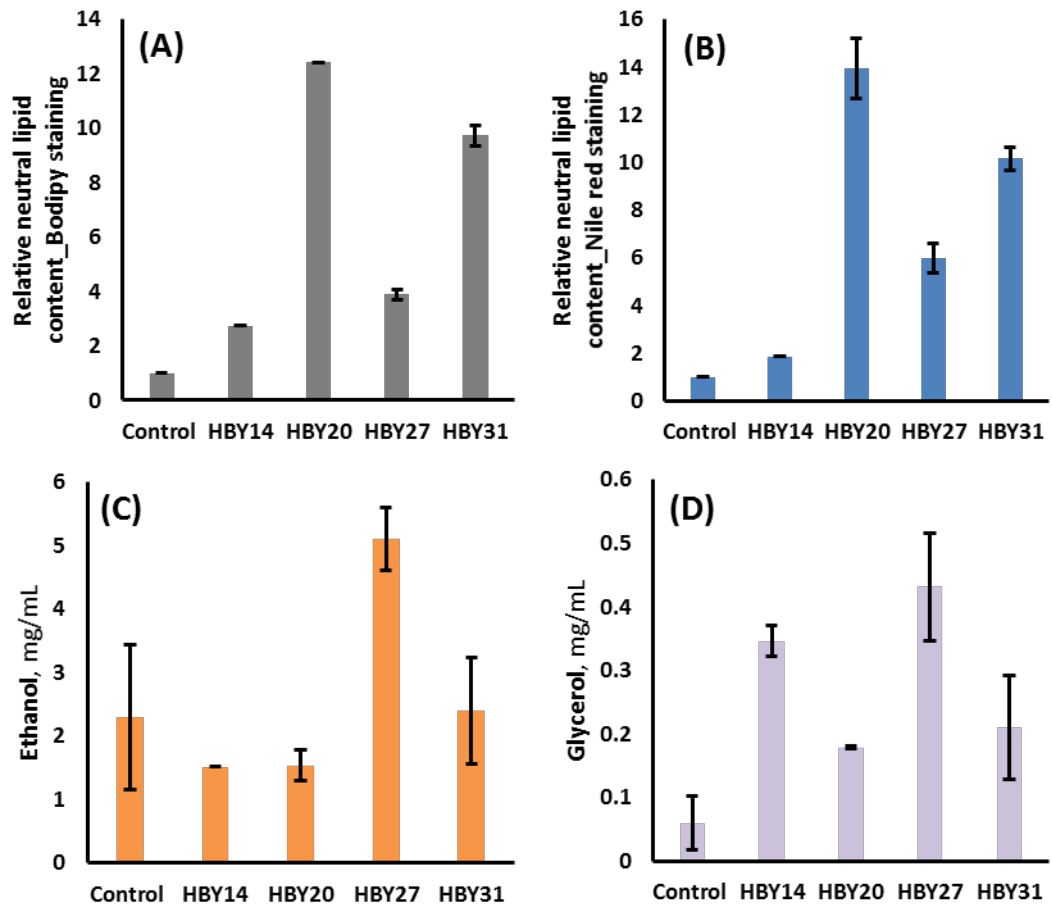


Figure 6.4

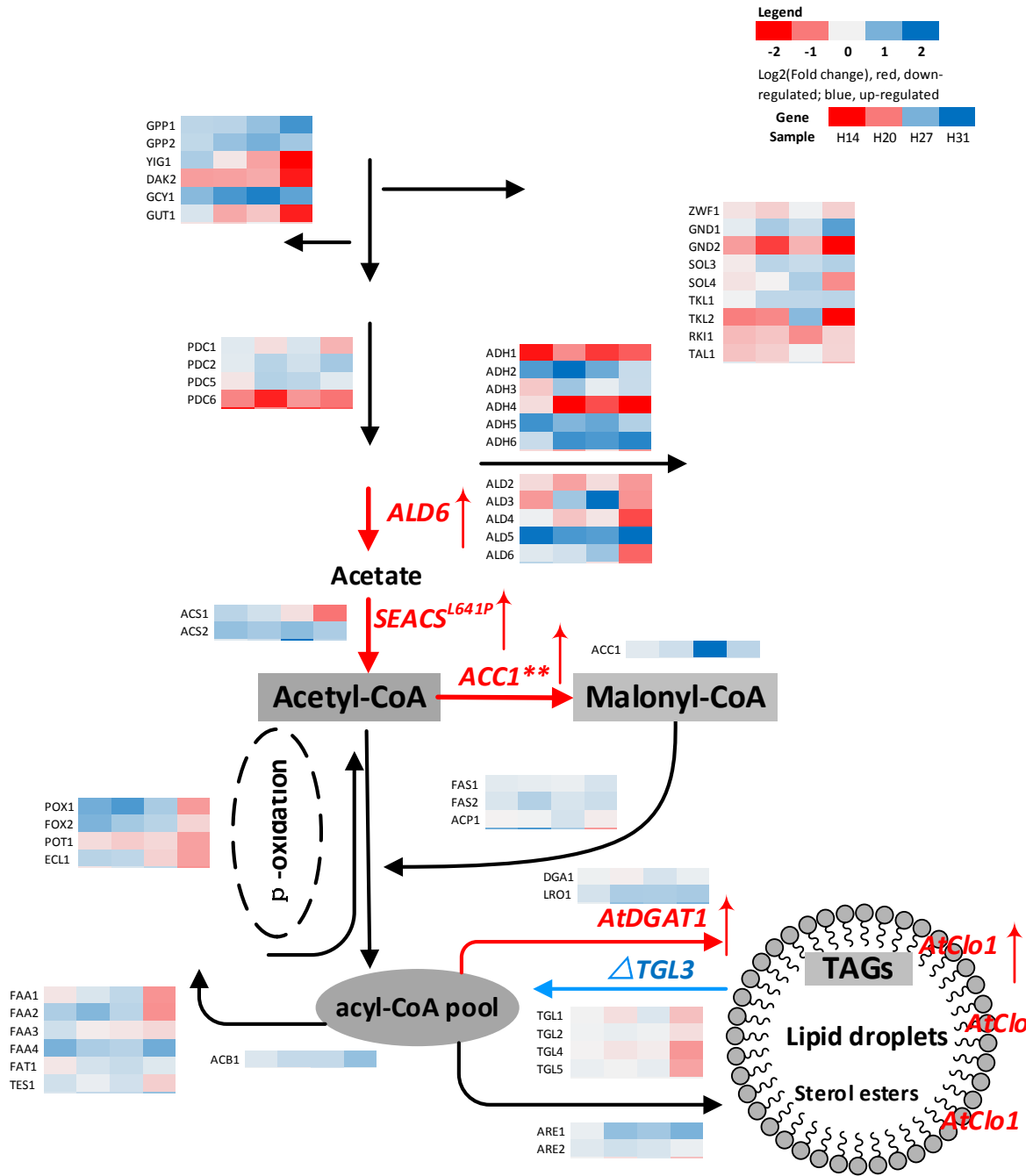


Figure 6.5

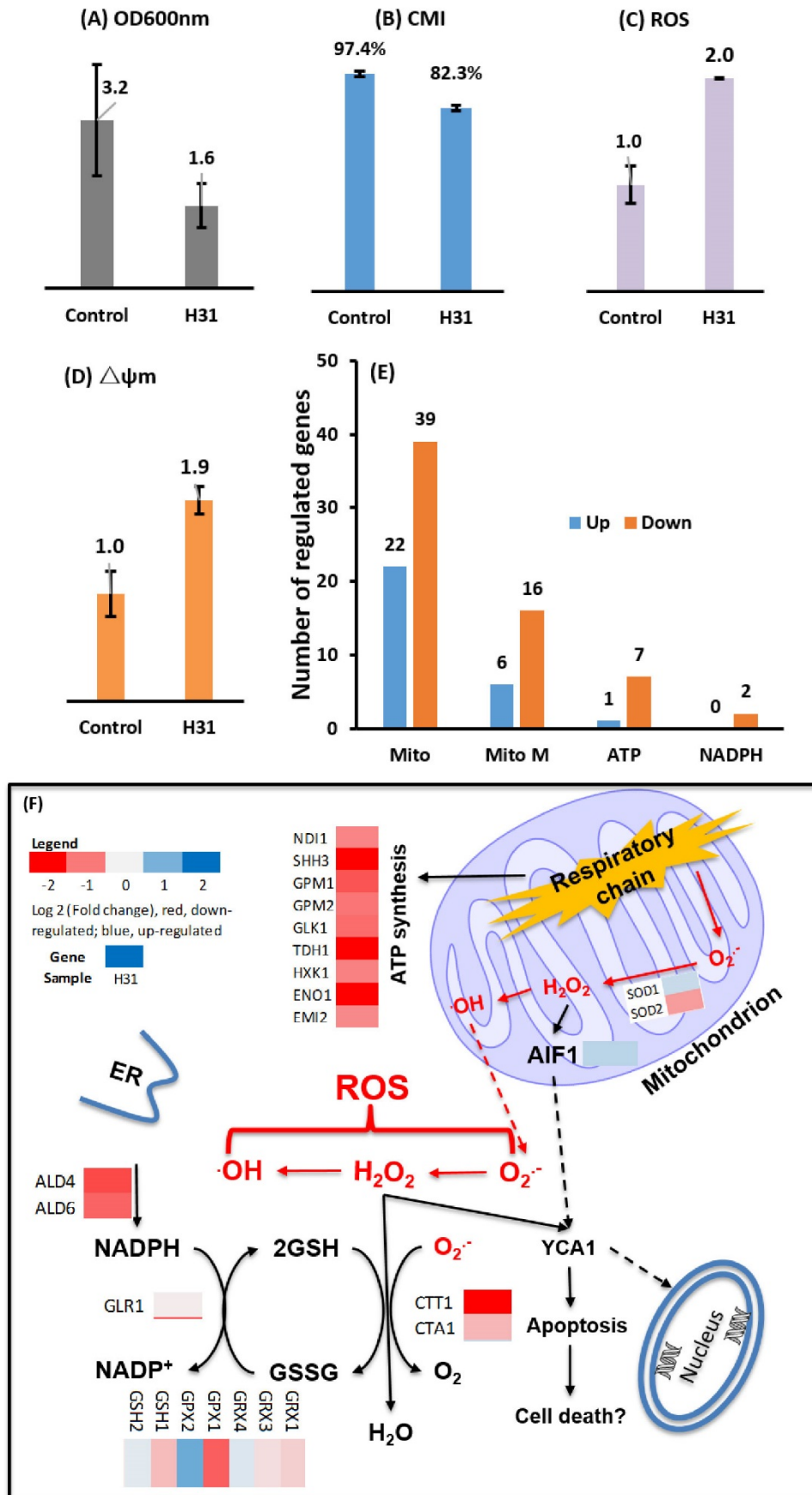


Figure 6.6

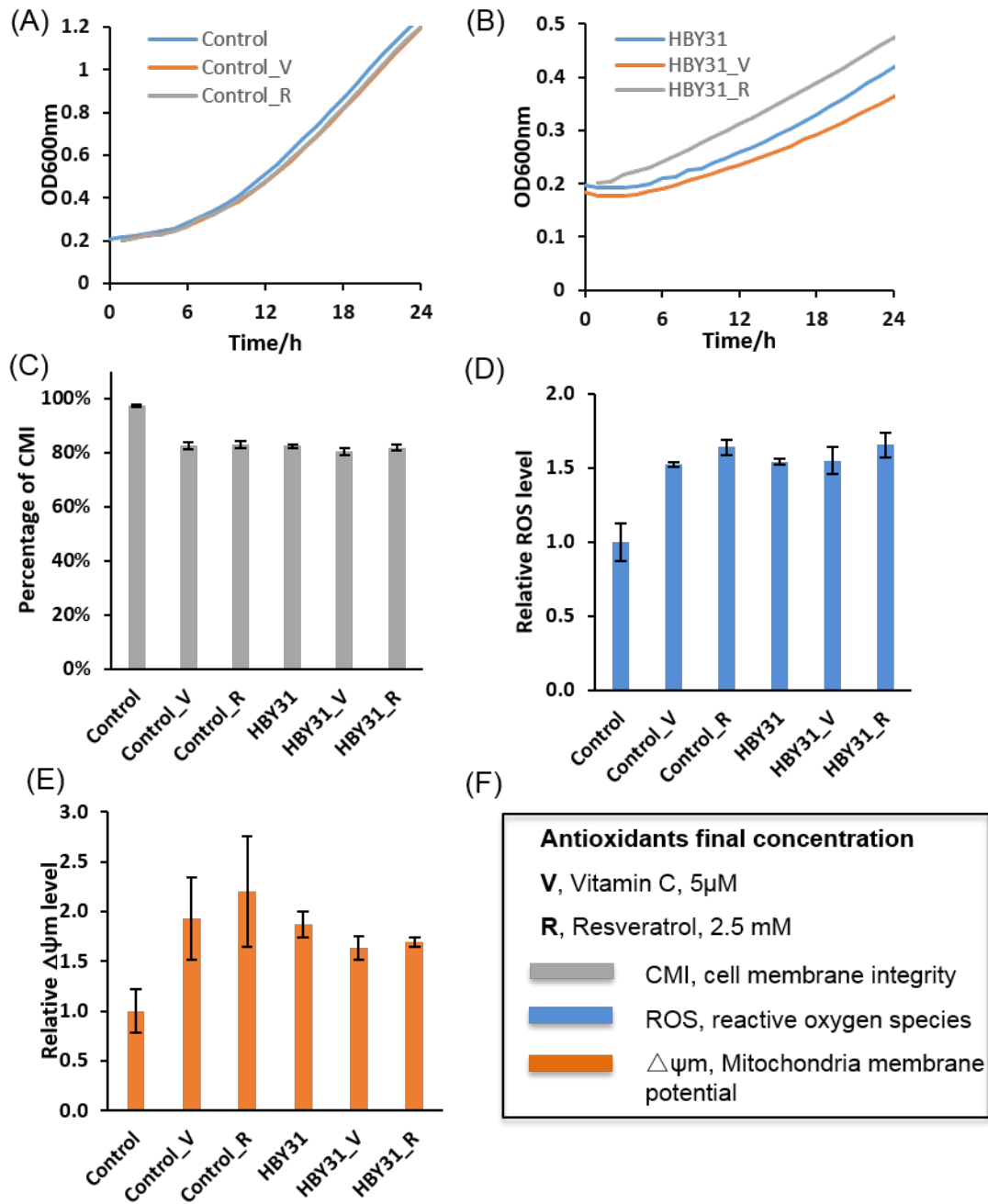


Figure 6.7

(A) Cell growth and FA distribution

Strain	OD600nm	Phospholipid	
		CFA%	UFAs %
Control	6.6	0	63.9
HBY20	3.6	0	52.4
CBY20	1.7	40	24.8

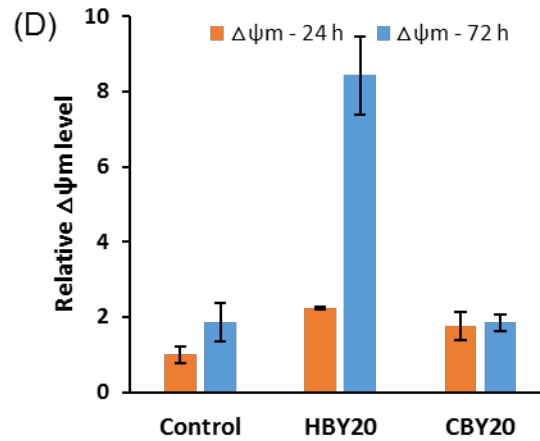
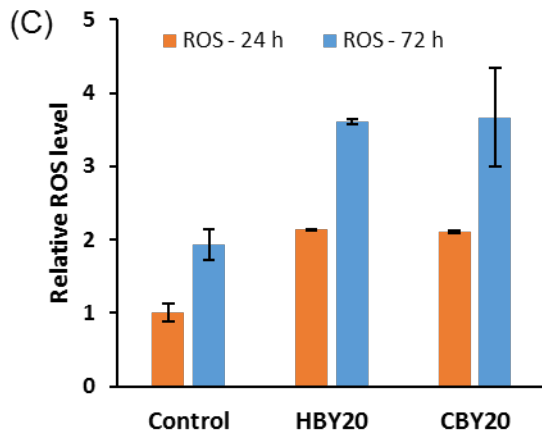
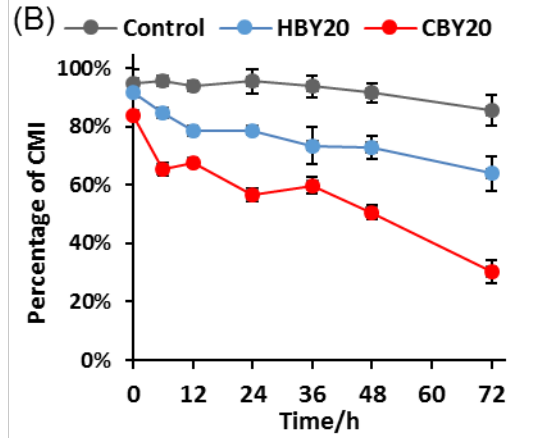


Figure 6.8

Appendix A. Supplementary material

Supplementary data associated with this article can be found in the online version.

RNA-seq analytical method

The following RNA-seq analytical method has been reproduced from Novogene company and Zhao et al. 2015 (Zhao et al., 2015) with slight modifications.

RNA isolation, examination and qualification

RNeasy Mini Kit (QIAGEN, Alameda, USA) was used to isolate and purify the total RNA as per the production protocol. 1% agarose gels and NanoPhotometer® spectrophotometer (IMPLEN, CA, USA) were used to check the RNA degradation, contamination and purity, respectively. Besides, RNA concentration and integrity were assessed by Qubit® RNA Assay Kit in Qubit® 2.0 Fluorometer (Life Technologies, CA, USA) and RNA Nano 6000 Assay Kit of the Bioanalyzer 2100 system (Agilent Technologies, CA, USA), respectively.

Library preparation for Transcriptome sequencing

A total amount of 3 mg RNA of each sample was used for the RNA sample preparations. Sequencing libraries were generated using NEBNext® Ultra™ RNA Library Prep Kit for Illumina® (NEB, USA) following manufacturer's instruction and index codes were added to attribute sequences to each sample. Briefly, mRNA was purified from total RNA using poly-T oligo-attached magnetic beads. Fragmentation was carried out using divalent cations under elevated temperature in NEBNext First-Strand Synthesis Reaction Buffer (5×). First strand cDNA was synthesized using random hexamer primer and M-MuLV Reverse Transcriptase (RNase H⁻). Second strand cDNA synthesis was subsequently performed using DNA polymerase I and RNase H. Remaining overhangs were converted into blunt ends via exonuclease/polymerase activities. After adenylation of 3'ends of DNA fragments, NEBNext

Adaptor with hairpin loop structure were ligated to prepare for hybridization. In order to select cDNA fragments of preferentially 150–200 bp in length, the library fragments were purified with AMPure XP system (Beckman Coulter, Beverly, USA). Then 3 mL USER Enzyme (NEB, USA) was used with size-selected, adaptor-ligated cDNA at 37 °C for 15 min followed by 5 min at 95 °C before PCR. Then PCR was performed with Phusion High-Fidelity DNA polymerase, Universal PCR primers and Index (X) Primer. At last, PCR products were purified (AMPure XP system) and library quality was assessed on the Agilent Bioanalyzer 2100 system (Agilent Technologies, Palo Alto, USA). The clustering of the index-coded samples was performed on a cBot Cluster Generation System using TruSeq PE Cluster Kit v3-cBot-HS (Illumina Inc., San Diego, CA, USA) according to the manufacturer's instructions. After cluster generation, the library preparations were sequenced on an Illumina HiSeq 2000 platform and 50 bp single-end reads were generated.

Transcriptome data analysis

All the analyses were based on the clean data with high quality after removing reads that containing adapter, poly-N and low quality reads from the raw data (reads). For the reads mapping, the reference genome and gene model annotation files of *S. cerevisiae* were downloaded from the *Saccharomyces* Genome Database (SGD). Index of the reference genome was built using Bowtie v2.2.3 and paired-end clean reads were aligned to the reference genome using TopHat v2.0.12. RPKM referred to the reads per kilobase of exon model per million mapped reads. Prior to differential gene expression analysis, HTSeq v0.6.1 was used to count the reads numbers mapped to each gene. And then the RPKM of each gene was calculated based on the length of the gene and reads count mapped to this gene (Mortazavi et al., 2008). For each sequenced library, the read counts were adjusted using the edgeR software package through one scaling normalized factor (Robinson et al., 2010). Differential expression analysis

of two conditions was performed using the DESeq R package (1.20.0) as described by Anders and Huber (Anders & Huber, 2010). The P values were adjusted using the Benjamini & Hochberg method. Corrected P-value of 0.005 and $\log_2(\text{Fold change})$ of 1 were set as the threshold for significantly differential expression. Gene ontology (GO) was implemented using the GOrse R package, in which gene length bias was adjusted (Trapnell et al., 2010). GO terms with corrected P-value less than 0.05 were considered significantly enriched by differential expressed genes. In order to examine the associated pathways and functions in the differential expressed genes, KOBAS software 2.0 was employed in KEGG pathway mapping analysis (Xie et al., 2011).

CHAPTER 7

CONCLUSION AND OUTLOOK

This page is intentionally blank

Chapter 7 Conclusion and outlook

The increasing demand for fatty acids and lipids from broad markets including nutrition, oleochemical and biofuels has driven the interest in the development of new strategies to produce and/or store high lipid content in microbes. An understanding of lipid metabolism and the consequences of its disruption due to metabolic engineering of these pathways is essential for the construction of a high lipid content yeast. This thesis has used the yeast *S. cerevisiae* as a model production host to test the effectiveness of different lipid metabolic engineering strategies on the enhancement of standard and unusual lipid stores and its impacts on cellular physiology. The major steps in lipid production were addressed systematically, including FA biosynthesis, FA modification, lipid accumulation and sequestration steps. The main contributions and limitations of this research are as follows.

Screen and comparing sources of lipid accumulation genes for efficacy in yeast

While lipid accumulation genes sourced from plants, microalgae and yeast have been previously characterised in separate studies, there was a lack of substantial evidence to support the selection of an effective lipid accumulation gene for enhancing lipid production in yeast. Chapter 3 compared and selected an effective lipid accumulation gene, specifically from among candidate diacylglycerol acyltransferases (DGAT) or related activities, for their performance in yeast. It evaluated the effectiveness of recombinant expression of 5 DGAT genes from plant and microalgae through establishing a set of validated analytical tools to measure intracellular lipid content in yeast. The established analytical procedures included Nile Red fluorescence, lipid droplet visualisation, fatty acid and lipid quantification. A DGAT1 from the plant *Arabidopsis thaliana*, *AtDGAT1*, was identified as an effective lipid accumulation gene (lipid yield 1.81-fold higher than control) in yeast and was selected for subsequent engineering.

Expression of another gene, *AtRODI* led to increased unsaturated fatty acid content in the yeast lipid.

Metabolic pathway engineering of yeast for high lipid productivity

Most metabolic engineering research in microbial lipids in yeast to date has targeted FA biosynthesis and lipid accumulation pathways. However, this approach overlooks the reversible nature of lipid storage and the immediate mobilisation of FA from lipid stores. Without intervention, increases in biosynthesis and flux of FA into TAG may be readily converted back into FA. Chapter 4 investigated the combination of genes for the individual steps toward improved lipid production, including FA synthesis, lipid accumulation and sequestration of the stored TAG. The metabolic engineering strategy developed here significantly improved cellular lipid content (up to 7.97% DCW basis, 2.6-fold over control) but severely reduced yeast growth and cell viability. To address this drawback, a two-stage bioprocess was designed to encourage cell growth in the first stage and improved cell viability by differential gene expression in the second stage, and consequently achieved very high lipid productivity (307 mg/L, 4.6-fold above control). This research also demonstrated that cell viability and other physiological measures are key indicators to guide successful metabolic engineering strategies.

Lipid pathway engineering for production of unusual fatty acids

Unusual FAs are those that are not generally produced within yeast but offer greater functionality and value for industrial applications compared with standard fatty acids. Modified FA also offer a greater challenge for metabolic engineering as additional steps are required for their production and their presence may not be tolerated within important organelles of the cell. The research in chapter 5 investigated the impact of expression of the cyclopropane fatty acid

synthetase gene within the highly engineered strains developed in Chapter 4 on their production and storage. This chapter has demonstrated that the lipid pathway engineering strategy developed for standard fatty acids is effective also for CFA production and accumulation in yeast although further improvement is needed in transferring CFA from phospholipid where it is generated into the storage TAG fraction for greater overall yields. To date, this research has achieved the highest reported intracellular CFA titre (68.3 mg/L) in *S. cerevisiae*.

Cellular physiological responses and transcriptome analysis of metabolically engineered cells

Among the metabolically engineered strains investigated in Chapter 4 & 5, those with the highest lipid content also displayed low cell growth accompanied by lower cell membrane integrity (cell viability). The research described in Chapter 6 measured cellular physiological responses and transcriptome analyses to examine the mechanisms of low growth and cell viability in yeast engineered for high lipid content. In addition to the regulated central carbon pathway, the reactive oxygen species (ROS) production was upregulated, and respiratory pathway (or energy synthesis such as NADPH, ATP) was downregulated in these cells. These insights also open up opportunities to ameliorate the side effects of lipid pathway engineering to deliver both high lipid yield and high cell viability in future.

Outlook

The outcomes of this thesis exemplified the construction of a yeast cell factory for high-level production and storage of standard and unusual lipids, which can be extended to other industrial microorganisms and valuable biochemicals. Built on these achievements, the following future work is recommended to further improve yeast lipid production without compromised cellular health.

Dynamic regulation to achieve greater balance in lipid pathway engineering

As shown in Chapter 4, the lipid pathway engineered through the combination of three steps of lipid metabolism produced a highly increased lipid yield but with low cell growth and low cell viability. Possible reasons behind this are that lipid production is involved with multiple synthesis steps and many metabolites and intermediates in the pathway. Each step is closely connected with other metabolic pathways in the cell and concentrations and availabilities of metabolites and cofactors may affect or limit the reaction. Thus, it is essential to regulate the pathways dynamically such as through the design of a dynamic biosensor, and fine-tune the supply of intermediates so as to avoid an unduly heavy metabolic burden or toxicity resulting from the build-up of precursors. Moreover, the direct engineering of the energy supply to improve the balance and supply of crucial reducing equivalents and energy carriers, NADPH and ATP, could also be a promising approach to improve lipid production.

Enhance CFA transfer from the point of production to storage

Cyclopropane fatty acid is synthesised from unsaturated fatty acids within the cell phospholipid membrane, then transfers from membrane phospholipid for storage within TAG. However, as shown in Chapter 5, there is a limitation in transferring CFA from PL to TAG. There are several possible strategies to overcome this bottleneck for intracellular lipid production, such as provide more substrates for CFA synthesis including palmitoleic acid and oleic acid by expressing additional $\Delta 9$ desaturase, and identify a DGAT enzyme having greater specificity for CFA compared with standard fatty acids e.g. sourced from a plant lychee that stores high level of CFA in TAG.

Combination of strategies

Lipid metabolic engineering is a complex goal. Taking a metabolic engineering strategy alone may not address or solve all the issues of an engineered microbial cell factory. Further examination and better methods to assess cellular physiology of engineered strains such as cell membrane integrity, reactive oxygen species, mitochondrial membrane potential and energy balances in the cell would greatly assist the diagnosis of the factors that hinder greater productivity. There is also potential extracellular production where fatty acids are secreted from the cell due to deletion of genes for fatty acid activation via Co-enzyme A and overexpressing TAG lipases to ensure TAG is mobilised. Furthermore, a better understanding of the nature and extent of cell to cell heterogeneity in lipid productivity among microbes may inspire new targets for yield improvement. New selection techniques which are already having an impact in the field of industrial microbiology such as artificial intelligence-assisted adaptive laboratory evolution, and new technologies, math modeling tools stemming from synthetic and systems biology, reverse engineering, and bioprocess engineering will also be valuable to increase yields and microbial culture performance. Thus, the combination of multiple strategies for improved lipid production could be the route to achieve better performance in the future.

This page is intentionally blank

Appendix I - Assessment of effect of additional lipid accumulation genes on cyclopropane fatty acid production

This addendum compares the effect of coexpression of *Escherichia coli* cyclopropane synthase (Ec.CFAS) with lipid accumulation genes *AtPDAT1*, *AtROD1* and *AtDGAT1* on cyclopropane fatty acid accumulation in yeast. In Chapter 3, *AtDGAT1* showed an effective ability to accumulate lipid in yeast (1.81-fold improvement) whereas *AtPDAT1* and *AtROD1* expression weakly compensated the TAG deficient strain H1246 in the oleic acid sensitivity assay. Here, we assessed the activities of *AtPDAT1* and *AtROD1* in CFA accumulation ability and compared them with *AtDGAT1* which was more comprehensively tested in Chapter 5. The combination of *Ec.CFAS* and *AtPDAT1* or *AtROD1* or *AtDGAT1* were constructed in *S. cerevisiae INVSc1*, and the standard lipid content and CFA content in both TAG fraction and phospholipid (PL) fraction were compared.

Interestingly, *Ec.CFAS* expression increased TAG content by 2.3 fold above control in this strain; this is unexpected as CFAS is considered a fatty acid modifying enzyme only. The combination of *AtDGAT1* and *Ec.CFAS* increased the TAG content by 4.4 fold above control, whereas the addition of *AtPDAT1* or *AtROD1* increased TAG content by just 1.8-1.9 fold (Fig. 1A). As expected, PL content was not significantly different between the engineered strains. Considering the CFA content in both TAG and PL fractions, no significant increases were found among the engineered strains including the *Ec.CFAS* and *AtDGAT1* combination, despite the increased overall lipid content (Fig. 1B). Therefore, *AtDGAT1* was shown again to be an effective standard lipid accumulation gene, while *AtPDAT1*, *AtROD1* didn't show obvious increases for standard or CFA lipid production.

Appendix I Additional lipid accumulation genes

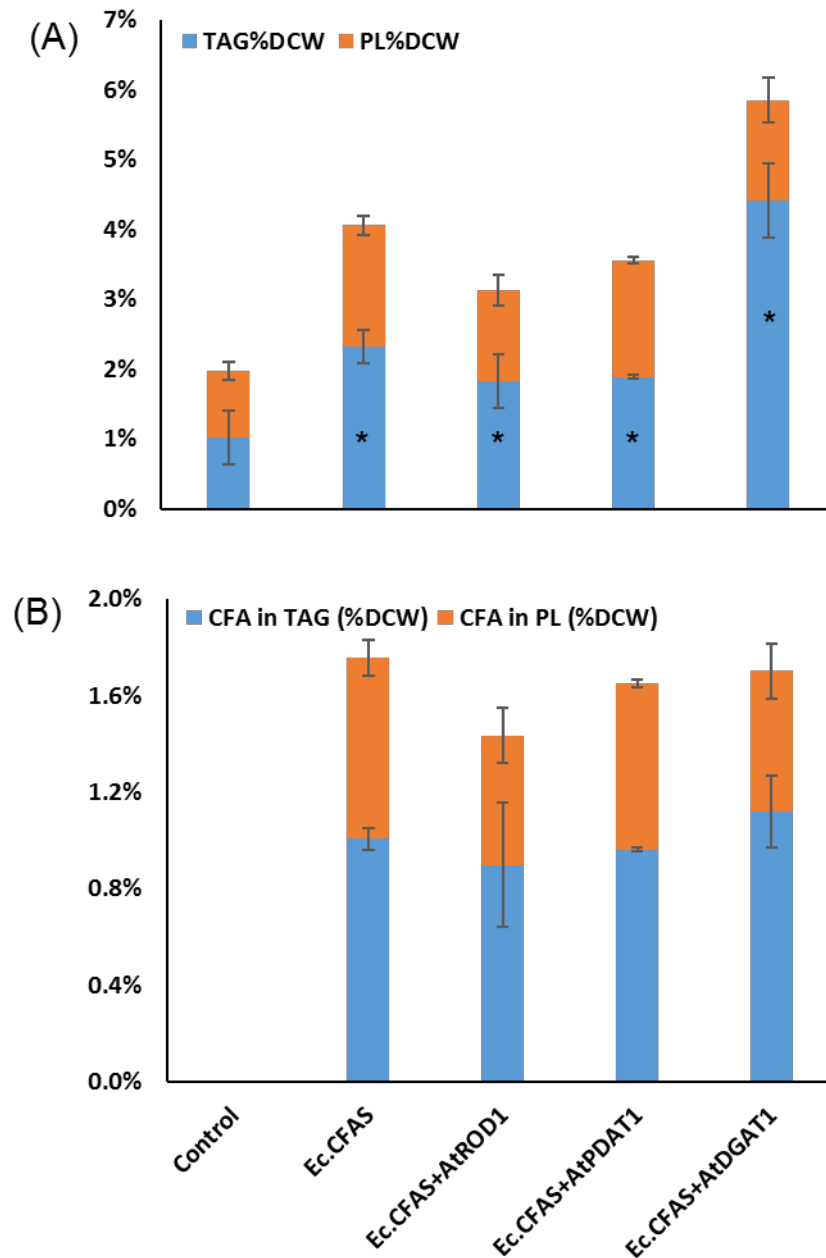


Fig. 1 Comparison of the coexpression of *Ec.CFAS* with lipid accumulation genes on CFA production (A) TAG content and PL content based on dry cell weight, (B) CFA content in TAG fraction and PL fraction based on dry cell weight. Student's t-test was performed based on the comparison of TAG and PL content of engineered strains with control, and the comparison of CFA content in TAG and PL fraction of engineered strains with strain expressing *Ec.CFAS*. *, P value of (T<=t) two-tail less than 0.05, alpha was 0.05.

RESEARCH

Open Access



Single cell assessment of yeast metabolic engineering for enhanced lipid production using Raman and AFM-IR imaging

Kamila Kochan^{1†}, Huadong Peng^{2†} , Bayden R. Wood¹ and Victoria S. Haritos^{2*}**Abstract**

Background: Biodiesel is a valuable renewable fuel made from derivatized fatty acids produced in plants, animals, and oleaginous microbes. Of the latter, yeasts are of special interest due to their wide use in biotechnology, ability to synthesize fatty acids and store large amounts of triacylglycerols while utilizing non-food carbon sources. While yeast efficiently produce lipids, genetic modification and indeed, lipid pathway metabolic engineering, is usually required for cost-effective production. Traditionally, gas chromatography (GC) is used to measure fatty acid production and to track the success of a metabolic engineering strategy in a microbial culture; here we have employed vibrational spectroscopy approaches at population and single cell level of engineered yeast while simultaneously investigating metabolite levels in subcellular structures.

Results: Firstly, a strong correlation ($r^2 > 0.99$) was established between Fourier transform infrared (FTIR) lipid in intact cells and GC analysis of fatty acid methyl esters in the differently engineered strains. Confocal Raman spectroscopy of individual cells carrying genetic modifications to enhance fatty acid synthesis and lipid accumulation revealed changes to the lipid body (LB), the storage organelle for lipids in yeast, with their number increasing markedly (up to tenfold higher); LB size was almost double in the strain that also expressed a LB stabilizing gene but considerable variation was also noted between cells. Raman spectroscopy revealed a clear trend toward reduced unsaturated fatty acid content in lipids of cells carrying more complex metabolic engineering. Atomic force microscopy-infrared spectroscopy (AFM-IR) analysis of individual cells indicated large differences in subcellular constituents between strains: cells of the most highly engineered strain had elevated lipid and much reduced carbohydrate in their cytoplasm compared with unmodified cells.

Conclusions: Vibrational spectroscopy analysis allowed the simultaneous measurement of strain variability in metabolite production and impact on cellular structures as a result of different gene introductions or knockouts, within a lipid metabolic engineering strategy and these inform the next steps in comprehensive lipid engineering. Additionally, single cell spectroscopic analysis measures heterogeneity in metabolite production across microbial cultures under genetic modification, an emerging issue for efficient biotechnological production.

Keywords: Lipid bodies, Spectroscopy, Metabolic engineering, Heterogeneity, Triacylglycerol, Fatty acids

Background

Biodiesel is a versatile renewable fuel composed of fatty acid methyl esters produced from animal and plant

lipids-triacylglycerols (TAGs) [1, 2]. Microbial oils also have advantages as a source of TAG: microorganisms can be grown on non-food sugars, are minimally affected by seasons, generally robust and have short life cycles [1]. Many types of oleaginous eukaryotic species accumulate TAG in lipid bodies (LB), intracellular organelles considered primarily as storage vesicles for neutral lipids, in amounts up to 70% of total DCW biomass [1, 3, 4].

*Correspondence: victoria.haritos@monash.edu

[†]Kamila Kochan and Huadong Peng contributed equally to this work

²Department of Chemical Engineering, Monash University, Clayton Campus, Clayton, VIC 3800, Australia

Full list of author information is available at the end of the article



However, for cost-effective and high yielding production of TAG in oleaginous organisms such as yeast, metabolic pathway engineering and maximizing yield across the cultures is necessary [1, 3, 5, 6].

The metabolic engineering strategies for improvement of lipid production include up and down regulation of genes involved in the main steps of yeast lipid production: fatty acid (FA) biosynthesis, lipid accumulation and sequestration [1, 7]. Increased fatty acid production can be achieved by higher expression of aldehyde dehydrogenase (ALD), acetyl-CoA synthetase (ACS) [8] and acetyl-CoA carboxylase (ACC) [9, 10] and FA accumulation in TAG is catalyzed by diacylglycerol acyltransferase (DGAT) [7] and other acyltransferases. Heterologous expression of highly active acyltransferases such as the DGAT1 from *Arabidopsis thaliana* has been shown to increase lipid yield in the yeast *Saccharomyces cerevisiae* [11] and similarly, LB stabilization proteins such as caleosin (AtClo1) [12] have been shown to support LB formation. Down regulation of lipid mobilization enzymes such as the major TAG lipase, Tgl3, in *S. cerevisiae*, can also increase lipid content of cells [13].

Another factor affecting the productivity of microbially produced lipids is heterogeneity in individual cell performance across a culture [14]. Some of the variance is due to the stochastic nature of biological processes within gene regulation, transcription and translation, but response can be further distorted by variable responses to environmental conditions [15] including genetic engineering. While heterogeneity in cellular processes among isogenic microbial cells in a population has been known for some time, recent developments in visualization technologies have allowed measurement and monitoring of metabolite production both of populations and single cells within.

The formation and growth of LBs in cells are most commonly analysed by fluorescence imaging or histochemical staining [16]; these enable the visualization of LBs in multiple cells at once, but without providing details of their chemical composition. Vibrational spectroscopy-based techniques such as infrared (IR) and Raman spectroscopy (RS) are used in combination with digital imaging to enable rare insights into single cells of microalgae and yeast [17–20]. In particular, confocal Raman spectroscopy (CRS) has revealed intracellular structures such as LBs, due to its high spatial resolution falling in the range of few hundred nm depending on the excitation wavelength [21] and chemical composition information of selected intracellular structures [18, 19, 22]. The spatial resolution of imaging with the use of conventional IR spectroscopy is restricted by wavelength diffraction spatial resolution limit ($\sim 5.5 \mu\text{m}$), making it less suitable for the study of intracellular structures of microorganisms.

Recently, however, a novel technique has been developed, based on a combination of IR spectroscopy and Atomic Force Microscopy (AFM–IR). In AFM–IR, IR absorption spectrum is acquired indirectly, by measuring the resulting thermal expansion of the sample. This approach overcomes the limitation of conventional IR-based imaging and achieves a spatial resolution of $\sim 100 \text{ nm}$, thus enabling analysis of cellular constituents at the single cell level.

The aims of this research were to determine the effectiveness of metabolic pathway engineering approaches for enhanced lipid content in yeast through an examination of subcellular structures including LBs and to examine the heterogeneity of response in *S. cerevisiae* yeast cultures via vibrational spectroscopic approaches. We measured the overall changes in lipid content and other metabolites at a population level in whole cells by ATR-FTIR following the introduction of genetic modifications, then undertook detailed studies of subcellular structures and changes in their chemical composition in single cells using CRS and AFM–IR. These approaches provided detailed, single cell information on subcellular structures at high-resolution for the engineered strains and also allowed representative sampling of the population for these traits. The increase in the total lipid content of engineered cells demonstrated in bulk samples reflected either a greatly increased number or greatly increased size of LBs; the increased size was likely due to the influence of the LB stabilizing protein, caleosin, expressed in these cells. In engineered yeast, LB fatty acid composition shifted towards lower content of UFA relative to SFA in the highly lipidic strains and cytoplasmic carbohydrate stores were heavily reduced. Vibrational spectroscopy analysis of yeast cells revealed unprecedented information on the effectiveness and effects of metabolic engineering strategies for higher lipid content that will also guide future approaches to the field.

Methods

Yeast cell lines and culture conditions

Four engineered strains of *S. cerevisiae* were evaluated in the study and compared with a control strain (CON) BY4741 (*MATa his3 Δ 1 leu2 Δ 0 met15 Δ 0 ura3 Δ 0*) transformed with three empty vectors. Genes selected for metabolic engineering are given in Table 1; the full description of the metabolic engineering strategy and selection and the combination of genes and expression plasmids are given in Ref. [23]. Expression of the introduced genes *AtDGAT1*, *SEACS^{L641P}*, *ACC1^{S659A}*, *S1157A*, *AtClo1* was regulated, respectively, by promoters GAL1, TEF1, PGK1 and GAL10.

Saccharomyces cerevisiae were maintained based on their auxotrophy using yeast synthetic complete (SC)

Table 1 *Saccharomyces cerevisiae* strain names and introduced genes

Strain	Genes expressed
CON	Empty vectors ^a
HBY03	<i>AtDGAT1</i>
HBY14	<i>AtDGAT1 Tgl3Δ</i>
HBY20	<i>AtDGAT1 Tgl3Δ Ald6 SEACS^{L641P}</i>
HBY31	<i>AtDGAT1 Tgl3Δ Ald6 SEACS^{L641P} ACC1^{S659A, S1157A} AtClo1</i>

Δ indicates endogenous gene was knocked out

^a pSP-GM2, pLYC04, pESC-leu2d

minimal medium, containing 6.7 g/L of yeast nitrogen base, 20 g/L glucose as well as a mixture containing appropriate nucleotide bases and amino acids for the various dropout options (SC-Leu, SC-His-Ura, SC-His-Leu-Ura). All strains were stored in 15% glycerol at $-80\text{ }^{\circ}\text{C}$ before being cultured in 5 mL yeast SC minimal medium and incubated at $30\text{ }^{\circ}\text{C}$, 250 rpm, overnight. The culture OD_{600 nm} was diluted to approximately 0.4 into 50 mL of SC induction medium containing 2% (w/v) galactose and 1% (w/v) raffinose in 250 mL flasks. The flasks were capped with aluminum foil and incubated at $30\text{ }^{\circ}\text{C}$, 250 rpm until cells were harvested at 72 h for the following analysis.

GC measurements of total fatty acid content

Harvested cells were pelleted by centrifugation at 3000 rpm for 5 min, frozen at $-80\text{ }^{\circ}\text{C}$ for ~ 1 h and subsequently freeze-dried overnight using a FreeZone[®] 4.5 Liter Freeze Dry Systems (Labconco Corporation, USA) to obtain the dry cell weight (DCW) of each culture. Dry cells (~ 20 mg) were treated with 2 mL methanol/hydrochloric acid/chloroform (10:1:1, v/v/v) and heated at $90\text{ }^{\circ}\text{C}$ for 1 h in sealed test tubes to convert lipids to fatty acid methyl ester (FAME). FAME was washed with 0.9% NaCl solution (1 mL) and extracted with hexane after mixing. FAME samples (1 μL) were analyzed by Agilent 7890A gas chromatography with flame ionization detection (GC-FID) as described previously [11].

Lipid body visualization using confocal fluorescence microscope

Imaging of lipid droplets after Nile red (Sigma-Aldrich, USA) staining of unfixed stationary phase yeast cells was undertaken 72 h after induction of gene expression [11, 24]. 1 mL of harvested cells were transferred into a 1.5 mL reaction tube and washed twice with 1 mL sterile 50 mM Tris-HCl (pH 7.5). 1 μL of Nile Red stock solution was added into the cell suspension to obtain the final concentration of 1 $\mu\text{g}/\text{mL}$, gently mixed, incubated for 20 min at room temperature and centrifuged at 1000g

for 2 min. 1 μL of dense cell suspension was mounted on a standard microscope slide and imaged by a Leica Microsystems SP5 confocal microscope coupled with HCX PL APO 63 \times /1.4 OIL CS oil-immersion objective in Monash Micro Imaging, Monash University and the data collected by Leica LAS X (Leica Microsystems, Inc.) microscope control software.

Sample preparation for vibrational spectroscopy-based techniques

Yeast cells in phosphate buffered saline (PBS) were collected by centrifugation (1000 rpm, 5 min) and the pellet resuspended in 500 μL of ultrapure water, gently mixed and again centrifuged. This step was repeated 3 times to ensure removal of any residual PBS. The final pellet was resuspended in 500 μL of ultrapure water. For each yeast strain, 100 μL of the suspension was placed on each of two CaF₂ slides and air-dried to obtain a dispersed layer of single cells. From each set of two samples, one was subjected to Raman measurements and the other was mounted on a flat magnetic stainless-steel substrate and designated for AFM-IR measurements. The remaining suspension (300 μL) was centrifuged and the pellet was placed directly on the Attenuated Total Reflection (ATR) crystal.

ATR-FTIR measurements

ATR-FTIR data were recorded using a Bruker Alpha FTIR (Ettlingen, Germany) spectrometer with an ATR sampling device containing a single bounce diamond internal reflection element and equipped with a global source, KBr beam splitter and a deuterated triglycine sulfate detector. Spectra were recorded at a resolution of 6 cm^{-1} in the spectral range of 4000–900 cm^{-1} . For each strain, 3 biological replicates were studied and for each of these, 3 technical replicates were recorded ($n_{\text{single_strain}}=9$, $n_{\text{total}}=45$). Background spectra were collected directly prior to each measurement (64 scans). After recording the background, 0.5 μL of yeast pellet was placed on the crystal and air-dried for approximately 10 min. Each spectrum was recorded using 64 co-added interferograms.

Raman measurements

Raman measurements were collected using WITec confocal CRM alpha 300 Raman microscope (WITec, Ulm, Germany). The spectrometer was equipped with an air-cooled solid-state laser operating at 532 nm, a CCD detector, cooled to $-60\text{ }^{\circ}\text{C}$ and 600 grooves/mm grating. The laser was coupled to the microscope via an optical fiber with a diameter of 50 μm . For data collection, a dry Olympus MPLAN (100 \times /0.90NA) objective was used. The monochromator of the spectrometer

was calibrated using Raman scattering line produced by a silicon plate (520.5 cm^{-1}). For each strain, 3 biological replicates were studied and for each of these replicates, 6 individual cells were mapped ($n_{\text{single_strain}} = 18$, $n_{\text{total}} = 90$). The size of mapped area was adapted individually, depending on the size of the cell. Data were collected in the spectral range of $3705\text{--}0\text{ cm}^{-1}$, with the spectral resolution of 3 cm^{-1} . The integration time for a single spectrum was $0.1\text{--}0.3\text{ s}$. Laser power was adjusted individually for each sample, not exceeding the range of $5\text{--}7\text{ mW}$. Raman measurements and initial data analysis were performed using WITec software (WITec Plus, Ulm Germany). Raman images were constructed by integration of selected marker bands without any preprocessing. Cluster analysis was carried out after cosmic spike removal (CRR) and background subtraction (polynomial fit, 2nd order). The Raman data were analyzed with *k*-means Clustering (KMC) using the Manhattan distance and Ward's algorithm.

AFM-IR measurements

AFM-IR measurements were performed with a NanoIR2 system (Anasys Instruments Inc., Santa Barbara, USA). The IR source was an optical parametric oscillator (OPO) laser, producing a 10 ns pulse at a 1 kHz repetition rate. A silicon cantilever (AppNano, Mountain View, CA 94043, USA) was used with nominal radius of 10 nm and a nominal spring constant of 0.5 N/m . The system was purged with N_2 to control humidity. For each strain, 3 biological replicates were studied, with 6 single cells investigated for each biological replicate ($n_{\text{single_strain}} = 18$, $n_{\text{total}} = 90$). All single spectra were collected in the range of $1800\text{--}900\text{ cm}^{-1}$ with a spectral resolution of 8 cm^{-1} and IR maps at fixed wavenumber values, to investigate the distribution of selected components (specific wavenumber values are given in Results). Simultaneously to each IR map, the AFM height and deflection images were acquired. The maps were subsequently combined in Matlab (Mathworks, Natick, USA), PLS_toolbox (Eigenvecor research, Manson, USA) and analyzed using *k*-means clustering to identify the presence and location of LBs. Following this analysis, single spectra were recorded from cytoplasm and LBs. All presented single spectra were normalized using the Standard Normal Variate (SNV) method and smoothed using the Savitzky-Golay algorithm with 13 smoothing points.

Statistical tests

Absorbance data obtained for the engineered and control yeast strains were assessed for statistical significance by one way analysis of variance (ANOVA) at $p < 0.01$, $\alpha = 0.05$; where significant differences were indicated,

Student's *t* test was applied the post hoc to data for engineered strains compared to control.

Results and discussion

Total fatty acid content: correlation between GC-FAME and ATR-FTIR spectroscopy

The cell lines were firstly characterized using gas chromatography (GC) and ATR-FTIR spectroscopy, to provide an overview of the total fatty acid content (Fig. 1). As can be seen from the GC results (Fig. 1c), the total fatty acid content increased in all modified cell lines compared to control. The most significant increase was observed in the HBY31 cell line carrying alterations in 6 lipid-modifying enzymes, and the increases in lipid were proportional to the number of introduced genes. The same trend was observed in the ATR-FTIR spectra, particularly using the spectral ranges between 1800 and 1500 (Fig. 1d, f) and $3050\text{--}2800\text{ cm}^{-1}$ (Fig. 1e, g).

The first region ($1800\text{--}1500\text{ cm}^{-1}$) includes the band at 1745 cm^{-1} (Fig. 1d, black arrow), attributed to stretching of $\text{C}=\text{O}$ groups of lipids, whereas the second one ($2800\text{--}3050\text{ cm}^{-1}$) contains a variety of bands originating from stretching of CH_2 and CH_3 groups in lipid chains [25]. Increase in the intensity of the band at 1745 cm^{-1} as well as the bands in the high wavenumber region between different cell lines is clearly visible (Fig. 1d–g) and follows the same trend as an increase in the total fatty acid content assessed from GC (Fig. 1c). Calculation of the ratio of those bands to the amide I band (Fig. 1a, b) enabled the visualization of changes in the lipid to protein ratio [26] in the studied cell lines, as it represents the total fatty acid content in the dried mass of cells. A PLS regression model, built on the basis of 2nd derivatives of ATR-FTIR spectra in the high wavenumber region, enabled the prediction of total fatty acid content (as a percentage of dry cell weight). The correlation between predicted and assessed from GC total fatty acid content for the validation set, together with the parameters of the PLS regression model, is shown in Fig. 1h. This approach provides a fast and straightforward measure of the effectiveness of lipid metabolic engineering strategy. The 2nd derivatives of ATR-FTIR spectra revealed significant variation in the band at 1636 cm^{-1} (Fig. 1f) assigned to deformation vibration of water, most likely due to intracellular water [27]. No correlation was observed between this and any of the lipid-related bands.

Our initial analysis of metabolically engineered cells undertaken on populations of whole cells addressed the basic question of lipid production between strains and demonstrated the power and rapid analysis of vibrational spectroscopy similar to that previously reported for naturally occurring yeasts by Ami et al. [28]. However, to enable us to address questions relating to subcellular structures and their chemical components and in regard

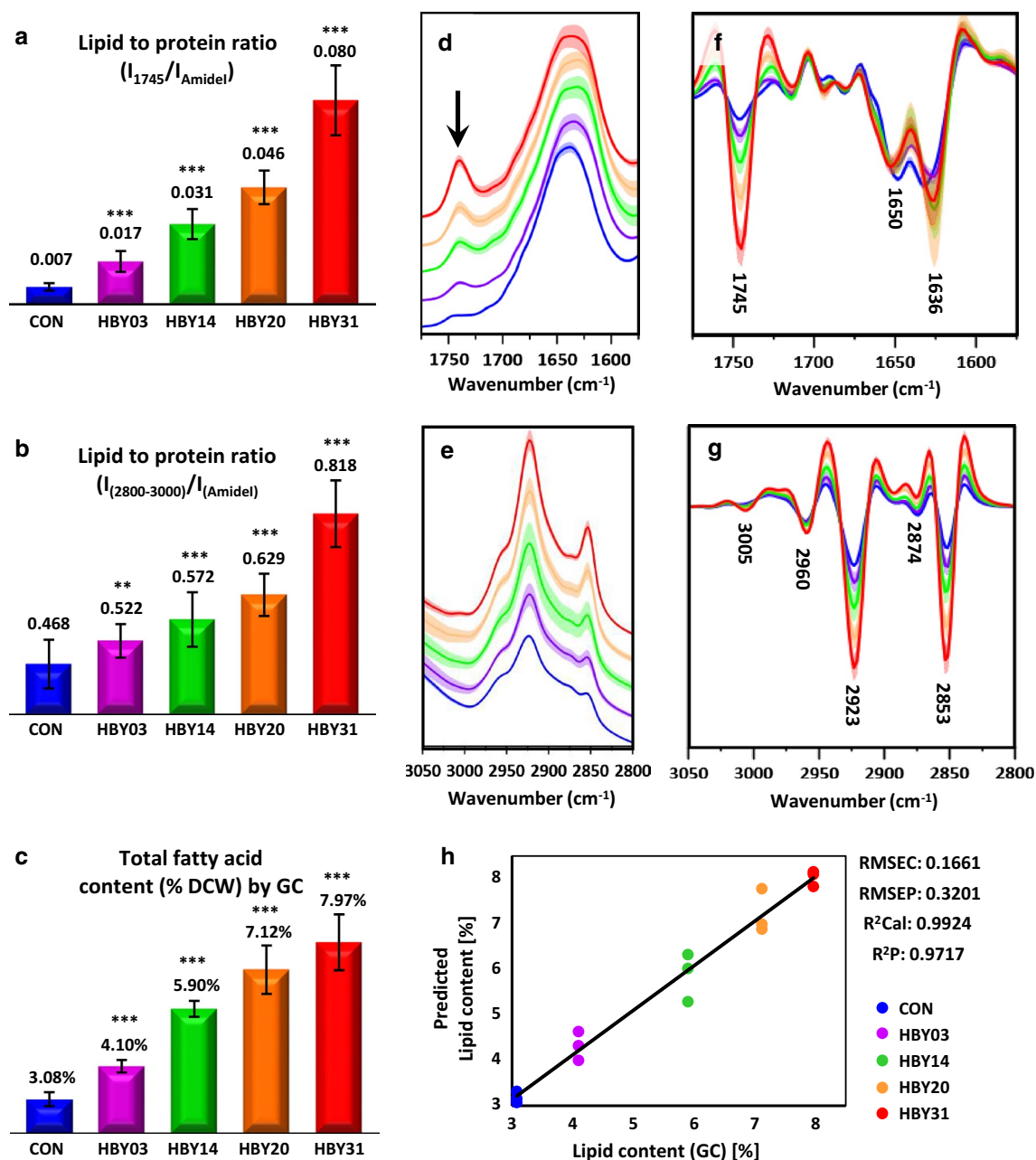


Fig. 1 Results of the assessment of total fatty acid content obtained via (a, b, d–h) ATR-FTIR and (c) GC for all studies cell lines (CON, HBY03, HBY14, HBY20 and HBY31). (a, b) The ratio of lipid to protein obtained on the basis of ATR-FTIR spectra calculated as the ratio of: a the band at 1745 cm^{-1} to the amide I band and b the bands in high wavenumber region to the amide I band. c The total fatty acid content obtained for all cell lines through GC. Detailed fatty acid quantification from GC is presented in Additional file 1: Table S1. All bar charts (a–c) show the results obtained together with their standard deviation (SD). d, e Average ATR-FTIR spectra (with SD) of all cell lines and g, h their 2nd derivatives (with SD) used for calculation of ratios presented in (a) and (b) are shown in the range (d, f) 1550–1800 cm^{-1} and (e, g) 2800–3050 cm^{-1} . Average ATR-FTIR spectra in the whole measured range (3600–600 cm^{-1}) are presented in Additional file 1: Fig. S1, S2. h Results of prediction of the total fatty acid content for the validation set by the PLS regression model (2800–3050 cm^{-1}) on the basis of 2nd derivatives of ATR-FTIR spectra. *** $p < 0.01$ vs control and ** $p < 0.05$ vs control

to cell-to-cell variability within metabolic engineered cells required spectroscopic approaches with greater spatial resolution power.

High-resolution CRS visualization and chemical analysis reveals subcellular structures and the impact of metabolic engineering

To confirm the presence of lipid bodies and estimate their amount, fluorescence imaging of the Nile Red stained cell lines was performed (Fig. 2). The results confirm the presence of LBs in all studied cell lines, with a clear increase in number in the engineered lines compared to control. In addition, amongst the highest engineered line (HBY31), numerous LBs of significantly larger diameter were observed (Fig. 2) but without providing any information about the composition of LBs or other intracellular structures. By comparison high spatial CRS imaging of HBY31 cells visualized LBs via lipid-related bands at 1444 cm^{-1} (bending mode of CH_2), 1656 cm^{-1} (stretching mode of $\text{C}=\text{C}$) or 1740 cm^{-1} (stretching mode $\text{C}=\text{O}$) and chemical content through spectra to reveal the presence of saturated (SFA, 1444 cm^{-1}), unsaturated fatty acids (UFA, 1656 cm^{-1}) as well as triglycerides (TAG, 1740 cm^{-1}) (Fig. 3). These confocal spectra ensured the collection of data only from a selected plane of given thickness and thus provide information exclusively about LBs, without interference of lipids from the cytoplasm and cell wall. Cell-to-cell variability in the presence of key metabolites within HBY31 cells is evident within the sample as shown in Fig. 3.

By imaging the cell in different planes, a three-dimensional chemical profile was mapped with the lipid-related bands, attributed to LBs, clearly visible within the cell (Fig. 4a). Via selection of the appropriate plane inside the cell covering a thickness of ~ 300 to 400 nm and spatial identification of LBs within this plane, spectra were obtained from LBs only. Simultaneously, all other cellular structures were studied by integration of marker bands related to their chemical components (Fig. 4b–f) and cluster analysis performed (Fig. 4g) from all spatially localised and averaged spectra obtained from subcellular structures (Fig. 4h). As can be seen, the LBs (Fig. 4b, g, h: red) contained bands attributed to SFAs (1444 , 1304 cm^{-1}), UFAs (1656 , 1268 cm^{-1}), TAGs (1742 cm^{-1}) and phospholipids (1085 cm^{-1}). The CRS spectrum of cell walls (Fig. 4g, h: dark blue) had a significantly different profile, characteristic of carbohydrates (e.g., 901 , 1075 cm^{-1}) with some protein contributions (1662 cm^{-1}). Cytoplasm (Fig. 4d, g, h: green) consisted mainly of protein (1662 , 1342 , 1314 cm^{-1}), including, e.g., phenylalanine (1007 cm^{-1}) and heme. Within the cytoplasm, areas of high heme content (1590 , 1132 , 753 cm^{-1}) can be identified (Fig. 4e, g, h: brown). Heme

(iron protoporphyrin IX) is an essential molecule for yeast; it serves as a prosthetic group in enzymes and proteins especially those involved in transporting oxygen or in oxidation reactions in addition to its many roles in cell signaling, etc. Furthermore, cluster analysis revealed the presence of a large structure (Fig. 4f–h: light blue), characterised by marker bands at 1160 and 693 cm^{-1} , attributed to inorganic polyphosphate (PolyP) [22]. PolyP has been reported to accumulate in a variety of organisms including yeast at up to 20% of dry cell weight [29] and while some biological functions of PolyP are known, its exact physiological role remains unclear. Here, PolyP accumulations were observed only in the most highly engineered cell line (HBY31).

Lipid body characteristics and fatty acid composition of individual engineered yeast cells

To investigate the variability in presence of LBs, their size and composition within the same metabolic engineered line and between the cell lines, CRS imaging was applied to a total of 90 cells drawn equally from all strains. The distribution of selected components (organic matter, lipids and heme) from a subgroup of these cells is shown in Fig. 5 together with the total number of observed LBs in each cell line and their average diameters. In the case of the control, HBY03 and HBY14 strains show single LBs (per cell) with a diameter of $\sim 1\text{ }\mu\text{m}$, or lacking obvious LBs, with a minor increase in the number of LBs in the engineered lines compared to control. A significant increase in the number of LBs in cells of HBY20 and HBY31 was observed, with HBY20 having the highest among all strains and with LBs present in every cell.

Interestingly, LBs in HBY20 were only slightly increased in size (diameter $1.21 \pm 0.40\text{ }\mu\text{m}$) compared to control (diameter $0.87 \pm 0.23\text{ }\mu\text{m}$) (Fig. 5). For HBY31 strain, LBs were observed in all cells, however, in two types of arrangements. Some cells, similarly to HBY20, contained multiple LBs with a diameter of approximately $1\text{ }\mu\text{m}$, but others contained a single large LB which filled the cell almost entirely (Fig. 5, HBY31 Panel G). This resulted in fewer but overall significantly larger LBs in HBY31 ($2.14 \pm 1.08\text{ }\mu\text{m}$) compared to any other strain. HBY31 was the only strain assessed in this study that expressed caleosin (Table 1), a lipid droplet stabilizing protein originating from plants which may account for the larger LBs observed here.

For a detailed investigation of LB composition, average spectra of each LB from each cell line (calculated from spectra of single LBs) were generated and variability measured (Fig. 6). Spectra of LBs contain several bands in the fingerprint region that are attributed to UFAs (1656 , 1268 cm^{-1}) and SFAs (1444 , 1304 cm^{-1}) with the ratio of intensities of I_{1656}/I_{1444} being among the best

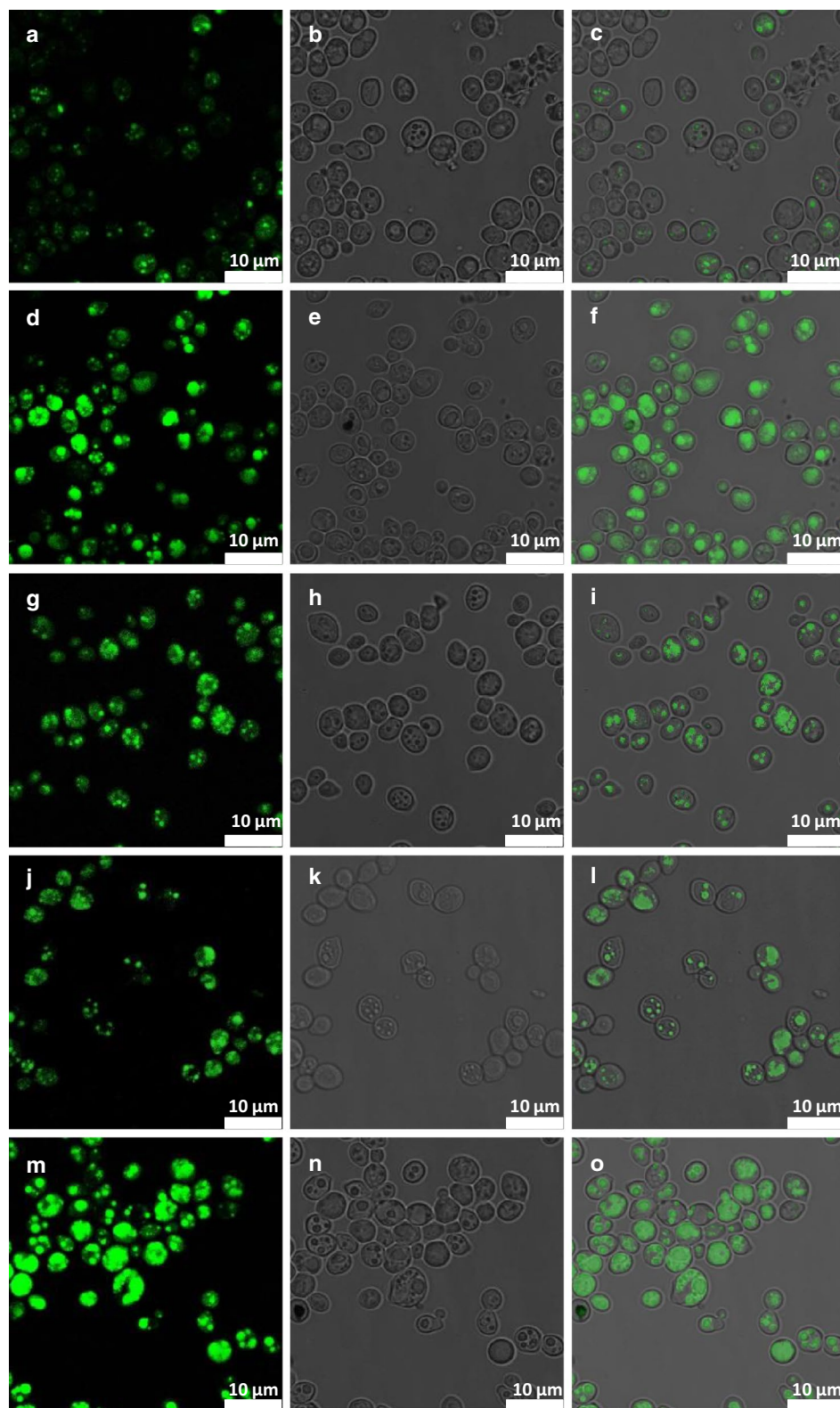
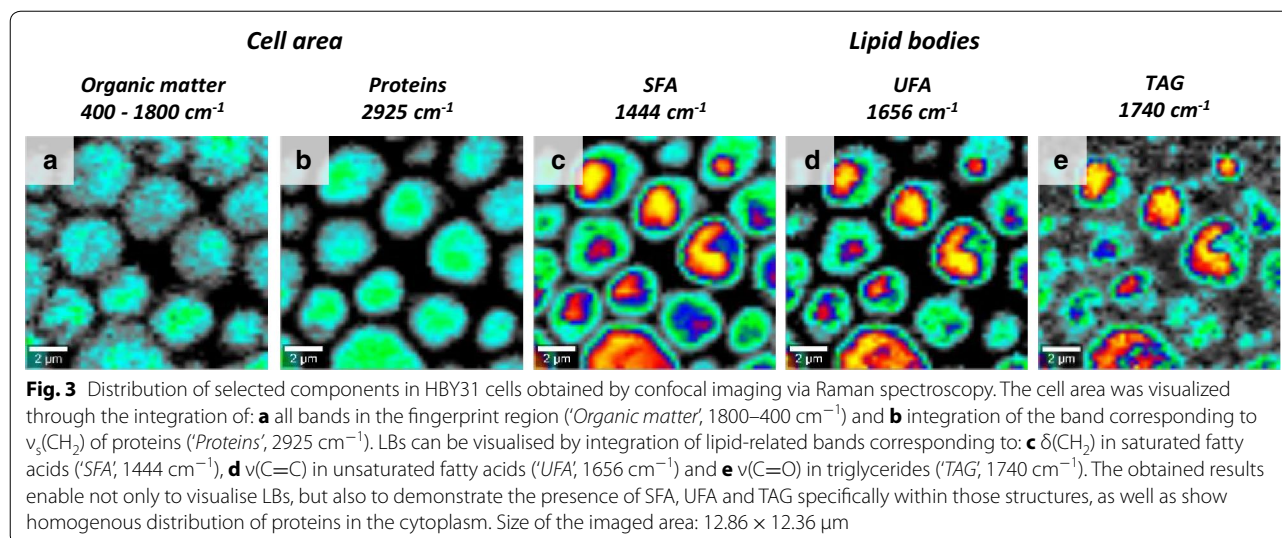


Fig. 2 Images showing: (a, d, g, j, m) fluorescence results, (b, e, h, k, n) visible image in transmission and (c, f, i, l, o) overlay of visible and fluorescence image obtained for the: (a–c) CON, (d–f) HBY03, (g–i) HBY14, (j–l) HBY20 and (m–o) HBY31 yeast cell line at 72 h culturing. The scale bar is presented at the bottom right corner of each image



indicators of fatty acid unsaturation [30]. An alternative approach for measuring fatty acid unsaturation by comparing intensities at 3012 and 2855 cm^{-1} is much less sensitive to unsaturation changes. No significant difference was found in the degree of unsaturation in LBs from HB Y03 and HB Y14 strains compared to control, but a significant decrease in unsaturation of LBs was observed for HB Y31 (0.32 ± 0.05), and to a lesser extent HB Y20 (Fig. 6). The observed decrease in fatty acid unsaturation was unlikely to be due to the larger size of LBs in HB Y31 as the reduction was also observed in HB Y20 for which no change in LB size was noted. This result indicated a shift to higher saturated fatty acid content in LBs in the more engineered strains measured via spectroscopy and the result was supported by GC analysis of fatty acid composition (Additional file 1: Table S1). It should be noted that CRS analysis was specifically measured in LB whereas GC analysis encompassed the whole cell fatty acid composition.

The shift to higher saturated fatty acid content in the most highly engineered strains was not only due to the specificity of the introduced acyltransferase, DGAT1, for saturated fatty acids as the *AtDGAT1* gene was expressed in all strains but maybe also due to limited quantities of unsaturated fatty acids available for conversion to triacylglycerol. $\Delta 9$ -Unsaturated fatty acids are essential components of plasma membranes of yeast [31] and may be preferentially directed to these locations potentially resulting in more saturated fatty acids directed to triacylglycerol production through the enhanced expression of diacylglycerol acyltransferases.

Comprehensive mapping of cellular constituents by AFM-IR

To obtain a comprehensive measure of biochemical changes in cells resulting from induced genetic modifications, further analysis of the composition of cytoplasm and, in particular, carbohydrate content was required. The ability to simultaneously study the composition of intracellular structures without the need to isolate them is an advantage of high spatial imaging via vibrational spectroscopy. However, as described earlier, the cytoplasm of engineered yeast contains significant and varying amounts of heme in the form of clusters and dispersed within the cytoplasm (Fig. 4e, g, h-Brown). The raised and variable Raman background due to heme content effectively conceals less intense signals such as carbohydrate-related bands excited at lower wavelengths and therefore, IR-based spectroscopy is more useful to investigate carbohydrate components at high spatial resolution. However, as the spatial resolution of conventional IR imaging does not exceed $\sim 5 \mu\text{m}$, a more sophisticated approach based on AFM-IR imaging was applied in our case. In AFM-IR the phenomenon of IR absorption is not measured directly, but by measuring the thermal expansion of the sample resulting from application. Therefore, the spatial resolution of imaging with the use of AFM-IR is no longer limited to $\sim 5 \mu\text{m}$, but can be significantly smaller ($\sim 100 \text{nm}$), enabling the measurement of spectra representing explicitly the composition of subcellular structures. AFM-IR mapping with selected bands corresponding to proteins, lipids and carbohydrates was performed on 6 replicate cells for each strain and the images were combined and analysed via cluster analysis to confirm presence (or absence) of LBs and determine their precise location within the

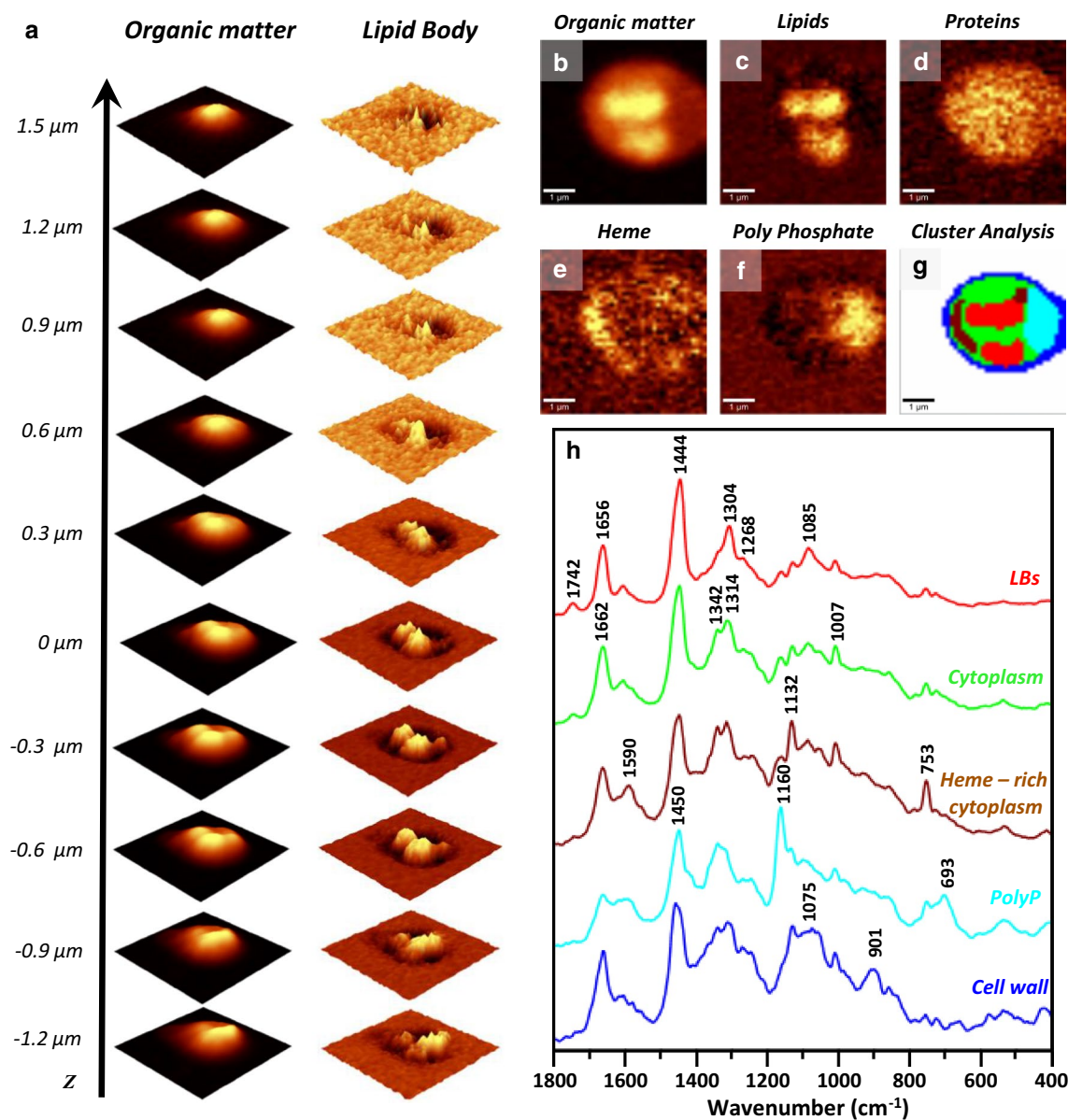
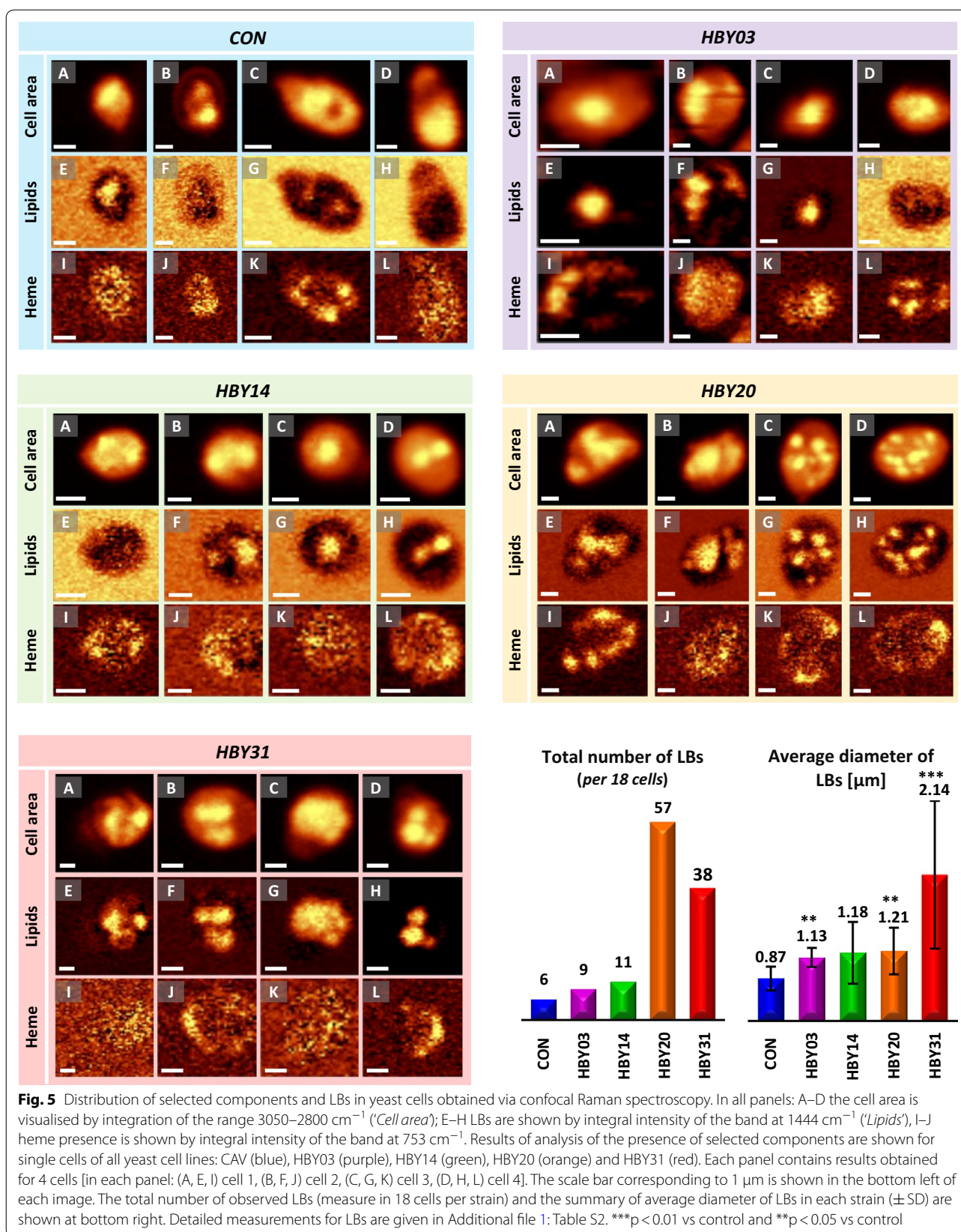
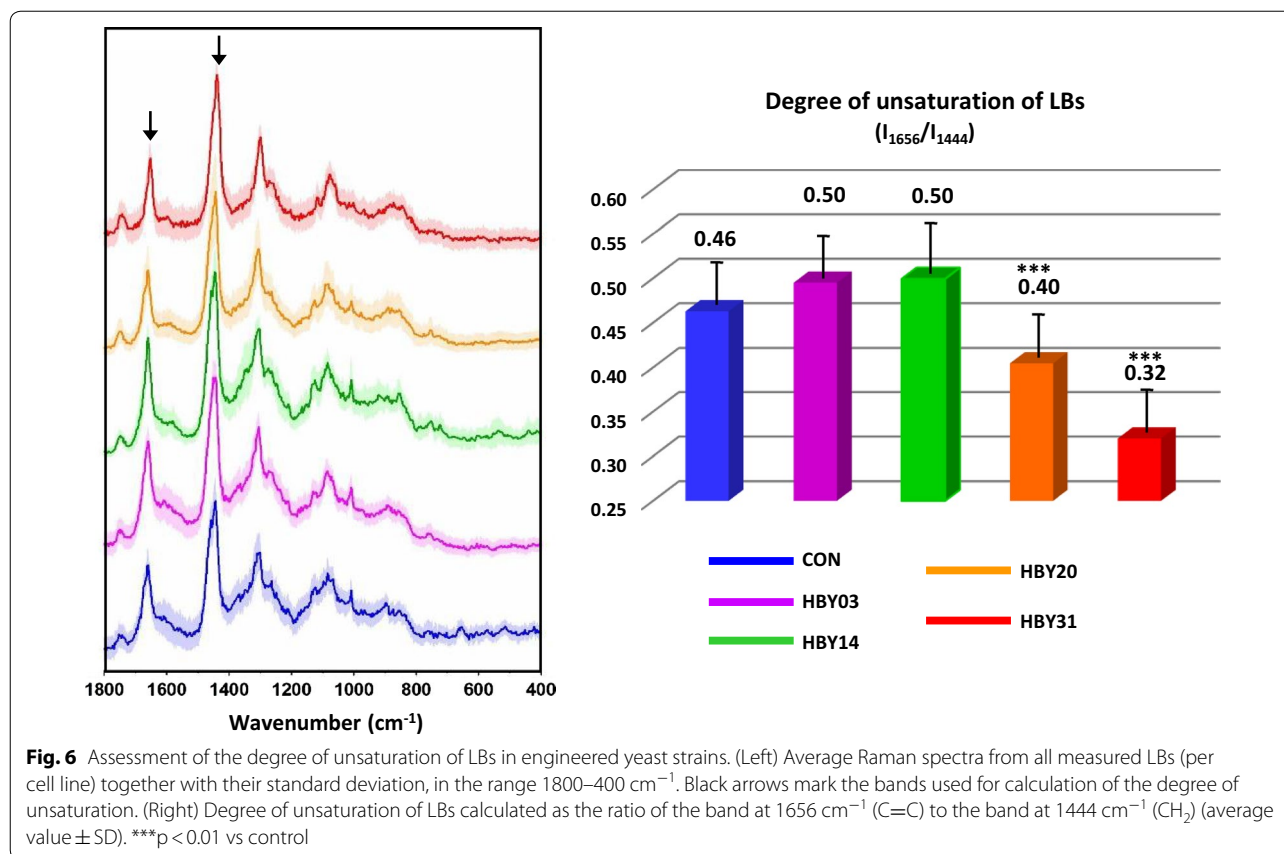


Fig. 4 Comprehensive analysis of individual HBY31 cells via confocal Raman spectroscopy. **a** Confocal imaging enables depth profiling showing the distribution of selected components. The depth profiling was done with a step size of 300 nm. The distribution of *Organic matter* is demonstrated on the basis of integration of bands in the range 3050–2800 cm^{-1} and visualises the cell. The integration of the band at 1444 cm^{-1} enables us to visualise *LBs*. As can be seen, the *LBs*' signals are present only within selected layers, corresponding to the inside of cell. **b–f** Distribution of selected components in a cell with polyphosphate vacuole, on the basis of integration of bands at: **(b)** 3050–2800 cm^{-1} (*Organic matter*), **(c)** 1444 cm^{-1} (*Lipids*), **(d)** 2925 cm^{-1} (*Proteins*), **(e)** 753 cm^{-1} (*heme*), **(e)** 1160 cm^{-1} (*Polyphosphate*). **g, h** Cluster analysis results obtained for the cell presented in **(b–f)**: **(g)** distribution of classes and **(h)** corresponding spectra of each class with marked selected bands. Size of the imaged area: **(a)** 5.32 \times 5.24 μm and **(b)** 5.22 \times 5.17 μm . With the use of 532 nm excitation wavelength the theoretical thickness of each plane, according to Rayleigh criterion, is 361 nm

cell. Subsequently, single spectra (5–10) were collected from areas corresponding to *LBs* and cytoplasm. A high prevalence of *LBs* in the HBY31 and HBY20 strains were observed, in agreement with results shown previously by other techniques applied in this study.

Focussing on HBY31 strain, Fig. 7a–d shows the AFM height profile recorded simultaneously with each AFM–IR map and the relatively even thickness of the cell (approximately 3 μm). The presence of *LBs* was revealed through imaging of the absorbance at 1740 cm^{-1}





(stretching of C=O from lipids) (Fig. 7f) and 1264 cm^{-1} (deformation of CH_2 of lipids) (Fig. 7g). The protein (Fig. 7e) and carbohydrate (Fig. 7h) distribution in the cells were homogenous, as these signals originate from both cytoplasm and cell wall, with the latter being of even thickness across the cell. A comparison between AFM-IR spectra of LB (Fig. 7i, red) and cytoplasm (Fig. 7i, black) of the same HBY31 cell showed large differences, the LB spectrum was dominated by lipid-related signals (1740, 1464, 1080 cm^{-1}) and an intense phospholipid band (1080 cm^{-1} , stretching of PO_2) originating from the LB membrane. The spectra of the HBY31 cytoplasm (Fig. 7i, black) has higher protein (1656 cm^{-1}) to lipid (1740 cm^{-1}) ratio compared with the LB spectra (Fig. 7i, red). A comparison of 2nd derivatives of AFM-IR spectra of cytoplasm from both HBY31 (Fig. 7j, black) and control (Fig. 7j, blue) showed interesting differences: although the HBY31 cytoplasm shows lower intensity due to lipids than LB from the same cell, it reveals a higher lipid content in the cytoplasm, compared to the control cell (Fig. 7j, blue). In terms of metabolic engineering, the measurement of significant quantities of lipid in the cytoplasm suggests the lipid accumulation and sequestration strategies for HBY31 cells are out of

balance with production, and lipid storage capacity of LBs in this strain has been overwhelmed. In addition, a band of significant intensity at 1044 cm^{-1} in control cells (Fig. 7j, blue) attributed to carbohydrate, was absent in the cytoplasm of HBY31 (Fig. 7j, black), suggesting an acute reduction of the carbohydrates in favour of enrichment of lipids in the cytoplasm of HBY31.

AFM-IR reveals cell-to-cell variability in concentrations of key metabolites

The AFM-IR spectra obtained from individual cells in all strains were analysed with respect to the relationship between carbohydrate and lipid content, and variance between samples. The average spectra for cytoplasm for each strain are shown in Fig. 8 together with the variance within the strain. The lipid content in the cytoplasm (e.g., 1740 cm^{-1}) undoubtedly increases, from low levels in control cells, through higher amounts for HBY03 and HBY14, to very high concentrations for HBY20 and HBY31 cell lines (Fig. 8a, c marked with a star), and the intra-strain variability in cytoplasm lipid increases. Concurrent with the increase of the intensity of lipid-related bands with more engineered strains, was a decrease in intensity of the bands in the range 1100–900 cm^{-1}

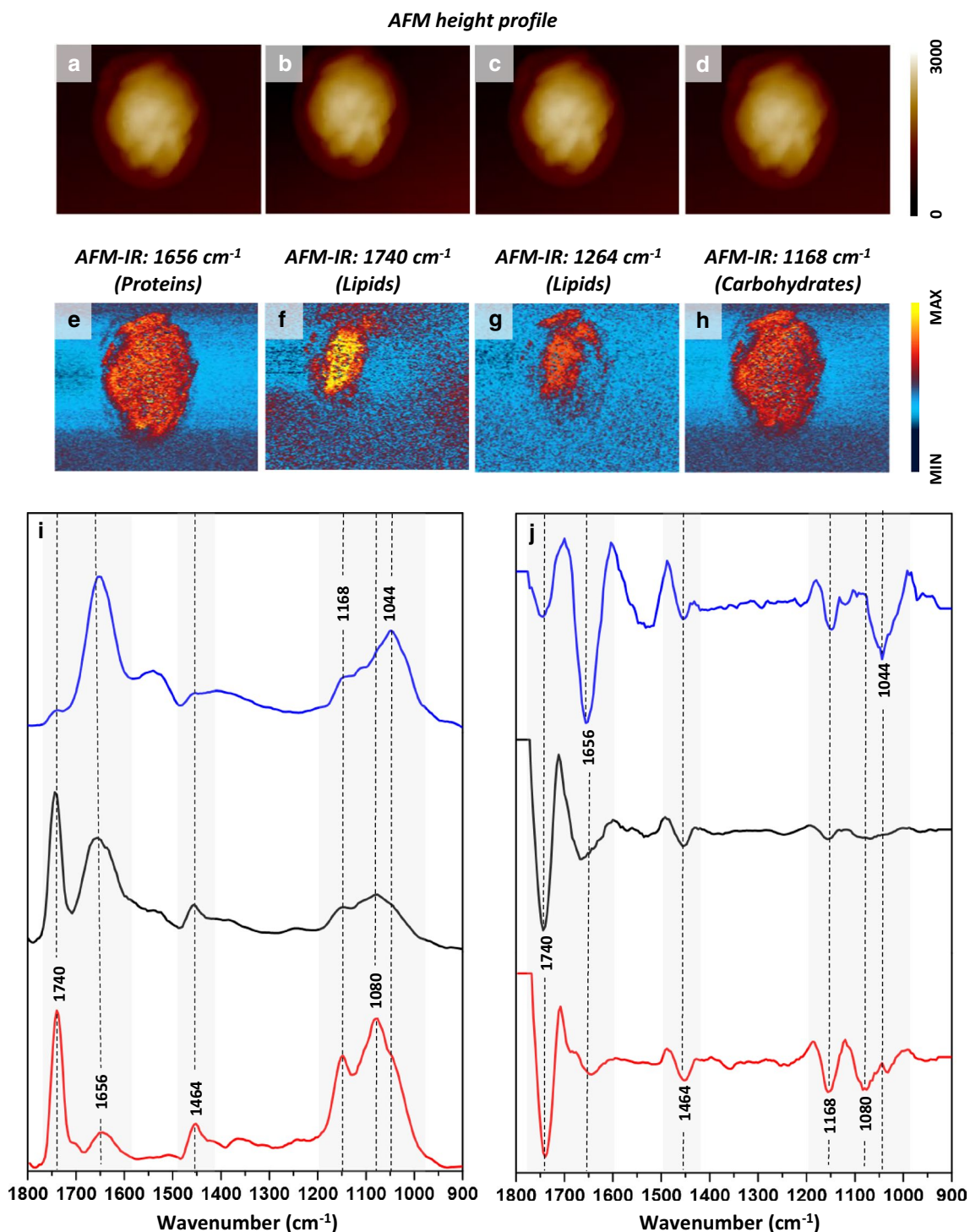


Fig. 7 AFM-IR analysis of HBY31 cells. **a-d** AFM height results recorded simultaneously with **e-h** AFM-IR imaging of selected wavenumbers, demonstrating the distribution of chosen components: **e** proteins (1656 cm^{-1}) (corresponding height: **a**), **f** lipids (1740 cm^{-1}) (corresponding height: **b**), **g** lipids (1264 cm^{-1}) (corresponding height: **c**) and **h** carbohydrates (cell wall, 1168 cm^{-1}) (corresponding height: **d**). The size of imaged area was $5.41 \times 4.47 \mu\text{m}$. The scale bar for AFM height is given in nm. **i** A comparison of AFM-IR spectra and **j** their 2nd derivatives in the range $1800\text{--}900 \text{ cm}^{-1}$ recorded from: LB (in red) of HBY31 cell, cytoplasm of HBY31 cell (in black) and cytoplasm of control cell (in blue). The spectral regions and bands showing most prominent differences were marked in grey background and black dash lines

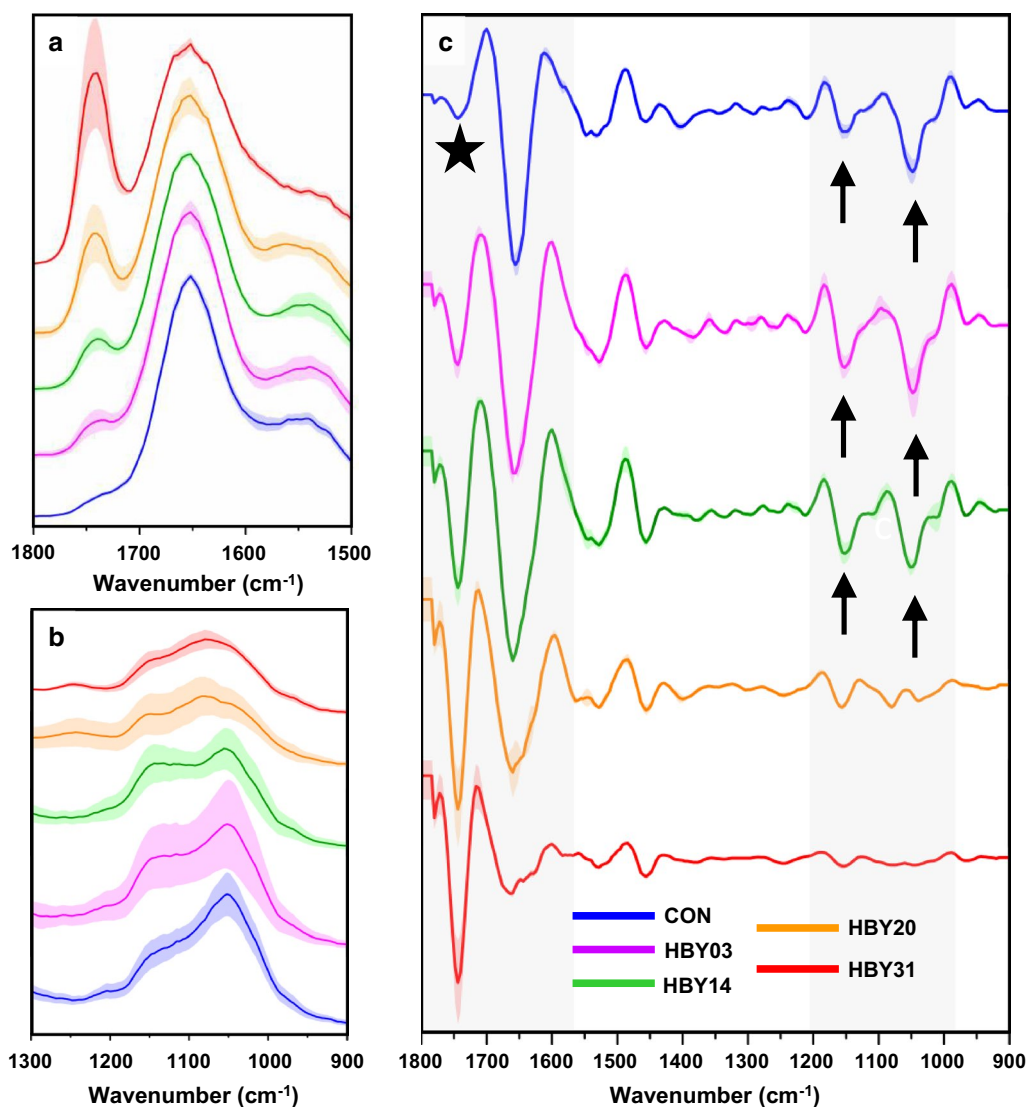


Fig. 8 Averaged AFM-IR spectra of cytoplasm of engineered yeast cells in the range **(a)** 1800–1500 cm^{-1} and **(b)** 1300–900 cm^{-1} together with **(c)** their 2nd derivative in the range 1800–900 cm^{-1} . Each presented average spectrum was obtained by averaging 30 single spectra collected for different cells (of the same strain) and is shown with SD. Each single spectrum in this study was collected from cytoplasm, after localization of the LB (or confirmation of its absence) through AFM-IR imaging. Grey area, black star and black arrows mark the most prominent differences

(Fig. 8b). A detailed comparison of 2nd derivative spectra revealed the contribution of different components in this region: for control, HBY03 and HBY14, the carbohydrate-related band at 1044 cm^{-1} was clearly present (Fig. 8c, black arrows) and of significant intensity. For cytoplasm of HBY20, the carbohydrate band was just visible but substantially lower and the emergence of the phospholipid band at 1080 cm^{-1} was evident (Fig. 8b). As discussed previously, the cytoplasm of HBY31 cells had almost no intensity at 1044 cm^{-1} whereas the band at 1080 cm^{-1} became more prominent (Fig. 8b). Altogether, the AFM-IR results demonstrate the increase in lipid content and a

simultaneous decrease in the carbohydrate content in the cytoplasm, from high carbohydrate and low lipid in control cells to the reversed ratio in the HBY31 strain.

Vibrational spectroscopy analysis has previously been shown to be highly informative for measurement and location of target metabolites such as lipids in cultured cells of wild-type microalgae and yeast [17, 19, 32–40] and in selected studies that include heterologous expression of lipid stabilizing proteins [41]. Our study is the first to our knowledge where the effects of the sequential introduction of a complex metabolic engineering pathway into an organism have been measured using

vibrational spectroscopy techniques and have revealed valuable insights into areas for further improvement.

Conclusions

Here, we have used vibrational spectroscopy techniques to measure the impact of metabolic engineering approaches for high lipid production in yeast at both the single cell level and averaged and detailed information about the chemical composition of subcellular structures. The ratio of lipid-related bands (e.g., 1740 cm^{-1}) to amide I was demonstrated to be useful as a quick marker of the total lipid content. An established PLS regression model allowed the successful prediction of total fatty acid content from the ATR-FTIR spectrum, demonstrating the ability of this technique to provide the same information as GC, but within few minutes and without the need for complex sample preparation. Fluorescence imaging enabled us to visualise LBs, confirming their highest prevalence and size in the HBY31 strain. Furthermore, two high spatial imaging techniques based on vibrational spectroscopies were applied (CRS, AFM-IR) and demonstrated substantial changes in intracellular composition with more complex metabolic engineering. CRS imaging provided an insight into LBs composition, revealing a significant decrease in the degree of unsaturation of lipids in the most highly engineered strain—HBY31. In addition, CRS imaging demonstrated significantly increased LB number in HBY20 and HBY31 strains together with a dramatic increase in LB size for HBY31 that expressed the LB stabilizing protein, caleosin. Finally, the AFM-IR imaging demonstrated large changes in the composition of cytoplasm between strains. A decrease in carbohydrate content with concurrent increase in lipid content of cytoplasm was observed, progressing from control through to HBY31 strains. The high concentration of lipid in the cytoplasm of HBY31, in particular, suggests lipid production rate in these engineered yeast is exceeding the rate of lipid sequestration in LBs which could lead to lipotoxicity. Additionally, the shift towards higher saturated fatty acids levels in stored lipids suggests a reduction in the availability of unsaturated fatty acids for TAG formation in the cells. Altogether, our results have demonstrated an increase in the total lipid content resulting from genetic modifications, with the multigene modification approach (*Ald6*, *SEACS*^{L64IP}, *ACC1*^{S659A}, *S1157A*, *AtDGAT1*, *AtClo1* and *Tgl3Δ*) in the HBY31 cell line being most effective. The vibrational spectroscopy approach allowed the simultaneous measurement of intra-strain variability in metabolite production and impact on cellular structures from metabolic engineering.

Additional file

Additional file 1. Supplementary Information.

Abbreviations

ACC: acetyl-CoA carboxylase; ACS: acetyl-CoA synthetase; AFM-IR: atomic force microscopy-infrared spectroscopy; ALD: aldehyde dehydrogenase; AtClo1: caleosin from *Arabidopsis thaliana*; ATR-FTIR: attenuated total reflection-Fourier transform infrared spectroscopy; CRS: confocal Raman spectroscopy; DCW: dry cell weight; DGAT1: diacylglycerol acyltransferase; FA: fatty acid; FAME: fatty acid methyl ester; GC: gas chromatography; GC-FID: gas chromatography with flame ionization detector; IR: infrared (spectroscopy); LB: lipid body; PBS: phosphate buffer solution; PLS: partial least square; PolyP: inorganic polyphosphate; RS: Raman spectroscopy; SFA: saturated fatty acid; SNV: standard normal variate; TAG: triacylglycerol; Tgl3: triacylglycerol lipase 3; UFA: unsaturated fatty acid.

Authors' contributions

KK collected ATR, Raman, AFM-IR, performed the data analysis, prepared the figures and drafted the manuscript. HP cultured the yeast cell lines, collected and analysed GC and fluorescence data and contributed to writing and correcting the manuscript. BR contributed to the experimental planning and corrected the manuscript. VH contributed to the design of the experiment, data interpretation and contributed to the writing of the manuscript. All authors read and approved the final manuscript.

Author details

¹ Centre for Biospectroscopy, School of Chemistry, Monash University, Clayton Campus, Clayton, VIC 3800, Australia. ² Department of Chemical Engineering, Monash University, Clayton Campus, Clayton, VIC 3800, Australia.

Acknowledgements

We thank Mr. Finlay Shanks for technical support of the instrumentals and are grateful to Ms. Yanqin Xu and Prof. Hongyuan Yang for the gift of the strains BY4741 and BY4741 *Tgl3Δ*.

Competing interests

The authors declare that they have no competing interests.

Availability of data and materials

The datasets used and/or analysed during the current study are available from the corresponding author on reasonable request.

Consent for publication

Not applicable.

Ethics approval and consent to participate

Not applicable.

Funding

We acknowledge the financial support from ARC linkage Project (LE160100185) and Monash University for the graduate and international postgraduate research scholarships awarded to HP. B.R.W. is supported by an Australian Research Council (ARC) Future Fellowship Grant FT120100926.

Publisher's Note

Springer Nature remains neutral with regard to jurisdictional claims in published maps and institutional affiliations.

Received: 19 February 2018 Accepted: 4 April 2018

Published online: 10 April 2018

References

- Liang MH, Jiang JG. Advancing oleaginous microorganisms to produce lipid via metabolic engineering technology. *Prog Lipid Res.* 2013;52(4):395–408.
- Lennen RM, Pflieger BF. Microbial production of fatty acid-derived fuels and chemicals. *Curr Opin Biotechnol.* 2013;24(6):1044–53.
- Lamers D, van Biezen N, Martens D, Peters L, van de Zilver E, Jacobs-van Dreumel N, Wijffels RH, Lokman C. Selection of oleaginous yeasts for fatty acid production. *BMC Biotechnol.* 2016;16(1):45.

4. Liu Y, Zhang C, Shen X, Zhang X, Cichello S, Guan H, Liu P. Microorganism lipid droplets and biofuel development. *BMB Rep.* 2013;46(12):575–81.
5. Zhou YJ, Buijs NA, Zhu Z, Qin J, Siewers V, Nielsen J. Production of fatty acid-derived oleochemicals and biofuels by synthetic yeast cell factories. *Nat Commun.* 2016;7:11709.
6. Sitepu IR, Garay LA, Sestric R, Levin D, Block DE, German JB, Boundy-Mills KL. Oleaginous yeasts for biodiesel: current and future trends in biology and production. *Biotechnol Adv.* 2014;32(7):1336–60.
7. Friedlander J, Tsakraklides V, Kaminen A, Greenhagen EH, Consiglio AL, MacEwen K, Crabtree DV, Afshar J, Nugent RL, Hamilton MA, et al. Engineering of a high lipid producing *Yarrowia lipolytica* strain. *Biotechnol Biofuels.* 2016;9(1):77.
8. Chen Y, Daviet L, Schalk M, Siewers V, Nielsen J. Establishing a platform cell factory through engineering of yeast acetyl-CoA metabolism. *Metab Eng.* 2013;15(Supplement C):48–54.
9. Ruenwai R, Cheevadhanarak S, Laoteng K. Overexpression of acetyl-CoA carboxylase gene of *Mucor rouxii* enhanced fatty acid content in *Hansenula polymorpha*. *Mol Biotechnol.* 2009;42(3):327–32.
10. Tai M, Stephanopoulos G. Engineering the push and pull of lipid biosynthesis in oleaginous yeast *Yarrowia lipolytica* for biofuel production. *Metab Eng.* 2013;15(Supplement C):1–9.
11. Peng H, Moghaddam L, Brinin A, Williams B, Mundree S, Haritos VS. Functional assessment of plant and microalgal lipid pathway genes in yeast to enhance microbial industrial oil production. *Biotechnol Appl Biochem* 2017;1–7. <https://doi.org/10.1002/bab.1573>.
12. Froissard M, D'Andrea S, Boulard C, Chardot T. Heterologous expression of AtClo1, a plant oil body protein, induces lipid accumulation in yeast. *FEMS Yeast Res.* 2009;9(3):428–38.
13. Dulermo T, Nicaud J-M. Involvement of the G3P shuttle and β -oxidation pathway in the control of TAG synthesis and lipid accumulation in *Yarrowia lipolytica*. *Metab Eng.* 2011;13(5):482–91.
14. Martins BM, Locke JC. Microbial individuality: how single-cell heterogeneity enables population level strategies. *Curr Opin Microbiol.* 2015;24:104–12.
15. Fritzsche FS, Dusny C, Frick O, Schmid A. Single-cell analysis in biotechnology, systems biology, and biocatalysis. *Ann Rev Chem Biomol Eng.* 2012;3:129–55.
16. Radulovic M, Knittelfelder O, Cristobal-Sarramian A, Kolb D, Wolinski H, Kohlwein SD. The emergence of lipid droplets in yeast: current status and experimental approaches. *Curr Genet.* 2013;59(4):231–42.
17. Smith R, Wright KL, Ashton L. Raman spectroscopy: an evolving technique for live cell studies. *Analyst.* 2016;141(12):3590–600.
18. Heraud P, Marzec KM, Zhang QH, Yuen WS, Carroll J, Wood BR. Label-free in vivo Raman microspectroscopic imaging of the macromolecular architecture of oocytes. *Sci Rep.* 2017;7(1):8945.
19. Kochan K, Kus E, Filipek A, Szafranska K, Chlopicki S, Baranska M. Label-free spectroscopic characterization of live liver sinusoidal endothelial cells (LSECs) isolated from the murine liver. *Analyst.* 2017;142(8):1308–19.
20. Perez-Guaita D, Kochan K, Martin M, Andrew DW, Heraud P, Richards JS, Wood BR. Multimodal vibrational imaging of cells. *Vib Spectrosc.* 2017;91(Supplement C):46–58.
21. Shao Y, Fang H, Zhou H, Wang Q, Zhu Y, He Y. Detection and imaging of lipids of *Scenedesmus obliquus* based on confocal Raman microspectroscopy. *Biotechnol Biofuels.* 2017;10:300.
22. Noothalapati H, Sasaki T, Kaino T, Kawamukai M, Ando M, Hamaguchi HO, Yamamoto T. Label-free chemical imaging of fungal spore walls by Raman microscopy and multivariate curve resolution analysis. *Sci Rep.* 2016;6:27789.
23. Peng H, He L, Haritos VS. Impact of yeast lipid pathway engineering and bioprocess strategy on cellular physiology and lipid content. *J Ind Microbiol Biotechnol.* 2018 (**under review**).
24. Wolinski H, Kohlwein SD. Microscopic and spectroscopic techniques to investigate lipid droplet formation and turnover in yeast. *Membrane Trafficking: Second Edition*; 2015. p. 289–305.
25. Cavagna M, Dell'Anna R, Monti F, Rossi F, Torriani S. Use of ATR-FTIR microspectroscopy to monitor autolysis of *Saccharomyces cerevisiae* cells in a base wine. *J Agric Food Chem.* 2010;58(1):39–45.
26. Kochan K, Maslak E, Chlopicki S, Baranska M. FT-IR imaging for quantitative determination of liver fat content in non-alcoholic fatty liver. *Analyst.* 2015;140(15):4997–5002.
27. Mojet BL, Ebbesen SD, Lefferts L. Light at the interface: the potential of attenuated total reflection infrared spectroscopy for understanding heterogeneous catalysis in water. *Chem Soc Rev.* 2010;39(12):4643–55.
28. Ami D, Posteri R, Mereghetti P, Porro D, Doglia SM, Branduardi P. Fourier transform infrared spectroscopy as a method to study lipid accumulation in oleaginous yeasts. *Biotechnol Biofuels.* 2014;7(1):12.
29. McGrath JW, Quinn JP. Intracellular accumulation of polyphosphate by the yeast *Candida humicola* G-1 in response to acid pH. *Appl Environ Microbiol.* 2000;66(9):4068–73.
30. Kochan K, Maslak E, Krafft C, Kostogrys R, Chlopicki S, Baranska M. Raman spectroscopy analysis of lipid droplets content, distribution and saturation level in non-alcoholic fatty liver disease in mice. *J Biophotonics.* 2015;8(7):597–609.
31. Stuke JE, McDonough VM, Martin CE. The OLE1 gene of *Saccharomyces cerevisiae* encodes the delta 9 fatty acid desaturase and can be functionally replaced by the rat stearoyl-CoA desaturase gene. *J Biol Chem.* 1990;265(33):20144–9.
32. Shao YN, Fang H, Zhou H, Wang Q, Zhu YM, He Y. Detection and imaging of lipids of *Scenedesmus obliquus* based on confocal Raman microspectroscopy. *Biotechnol Biofuels.* 2017;10:300.
33. Wang TT, Ji YT, Wang Y, Jia J, Li J, Huang S, Han DX, Hu Q, Huang WE, Xu J. Quantitative dynamics of triacylglycerol accumulation in microalgae populations at single-cell resolution revealed by Raman microspectroscopy. *Biotechnol Biofuels.* 2014;7:58.
34. Chiu LD, Ho SH, Shimada R, Ren NQ, Ozawa T. Rapid in vivo lipid/carbohydrate quantification of single microalgal cell by Raman spectral imaging to reveal salinity-induced starch-to-lipid shift. *Biotechnol Biofuels.* 2017;10:9.
35. He YH, Zhang P, Huang S, Wang TT, Ji YT, Xu J. Label-free, simultaneous quantification of starch, protein and triacylglycerol in single microalgal cells. *Biotechnol Biofuels.* 2017;10:275.
36. Noothalapati H, Sasaki T, Kaino T, Kawamukai M, Ando M, Hamaguchi H, Yamamoto T. Label-free chemical imaging of fungal spore walls by Raman microscopy and multivariate curve resolution analysis. *Sci Rep.* 2016;6:27789.
37. Huang CK, Hamaguchi H, Shigeto S. In vivo multimode Raman imaging reveals concerted molecular composition and distribution changes during yeast cell cycle. *Chem Commun.* 2011;47(33):9423–5.
38. Heraud P, Marzec KM, Zhang QH, Yuen WS, Carroll J, Wood BR. Label-free in vivo Raman microspectroscopic imaging of the macromolecular architecture of oocytes. *Sci Rep.* 2017;7:8945.
39. Perez-Guaita D, Kochan K, Martin M, Andrew DW, Heraud P, Richards JS, Wood SR. Multimodal vibrational imaging of cells. *Vib Spectrosc.* 2017;91:46–58.
40. Deniset-Besseau A, Prater CB, Vïrolle MJ, Dazzi A. Monitoring triacylglycerols accumulation by atomic force microscopy based infrared spectroscopy in *Streptomyces* species for biodiesel applications. *J Phys Chem Lett.* 2014;5(4):654–8.
41. Jamme F, Vindigni J-D, Mèchin V, Cherifi T, Chardot T, Froissard M. Single cell synchrotron FT-IR microspectroscopy reveals a link between neutral lipid and storage carbohydrate fluxes in *S. cerevisiae*. *PLoS ONE.* 2013;8(9):e74421.

Additional materials

For submission to: *Biotechnology for Biofuels*

Section: *Research*

***Single cell assessment of yeast metabolic engineering for enhanced lipid
production using Raman and AFM-IR imaging***

Kamila Kochan^{1†}, Huadong Peng^{2†}, Bayden R. Wood¹, Victoria S. Haritos^{2,*}

¹*Centre for Biospectroscopy, School of Chemistry, Monash University, Clayton Campus,
3800, Victoria, Australia*

²*Department of Chemical Engineering, Monash University, Clayton Campus, 3800, Victoria,
Australia*

†Equal contributors

Author for correspondence:

Assoc Prof Victoria Haritos,

Department of Chemical Engineering,

Monash University, Clayton 3800, Victoria Australia

Phone: +61 3 9905 6873

email: victoria.haritos@monash.edu

Table S1. GC analysis of total fatty acid content in yeast strains.

Sample	Total fatty acid content [% of dry cell weight]		Fatty acid composition [% of total fatty acid content]						
	Mean	SD	C10:0	C12:0	C14:0	C16:1	C16:0	C18:1	C18:0
CON	3.08	0.22	0.00	0.61	0.00	54.67	19.06	17.14	8.52
HBY03	4.10	0.19	0.00	0.88	1.32	47.47	22.04	16.59	11.70
HBY14	5.90	0.25	1.28	1.24	1.97	45.25	23.55	16.26	10.44
HBY20	7.12	0.75	1.80	1.54	2.61	38.30	28.96	14.09	12.71
HBY31	7.97	0.87	1.92	1.63	2.82	37.68	29.59	13.53	12.84

Table S2. The average diameter (μm) of LBs in yeast strains together with standard deviation (SD) measured by confocal Raman spectroscopy. (The values are represented as a bar chart in Fig. 5.)

CON		HBY 03		HBY 14		HBY 20		HBY 31	
<i>Mean</i>	<i>SD</i>								
0.87	0.23	1.13	0.16	1.18	0.53	1.21	0.40	2.14	1.08

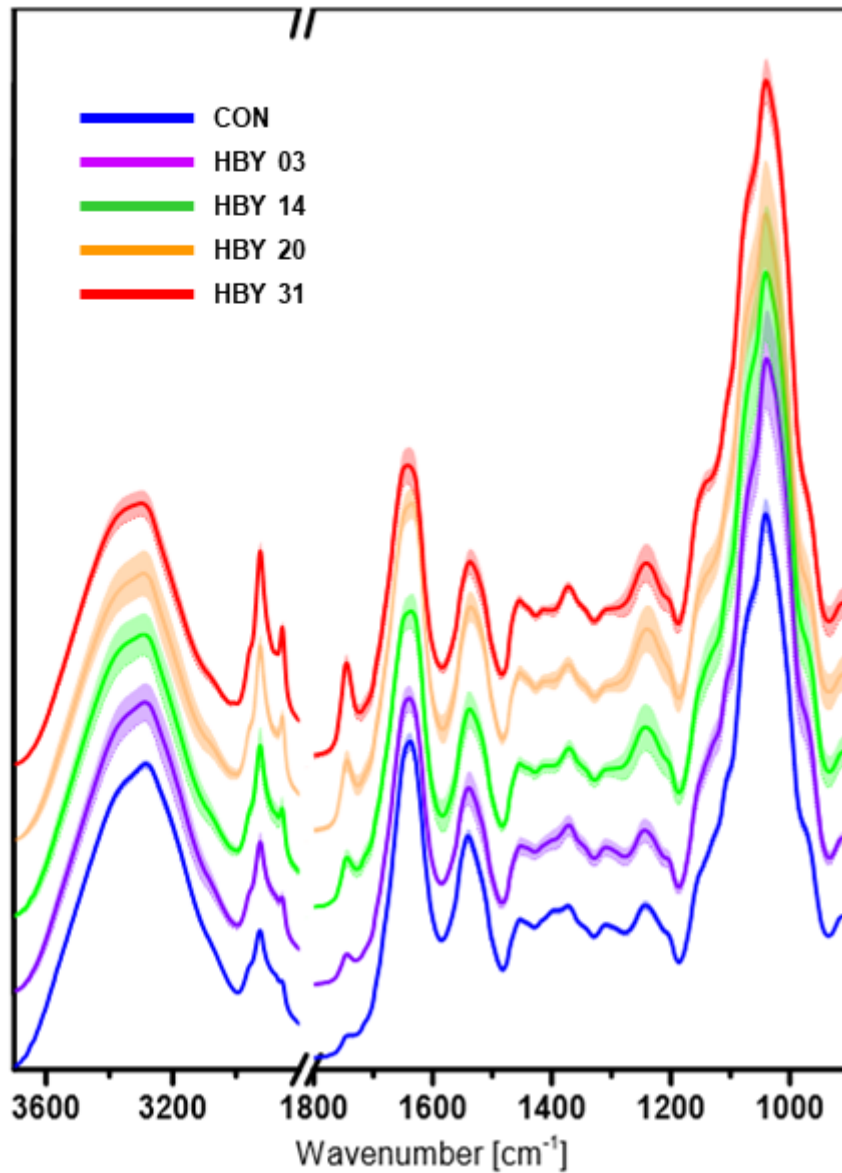


Figure S1. ATR-FTIR average spectra (and SD) of all measured cell lines in the range 3700 – 900 cm^{-1} . Each spectrum is an average of 9 single spectra (3 technical replicates of 3 biological replicates.).

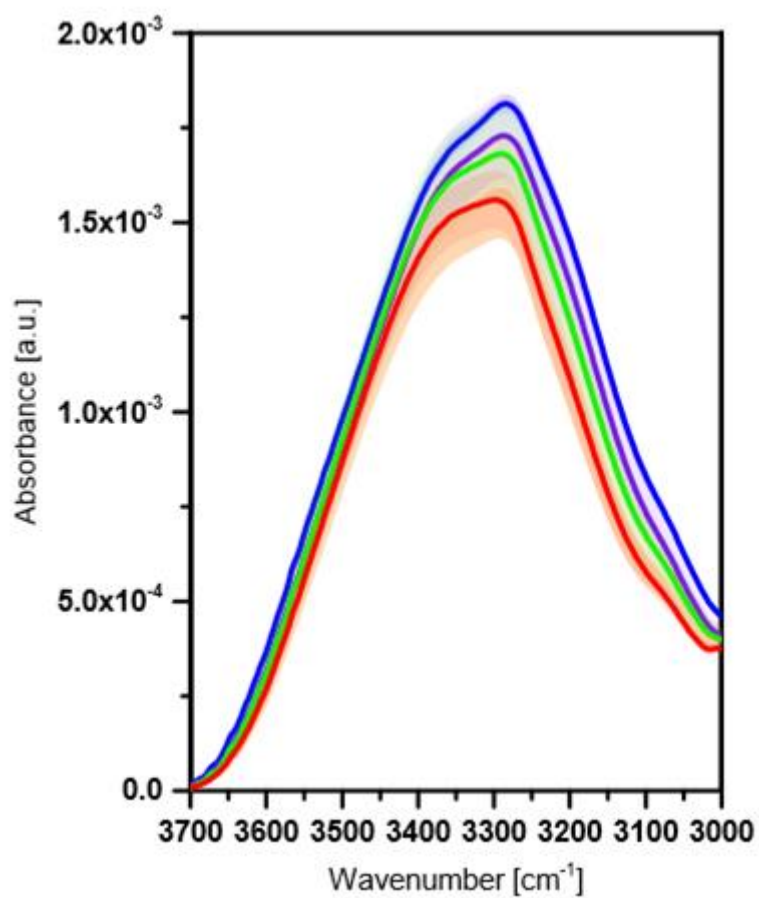


Figure S2. ATR-FTIR average spectra (and SD) of all measured cell lines in the range 3700 – 3000 cm^{-1} . Each spectrum is an average of 9 single spectra (3 technical replicates of 3 biological replicates.). Colour coding of spectra is presented in Figure S1.

This page is intentionally blank



Cite this: DOI: 10.1039/c8an01477a

Raman spectroscopy as a tool for tracking cyclopropane fatty acids in genetically engineered *Saccharomyces cerevisiae*†

Kamila Kochan,^a Huadong Peng,^b Eunice S. H. Gwee,^{a,c}
Ekaterina Izgorodina,^c Victoria Haritos^{*b} and Bayden R. Wood^{†*a}

Cyclopropane fatty acids (CFAs) are a group of lipids with unique physical and chemical properties between those of saturated and monounsaturated fatty acids. The distinctive physicochemical characteristics of CFAs (e.g. oxidative stability, self-polymerization at high temperatures, etc.) results from the presence of a cyclopropane ring within their structure making them highly useful in industrial applications. CFAs are present in several species of plants and bacteria and are typically detected with standard lipid profiling techniques, such as gas or liquid chromatography. In this work we investigated several strains of *S. cerevisiae*, genetically modified to introduce the production of CFAs, in comparison to control strain using confocal Raman spectroscopy (CRS). The aim of our work was to demonstrate the potential of CRS not only to detect changes introduced due to the CFAs presence, but also to track CFAs within the cells. We present for the first time Raman and IR spectra of CFA standard (*cis*-9,10-methyleneoctadecanoic acid), completed with quantum chemical calculations and band assignment. We identified marker bands of CFA (e.g. 2992, 1222, 942 cm⁻¹) attributed to the vibrations of the cyclopropyl ring. Furthermore, we analysed lipid bodies (LBs) from modified and control yeast using CRS imaging and identified multiple changes in size, number and composition of LBs from engineered strains. We observed a significant reduction in the degree of unsaturation of LBs using the ratio of bands located at 1660 cm⁻¹ (ν (C=C)) and 1448 cm⁻¹ (δ (CH₂)) in the modified cell lines. In addition, we were able to detect the presence of CFAs in LBs, using the established marker bands. CRS shows tremendous potential as technique to identify CFAs in lipid bodies providing a new way to track lipid production in genetically modified single yeast cells.

Received 2nd August 2018,
Accepted 2nd September 2018

DOI: 10.1039/c8an01477a

rsc.li/analyst

Introduction

The emerging interest in the development of new engineering strategies aimed at enhancing lipid production in yeast is dictated by their potential for industrial applications. Amongst those, the most commonly mentioned is biodiesel production.^{1–3} Biodiesel is an alternative, biodegradable and renewable energy source produced from triacylglycerols (TAGs), obtained from animal, plant or microbial oils.^{1–3} The latter is considered the most promising TAG source due to the low cost of production, short life cycle of the microorganism,

independence from the climate, season, etc.^{1–3} A realistic alternative fuel should not only produce significant environmental and economic benefits, but also be amenable to large scale production and provide a net energy gain over the energy used for production.² Consequently, special attention is devoted to microorganisms capable of accumulating significant amounts of lipids.² Oleaginous microorganisms are a group of microorganisms, including microalgae, fungi, yeast and bacteria, characterised by the content of lipid being in excess of 20% in biomass weight.^{1–3} However, the amount of lipids accumulated by oleaginous organisms can be substantially higher.^{1–3} In fact, some microbes (such as *Rhodospiridium* sp., *Rhodotorula* sp. and *Lipomyces* sp.) have enormous capabilities of accumulating intracellular lipids, with some producing 70% of their total biomass dry weight.^{2,4,5} The high yield of TAG production by oleaginous microorganisms is very beneficial for industrial applications (including, but not limited to, biodiesel production) and can be achieved *via* genetic engineering. This has resulted in growing interest in various engineering strategies aiming at

^aCentre for Biospectroscopy, School of Chemistry, Monash University, Clayton Campus, 3800 Victoria, Australia. E-mail: bayden.wood@monash.edu

^bDepartment of Chemical Engineering, Monash University, Clayton Campus, 3800 Victoria, Australia. E-mail: victoria.haritos@monash.edu

^cSchool of Chemistry, Monash University, 17 Rainforest Walk, Clayton, VIC, 3800, Australia. E-mail: katya.pas@monash.edu

†Electronic supplementary information (ESI) available. See DOI: 10.1039/c8an01477a

enhancing TAG production and accumulation in microorganisms. The detailed lipid content and fatty acid profile differs between species but most produce TAGs formed from several saturated and unsaturated fatty acid chains.⁶

Cyclopropane fatty acids (CFAs) are a subgroup of fatty acids, containing a cyclopropane ring within their structure. They occur infrequently in plants (such as gymnosperms, Malvales, Litchi and other Sapindales)^{7,8} and bacteria (such as *Escherichia coli*, *Streptococcus* sp. and *Salmonella* sp.).^{9,10} CFAs are derived from corresponding unsaturated fatty acids (UFAs) and are formed through cyclopropanation, catalysed by cyclopropane synthases (CPSs).^{7,9,10} In bacteria, CFAs occur in the cell membranes, with the vast majority in the *cis* form.¹⁰ However, the presence of the *trans* form was also detected in the cell envelope of *Mycobacterium tuberculosis*, where it was involved in the regulation of *Mycobacterium* virulence.¹¹ In general, CFAs are considered to enhance the chemical and physical stability of membranes.⁹ It was suggested that the CFAs reduce the fluidity of membranes, therefore reducing their permeability.^{9,12} The presence of CFAs was also demonstrated to increase the tightness of packing within lipid bilayers.^{13,14} In addition, lipid bilayers containing CFAs compared to lipid bilayers containing UFAs, exhibit a greater chain order.¹⁴ The influence of CFAs presence on the properties of the membrane was postulated to result from the cyclopropane moiety acting as a barrier preventing the propagation of motion from one chain to another.¹⁵

The presence of the ring within the CFAs structures translates into their unique physical and chemical properties, placed in between those of saturated (SFAs) and monounsaturated fatty acids (MUFAs).⁷ For instance, hydrogenation of CFAs results in ring opening and formation of methyl-branched fatty acids, exhibiting low temperature properties similar to MUFAs, while at the same time demonstrating the oxidative stability characteristic for SFAs (non-susceptibility for oxidation).^{7,9} The unique physical and chemical properties of CFAs make them highly desirable for industrial applications (production of lubricants, coatings, polymers, *etc.*)⁷ However, currently none of the natural sources of CPSs are suitable for commercial production.⁸

The lipid composition of cells can be studied using various experimental techniques. Traditionally, the most widely used include gas chromatography (GC) and fluorescence staining. GC enables one to obtain the total lipid profile for whole cells, however, without any information upon their spatial distribution. Fluorescence staining, on the other hand, allows one to visualise LBs, but does not provide information about their composition.¹⁶ Both methods, although very useful, are burdened by the lack of ability to provide spatially localised chemical information. This gap was recently fulfilled by micro-scale imaging *via* molecular-based techniques such as Raman spectroscopy (RS). RS is a non-invasive and non-destructive technique requiring minimal sample preparation and enabling *in situ*, online analysis. In recent years imaging by confocal Raman spectroscopy (CRS) has been broadly applied to various cells, including red blood cells,¹⁷ white blood cells,¹⁸ endo-

thelial cells,¹⁹ hepatocytes,²⁰ algae,²¹ yeast^{16,22} and many others.²³

Although, RS provides the ability to simultaneously obtain information about multiple chemical components (*e.g.* pigments, proteins, carbohydrates, *etc.*), it is particularly suitable to study lipids²⁴ because lipids contain multiple non-polar groups (C–C, C=C), making them strong Raman scatterers.²⁴ Primarily, RS offers the possibility to identify various groups of lipids (free fatty acids, TAGs, phospholipids, cholesterol, *etc.*) and discriminate between them.²⁵ This enables the differentiation between esterified and non-esterified forms *via* the presence of the ester carbonyl band located at $\sim 1740\text{ cm}^{-1}$ ($\nu(\text{C}=\text{O})$), enabling one to determine the presence of TAGs.^{16,20} Furthermore, it allows the discrimination between UFAs and SFAs^{25,26} and can be used to determine their relative content (using ratios of UFA-related bands located at $\sim 3012\text{ cm}^{-1}$, $\sim 1656\text{ cm}^{-1}$, $\sim 1301\text{ cm}^{-1}$ and SFA-related bands located at $\sim 2855\text{ cm}^{-1}$, $\sim 1444\text{ cm}^{-1}$, $\sim 1266\text{ cm}^{-1}$).^{27–29} Raman spectra of various, biologically relevant lipids have been demonstrated in several reviews.^{25,26,30} However, hitherto there are no experimental or theoretical spectra of CFAs available in the literature.

In our previous work, we demonstrated several single- and multigene engineering approaches enabling the increase in amount of intracellular lipids (TAGs) in *Saccharomyces cerevisiae*.^{16,31} In the next stage, we focused on investigating whether those strategies can also be applied for CFAs, which are highly valued in industry. Currently, the detection of CFAs is based on either liquid³² or gas chromatography,³³ although recently a ¹H NMR approach was shown.³⁴ Here, we demonstrate for the first time the application of CRS imaging for determining the presence of CFAs in several engineered *Saccharomyces cerevisiae* strains. We first obtained spectra (Raman and IR) of the CFA standard and assigned the bands *via* theoretical calculations. Subsequently, we performed CRS imaging of single cells from various strains to determine the presence, composition and heterogeneity of LBs. Finally, we investigated the presence of CFAs in the engineered cell lines by comparing Raman spectra of the lipid bodies with the CFA standard and using Partial Least Square Discriminant Analysis (PLS-DA) to predict lipid body composition.

Materials and methods

Yeast cell lines and culture condition

Five engineered strains of *S. cerevisiae* (CP1, CP4, CP5, CP6, CP7) in comparison to a control strain (CON) were compared. Details of all strains are given in Table 1. Cyclopropane fatty acid synthase from *E. coli* (Ec.CFAS) was regulated by promoter GAL1. The details of other genes including *Ald6*, *SeACS^{L641P}*, *AtDGAT1*, *AtClo1* can be found in our previous paper.³¹ Based on the auxotrophy difference (SC-Leu, SC-His-Ura, SC-His-Leu-Ura), the engineered yeast strains were maintained using synthetic complete (SC) minimal medium. Then, induced by galactose and incubated at 30 °C, 250 rpm in 250 mL flasks

Table 1 Engineered *Saccharomyces cerevisiae* strain names and introduced genes

Strain	Description
CON	BY4741 – empty vectors ^a
CP1	BY4741 – <i>Ec.CFAS</i>
CP4	BY4741 – <i>Ec.CFAS</i> – <i>AtDGAT1</i>
CP5	BY4741 – <i>Ec.CFAS</i> – <i>AtDGAT1</i> – $\Delta Tgl3$
CP6	BY4741 – <i>Ec.CFAS</i> – <i>AtDGAT1</i> – $\Delta Tgl3$ – <i>Ald6</i> – <i>SeACS</i> ^{L641P}
CP7	BY4741 – <i>Ec.CFAS</i> – <i>AtDGAT1</i> – $\Delta Tgl3$ – <i>Ald6</i> – <i>SeACS</i> ^{L641P} – <i>Atclo1</i>

^a pSP-GM2, pIYC04, pESC-leu2d. Δ indicates endogenous gene was knocked out.

until cells were harvested at 72 h for the following analysis. Detailed cell culture conditions have previously been described.^{16,31}

Lipid analysis and quantification by gas chromatography (GC)

Harvested cell pellets were freeze-dried overnight to obtain the dry cell weight (DCW) of each culture. Slightly modified Bligh Dyer extraction procedure³⁵ was used to extract yeast lipids, then dissolved in the chloroform layer, which was loaded on the thin layer chromatography (TLC) plate to separate the phospholipids and triacylglycerols (TAGs).³⁶ Then, scraped TAG and phospholipids silica spots from TLC plates were methylated to form the fatty acid methyl esters (FAME), which were quantified by GC as described previously.³⁷

Sample preparation for Raman spectroscopy

Yeast cells in Phosphate Buffer Solution (PBS) were centrifuged (1000 rpm, 5 min) in order to obtain a pellet. The supernatant was then removed; the pellet was re-suspended in 500 μ L of ultrapure water, vortexed for 2 min and centrifuged again. This step was repeated three times to ensure complete removal of any residual PBS. The final pellet was resuspended in 500 μ L of ultrapure water and gently mixed. 100 μ L of the yeast solution was placed on a Raman grade CaF₂ window (Crystran Pty. Ltd, UK) and air-dried. From each cell line, at least three independent samples were prepared. The cyclopropane fatty acid (CFA) standard: *cis*-9,10-methyleneoctadecanoic acid (CycC19) and fatty acid standard: stearic acid (SA) were purchased from Sigma Aldrich and prepared directly prior to measurement by placing them on a Raman grade CaF₂ slide (both in solid state).

Raman spectroscopy of yeast cells

Raman spectroscopy measurements were performed using WITec confocal CRM alpha 300 Raman microscope, equipped with a CCD detector (cooled to -60 °C), 600 grooves per mm grating and an air-cooled solid-state laser operating at 532 nm, coupled to the microscope with an optical fibre with a diameter of 50 μ m. All data was collected using a dry Olympus MPLAN (100 \times /0.90 NA) objective. Prior to data collection, the monochromator of the spectrometer was calibrated using Raman scattering line produced by a silicon plate (520.5 cm^{-1}). The size of mapped area was adjusted individu-

ally, depending on the cell size, with sampling step of 0.3 μ m. The laser power was 7 mW. All spectra were collected in the spectral range 0–3725 cm^{-1} and with spectral resolution of 3 cm^{-1} . The integration time for each spectrum was 0.5 s.

Vibrational spectroscopy measurements of the CFA standard

Raman measurements of the CFA and fatty acid standards (CycC19 & SA) were performed using the system described in the previous section. RS spectrum of each standard was obtained by averaging three individual spectra, each collected in the spectral range of 0–3725 cm^{-1} , with spectral resolution of 3 cm^{-1} , integration time of 1 s and 100 accumulations. The Attenuated Total Reflectance-Fourier Transform Infrared (ATR-FTIR) spectra of CFA standard were recorded using a Bruker Alpha FTIR (Ettlingen, Germany) spectrometer with a global source, KBr beam splitter, a deuterated triglycine sulfate (DTGS) detector and an Attenuated Total Reflection (ATR) sampling device containing a single bounce diamond internal reflection element (IRE). The ATR-FTIR spectrum of the CFA standard was obtained by averaging three individual spectra, each collected in the spectral range of 600–4000 cm^{-1} with spectral resolution of 8 cm^{-1} and accumulation of 64 interferograms. The collection of each ATR-FTIR spectrum was preceded by collection of background (128 interferograms).

Data analysis

Directly after collection, all Raman spectra were subjected to cosmic spike removal (CRR)(filter size: 2, dynamic factor: 4). The ATR-FTIR spectrum of CFA was smoothed using Savitzky-Golay algorithm with 9 smoothing points (polynomial fit 2). The quantum chemical calculations were performed using ethyl and butyl groups as side chains, two different functionals (M06-2X and wB97XD) and two different basis sets (cc-pVDZ and aug-cc-pVDZ). The high wavenumber region of the spectra was scaled using scaling factors (ESI, Table 1[†]) because the calculations assume harmonic oscillations. The maps of distribution of components were created by displaying the integrated intensity of selected Raman bands in the ranges: 3050–2800 cm^{-1} (organic components) and 1460–1420 cm^{-1} (lipids). To obtain the average LB spectrum for each cell line the following procedure was implemented. For each LB from each measured cell an average LB spectrum was obtained by *k*-means cluster analysis (KMC) (spectral range: 1800–600 cm^{-1}) and extracted. Subsequently, all spectra of LBs originating from cells of selected cell lines were averaged. For PLS-DA, 630 spectra extracted from LBs of all cell lines were used ($n_{\text{CON}} = 274$, $n_{\text{CFAS}} = 356$). Spectra from LBs from all modified cell lines (CP1, CP4, CP5, CP6, and CP7) were assigned to CFA-containing group. The dataset was randomly divided into calibration and validation subsets, with 66% of spectra kept in the calibration subset. PLS-DA was performed on 2nd derivatives of RS spectra from LBs. Prior to analysis spectra were smoothed, using Savitzky-Golay algorithm with 11 smoothing points (polynomial fit 2) and normalised using the Standard Normal Variate (SNV) method. 2nd derivatives were calculated using 11 smoothing points (Savitzky-Golay algorithm) and

mean centred before PLS-DA. The presented PLS-DA model was created using the spectral ranges of 3100–2800 cm^{-1} and 1800–650 cm^{-1} and 5 latent variables.

Results and discussion

Vibrational spectroscopic characterisation of CFA standard

First, we collected Raman spectra of a CFA standard: *cis*-9,10-methyleneoctadecanoic acid and of a fatty acid standard: stearic acid (C18:0). A direct comparison between the average spectra of those compounds is presented in Fig. 1 (1800–200 cm^{-1}) and Fig. 2 (3200–2800 cm^{-1}). The RS spectrum of the CFA standard shows bands typical for vibrations of FA chains along with additional modes, originating from vibrations of the cyclopropane ring. The bands associated with vibrations related to FA chain are marked with dashed lines in Fig. 1 and 2. These include bands located at: 2882 cm^{-1} , 2846 cm^{-1} , 1466 cm^{-1} , 1442 cm^{-1} , 1298 cm^{-1} , *etc.*, originating from stretching and deformation modes of CH_2 & CH_3 groups.^{25,26,30} The bands located between 1100–1000 cm^{-1} (1173, 1127, 1104, 1065 cm^{-1}) are associated with C–C stretching modes and were also reported for saturated FAs.²⁵ Minor shifts in the bands related to FA chain between SA and CFA spectrum can be observed. The relative intensity of various bands also differs between SA and CFA spectra (particularly in the region 1200–1000 cm^{-1}). Despite this, the presence and

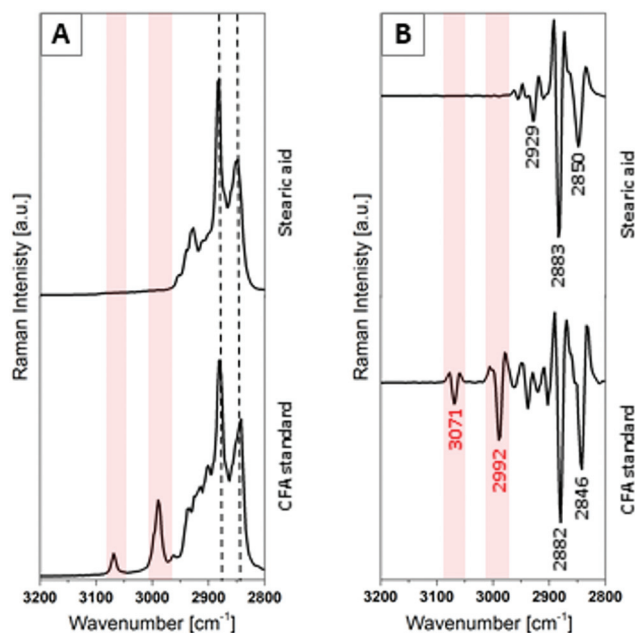


Fig. 2 (A) Raman spectra (in the range 3200–2800 cm^{-1}) of the CFA standard (bottom) and stearic acid (C18:0) (top) together with (B) their 2nd derivatives. Corresponding bands in both spectra, associated with vibrations of FA chain, are marked with black dashed lines in (A). Red background in (A) and (B) marks the region with bands present in the Raman spectrum of CFA, but absent in the Raman spectrum of stearic acid. The precise band positions are given in (B).

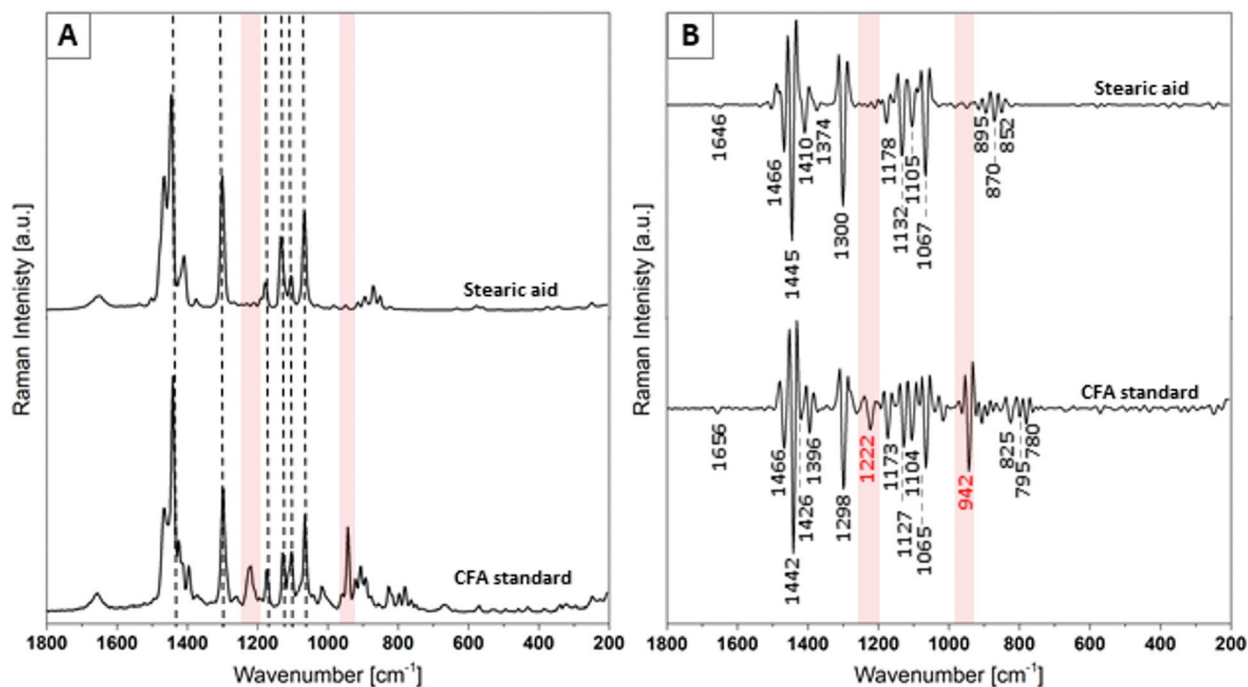


Fig. 1 (A) Raman spectra (in the range 1800–200 cm^{-1}) of the CFA standard (bottom) and stearic acid (C18:0) (top) together with (B) their 2nd derivatives. Corresponding bands in both spectra, associated with FA chain vibrations, are marked with black dashed lines in (A). Red background in (A) and (B) marks the region where bands are present in the Raman spectrum of CFA, but absent in the Raman spectrum of stearic acid. The precise band positions are given in (B).

compatibility of the aforementioned bands in SA and CFA spectra indicates that they originate from vibrations of the FA chain. Vibrations associated with the functional groups within the cyclopropane ring most probably also contribute to those bands, although none of them is specific for the cyclopropane ring, as all were previously reported for chain FAs.^{25,26,30} However, the CFA spectrum compared to SA spectrum contains multiple additional bands (Fig. 1 and 2, red background), located in the high wavenumber region ($3071, 2992\text{ cm}^{-1}$) and in the fingerprint region ($1222\text{ cm}^{-1}, 942\text{ cm}^{-1}$ and several low intensity bands between $830\text{--}780\text{ cm}^{-1}$), absent in Raman spectrum of SA (Fig. 1 and 2), along with spectra of other chain FAs.²⁵

To confirm the contribution of the ring vibrations to the aforementioned bands and their assignment, we performed Density Functional Theory (DFT) calculations of two model systems, 3-(2-ethylcyclopropyl)propanoic acid and 5-(2-butylcyclopropyl)pentanoic acid using M06-2X³⁸ and ω B97XD³⁹ functionals combined with cc-pVDZ and aug-cc-pVDZ basis sets.⁴⁰ We used two different lengths of a side chain to further study the effect of the side chain on the cyclopropyl ring vibrations. The predicted Raman spectra are presented in Fig. 3 and their detailed band assignment is presented in ESI (see Table S1†). The model system with the ethyl chain is given in Fig. 3A and B, whereas the model with the butyl chain in Fig. 3C and D. The fingerprint region for both models (normalized to one) is presented in Fig. 3B for ethyl and 3D for butyl. Initially, it appears that the presence of the ethyl groups resulted in spectra exhibiting more bands than in the case of the butyl groups. However, a similar number of bands are present in both spectra. The main difference between the spectra came from the relative intensity of some bands. Since the butyl group is longer than the ethyl one by 2 carbon atoms, Raman spectra of the butyl model showed higher intensity of bands originating from vibrations of the side chains compared to those originating from the cyclopropyl ring. The predicted spectra above 2800 cm^{-1} were scaled to reproduce the 2847.27 cm^{-1} band that is assigned experimentally to $\nu_s(-\text{CH}_2)$. The scaling parameters are included in the ESI.† The rest of the spectra were left unscaled. Analysis of the predicted spectra for the two DFT functionals and four different basis sets revealed small variations in the bands. It was observed that the complexity of vibrations increased with the length of the alkyl chain, giving rise to an increase in coupled vibrations and a decrease in pure vibrations. The longer butyl alkyl chain appeared to also influence intensities of the predicted bands. Upon comparison, both ethyl and butyl side chains predicted similar assignment of the fingerprint region, which confirms that the alkyl chain length has a minimal effect on the predicted Raman spectra. Furthermore, in the text we only discuss results obtained with ω B97XD/aug-cc-pVDZ for the butyl model system. Experimentally, there are 3 distinct peaks assigned to bands arising from the cyclopropyl ring – 942 cm^{-1} , 1222 cm^{-1} and 2992 cm^{-1} and this assignment agrees well with the predicted spectra. 942 cm^{-1} (calculated to be at 958 cm^{-1}) corresponds to $\alpha(-\text{C}-\text{C}-\text{C}-)$ (ring), whereas the

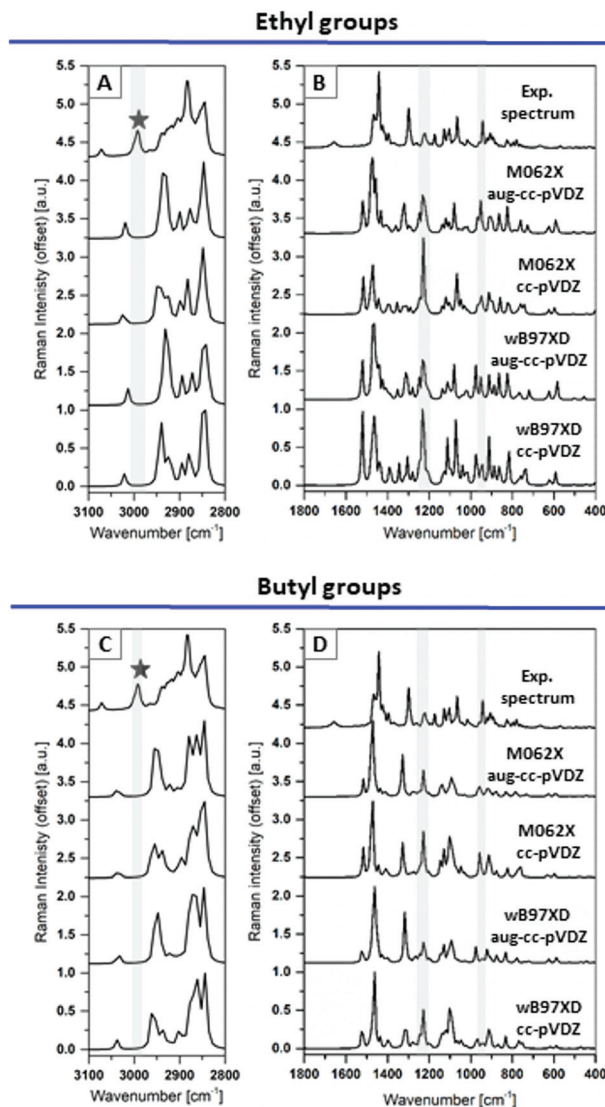


Fig. 3 A comparison of the experimental Raman spectrum of CFA standard with calculated Raman spectra using varying length of side chains: (A, B) ethyl and (C, D) butyl groups. For each length of side chains spectra were calculated using combinations of functionals: M06-2X, ω B97XD and basic sets: cc-pVDZ, aug-cc-pVDZ, as annotated on the figure. Spectra are presented in spectral ranges: (A, C) $3100\text{--}2800\text{ cm}^{-1}$ and (B, D) $1800\text{--}400\text{ cm}^{-1}$. The scaling factors for each calculated spectrum are given in ESI, Table S1.† All spectra in (A, C) were normalized to 1 in the range $3100\text{--}2800\text{ cm}^{-1}$. All spectra in (B, D) were normalised to 1 in the range $1800\text{--}400\text{ cm}^{-1}$. Grey background highlights the spectral regions of: (A, C) $3010\text{--}2980\text{ cm}^{-1}$, (B, D) $1260\text{--}1200\text{ cm}^{-1}$ and $960\text{--}920\text{ cm}^{-1}$. Black stars mark the band located at 2992 cm^{-1} in the experimental spectrum.

bands at 1222 cm^{-1} (calculated to 1226 cm^{-1}) can be confidently assigned to a combination of stretching and bending vibrations of the ring (labelled as $\nu_s(-\text{C}-\text{C}-)$ (ring)) + $\tau(-\text{CH}_2(\text{ring}))$ + $\alpha(\text{H}-\text{C}-\text{C}-\text{H}(\text{ring}))$ in Table S1†). The band at 2992 cm^{-1} (calculated to be 2958 cm^{-1} after scaling) was assigned to a combination of stretching vibrations such as $\nu_s(-\text{CH}_2(\text{ring}))$ and $\nu(-\text{CH}(\text{ring}))$. To this end, the calculated

spectra, regardless of level of theory chosen in this study and length of alkyl side chain, were able to reliably predict and assign characteristic vibrations of the cyclopropyl ring, confirming the identified CFA marker bands above (with the main ones located at 1222 and 2992 cm^{-1}).

Raman spectral characteristics of the CFA standard (experimental spectrum as well as theoretical calculations) was additionally supplemented with results from a complementary technique – ATR-FTIR. The ATR-FTIR spectrum of a CFA standard, theoretical calculations using the same approach as for RS spectra and a table with band assignments are presented in ESI (Fig. S1, S2 and Table S2†).

Multigene modification of yeast leads to significant increase in number of LBs with heterogeneous size

In the next step, we collected Raman maps of single cells ($n = 126$) from all studied strains ($n = 6$). Raman mapping enabled us to quickly visualise the cell area, by integrating the area under the bands in the region 3050–2800 cm^{-1} (corresponding to symmetric and asymmetric stretching of C–H groups from all organic components) along with the presence of LBs (by integrating the area under the lipid-originating band *e.g.* at $\sim 1444 \text{ cm}^{-1}$). Representative results obtained for three cells from each strain are presented in Fig. 4 (cell area together with LBs). The control cells rarely demonstrated LBs and if so – they were usually rather small ($< 1 \mu\text{m}$) (Fig. 4: 1b). A similar situation was observed for the CP1 strain, with only a slight increase in the number of cells containing single LBs only. Of note is that the CP1 strain was modified only to induce the production of CFAs, however, without any modifications aimed at increasing the overall lipid yield. For the CP4 and CP5 strains an increase in the prevalence of LBs can be observed. Even though they remain rather small (majority with a diameter $\leq 1 \mu\text{m}$), they began to appear in multiple numbers in one cell (Fig. 4: 8b, 10b). A clear and significant increase in the prevalence of LBs is visible for CP6 and CP7 (Fig. 4: 13–18). Overall, LBs of CP6 and CP7 strains are larger than in other cell lines (*e.g.* Fig. 4: 13b and 16b), however, at the same time they demonstrate a substantial heterogeneity in size (*e.g.* Fig. 4: 15b), even within a single cell.

Fig. 5 shows the results of analysis of all collected Raman maps. The percentage of cells with LBs (Fig. 5A) demonstrates the prevalence of LBs in each cell line, whereas the ratio of the number of LBs to the number of cells with LBs for each cell line (Fig. 5B) shows the tendency to occur as individual or several LBs per cell. The value equal to 1 indicates the presence of only single LB per cell, whereas the value above 1 shows the presence of multiple LBs per cell. The CP1 strain exhibits similar characteristic to the control, with only slightly increased prevalence of LBs (Fig. 5A). In both cases, LBs always occur individually per cell (Fig. 5B). In addition, for all those strains (CP4, CP5, CP6 and CP7) the ratio of the number of LBs to the number of cells containing LBs exceeds 1, indicating that for each strain it was possible to identify cells with multiple LBs (Fig. 5B). This ratio is higher for the strains CP4, CP5, CP6 than CP7, as in those strains at least half of all

measured cells contained min. 2 LBs. Particularly for CP6, LBs often were heterogeneous in size. In case of the CP7, the number of cells with ≥ 2 LBs was smaller than in CP4, CP5, and CP6, although such cells were still observed. Most of the LBs in CP7 were large (diameter $> 1 \mu\text{m}$), often with a single LB filling most of a cell. Altogether, these results demonstrate that a single gene modification, aimed at inducing the production of CFAs (CP1 strain) did not influence the overall LB formation. At the same time, the multi-gene-based engineering strategies (CP6, CP7 strains) were shown to remain effective in enhancing lipid production, even when combined with modification aimed at introduction of CFA production. The excessive lipids were stored in the form of LBs, however, demonstrated significant heterogeneity in their size not only within the cell line, but even within individual cells.

All engineered strains exhibit LBs with altered UFA/SFA ratio

The average spectra of LBs (together with their standard deviation) from all modified cell lines in comparison to control are presented in Fig. 6 (RS spectrum of LBs with marked all band positions is presented in ESI, Fig. S3†). In all cases, spectra show a typical lipid profile, indicating the presence of TAGs, containing both UFA and SFA chains. The high lipid contribution to the spectra of LBs from all cell lines is also clearly visible *via* the high wavenumber region (3100–2800 cm^{-1}), particularly through the presence of a band at 2855 cm^{-1} ($\nu(\text{CH}_2)$) (ESI, Fig. S4†). The presence of TAGs is confirmed by the band, located at 1747 cm^{-1} and assigned to ester carbonyl stretching.²⁵ The SFAs are primarily manifested in the spectrum by the presence of bands at $\sim 1448 \text{ cm}^{-1}$ ($\delta(\text{CH}_2)$) and $\sim 1308 \text{ cm}^{-1}$ ($\tau(\text{CH})$) (Fig. 6) along with the aforementioned band at 2855 cm^{-1} (ESI, Fig. S4†). The main evidence of the UFA presence is the band located at 1660 cm^{-1} originating from C=C stretching (Fig. 6, marked with a star). The second typical UFA band in the fingerprint region is located around 1270 cm^{-1} ($\delta(=\text{C}-\text{H})$) (Fig. 6, marked with an arrow). This band is a part of a characteristic doublet ($\sim 1308 \text{ cm}^{-1}$ and $\sim 1270 \text{ cm}^{-1}$) observed for mixtures of UFA and SFA.^{25,26,30} Although, this doublet might be used as a measure of degree of unsaturation for lipid mixtures,⁴¹ in case of biological materials its usefulness is limited because both bands are often not well resolved and strongly affected by baseline changes and the presence of compounds such as haem (inducing a photothermal raise of background).⁴² Even though haem itself is not located within LBs, its presence around them may affect the average spectra of LBs. This is particularly the case for small LBs (diameter $\leq 1 \mu\text{m}$) because of spatial resolution depth probed by CRS. The haem from outside of small LBs may still contribute to their spectra. Some contribution from haem can be seen *e.g.* in the average RS spectrum of LBs from control (Fig. 6 and Fig S3†) through the presence of bands located at 757 cm^{-1} ($\nu(\text{pyr}$ breathing); $\nu(\text{C}_\alpha\text{C}_\beta)$), 1127 cm^{-1} ($\nu(\text{C}-\text{C})$) and 1588 cm^{-1} ($\nu(\text{C}_\alpha\text{C}_m)_{\text{asym}}$).

A comparison between RS spectra of LBs from all studied strains shows a clear difference between control (CON) and all modified strains. The relative intensity of the UFA-related

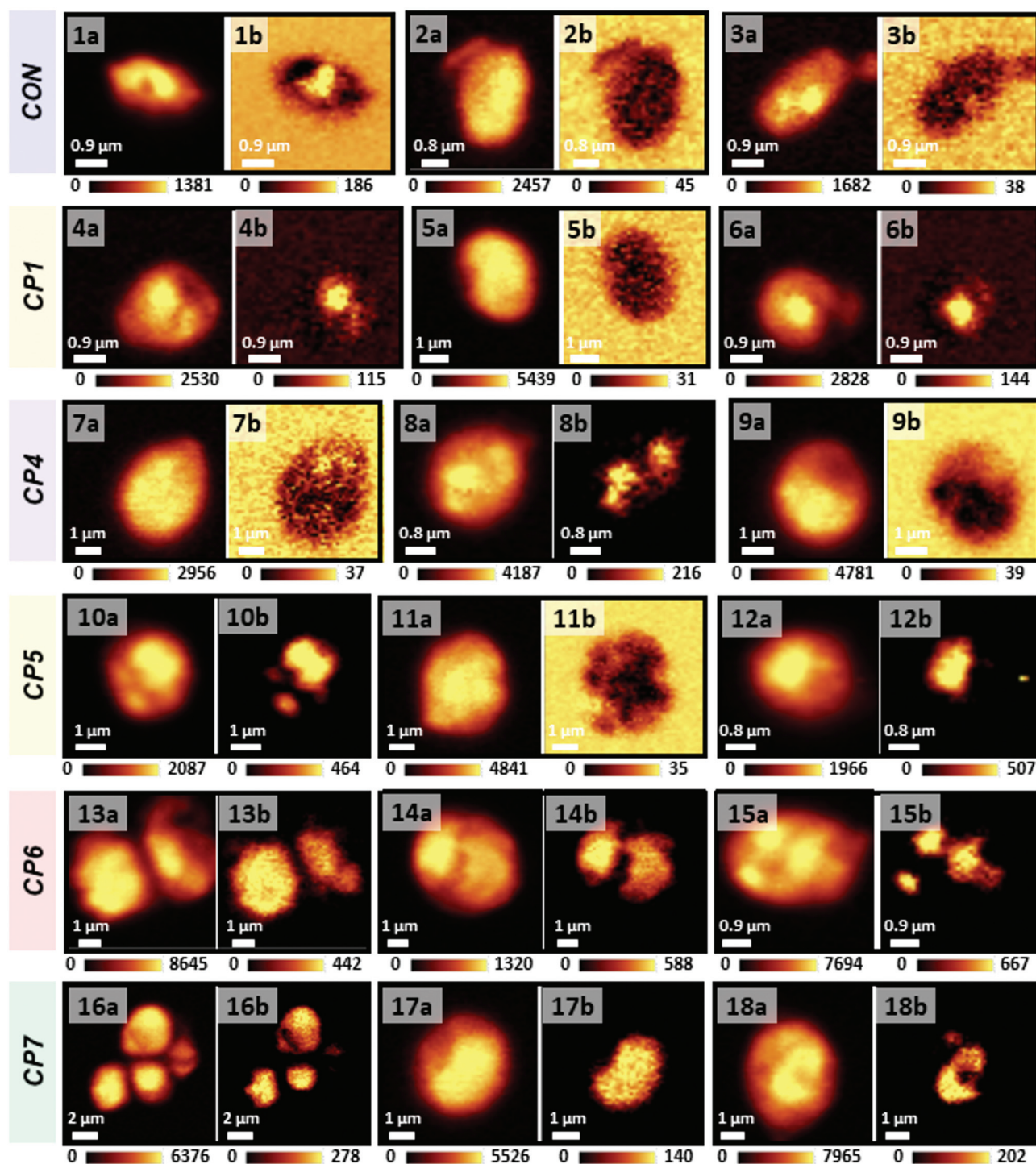


Fig. 4 Maps of distribution of selected components for three representative cells from each cell line obtained by integration the area under the Raman bands in the range: (a) 3050–2800 cm^{-1} (representing the area of the cell) and (b) 1460–1420 cm^{-1} (representing the lipids and visualising the LBs). Each row contains cells from different cell line (CON, CP1, CP4, CP5, CP6, CP7). Each number (1–18) corresponds to a different cell. For each cell a map of distribution of organic components (visualising the cell area and labelled 'a') and of lipids (visualising LBs and labelled 'b') is presented. The colour scale for each map was adjusted individually to visualise LBs and is presented below (values given in CCDs).

bands (1270, 1660, and 3009 cm^{-1}) to the SFA-related bands (1308, 1448, and 2855 cm^{-1}) is significantly higher for the control strain.

This is particularly visible using the set of bands at 1660 and 1448 cm^{-1} . Fig. 6 presents spectra normalized to the lateral, with the blue dashed line indicating the height of the

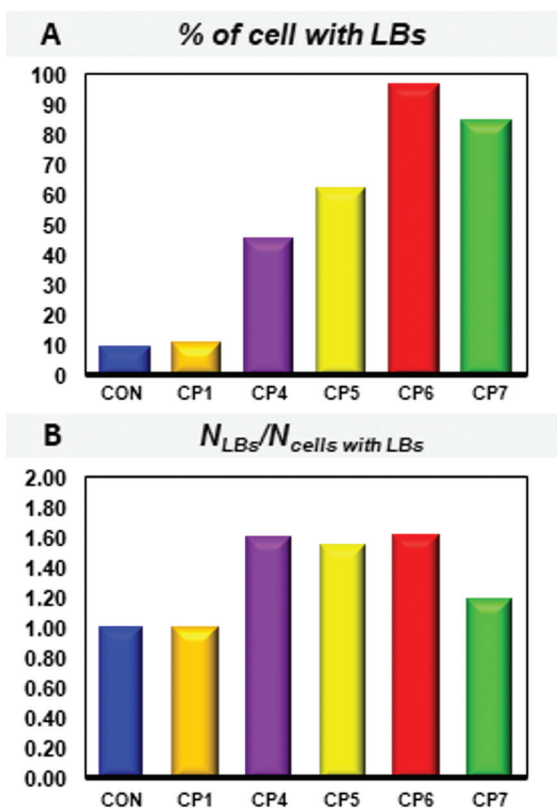


Fig. 5 (A) Bar chart showing the percentage of all measured *via* CRS cells that showed the presence of LBs for each cell line. (B) Bar chart showing the ratio of the number of LBs to the number of cells demonstrating the presence of LBs for each cell line (on the basis of CRS measurements). Ratio equal to 1 indicates that for all cells containing a LB, only single LBs per cell were present. Ratio above 1 indicates the presence of multiple LBs in single cells.

band at 1660 cm^{-1} in LBs from control strain and the red dashed line – height of this band in all modified strains. Interestingly, the UFA-related band from stretching of C=C (1660 cm^{-1}) shows similar height in all modified cell lines, with only minor variations (within the SD). Higher UFA chains content in the LBs of the control strain manifest itself in spectra also *via* the band at 1270 cm^{-1} . Although it shows low intensity, it is still noticeable for the LBs from CON strain (Fig. 6, black arrow). For all modified strains however, even though some increase in intensity of Raman signal in this region can be observed, it remains clearly smaller than in LBs from CON line and with no distinct peak. A similar situation is observed for the band at 3009 cm^{-1} (ESI, Fig. S4†) with the band being clearly more pronounced for LBs of CON strain compared to LBs from the modified strain. These results remain in good correlation with the FA profile obtained *via* GC (ESI, Table S3†), clearly indicating a substantially higher UFA/SFA ratio for control compared to all modified strains (similar between each other). It is important to underline that the lipid profile obtained by GC reflects the overall lipid composition (including *e.g.* membrane lipids). Therefore, for cell lines with high LB content the GC results will reflect primarily the LBs

composition and very likely correspond to it with high accuracy. However, for cell lines with low content of LBs (such as CON), the composition of LBs may have a limited impact on the overall lipid composition. Although the overall lipid composition from GC for such cell lines (low content of LBs) may still be indicative of LBs composition (*e.g.* point towards higher UFA/SFA ratio, as in this case), it does not necessarily represent it exactly. Therefore, the exact lipid composition estimated *via* GC for cell lines with low LB content does not necessarily correspond exactly to the composition of their LBs. However, GC results, accurate with the respect to whole cells and indicative for LBs, combined with high spatial resolution CRS aimed at LBs explicitly, together provide a strong proof of a change in the composition of LBs resulting from the introduced modifications. In all modified strains, despite the influence of the introduced modifications on total lipid content along with the number and size of LBs results in a significant reduction in the ratio of UFA to SFA chains. Interestingly, the ratio of UFA/SFA chains remained similar in LBs for all modified strains, independently of the engineering strategies (single, multigene) and their efficiency towards increasing the total lipid content. This change in the ratio of UFA/SFA chains might therefore be attributed to the introduction of the cyclopropane fatty acid synthase from *E. coli*, as this modification was shared for all lines. Furthermore, this modification aimed at inducing the production of CFAs, deriving from UFA through cyclopropanation.

RS enables the detection CFAs in LBs

GC results confirmed the presence of CFAs in all modified strains (ESI, Table S3†). However, as mentioned before they reflect the overall composition of cells, without providing any specific information about the localisation of chosen lipids. The location of CFAs within the yeast cell is important, as for industrial applications the desired position for CFAs are LBs. However, at the same time CFAs are known to be associated mainly with membranes.^{9–14} In order to confirm that the CFAs produced by engineered cell lines are in LBs and are not only within the membranes, we isolated and separated the TAGs and phospholipids (PLs) and subsequently determined the composition of both fractions using GC. The results (ESI, Table S4†) confirmed the presence of CFAs in both fractions, indicating that at least a part of produced CFAs is associated with TAGs (and therefore – with high probability present in LBs). We further investigated whether it is possible to detect the presence of CFAs in the LBs of modified cell lines using CRS. For this purpose we used a set of 630 spectra ($n_{CFAs} = 356$, $n_{CON} = 274$) extracted from LBs of all cell lines and analysed them using Partial Least Square Discriminant Analysis (PLS-DA). As the CFAs were detected in TAG fractions of all modified cell lines (ESI, Table S4†), LBs from all engineered cell lines were assigned as containing CFAs. The results of the PLS-DA are presented in Fig. 7.

The PLS-DA model was able to discriminate between CON and CFA-containing LBs on the basis of their RS spectra with 98% sensitivity and 100% specificity (Fig. 7A). The regression

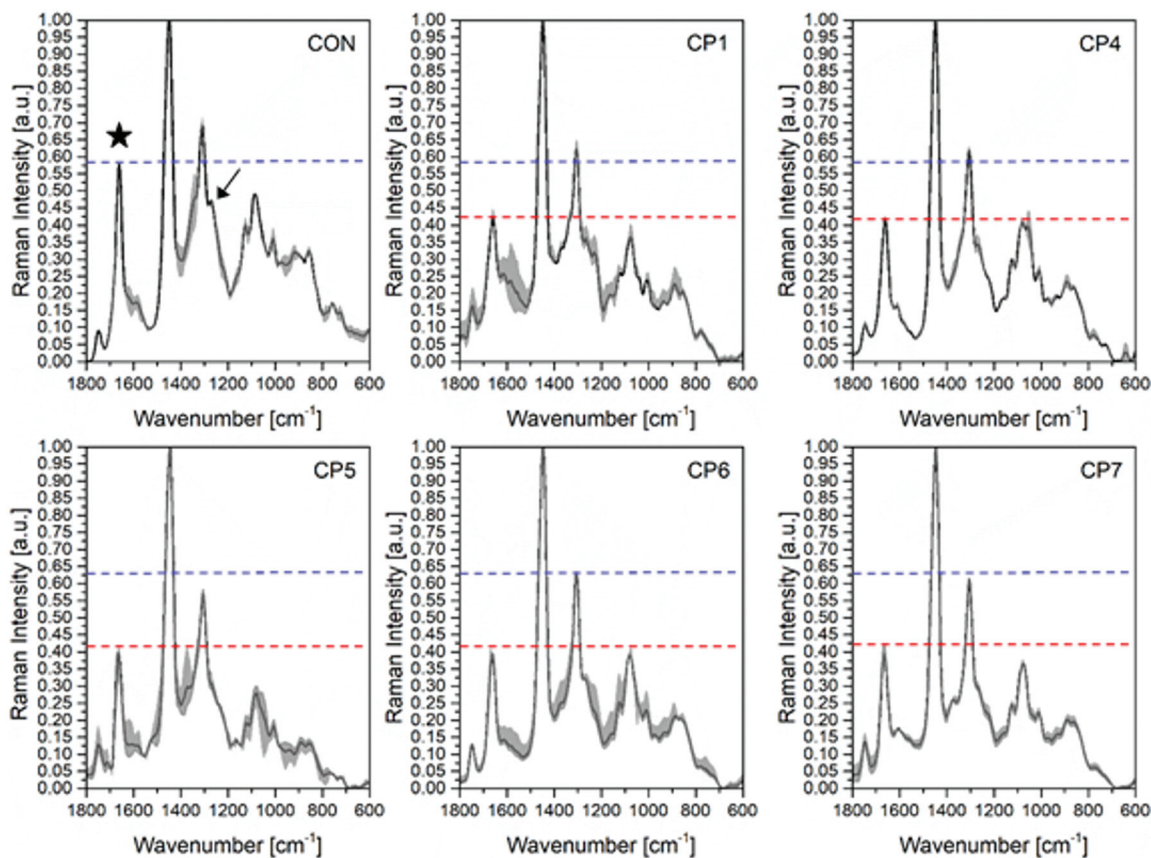


Fig. 6 Average Raman spectra (in the range 1800–600 cm^{-1}) of LBs from each cell line (black line, in each panel) together with standard deviation (grey background, in each panel). Each spectrum was obtained by averaging all average spectra of LBs originating from the selected cell line (more details are given in the 'Materials and methods' section). The black star marks the position of the band originating from $\nu(\text{C}=\text{C})$, located at 1660 cm^{-1} and the black arrow marks the band located at 1270 cm^{-1} ($\delta(\text{C}=\text{H})$). All spectra were normalized to the band located at 1448 cm^{-1} ($\delta(\text{CH}_2)$) marker band for SFA). Blue dashed line marks the height of the band in control. The red dashed line marks the position of band in all modified lines.

vectors (Fig. 7B and C) show a series of discriminative bands. However, from the regression vectors it is obvious that the major differentiating feature between the CON and CFA groups was not the presence/absence of CFAs, but rather the differences in UFA/SFA ratio. The regression vector for the control group shows bands characteristic for UFAs (3012, 1656, 1272 cm^{-1}), whereas the regression vector for CFA-containing group demonstrates bands related to SFAs (2855, 1444, 1302 cm^{-1}). This result is not unexpected, since the differences in the UFA/SFA ratio is known to be well reflected in Raman spectra and have a large impact on them.^{19,25,28} Furthermore, the differences in UFA/SFA ratio between LBs from control and modified cell lines were visible already in the average spectra (Fig. 6) and indicated by the overall lipid profile obtained through GC (ESI, Tables S3 and S4†).

However, despite of the differences in UFA/SFA ratio being the dominant differentiating feature between both groups, the regression vector for the CFA-containing LBs exhibits some bands not associated with the changes in UFA/SFA relative content (Fig. 7C, black stars). In particular, the bands at 2994 and 1223 cm^{-1} can be observed. These bands are not present

in Raman spectra of TAGs and FA constructed from saturated and/or unsaturated chains.²⁵

Both bands are however present in the Raman spectrum of CFAs standard (Fig. 1 and 2). A direct comparison of Raman spectra of stearic acid (C18:0) and CFA standard (Fig. 3) as well as quantum chemical calculations clearly indicated that they originate from the cyclopropane ring vibrations. The possibility of these bands resulting from protein contribution to the spectrum is highly unlikely. As discussed in the previous section the CFA-containing group (CP1, CP4, CP5, CP6, CP7) consisted in the majority of spectra from larger LBs than the CON group (Fig. 4). The potential contribution of non-lipid material from outside of the LB (such as proteins) is a result of possible to achieve depth and spatial resolution. A larger protein contribution can be expected for smaller lipid bodies, with a size below the depth and spatial resolution. Therefore, in the discussed results the possible contribution of proteins would be expected to be much higher for the control group. Altogether, this suggests that the bands at 2994 and 1223 cm^{-1} , observed in the regression vector of the CFA-containing group, are in fact markers of the CFAs presence in the

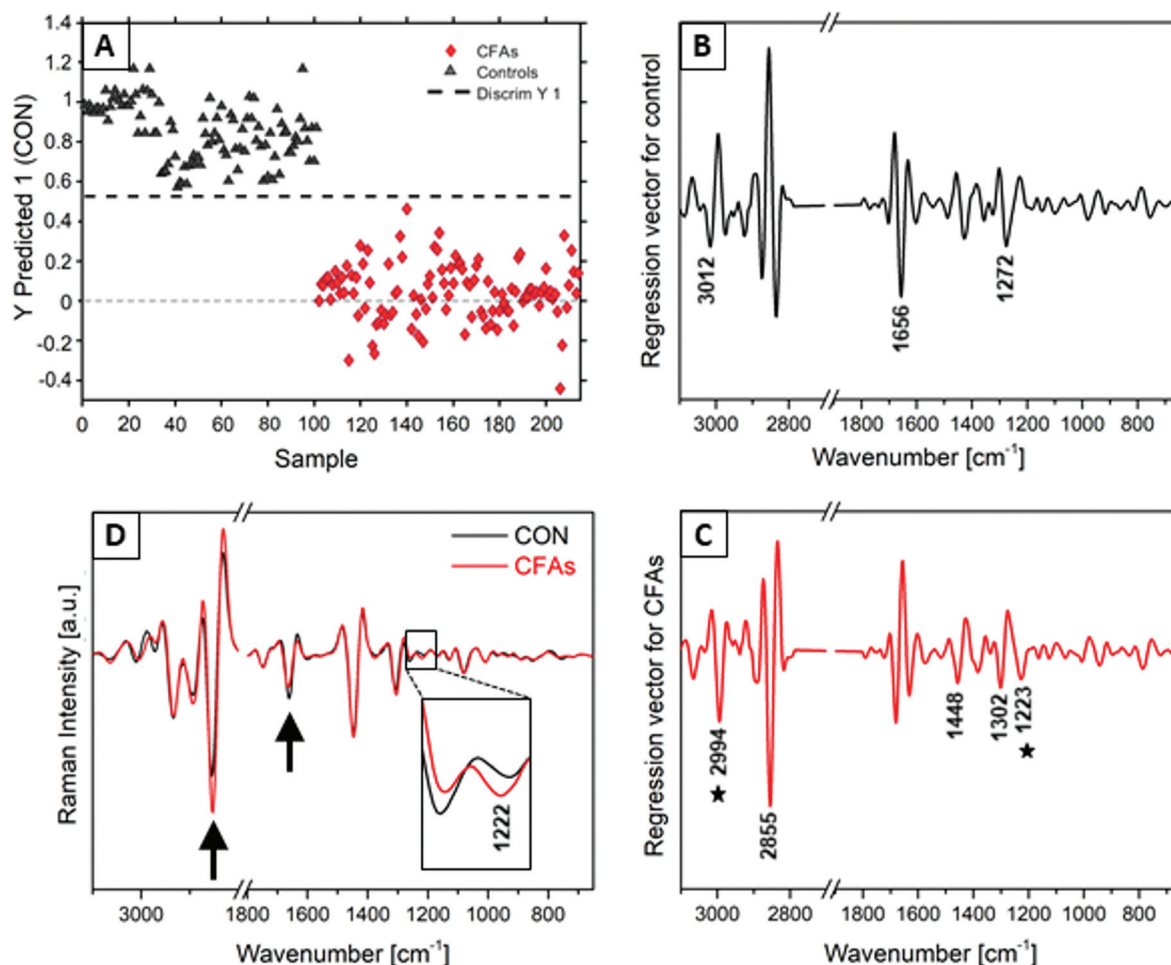


Fig. 7 Results of PLS-DA on a set of 630 Raman spectra ($n_{\text{CFAs}} = 356$, $n_{\text{CON}} = 274$) extracted from LBs of *S. cerevisiae* cells, genetically engineered to produce CFAs (marked with red diamonds and red lines) as well as *S. cerevisiae* control cell line (marked with black triangles and black lines). (A) Predicted class membership based on RS spectra and PLS-DA model for validation set together with regression vectors for (B) control and (C) CFAs-containing LBs with most prominent bands indicated. The stars in (C) mark bands discriminative for the CFA-containing group (in reference to control), but not associated with the differences in UFA/SFA ratio between both groups. PLS-DA was performed on 2nd derivatives of spectra after pre-processing (described in the 'Materials and methods' section) using the spectral ranges: 3100–2800 and 1800–650 cm^{-1} . The average 2nd derivatives of Raman spectra of both groups (control vs. CFAs) are presented in (D). Black arrows mark the bands associated with the differences in UFA/SFA ratio (2855 and 1660 cm^{-1}). The spectral region between 1280 and 1200 cm^{-1} was magnified to visualise the differences in this region.

LBs and demonstrates the ability of RS to detect and track CFAs in LBs.

Conclusion

Cyclopropane fatty acids are a group of lipids with an unusual structure, containing a cyclopropane ring. This translates directly to their unique physicochemical properties, which makes them highly desirable for industrial applications. CFAs are produced by several species of plants and bacteria. Currently however none of the natural sources of CFAs is sustainable for commercial use. At the same time, due to the untypical properties and potential applications, there is an emerging interest in studies focused on CFAs, as well as on sensitive methods for their detection.

Here, we demonstrated an approach, based on confocal Raman imaging, for determination of the CFA presence within *S. cerevisiae* strains, genetically engineered to induce the CFA production. The study of yeast cells was preceded by detailed spectral characterisation of CFA standard. We present for the first time the experimental Raman spectrum of a CFA standard (*cis*-9,10-methyleneoctadecanoic acid) along with quantum chemical calculations accompanied by detailed band assignments. Using the calculated spectra and through direct comparison with spectra of FA chains, we were able to identify bands associated with vibrations of cyclopropane ring (including primarily 2994 and 1222 as well as 3071 and 942 cm^{-1}), constituting marker bands for this group of lipids. We supplemented this work with experimental spectra, quantum chemical calculations and band assignments for the CFA standard in IR, to provide its full vibrational characteristics.

Furthermore, we investigated several engineered cell lines in comparison to control. We were able to determine the impact of induced genetic modifications on the number, size and heterogeneity of produced LBs. Moreover, CRS demonstrated a significant decrease in the unsaturation of LBs (through the ratio of bands at 1660 and 1448 cm^{-1}) in all modified cell lines compared to controls. The unsaturation level of LBs remained constant between the modified cell lines, regardless of the effectiveness of the engineering strategies towards increasing total lipid content. This indicates that the decrease of unsaturation in the modified cell lines is associated with the introduction of CFA production, as all engineered lines shared this modification. Finally, we were able to detect the presence of the CFAs within the LBs of modified cell lines, using CRS combined with PLS-DA. Even though the discrimination between LBs from control and engineered cell lines was dominated by spectral signatures related to differences in unsaturation, the regression vector of LBs from modified cell lines showed also the identified previously CFA marker bands (2992, 1222 cm^{-1}). This demonstrated the potential of CRS for CFA spatially localised detection.

Conflicts of interest

There are no conflicts to declare.

Acknowledgements

We acknowledge the financial support from ARC linkage project (LE160100185) and Monash University for the graduate and international postgraduate research scholarships awarded to HP. B. R. W. is supported by an Australian Research Council (ARC) Future Fellowship grant FT120100926. We thank Mr Finlay Shanks for instrumental support. The authors would also like to acknowledge the allocation of computational resources through the Monash eResearch Centre and the National Computational Infrastructure in Canberra.

References

- M.-H. Liang and J.-G. Jiang, *Prog. Lipid Res.*, 2013, **52**, 395–408.
- X. Meng, J. Yang, X. Xu, L. Zhang, Q. Nie and M. Xian, *Renewable Energy*, 2009, **34**, 1–5.
- H. U. Cho and J. M. Park, *Bioresour. Technol.*, 2018, **256**, 502–508.
- Y. Li, Z. Zhao and F. Bai, *Enzyme Microb. Technol.*, 2007, **41**, 312–317.
- Z. Zhu, S. Zhang, H. Liu, H. Shen, X. Lin, F. Yang, Y. J. Zhou, G. Jin, M. Ye, H. Zou and Z. K. Zhao, *Nat. Commun.*, 2012, **3**, 1112.
- F. Thevenieau and J.-M. Nicaud, *OCL*, 2013, **20**, D603.
- X.-H. Yu, R. Rawat and J. Shanklin, *BMC Plant Biol.*, 2011, **11**, 97–97.
- X.-H. Yu, R. R. Prakash, M. Sweet and J. Shanklin, *Plant Physiol.*, 2014, **164**, 455–465.
- D. W. Grogan and J. E. Cronan, *Microbiol. Mol. Biol. Rev.*, 1997, **61**, 429–441.
- D. Poger and A. E. Mark, *J. Phys. Chem. B*, 2015, **119**, 5487–5495.
- M. S. Glickman, S. M. Cahill and W. R. Jacobs Jr., *J. Biol. Chem.*, 2001, **276**, 2228–2233.
- C. Ying-Ying and J. E. Cronan, *Mol. Microbiol.*, 1999, **33**, 249–259.
- N. Loffhagen, C. Härtig, W. Geyer, M. Vovevoda and H. Harms, *Eng. Life Sci.*, 2007, **7**, 67–74.
- R. A. Moss, T. Fujita, Y. Okumura, Z. Hua, R. Mendelsohn and L. Senak, *Langmuir*, 1992, **8**, 1731–1735.
- E. J. Dufourc, I. C. P. Smith and H. C. Jarrell, *Biochemistry*, 1984, **23**, 2300–2309.
- K. Kochan, H. Peng, B. R. Wood and V. S. Haritos, *Biotechnol. Biofuels*, 2018, **11**, 106.
- B. R. Wood, A. Hermelink, P. Lasch, K. R. Bambery, G. T. Webster, M. A. Khiavi, B. M. Cooke, S. Deed, D. Naumann and D. McNaughton, *Analyst*, 2009, **134**, 1119–1125.
- T. Ichimura, L.-d. Chiu, K. Fujita, H. Machiyama, T. Yamaguchi, T. M. Watanabe and H. Fujita, *Sci. Rep.*, 2016, **6**, 37562.
- K. Majzner, A. Kaczor, N. Kachamakova-Trojanowska, A. Fedorowicz, S. Chlopicki and M. Baranska, *3D confocal Raman imaging of endothelial cells and vascular wall: Perspectives in analytical spectroscopy of biomedical research*, 2012.
- K. Kochan, E. Kus, A. Filipek, K. Szafranska, S. Chlopicki and M. Baranska, *Analyst*, 2017, **142**, 1308–1319.
- D. Perez-Guaita, K. Kochan, M. Martin, D. W. Andrew, P. Heraud, J. S. Richards and B. R. Wood, *Vib. Spectrosc.*, 2017, **91**, 46–58.
- A. F. Palonpon, M. Sodeoka and K. Fujita, *Curr. Opin. Chem. Biol.*, 2013, **17**, 708–715.
- A. S. Stender, K. Marchuk, C. Liu, S. Sander, M. W. Meyer, E. A. Smith, B. Neupane, G. Wang, J. Li, J.-X. Cheng, B. Huang and N. Fang, *Chem. Rev.*, 2013, **113**, 2469–2527.
- B. Vincent, *Lipid Technol.*, 2010, **22**, 36–38.
- K. Czamara, K. Majzner, M. Z. Pacia, K. Kochan, A. Kaczor and M. Baranska, *J. Raman Spectrosc.*, 2015, **46**, 4–20.
- H. Wu, J. V. Volponi, A. E. Oliver, A. N. Parikh, B. A. Simmons and S. Singh, *Proc. Natl. Acad. Sci. U. S. A.*, 2011, **108**, 3809–3814.
- O. Samek, A. Jonas, Z. Pilat, P. Zemanek, L. Nedbal, J. Triska, P. Kotas and M. Trtilek, *Sensors*, 2010, **10**, 8635–8651.
- K. Kochan, E. Maslak, C. Krafft, R. Kostogryns, S. Chlopicki and M. Baranska, *J. Biophotonics*, 2015, **8**, 597–609.
- U. Munchberg, L. Wagner, C. Rohrer, K. Voigt, P. Rosch, G. Jahreis and J. Popp, *Anal. Bioanal. Chem.*, 2015, **407**, 3303–3311.

- 30 J. D. Gelder, K. D. Gussem, P. Vandenabeele and L. Moens, *J. Raman Spectrosc.*, 2007, **38**, 1133–1147.
- 31 H. Peng, L. He and V. S. Haritos, *J. Ind. Microbiol. Biotechnol.*, 2018, 1–11.
- 32 J. C. Obert, D. Hughes, W. R. Sorenson, M. McCann and W. P. Ridley, *J. Agric. Food Chem.*, 2007, **55**, 2062–2067.
- 33 A. Caligiani, M. Nocetti, V. Lolli, A. Marseglia and G. Palla, *J. Agric. Food Chem.*, 2016, **64**, 4158–4164.
- 34 V. Lolli, A. Marseglia, G. Palla, E. Zanardi and A. Caligiani, *J. Anal. Methods Chem.*, 2018, **2018**, 8034042.
- 35 E. G. Bligh and W. J. Dyer, *Can. J. Biochem. Physiol.*, 1959, **37**, 911–917.
- 36 O. L. Knittelfelder and S. D. Kohlwein, *Cold Spring Harb. Protoc.*, 2017, **5**, 408–411.
- 37 H. Peng, L. Moghaddam, A. Brinin, B. Williams, S. Mundree and V. S. Haritos, *Biotechnol. Appl. Biochem.*, 2018, **65**, 138–144.
- 38 Y. Zhao and D. G. Truhlar, *Theor. Chem. Acc.*, 2008, **120**, 215–241.
- 39 J.-D. Chai and M. Head-Gordon, *Phys. Chem. Chem. Phys.*, 2008, **10**, 6615–6620.
- 40 D. E. Woon and T. H. Dunning Jr., *J. Chem. Phys.*, 1994, **100**, 2975–2988.
- 41 K. Majzner, K. Kochan, N. Kachamakova-Trojanowska, E. Maslak, S. Chlopicki and M. Baranska, *Anal. Chem.*, 2014, **86**, 6666–6674.
- 42 K. Kochan, K. M. Marzec, E. Maslak, S. Chlopicki and M. Baranska, *Analyst*, 2015, **140**, 2074–2079.

SUPPLEMENTARY MATERIALS

Raman spectroscopy as tool for tracking cyclopropane fatty acids in genetically engineered *Saccharomyces cerevisiae*

Kamila Kochan,^a Huadong Peng,^b Eunice S. H. Gwee,^{a,c} Ekaterina Izgorodina,^c Victoria
Haritos^{b, *} and Bayden R. Wood^{a, *}

^aCentre for Biospectroscopy, School of Chemistry, Monash University, Clayton Campus,
3800, Victoria, Australia. Email: Bayden.wood@monash.edu.

^bDepartment of Chemical Engineering, Monash University, Clayton Campus, 3800, Victoria,
Australia. Email: victoria.haritos@monash.edu.

^cSchool of Chemistry, Monash University, 17 Rainforest Walk, Clayton, VIC, 3800, Australia.
E-mail: katya.pas@monash.edu.

Appendix III Raman track CFA

Table S1. Band position and assignment in the theoretically calculated Raman spectra of *cis*-9,10-methyleneoctadecanoic acid, using different combinations of length of side chains, basic sets and functionals. The band used for scaling in each spectrum is highlighted in light grey and the scaling factor for each spectrum is highlighted in orange.

Functional	Basis set	Ethyl			Butyl		
		Theoretical Wavenumber (cm ⁻¹)			Theoretical Wavenumber (cm ⁻¹)		
		Raman (cm ⁻¹)	Intensity	Assignment	Raman (cm ⁻¹)	Intensity	Assignment
wB97XD	cc-pVDZ	589.19	4.5656	$\gamma(-\text{COOH})$	593.04	3.4314	$\gamma(-\text{COOH})$
		626.73	2.3479	$\alpha(-\text{COO}) + \delta(-\text{COH})$	628.74	2.886	$\gamma(-\text{COOH}) + \alpha(-\text{COO})$
		725.66	2.567	$\gamma(-\text{COOH}) + \rho(-\text{CH}_2(\text{ethyl}))$	730.44	1.8791	$\gamma(-\text{COOH}) + \rho(-\text{CH}_2(\text{butyl}))$
		762.4	4.1035	$\rho(-\text{CH}_2(\text{ethyl})) + \omega(-\text{CH}_2(\text{ring})) + \rho(-\text{C-C-C}(\text{ring}))$	783.1	5.3038	$\gamma(-\text{COOH}) + \rho(-\text{CH}_2(\text{butyl})) + \omega(-\text{CH}_2(\text{ring})) + \delta(-\text{CH}(\text{ring})) + \tau(-\text{CH}_2(\text{butyl}))$
		788.2	1.0699	$\rho(-\text{CH}_2(\text{ethyl})) + \tau(-\text{CH}_2(\text{ring}))$	828.49	5.15	$\rho(-\text{CH}_2(\text{butyl})) + \alpha(-\text{C-C-C}(\text{ring})) + \tau(-\text{CH}_2(\text{ring}))$
		823	6.7405	$\rho(-\text{CH}_2(\text{ethyl})) + \rho(-\text{CH}_2(\text{ring})) + \delta(-\text{CH}(\text{ring}))$	880.82	3.9963	$\rho(-\text{CH}_2(\text{butyl})) + \tau(-\text{CH}_2(\text{ring})) + \omega(-\text{CH}(\text{ring}))$
		861.74	6.1143	$\nu(-\text{C-C-O}) + \tau(-\text{CH}_2(\text{ring})) + \delta(-\text{CH}(\text{ring})) + \nu(-\text{C-C-C})$	912.47	3.6228	$\rho(-\text{CH}_2(\text{ring})) + \tau(-\text{CH}_2(\text{butyl}))$
		897.87	2.6001	$\tau(-\text{CH}_2(\text{ethyl})) + \rho(-\text{CH}_2(\text{ring})) + \rho(\text{H-C-C-H}(\text{ring}))$	924.43	5.7959	$\delta(-\text{COH}) + \rho(-\text{CH}_2(\text{butyl})) + \tau(-\text{CH}_2(\text{butyl})) + \tau(-\text{CH}_2(\text{ring})) + \delta(-\text{CH}(\text{ring}))$
		908.28	6.8929	$\nu(-\text{COO}) + \tau(-\text{CH}_2(\text{ring})) + \alpha(\text{H-C-C-H}(\text{ring}))$	961.9	10.3272	$\alpha(-\text{C-C-C}(\text{ring})) + \omega(-\text{CH}_2(\text{butyl}))$
		950.44	8.8181	$\nu(-\text{COO}) + \alpha(-\text{C-C-C}) + \tau(-\text{CH}_2(\text{ethyl})) + \rho(-\text{CH}_3) + \omega(-\text{CH}_2(\text{ethyl})) + \alpha(-\text{C-C-C}(\text{ring}))$	1075.24	3.9951	$\nu(-\text{C-C-C}) + \omega(-\text{CH}_2(\text{butyl})) + \omega(-\text{CH}_2(\text{ring})) + \omega(\text{H-C-C-H}(\text{ring}))$
		965.42	7.5527	$\rho(-\text{CH}_2) + \tau(-\text{CH}_2(\text{ring}))$	1083.94	6.4244	$\nu(-\text{C-C}(\text{butyl})) + \omega(-\text{CH}_2(\text{ring}))$
		1019.14	2.4452	$\omega(-\text{CH}_2(\text{ring})) + \delta(-\text{CH}(\text{ring})) + \alpha(\text{H-C-C-H}(\text{ring}, \text{ethyl})) + \rho(-\text{CH}_3)$	1095.17	10.662	$\omega(-\text{CH}_2(\text{butyl})) + \tau(-\text{CH}_2(\text{ring})) + \delta(-\text{CH}(\text{ring})) + \nu(-\text{CH}_2(\text{butyl}))$
		1033.9	1.4906	$\omega(-\text{CH}_2(\text{ring})) + \omega(-\text{CH}_2(\text{ethyl})) + \omega(\text{H-C-C-H}(\text{ring}))$	1134.83	11.3164	$\tau(-\text{CH}_2(\text{butyl})) + \tau(-\text{CH}_2(\text{ring})) + \omega(\text{H-C-C-H}(\text{ring}))$
		1052.28	1.3821	$\omega(-\text{CH}_2(\text{ring})) + \alpha(\text{H-C-C-H}(\text{ring}, \text{ethyl}))$	1147.15	4.8086	$\tau(-\text{CH}_2(\text{butyl})) + \omega(\text{H-C-C-H}(\text{ring}))$
		1078.42	8.7501	$\nu(-\text{C-C-C}) + \tau(-\text{CH}_2(\text{ring})) + \delta(-\text{CH}(\text{ring}))$	1226.28	20.3851	$\delta(-\text{COH}) + \rho(-\text{CH}_2(\text{butyl})) + \alpha(-\text{CH}_2(\text{ring})) + \alpha(\text{H-C-C-H}(\text{ring}))$
		1106.77	1.8724	$\alpha(\text{H-C-C-H}(\text{ring})) + \tau(-\text{CH}_2(\text{ethyl})) + \tau(-\text{CH}_2(\text{ring}))$	1249.65	4.0139	$\delta(-\text{COH}) + \rho(-\text{CH}_2(\text{butyl})) + \tau(-\text{CH}_2(\text{ring})) + \tau(-\text{CH}_2(\text{butyl}))$
		1120.37	3.5269	$\alpha(\text{H-C-C-H}(\text{ring})) + \tau(-\text{CH}_2(\text{ethyl})) + \tau(-\text{CH}_2(\text{ring}))$	1277.63	5.7097	$\tau(-\text{CH}_2(\text{butyl})) + \omega(-\text{CH}_2(\text{butyl})) + \omega(-\text{CH}(\text{ring}))$
		1138.13	2.613	$\alpha(-\text{C-C-H}(\text{ring})) + \rho(-\text{CH}_2(\text{ethyl})) + \tau(-\text{CH}_2(\text{ring}))$	1328.52	20.6676	$\tau(-\text{CH}_2(\text{butyl}))$
1206.21	1.4255	$\rho(-\text{CH}_2(\text{ring})) + \omega(-\text{CH}(\text{ring})) + \nu(-\text{C-C-C})$	1405.59	2.2334	$\tau(-\text{CH}_2(\text{butyl})) + \omega(-\text{CH}_2(\text{butyl})) + \alpha(-\text{CH}_2(\text{ring}))$		
1217.06	4.2574	$\delta(-\text{COH}) + \tau(-\text{CH}_2(\text{ethyl})) + \rho(-\text{CH}_2(\text{ethyl})) + \rho(-\text{C-C-H}(\text{ring}))$	1434.5	4.5	$\alpha(-\text{CH}_2(\text{ring})) + \omega(-\text{CH}_2(\text{butyl})) + \alpha(\text{H-C-C-H}(\text{ring}))$		

Appendix III Raman track CFA

Functional	Basis set	Ethyl			Butyl		
		Theoretical Wavenumber (cm ⁻¹)			Theoretical Wavenumber (cm ⁻¹)		
		Raman (cm ⁻¹)	Intensity	Assignment	Raman (cm ⁻¹)	Intensity	Assignment
		1228.48	16.9717	vs(-C-C-C- (ring)) + τ(-CH2(ring)) + α(H-C-C-H (ring))	1472.25	25.172	α(-CH2(butyl)) + α(-CH3)
		1247.15	4.8065	δ(-COH) + τ(-CH2(ethyl)) + τ(-CH2(ring))	1516.78	12.5005	α(-CH2(ring)) + vs(-C-C-C-(ring))
		1292.44	2.7922	ω(-CH2(ethyl)) + τ(-CH2(ring)) + ω(-CH (ring)) + τ(-CH2 (ethyl))	3028.34	177.596	vs(-CH2(butyl))
		1317.94	8.9215	τ(-CH2(ethyl)) + τ(-CH2(ring))	3043.76	182.6362	vs(-CH3(butyl))
		1328.4	4.7735	ρ(H-C-C-H (ring, ethyl))	3058.77	157.4713	vass(-CH2(butyl))
		1361.88	2.3049	ω(-CH2(ethyl))	3065.01	53.7627	vs(-CH2(butyl))
		1396.33	2.0617	α(-COH) + ω(-CH2(ethyl)) + ω(H-C-C-H (ring))	3089.38	24.6143	vass(-CH2(butyl))
		1432.39	5.4502	α(-CH2(ring))	3107.31	45.608	vass(-CH2(butyl))
		1455.67	12.8005	α(-CH2(ethyl))	3135.24	42.5471	vass(-CH3) + vs(-CH2(ring)) + δ(-CH(ring))
		1469.34	19.3327	α(-CH2(ethyl)) + α(-CH2(ring)) + α(-CH3)	3142.8	155.7186	vs(-CH2(ring)) + v(-CH(ring))
		1477.97	5.7917	α(-CH2(ethyl))	3231.23	48.1213	vass(-CH2(ring))
		1517.34	12.7175	vs(-C-C-C- (ring)) + α(-CH2(ring)) + δ(-CH(ring))	3800.63	128.5	v(-OH)
		1882.83	6.9764	v(C=O) + α(-COH) + τ(-CH2(ethyl))	SCALING FACTOR	0.939782191	
		3046.79	162.5392	vs(-CH3) + vs(-CH2(ethyl))			
		3068.89	39.0607	vs(-CH2(ethyl))			
		3082.11	96.3816	vass(-CH3) + vass(-CH2(ethyl))			
		3105.47	79.9938	vass(-CH2(ethyl)) + v(-CH(ring))			
		3136.71	99.3456	vass(-CH3)			
		3144.12	90.9367	vass(-CH2(ethyl)) + v(-CH(ring)) + vs(-CH2(ring))			
		3231.25	50.5085	vass(-CH2(ring))			
		3800.48	123.663	v(-OH)			
		SCALING FACTOR	0.93409129				
	aug-cc-pVDZ	596.73	1.7143	γ(-COOH)	599.08	1.2506	γ(-COOH)
	aug-cc-pVDZ	626.38	1.2625	γ(-COOH) + α(-COO)	630.78	1.2531	γ(-COOH) + α(-COO)

Appendix III Raman track CFA

Functional	Basis set	Ethyl			Butyl		
		Theoretical Wavenumber (cm ⁻¹)			Theoretical Wavenumber (cm ⁻¹)		
		Raman (cm ⁻¹)	Intensity	Assignment	Raman (cm ⁻¹)	Intensity	Assignment
		745.23	3.6559	$\rho(-CH_2) + \rho(-C-C-C) + \gamma(-COOH)$	762.38	4.2555	$\rho(-C-C-C) + \gamma(-COOH)$
		763.3	3.7594	$\rho(-CH_2 \text{ (ethyl)}) + \omega(-COH)$	773.42	3.7797	$\rho(-CH_2(\text{butyl})) + \tau(-CH_2(\text{butyl})) + \alpha(-C-C-C \text{ (ring)})$
		818.97	5.6014	$\rho(-CH_2(\text{ethyl})) + \rho(-CH_2(\text{ring}))$	825.23	3.9401	$\rho(-CH_2(\text{butyl})) + \tau(-CH_2(\text{butyl})) + \rho(-CH_2(\text{ring})) + \alpha(-C-C-C \text{ (ring)})$
		858.85	4.0416	$vs(-O-C-C) + \tau(-CH_2(\text{ring})) + \alpha(H-C-C-H(\text{ring}))$	877.95	1.954	$\rho(-CH_2(\text{butyl})) + \tau(-CH_2(\text{ring})) + \alpha(H-C-C-H(\text{ring}))$
		895.28	2.5179	$\rho(-CH_2(\text{ring})) + \rho(H-C-C-H(\text{ring})) + \tau(-CH_2(\text{ethyl}))$	910.76	8.8352	$vs(-COO) + \rho(-CH_2(\text{butyl})) + \rho(-CH_2(\text{ring})) + \alpha(-C-C-C \text{ (ring)})$
		909.85	8.4364	$vs(-C-C-O) + \tau(-CH_2(\text{ring})) + \alpha(H-C-C-H(\text{ring}))$	921.86	2.787	$\rho(-CH_2(\text{butyl})) + \tau(-CH_2(\text{butyl})) + \alpha(-C-C-C \text{ (ring)})$
		946.36	6.0068	$vs(-COO) + \omega(-CH_2(\text{ethyl})) + \alpha(-C-C-C \text{ (ring)})$	957.54	6.904	$\alpha(-C-C-C \text{ (ring)}) + \omega(-CH_2(\text{butyl}))$
		962.82	4.723	$\alpha(-C-C-C \text{ (ring)}) + \rho(-CH_2(\text{ethyl}))$	1028.89	1.1162	$\tau(-CH_2(\text{butyl})) + \alpha(-C-C-C \text{ (ring)}) + \omega(-CH_2(\text{ring})) + \omega(-CH \text{ (ring)})$
		1016.32	1.6788	$vs(-C-C-C \text{ (ring)}) + \tau(-CH_2(\text{ethyl})) + vs(-C-C-C \text{ (ethyl, ring)})$	1046.89	3.0882	$vass(-C-C \text{ (ring)}) + \omega(-CH_2(\text{ring}))$
		1031.18	1.9613	$\omega(-CH_2(\text{ring})) + \omega(H-C-C-H \text{ (ring)}) + vs(-C-C-C \text{ (ethyl, ring)})$	1070.12	4.4119	$\tau(-CH_2(\text{butyl})) + \rho(-CH_2(\text{ring})) + \omega(H-C-C-H \text{ (ring)})$
		1047.05	3.4118	$\omega(-CH_2(\text{ring}))$	1082.08	4.9613	$vass(-C-C-C(\text{butyl}))$
		1067.88	12.6149	$\tau(H-C-C-H \text{ (ring)}) + vass(-C-C-C \text{ (ethyl)})$	1091.04	9.3555	$vass(-C-C-C(\text{butyl}))$
		1102.02	2.1276	$\tau(-CH_2(\text{ring})) + \alpha(H-C-C-H \text{ (ring)}) + \tau(-CH_2(\text{ethyl}))$	1102.02	9.7095	$v(-C-C-C \text{ (butyl)}) + \tau(-CH_2(\text{ring})) + \omega(-CH \text{ (ring)})$
		1117.34	5.9982	$\tau(-CH_2(\text{ethyl})) + \rho(-CH_2(\text{ring}))$	1126.91	11.6793	$\tau(-CH_2(\text{butyl})) + \omega(H-C-C-H \text{ (ring)})$
		1136.08	2.3629	$\alpha(-COH) + \tau(-CH_2(\text{ethyl})) + \tau(-CH_2(\text{ring})) + \omega(H-C-C-H \text{ (ring)})$	1144.61	7.3543	$\tau(-CH_2(\text{butyl})) + vs(-C-C-C \text{ (butyl)}) + \rho(H-C-C-H \text{ (ring)}) + \omega(-CH_2(\text{butyl}))$
		1228.25	20.068	$\delta(-COH) + vs(-C-C-C \text{ (ring)}) + \alpha(H-C-C-H \text{ (ring)}) + \tau(-CH_2(\text{ethyl}))$	1226.03	17.4839	$\rho(-COH) + \alpha(H-C-C-H \text{ (ring)}) + vs(-C-C-C \text{ (ring)})$
		1247.48	3.736	$\delta(-COH) + \tau(-CH_2(\text{ethyl})) + \rho(-CH_2(\text{ring}))$	1248.69	3.8315	$\tau(-CH_2(\text{butyl})) + \omega(-CH_2(\text{butyl})) + \alpha(H-C-C-H \text{ (ring)}) + \tau(-CH_2 \text{ (ring)})$
		1290.67	1.6819	$\tau(-CH_2(\text{ring})) + \omega(-CH \text{ (ring)}) + \tau(-CH_2(\text{ring}))$	1276.75	2.9531	$\delta(-COH) + \tau(-CH_2(\text{butyl}))$
		1313.06	4.2475	$\delta(-COH) + \tau(-CH_2(\text{ethyl})) + \tau(-CH_2(\text{ring})) + \delta(-CH \text{ (ring)})$	1294.29	1.6641	$\omega(-CH_2(\text{butyl})) + \omega(-CH \text{ (ring)}) + \delta(-COH)$
		1326.81	1.6932	$\tau(-CH_2(\text{ethyl})) + \omega(H-C-C-H \text{ (ring)})$	1324.95	5.4819	$\tau(-CH_2(\text{butyl}))$
		1354.05	3.1705	$\omega(-CH_2(\text{ethyl})) + \omega(-C-H \text{ (ring)})$	1408.88	2.4142	$\omega(-CH_2(\text{butyl})) + \omega(-CH \text{ (ring)}) + \alpha(-CH_2 \text{ (ring)})$
		1396.21	3.4731	$\alpha(-COH) + \omega(-CH_2(\text{ethyl})) + \omega(-CH \text{ (ring)})$	1442.66	4.3967	$\alpha(-CH_2(\text{ring})) + \alpha(H-C-C-H \text{ (ring)})$
		1441.63	5.422	$\alpha(-CH_2(\text{ethyl})) + \alpha(-CH_2(\text{ring})) + \alpha(H-C-C-H \text{ (ring)})$	1473.96	27.2866	$\alpha(-CH_2(\text{butyl})) + \alpha(-CH_2(\text{ring}))$

Appendix III Raman track CFA

Functional	Basis set	Ethyl			Butyl		
		Theoretical Wavenumber (cm ⁻¹)			Theoretical Wavenumber (cm ⁻¹)		
		Raman (cm ⁻¹)	Intensity	Assignment	Raman (cm ⁻¹)	Intensity	Assignment
		1472.96	8.0436	α(-CH2(ethyl))	1517.72	13.3833	α(-CH2(ring)) + vs(-C-C-C- (ring))
		1518.05	13.3123	v(-C-C-C- (ring)) + α(-CH2(ring)) + δ(-CH(ring))	1844.12	16.6225	v(C=O) + α(-COH) + τ(-CH2(ethyl))
		1843.41	17.1462	v(C=O) + α(-COH) + τ(-CH2(ethyl))	3029.13	140.7988	vs(-CH2(butyl))
		3043.39	263.9167	vs(-CH2(ethyl)) + vs(-CH3)	3040.94	253.4047	vs(-CH3)
		3051.93	125.2432	vs(-CH2(ethyl))	3057.02	131.2962	vass(-CH2(butyl))
		3082.37	81.8897	vass(-CH3) + vass(-CH2(ethyl))	3064.72	109.7682	vass(-CH2(butyl))
		3100.99	62.5775	vass(-CH2(ethyl)) + v(-CH(ring))	3084.28	56.6679	vass(-CH2(butyl)) + vs(-CH2(butyl))
		3129.65	79.2444	vass(-CH3) + vass(-CH2(ethyl))	3105.31	23.9724	vass(-CH2(butyl))
		3138.79	56.0535	vs(-CH2(ring)) + v(-CH (ring))	3127.8	98.3032	v(-CH3)
		3148.87	156.6131	vs(-CH2(ethyl)) + v(-CH(ring))	3147.95	175.9082	vs(-CH2(ring)) + v(-CH(ring))
		3232.1	44.1849	vass(-CH2(ethyl))	3230.87	42.6271	vass(-CH2(ring)) + v(-CH(ring))
		3828.31	108.7194	v(-OH)	3828.77	112.7502	v(-OH)
		SCALING FACTOR	0.935134833		SCALING FACTOR	0.939537095	
M06-2X	cc-pVDZ	585.88	4.7152	γ(-COOH)	586.45	3.767	γ(-COOH)
		625.69	2.1367	γ(-COOH) + α(-COO)	626.78	2.5408	γ(-COOH) + α(-COO)
		718.35	2.47	γ(-COOH) + ρ(-CH2(ethyl))	720.23	1.6915	γ(-COOH) + ρ(-CH2(butyl))
		764.55	2.5088	ρ(-CH2(ethyl)) + ω(-CH2(ring))	779.79	2.9847	ρ(-CH2(butyl)) + τ(-CH2(ring)) + τ(-CH2(butyl))
		821.11	7.7815	ρ(-CH2(ethyl)) + τ(-CH2(ring)) + δ(-CH(ring))	833.75	6.7483	τ(-CH2(butyl)) + ρ(-C-C-C- (ring)) + ρ(-CH2(butyl))
		863.39	5.909	vs(-C-C-O) + τ(-CH2(ring)) + τ(-CH2(ethyl)) + ω(-CH(ring))	875.32	3.6071	ρ(-CH2(butyl)) + τ(-CH2(ring)) + α(H-C-C-H (ring))
		888.82	3.1565	ρ(-CH2(ethyl)) + τ(-CH2(ethyl)) + ρ(-CH2(ring)) + ρ(H-C-C-H (ring))	907.91	3.0312	ρ(-CH2(ring)) + ρ(-CH2 (butyl)) + vs(-C-C-O-)
		910.53	6.2592	vs(-C-C-O) + τ(-CH2(ring)) + α(H-C-C-H (ring))	921.15	7.0976	ρ(-CH2(butyl)) + τ(-CH2(butyl)) + τ(-CH2(ring)) + δ(-CH(ring))
		950.41	5.7795	τ(-CH2(ring)) + τ(-CH2(ethyl)) + ω(-CH (ring))	944.64	3.3727	τ(-CH2(butyl)) + ρ(-C-C-C-(ring))
		976.87	8.182	α(-C-C-C- (ring)) + ρ(-CH2(ethyl))	974.72	9.5596	α(-C-C-C- (ring)) + α(-C-C-C- (ring, butyl))
		1018.81	2.4065	ω(-CH2 (ring)) + ω(-CH (ring)) + τ(-CH2(ethyl))	1069.07	2.071	ω(-CH2 (butyl)) + ρ(-CH2(ring)) + ω(H-C-C-H (ring))

Appendix III Raman track CFA

Functional	Basis set	Ethyl			Butyl		
		Theoretical Wavenumber (cm ⁻¹)			Theoretical Wavenumber (cm ⁻¹)		
		Raman (cm ⁻¹)	Intensity	Assignment	Raman (cm ⁻¹)	Intensity	Assignment
		1080.78	8.571	$\tau(-\text{CH}_2(\text{ethyl})) + \tau(-\text{CH}_2(\text{ring})) + \delta(-\text{CH}(\text{ring})) + \text{vass}(-\text{C}-\text{C}-\text{C}-)$	1084.52	6.0568	$\text{vass}(-\text{C}-\text{C}-\text{C}- (\text{butyl})) + \tau(-\text{CH}_2(\text{ring})) + \alpha(\text{H}-\text{C}-\text{C}-\text{H} (\text{ring}))$
		1113.73	4.2913	$\tau(-\text{CH}_2(\text{ethyl})) + \tau(-\text{CH}_2(\text{ring})) + \alpha(\text{H}-\text{C}-\text{C}-\text{H} (\text{ring}))$	1095.05	9.1696	$\tau(-\text{CH}_2(\text{ring})) + \alpha(\text{H}-\text{C}-\text{C}-\text{H} (\text{ring})) + \text{vass}(-\text{C}-\text{C}-\text{C}- (\text{butyl}))$
		1133.68	3.2175	$\rho(-\text{CH}_2(\text{ethyl})) + \tau(-\text{CH}_2(\text{ethyl})) + \omega(\text{H}-\text{C}-\text{C}-\text{H} (\text{ring}))$	1112.01	3.4197	$\rho(-\text{CH}_2 (\text{ring})) + \rho(\text{H}-\text{C}-\text{C}-\text{H} (\text{ring})) + \text{vass}(-\text{C}-\text{C}-\text{C}- (\text{butyl}, \text{ring}))$
		1212.35	3.8319	$\delta(-\text{COH}) + \tau(-\text{CH}_2(\text{ethyl})) + \rho(-\text{CH}_2(\text{ring})) + \alpha(\text{H}-\text{C}-\text{C}-\text{H} (\text{ring}))$	1131	11.7461	$\tau(-\text{CH}_2(\text{butyl})) + \alpha(-\text{C}-\text{C}-\text{C}- (\text{ring})) + \delta(-\text{CH}(\text{ring}))$
		1228.2	17.7471	$\delta(-\text{COH}) + \tau(-\text{CH}_2(\text{ethyl})) + \tau(-\text{CH}_2(\text{ring})) + \alpha(\text{H}-\text{C}-\text{C}-\text{H}(\text{ring}))$	1144.14	6.2076	$\tau(-\text{CH}_2(\text{butyl})) + \omega(-\text{CH}(\text{ring})) + \omega(-\text{CH}_2(\text{butyl}))$
		1248.48	3.807	$\delta(-\text{COH}) + \tau(-\text{CH}_2(\text{ethyl}))$	1224.77	18.1052	$\tau(-\text{CH}_2(\text{butyl})) + \rho(-\text{CH}_2(\text{butyl})) + \alpha(-\text{CH}_2(\text{ring})) + \text{vs}(-\text{C}-\text{C}-\text{C}- (\text{ring}))$
		1281.14	2.8401	$\tau(-\text{CH}_2 (\text{ethyl})) + \tau(-\text{CH}_2 (\text{ring})) + \omega(-\text{CH} (\text{ring}))$	1245.82	3.956	$\alpha(-\text{COH}) + \text{vass}(-\text{O}-\text{C}-\text{C}-) + \tau(-\text{CH}_2(\text{butyl})) + \tau(-\text{CH}_2(\text{ring})) + \omega(-\text{CH} (\text{ring}))$
		1307.85	9.2933	$\tau(-\text{CH}_2(\text{ethyl})) + \tau(-\text{CH}_2(\text{ring})) + \delta(-\text{CH}(\text{ring}))$	1267.68	6.3262	$\delta(-\text{COH}) + \tau(-\text{CH}_2(\text{butyl})) + \rho(-\text{CH}_2(\text{butyl})) + \tau(-\text{CH}_2(\text{ring})) + \omega(-\text{CH}_2(\text{butyl})) + \omega(-\text{CH} (\text{ring}))$
		1351.23	2.4718	$\omega(-\text{CH}_2 (\text{ethyl})) + \omega(-\text{CH} (\text{ring})) + \alpha(-\text{CH}_2(\text{ring}))$	1315.3	20.377	$\tau(-\text{CH}_2(\text{butyl}))$
		1422.1	5.06	$\alpha(-\text{CH}_2 (\text{ring})) + \omega(-\text{CH}_2 (\text{ethyl}))$	1397	2.2093	$\omega(-\text{CH}_2(\text{butyl})) + \alpha(-\text{CH}_2 (\text{ring}))$
		1443.33	13.1987	$\alpha(-\text{CH}_2(\text{ethyl}))$	1423.96	4.5357	$\alpha(-\text{CH}_2(\text{ring})) + \omega(-\text{CH}_2(\text{butyl})) + \omega(-\text{CH} (\text{ring}))$
		1460.88	19.5208	$\alpha(-\text{CH}_2(\text{ethyl})) + \text{vs}(-\text{C}-\text{C}-\text{C}- (\text{ring})) + \alpha(-\text{CH}_2(\text{ring}))$	1459	21.6703	$\text{vs}(-\text{C}-\text{C}-\text{C}- (\text{ring})) + \alpha(-\text{CH}_2(\text{ring})) + \omega(-\text{CH} (\text{ring}))$
		1470.46	16.0968	$\alpha(-\text{CH}_3)$	1472.79	14.3098	$\alpha(-\text{CH}_2(\text{butyl})) + \alpha(-\text{CH}_3)$
		1522.05	12.9312	$\alpha(-\text{CH}_2(\text{ring})) + \text{vs}(-\text{C}-\text{C}-\text{C}- (\text{ring}))$	1521.36	12.5989	$\alpha(-\text{CH}_2(\text{ring})) + \text{vs}(-\text{C}-\text{C}-\text{C}- (\text{ring}))$
		1904.45	7.7864	$\text{v}(\text{C}=\text{O}) + \alpha(-\text{COH}) + \tau(-\text{CH}_2(\text{ethyl}))$	1904.38	7.5641	$\text{v}(\text{C}=\text{O}) + \alpha(-\text{COH}) + \tau(-\text{CH}_2(\text{ethyl}))$
		3060.17	269.957	$\text{vs}(-\text{CH}_2(\text{ethyl})) + \text{vs}(-\text{CH}_3)$	3036.49	208.3453	$\text{vs}(-\text{CH}_2(\text{butyl}))$
		3089.88	105.1511	$\text{vass}(-\text{CH}_2(\text{ethyl})) + \text{vass}(-\text{CH}_3)$	3057.14	136.847	$\text{vs}(-\text{CH}_2(\text{butyl}))$
		3111.21	84.3875	$\text{vass}(-\text{CH}_2(\text{ethyl}))$	3064.53	164.9593	$\text{vass}(-\text{CH}_2(\text{butyl}))$
		3152.19	149.8719	$\text{vass}(-\text{CH}_2(\text{ethyl})) + \text{vs}(-\text{CH}_2(\text{ring})) + \text{v}(-\text{CH}(\text{ring}))$	3070.83	130.1758	$\text{vass}(-\text{CH}_2(\text{butyl}))$
		3239.45	53.2957	$\text{vass}(-\text{CH}_2(\text{ring}))$	3095.84	31.0422	$\text{vass}(-\text{CH}_2(\text{butyl}))$
		3782.89	121.073	$\text{v}(-\text{OH})$	3114.24	51.2442	$\text{vass}(-\text{CH}_2(\text{butyl}))$
		SCALING FACTOR	0.930007156		3142.95	120.7271	$\text{v}(-\text{CH}_3)$
					3150	168.4671	$\text{vs}(-\text{CH}_2(\text{ring})) + \text{v}(-\text{CH}(\text{ring}))$

Appendix III Raman track CFA

Functional	Basis set	Ethyl			Butyl		
		Theoretical Wavenumber (cm ⁻¹)			Theoretical Wavenumber (cm ⁻¹)		
		Raman (cm ⁻¹)	Intensity	Assignment	Raman (cm ⁻¹)	Intensity	Assignment
					3237.92	50.4399	vass(-CH2(ring))
					3785.39	125.6187	v(-OH)
					SCALING FACTOR	0.937259797	
	aug-cc-pVDZ	591.91	1.8192	γ(-COOH)	590.82	1.319	γ(-COOH)
		620.77	1.1878	γ(-COOH) + α(-COO)	620.15	1.237	γ(-COOH) + α(-COO)
		739.63	4.1026	γ(-COOH) + ρ(-CH2(ethyl))	754.51	3.5695	γ(-COOH) + ρ(-CH2(butyl))
		758.02	1.3269	α(-C-C-C- (ring)) + ρ(-CH2(ethyl))	769.5	2.5494	τ(-CH2 (butyl)) + ρ(-CH2 (butyl)) + ρ(-C-C-C- (ring))
		772.21	1.0031	ρ(-CH2(ethyl)) + τ(-CH2 (ring)) + ω(-CH (ring))	830.9	4.8707	α(-C-C-C- (ring)) + ρ(-CH2(butyl))
		818.53	6.6936	ρ(-CH2(ethyl)) + τ(-CH2(ring)) + δ(-CH(ring)) + α(-C-C-C- (ring))	869.69	1.064	τ(-CH2 (ring)) + ω(-CH (ring)) + ρ(-CH2 (butyl)) +
		861.28	3.6811	vs(-C-C-O-) + τ(-CH2(ring)) + τ(-CH2(ethyl)) + ω(-CH (ring))	909.82	10.0107	vs(-C-C-O) + τ(-CH2(butyl)) + τ(-CH2(ring)) + ρ(-CH3)
		886.15	2.9925	ρ(-CH2(ethyl)) + τ(-CH2(ethyl)) + ρ(-CH2(ring)) + ρ(H-C-C-H (ring))	919.9	2.9026	ρ(-CH2 (butyl)) + τ(-CH2 (butyl)) + τ(-CH2(ring)) + α(H-C-C-H (ring))
		911.41	7.0368	vs(-C-C-O) + τ(-CH2(ring)) + α(H-C-C-H (ring))	944.31	3.4635	τ(-CH2 (butyl)) + ρ(-CH2 (butyl)) + ρ(-C-C-C- (ring))
		947.42	4.8069	vs(-C-C-O) + τ(-CH2(ring)) + τ(-CH2(ethyl)) + ω(-CH (ring))	970.82	6.9362	α(-C-C-C- (ring)) + ω(-CH2(butyl))
		973.05	6.7812	ρ(-CH2(ethyl)) + α(-C-C-C- (ring))	1024.44	0.77	ω(-CH2 (ring)) + ω(-CH (ring)) + τ(-CH2 (butyl))
		1039.3	2.6983	ω(-CH2 (ring)) + ω(-CH (ring)) + ω(-CH2(ethyl))	1037.96	1.1679	vass(-C-C-C- (butyl)) + ω(-CH2 (ring)) + ω(-CH (ring))
		1069.74	12.7101	τ(-CH2(ring)) + δ(-CH(ring)) + vass(-C-C-C-)	1050.18	3.5128	vass(-C-C-C- (butyl))
		1093.9	1.4505	τ(-CH2(ethyl)) + ρ(-CH2(ring))	1064.69	2.4653	ω(-CH2 (butyl)) + ρ(-CH2 (ring)) + ρ(H-C-C-H (ring))
		1110.73	7.5841	τ(-CH2(ethyl)) + τ(-CH2(ring)) + α(H-C-C-H (ring))	1083.22	4.5204	vass(-C-C-C- (butyl)) + ω(-CH (ring))
		1131.34	2.7991	ρ(-CH2(ethyl)) + τ(-CH2(ethyl)) + ω(H-C-C-H (ring))	1091.45	1.0815	τ(-CH2 (ring)) + vass(-C-C-C- (butyl))
		1228.59	19.7083	vs(-C-C-C-) + τ(-CH2(ring)) + α(H-C-C-H (ring)) + τ(-CH2(ethyl))	1104.03	17.1359	vs(-C-C-C- (butyl)) + ω(-CH (ring))
		1243.44	2.8818	τ(-CH2 (ring)) + ω(-CH2 (ethyl)) + ρ(-COH)	1123.87	11.3234	τ(-CH2(butyl)) + ω(-CH (ring))
	1250.64	2.2487	δ(-COH) + ω(-CH2(ethyl))	1141.75	9.2098	vs(-C-C-C- (butyl)) + τ(-CH2 (butyl)) + α(-C-C-C- (ring))	
	1281.08	1.9264	ω(-CH (ring)) + τ(-CH2 (ethyl))	1199.92	1.4104	ρ(-CH2(butyl)) + ω(-CH (ring)) + ω(-CH2(butyl))	

Appendix III Raman track CFA

Functional	Basis set	Ethyl			Butyl		
		Theoretical Wavenumber (cm ⁻¹)			Theoretical Wavenumber (cm ⁻¹)		
		Raman (cm ⁻¹)	Intensity	Assignment	Raman (cm ⁻¹)	Intensity	Assignment
		1304.46	4.3358	τ (-CH2(ethyl)) + τ (-CH2(ring)) + δ (-CH(ring))	1226.84	15.9591	α (-CH2 (ring)) + τ (-CH2 (butyl)) + α (H-C-C-H (ring))
		1344.18	3.4007	ω (-CH2(ethyl)) + α (-CH2(ring)) + δ (-CH(ring)) + α (-COH)	1242.52	8.167	ρ (-COH) + τ (-CH2 (butyl)) + τ (-CH2 (butyl)) + α (H-C-C-H (ring))
		1389.98	2.4369	α (-COH) + α (-CH2(ethyl)) + α (-CH2(ring)) + ω (-CH3)	1268.9	2.7699	δ (-COH) + τ (-CH2(butyl)) + ρ (-CH2(butyl)) + τ (-CH2(ring)) + ω (-CH2(butyl))
		1436.41	5.6878	α (-CH2(ethyl)) + α (-CH2(ring)) + α (H-C-C-H(ring))	1281.9	2.0443	ω (-CH2 (butyl)) + α (H-C-C-H (ring))
		1458.44	8.6226	α (-CH2(ethyl))	1313.12	5.5122	τ (-CH2 (butyl))
		1465.75	8.7749	α (-CH3) + α (-CH2(ethyl))	1396.43	3.4201	ω (-CH2 (butyl)) + α (-CH2 (ring)) + α (H-C-C-H (ring))
		1474.16	5.2024	α (-CH3)	1436.51	4.8579	α (-CH2 (ring)) + vs(-C-C-C- (ring)) + α (-CH2 (butyl))
		1521.86	14.8475	α (-CH2(ring)) + vs(-C-C-C-(ring))	1464.5	24.602	α (-CH2(butyl))
		1867.11	17.1562	ν (C=O) + α (-COH) + τ (-CH2(ethyl))	1521.03	14.3208	α (-CH2 (ring)) + vs(-C-C-C- (ring)) + α (H-C-C-H (ring))
		3059.53	147.4468	vs(-CH3)	1866.01	16.6873	ν (C=O) + α (-COH) + τ (-CH2(butyl))
		3093.96	90.4507	vass(-CH2(ethyl)) + vass(-CH3)	3039.26	225.3399	vs(-CH2(butyl))
		3111.76	65.332	vass(-CH2(ethyl))	3056.78	150.3069	vs(-CH2(butyl)) + vs(-CH3)
		3141.76	99.8112	vass(-CH3)	3068.07	139.4147	vass(-CH2 (butyl))
		3160.52	155.8493	vass(-CH2(ethyl)) + vs(-CH2(ring)) + ν (-CH(ring))	3095.93	69.8328	vs(-CH2(butyl))
		3246.86	47.8349	vass(-CH2(ring))	3114.41	25.9871	vass(-CH2(butyl))
		3816.41	107.3022	ν (-OH)	3139.34	108.8872	vass(-CH3)
		SCALING FACTOR	0.930201698		3159.14	201.567	vs(-CH2(ring)) + ν (-CH(ring))
					3244.48	45.297	vass(-CH2(ring))
					3816.11	111.2333	ν (-OH)
					SCALING FACTOR	0.936405572	

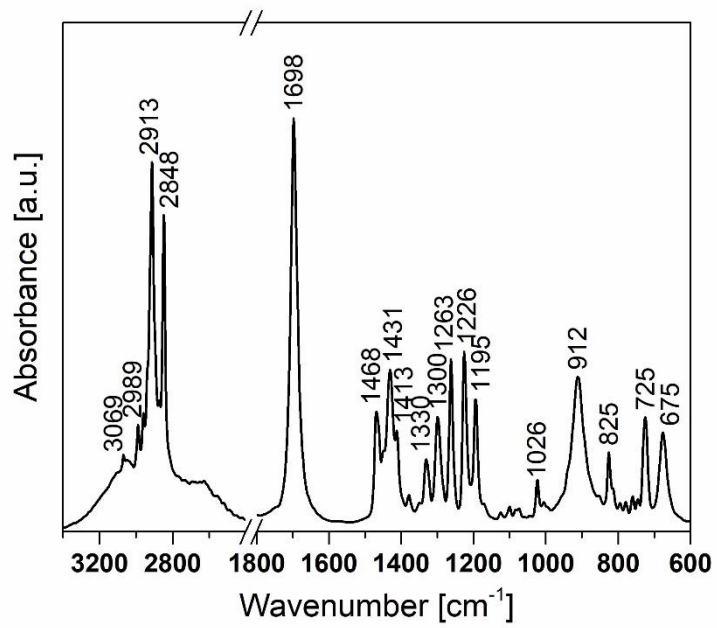


Figure S1. ATR-FTIR spectrum of the CFA standard (*cis*-9,10-methyleneoctadecanoic acid (CycC19)) with marked band positions.

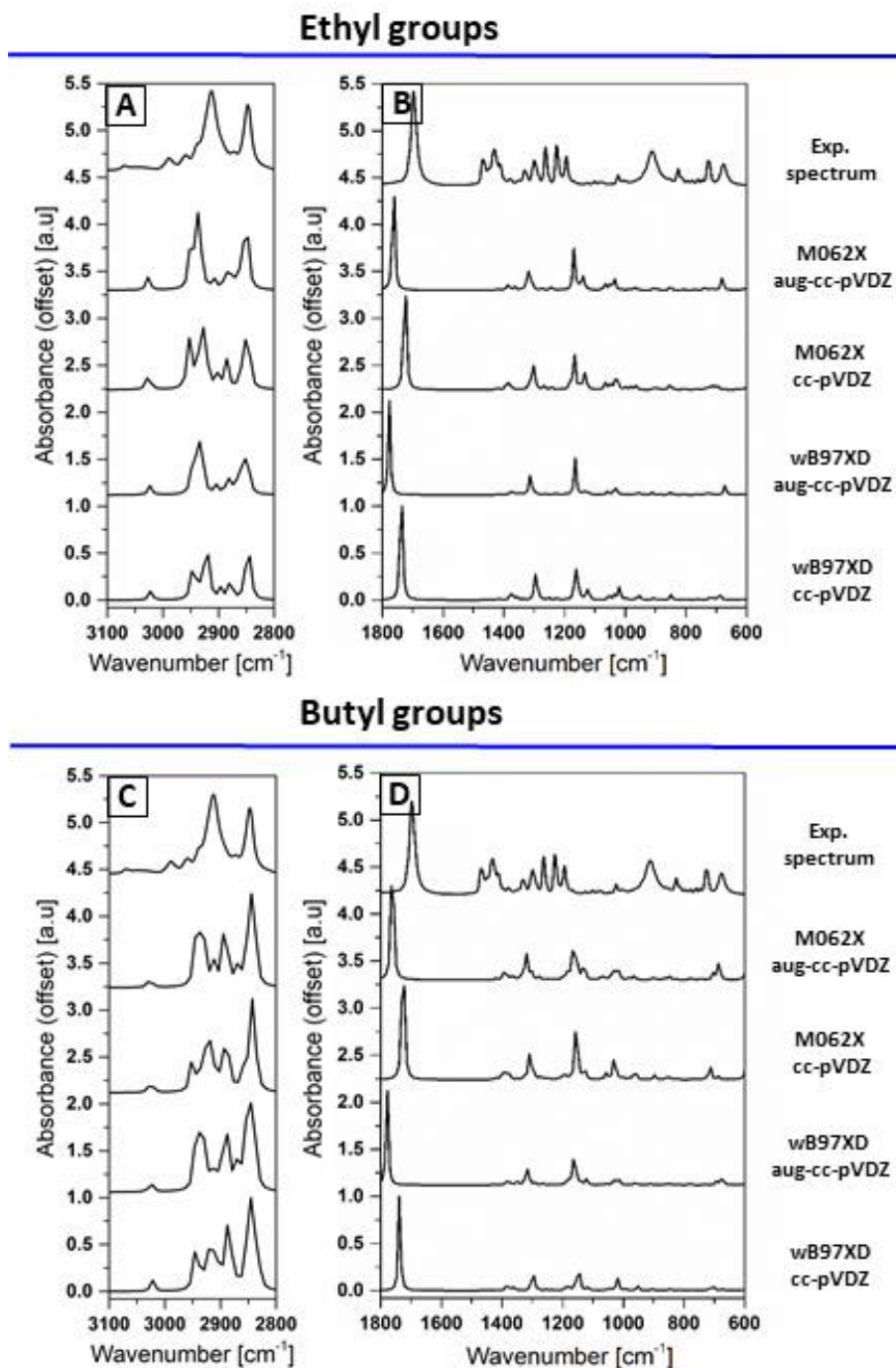


Figure S2. A comparison of the experimental ATR-FTIR spectrum of CFA standard with calculated IR spectra using various length of side chains: (A, B) ethyl and (C, D) butyl groups. For each length of side chains spectra were calculated using combinations of functionals: M06-2X, wB97XD and basic sets: cc-pVDZ, aug-cc-pVDZ, as marked on the right side of spectra. Spectra are presented in spectral ranges: (A, C) 3100 – 2800 cm^{-1} and (B, D) 1800 – 600 cm^{-1} . The scaling factors for each calculated spectrum are given in Supplementary Materials, Table S2. All spectra in (A, C) were normalized to 1 in the range 3100-2800 cm^{-1} . All spectra in (B, D) were normalised to 1 in the range 1800 – 600 cm^{-1} .

Appendix III Raman track CFA

Table S2. Band position and assignment in the theoretically calculated ATR-FTIR spectra of *cis*-9,10-methyleneoctadecanoic acid, using different combinations of length of side chains, basic sets and functionals. The band used for scaling in each spectrum is highlighted in light grey and the scaling factor for each spectrum is highlighted in orange.

Functional	Basis set	Ethyl			Butyl		
		Theoretical Wavenumber (cm ⁻¹)			Theoretical Wavenumber (cm ⁻¹)		
		IR (cm ⁻¹)	Intensity	Assignment	IR (cm ⁻¹)	Intensity	Assignment
wb97XD	cc-pVDZ	589.19	53.2784	γ (-COOH)	593.04	51.6178	γ (-COOH)
		626.73	65.62	γ (-COOH) + α (-COO)	628.74	67.9427	γ (-COOH) + α (-COO)
		725.66	41.5133	γ (-COOH) + ρ (-CH2(ethyl))	730.44	40.673	γ (-COOH) + ρ (-CH2(butyl))
		788.2	10.0407	ρ (-CH2) + τ (-CH2 (ring))	749.71	11.2401	ρ (-CH2(butyl))
		908.28	11.858	ν s(-C-C-O) + τ (-CH2(ring)) + α (H-C-C-H (ring))	828.49	5.1566	ρ (-CH2(butyl)) + α (-C-C-C- (ring)) + τ (-CH2(ring))
		965.42	7.5227	ρ (-CH2) + τ (-CH2 (ring))	904.85	6.1701	ν s(-C-C-O) + ρ (-CH2(ring))
		1033.9	9.1491	ω (-CH2(ring)) + ω (-CH2(ethyl)) + ω (H-C-C-H(ring))	924.43	2.8065	τ (-CH2(butyl)) + ρ (-CH2(butyl)) + τ (-CH2(ring))
		1106.77	19.777	α (H-C-C-H (ring)) + τ (-CH2(ethyl)) + τ (-CH2(ring))	961.9	6.0458	α (-C-C-C- (ring)) + ω (-CH2(butyl))
		1120.37	13.2446	α (H-C-C-H (ring)) + τ (-CH2(ethyl)) + τ (-CH2(ring))	1027.81	6.8145	τ (-CH2(butyl)) + ω (-CH2(ring)) + ω (-CH (ring))
		1138.13	20.0366	α (-C-C-H (ring)) + ρ (-CH2(ethyl)) + τ (-CH2(ring))	1049.26	3.8461	ω (-CH2(ring))
		1217.06	34.5956	δ (-COH) + τ (-CH2(ethyl)) + ρ (-CH2(ethyl)) + ρ (-C-C-H (ring))	1083.94	14.696	ν ass(-C-C- (butyl)) + ω (-CH2(ring))
		1247.15	111.5994	δ (-COH) + τ (-CH2(ethyl)) + τ (-CH2(ring))	1097.82	30.7353	τ (-CH2(butyl)) + τ (-CH2(ring))
		1328.4	7.3429	ρ (H-C-C-H (ring, ethyl))	1134.83	7.5333	τ (-CH2(butyl)) + τ (-CH2(ring)) + ω (H-C-C-H (ring))
		1361.88	5.05	ω (-CH2(ethyl))	1147.15	4.0593	τ (-CH2(butyl)) + ω (H-C-C-H (ring))
		1396.33	24.9744	α (-COH) + ω (-CH2(ethyl)) + ω (H-C-C-H (ring))	1206.33	33.7072	ρ (-COH) + τ (-CH2(butyl)) + ρ (-CH2(butyl)) + τ (-CH2(ring)) + ω (-C-H (ring))
		1406.19	42.0823	α (-COH) + ω (-CH3)	1233.26	33.0586	δ (-COH) + ω (-CH2(butyl)) + τ (-CH2(butyl)) + ρ (-CH2(ring)) + ρ (H-C-C-H (ring))
		1412.36	25.297	α (-COH) + ω (-CH2(ethyl)) + α (-CH2(ring))	1242.63	70.1082	ω (-CH2(butyl)) + α (-COH)
		1432.39	2.0404	α (-CH2(ring)) + α (-C-C-H (ring))	1263.97	12.0534	δ (-COH) + ω (-CH2(butyl)) + ω (H-C-C-H (ring))
1455.67	8.587	α (-CH2(ethyl))	1277.63	8.7411	τ (-CH2(butyl)) + ω (-CH2(butyl)) + ω (-CH(ring))		
1477.62	8.2001	α (-CH3)	1365.89	8.4521	α (-COH) + ω (-CH2(butyl)) + δ (-CH(ring))		

Appendix III Raman track CFA

Functional	Basis set	Ethyl			Butyl		
		Theoretical Wavenumber (cm ⁻¹)			Theoretical Wavenumber (cm ⁻¹)		
		IR (cm ⁻¹)	Intensity	Assignment	IR (cm ⁻¹)	Intensity	Assignment
		1882.73	353.795	$\nu(\text{C}=\text{O}) + \alpha(-\text{COH}) + \tau(-\text{CH}_2(\text{ethyl}))$	1390.44	12.7833	$\alpha(-\text{COH}) + \omega(-\text{CH}_2(\text{butyl})) + \alpha(-\text{CH}_2(\text{ring})) + \omega(\text{H-C-C-H}(\text{ring}))$
		3040.21	35.3464	$\nu\text{s}(-\text{CH}_2(\text{ethyl}))$	1411.14	38.6131	$\alpha(-\text{COH}) + \omega(-\text{CH}_2(\text{butyl})) + \delta(-\text{CH}(\text{ring}))$
		3046.79	27.3126	$\nu\text{s}(-\text{CH}_3) + \nu\text{s}(-\text{CH}_2(\text{ethyl}))$	1456.95	10.3466	$\alpha(-\text{CH}_2(\text{butyl}))$
		3136.71	34.4759	$\nu\text{ass}(-\text{CH}_3) + \nu\text{ass}(-\text{CH}_2(\text{ethyl}))$	1479.96	7.2514	$\alpha(-\text{CH}_3)$
		3149.58	36.8001	$\nu\text{ass}(-\text{CH}_2(\text{ethyl})) + \nu(-\text{CH}(\text{ring}))$	1489.2	7.5028	$\alpha(-\text{CH}_2(\text{butyl}))$
		3231.25	10.9901	$\nu\text{ass}(-\text{CH}_2(\text{ring}))$	1881.01	347.6157	$\nu(\text{C}=\text{O}) + \alpha(-\text{COH}) + \tau(-\text{CH}_2(\text{butyl}))$
		3800.48	80.3813	$\nu(-\text{OH})$	3036.65	78.7837	$\nu\text{s}(-\text{CH}_3) + \nu\text{s}(-\text{CH}_2(\text{butyl}))$
		SCALING FACTOR	0.936537279		3089.38	63.0143	$\nu\text{ass}(-\text{CH}_3) + \nu\text{ass}(-\text{CH}_2(\text{butyl}))$
					3125.68	47.6656	$\nu\text{ass}(-\text{CH}_3) + \nu\text{ass}(-\text{CH}_2(\text{butyl}))$
					3135.24	36.6548	$\nu\text{ass}(-\text{CH}_3) + \nu\text{s}(-\text{CH}_2(\text{butyl})) + \nu(-\text{CH}_2(\text{ring}))$
				3145.54	32.3427	$\nu(-\text{CH}(\text{ring}))$	
				3231.23	12.3742	$\nu\text{ass}(-\text{CH}_2(\text{ring}))$	
				3800.63	80.9905	$\nu(-\text{OH})$	
				SCALING FACTOR	0.937635223		
	aug-cc-pVDZ	596.73	63.7292	$\gamma(-\text{COOH})$	599.08	57.8357	$\gamma(-\text{COOH})$
		626.38	69.3445	$\gamma(-\text{COOH}) + \alpha(-\text{COO})$	630.78	73.4059	$\gamma(-\text{COOH}) + \alpha(-\text{COO})$
		745.23	13.3142	$\rho(-\text{CH}_2) + \rho(-\text{C-C-C-}) + \gamma(-\text{COOH})$	762.38	31.0397	$\rho(-\text{C-C-C-}) + \gamma(-\text{COOH})$
		763.3	14.7572	$\rho(-\text{CH}_2(\text{ethyl})) + \omega(-\text{COH})$	910.76	4.8018	$\nu\text{s}(-\text{C-C-O}) + \rho(-\text{CH}_2(\text{ring})) + \omega(-\text{CH}_2(\text{butyl}))$
		781.63	6.0197	$\rho(-\text{CH}_2(\text{ethyl})) + \tau(-\text{CH}_2(\text{ring}))$	957.54	8.1779	$\alpha(-\text{C-C-C-}(\text{ring})) + \omega(-\text{CH}_2(\text{butyl}))$
		909.85	15.8449	$\nu\text{s}(-\text{C-C-O}) + \tau(-\text{CH}_2(\text{ring})) + \alpha(\text{H-C-C-H}(\text{ring}))$	1023.34	11.6104	$\tau(-\text{CH}_2(\text{butyl})) + \nu\text{s}(-\text{C-C-C-}(\text{butyl, ring})) + \omega(-\text{CH}_2(\text{ring}))$
962.82		7.234	$\alpha(-\text{C-C-C-}(\text{ring})) + \rho(-\text{CH}_2(\text{ethyl}))$	1070.12	6.0733	$\tau(-\text{CH}_2(\text{butyl})) + \omega(-\text{CH}_2(\text{ring})) + \omega(\text{H-C-C-H}(\text{ring}))$	
1031.18		9.2902	$\omega(-\text{CH}_2(\text{ring})) + \omega(-\text{CH}_2(\text{ethyl})) + \omega(\text{H-C-C-H}(\text{ring}))$	1098.48	51.1369	$\rho(-\text{COH}) + \tau(-\text{CH}_2(\text{butyl})) + \rho(-\text{CH}_2(\text{ring}))$	
1047.05		6.7059	$\omega(-\text{CH}_2(\text{ring}))$	1126.91	14.772	$\tau(-\text{CH}_2(\text{butyl})) + \omega(\text{H-C-C-H}(\text{ring}))$	

Appendix III Raman track CFA

Functional	Basis set	Ethyl			Butyl		
		Theoretical Wavenumber (cm ⁻¹)			Theoretical Wavenumber (cm ⁻¹)		
		IR (cm ⁻¹)	Intensity	Assignment	IR (cm ⁻¹)	Intensity	Assignment
		1067.88	6.6895	$\tau(\text{H-C-C-H (ring)}) + \text{vass(-C-C-C- (ethyl))}$	1204.91	21.6323	$\rho(-\text{CH}_2(\text{butyl})) + \tau(-\text{CH}_2(\text{ring})) + \omega(-\text{CH (ring)})$
		1097.05	35.5219	$\rho(-\text{COH}) + \tau(-\text{CH}_2(\text{ethyl})) + \rho(-\text{CH}_2(\text{ring}))$	1235.29	92.2637	$\delta(-\text{COH}) + \omega(-\text{CH}_2(\text{butyl}))$
		1117.34	15.2285	$\tau(-\text{CH}_2(\text{ethyl})) + \rho(-\text{CH}_2(\text{ring}))$	1276.75	14.672	$\delta(-\text{COH}) + \tau(-\text{CH}_2(\text{butyl}))$
		1136.08	19.5905	$\alpha(-\text{COH}) + \tau(-\text{CH}_2(\text{ethyl})) + \tau(-\text{CH}_2(\text{ring})) + \omega(\text{H-C-C-H (ring)})$	1359.03	7.5185	$\omega(-\text{CH}_2(\text{butyl})) + \omega(-\text{CH (ring)}) + \alpha(-\text{COH})$
		1212.13	42.341	$\delta(-\text{COH}) + \tau(-\text{CH}_2(\text{ethyl})) + \tau(-\text{CH}_2(\text{ring}))$	1384.13	13.196	$\alpha(-\text{COH}) + \omega(-\text{CH}_2(\text{butyl})) + \alpha(\text{H-C-C-H (ring)})$
		1247.48	90.5494	$\delta(-\text{COH}) + \tau(-\text{CH}_2(\text{ethyl})) + \rho(-\text{CH}_2(\text{ring}))$	1396.19	65.1871	$\alpha(-\text{COH}) + \omega(-\text{CH}_2(\text{butyl})) + \omega(-\text{CH (ring)})$
		1260.47	18.5188	$\delta(-\text{COH}) + \omega(-\text{CH}_2(\text{ethyl})) + \omega(-\text{C-H (ring)})$	1468.49	11.8409	$\alpha(-\text{CH}_2(\text{butyl}))$
		1290.67	1.3773	$\omega(-\text{CH}_2(\text{ethyl})) + \tau(-\text{CH}_2(\text{ring})) + \tau(-\text{CH}_2(\text{ethyl}))$	1481.08	7.9592	$\alpha(-\text{CH}_3)$
		1326.81	6.0138	$\tau(-\text{CH}_2(\text{ethyl})) + \omega(\text{H-C-C-H (ring)})$	1491.96	13.6855	$\alpha(-\text{CH}_2(\text{butyl}))$
		1354.05	8.0805	$\omega(-\text{CH}_2(\text{ethyl})) + \omega(-\text{C-H (ring)})$	1844.12	372.4437	$\nu(\text{C=O}) + \alpha(-\text{COH}) + \tau(-\text{CH}_2(\text{butyl}))$
		1388.28	57.9513	$\alpha(-\text{COH}) + \tau(-\text{CH}_2(\text{ethyl})) + \omega(-\text{CH}(\text{ring}))$	3038.63	80.9691	$\text{vs}(-\text{CH}_3) + \text{vs}(-\text{CH}_2(\text{butyl}))$
		1396.21	23.7076	$\alpha(-\text{COH}) + \omega(-\text{CH}_2(\text{ethyl})) + \omega(-\text{CH}(\text{ring}))$	3052.49	30.8586	$\text{vs}(-\text{CH}_2(\text{butyl}))$
		1468.4	6.9945	$\alpha(-\text{CH}_2(\text{ethyl}))$	3088.89	56.4046	$\text{vass}(-\text{CH}_3) + \text{vass}(-\text{CH}_2(\text{butyl}))$
		1483.92	14.8575	$\alpha(-\text{CH}_2(\text{ethyl}))$	3105.31	39.8738	$\text{vass}(-\text{CH}_2(\text{butyl}))$
		1843.41	380.9819	$\nu(\text{C=O}) + \alpha(-\text{COH}) + \tau(-\text{CH}_2(\text{ethyl}))$	3119.1	60.0423	$\text{vass}(-\text{CH}_3) + \text{vass}(-\text{CH}_2(\text{butyl}))$
		3041.64	43.4321	$\text{vs}(-\text{CH}_3) + \text{vs}(-\text{CH}_2(\text{ethyl}))$	3127.8	41.4733	$\text{vass}(-\text{CH}_3)$
		3082.37	14.0301	$\text{vass}(-\text{CH}_3) + \text{vass}(-\text{CH}_2(\text{ethyl}))$	3150.99	32.6728	$\nu(-\text{CH}(\text{ring}))$
		3129.65	39.4178	$\text{vass}(-\text{CH}_3) + \text{vass}(-\text{CH}_2(\text{ethyl}))$	3230.87	15.9274	$\text{vass}(-\text{CH}_2(\text{ring}))$
		3155.6	28.8659	$\text{vass}(-\text{CH}_2(\text{ethyl})) + \nu(-\text{CH}(\text{ring}))$	3828.77	77.7509	$\nu(-\text{OH})$
		3232.1	13.7274	$\text{vass}(-\text{CH}_2(\text{ring}))$	SCALING FACTOR	0.937024251	
		3828.31	77.2783	$\nu(-\text{OH})$			
		SCALING FACTOR	0.936096974				
M06-2X	cc-pVDZ	585.88	54.008	$\gamma(-\text{COOH})$	586.45	55.8901	$\gamma(-\text{COOH})$
		626.69	65.6301	$\gamma(-\text{COOH}) + \alpha(-\text{COO})$	626.78	66.5047	$\gamma(-\text{COOH}) + \alpha(-\text{COO})$

Appendix III Raman track CFA

Functional	Basis set	Ethyl			Butyl		
		Theoretical Wavenumber (cm ⁻¹)			Theoretical Wavenumber (cm ⁻¹)		
		IR (cm ⁻¹)	Intensity	Assignment	IR (cm ⁻¹)	Intensity	Assignment
		718.35	42.6179	$\gamma(-\text{COOH}) + \rho(-\text{CH}_2(\text{ethyl}))$	720.23	36.1121	$\gamma(-\text{COOH}) + \rho(-\text{CH}_2(\text{butyl}))$
		780.02	11.6458	$\rho(-\text{CH}_2(\text{ethyl})) + \tau(-\text{CH}_2(\text{ring}))$	740.1	13.4172	$\rho(-\text{CH}_2(\text{butyl}))$
		910.53	10.7298	$\nu(-\text{C}-\text{C}-\text{O}) + \tau(-\text{CH}_2(\text{ring})) + \alpha(\text{H}-\text{C}-\text{C}-\text{H}(\text{ring}))$	833.75	5.9748	$\tau(-\text{CH}_2(\text{butyl})) + \alpha(-\text{C}-\text{C}-\text{C}(\text{ring})) + \rho(-\text{CH}_2(\text{butyl}))$
		976.87	8.6217	$\alpha(-\text{C}-\text{C}-\text{C}(\text{ring})) + \rho(-\text{CH}_2(\text{ethyl}))$	907.91	4.3416	$\nu(-\text{C}-\text{C}-\text{O}) + \tau(-\text{CH}_2(\text{butyl})) + \rho(-\text{CH}_2(\text{ring}))$
		1026.86	8.6262	$\omega(-\text{CH}_2(\text{ring})) + \omega(-\text{CH}_2(\text{ethyl})) + \omega(\text{H}-\text{C}-\text{C}-\text{H}(\text{ring}))$	974.72	4.7532	$\alpha(-\text{C}-\text{C}-\text{C}(\text{ring})) + \omega(-\text{CH}_2(\text{butyl}))$
		1102.43	26.2195	$\tau(-\text{CH}_2(\text{ethyl})) + \rho(-\text{CH}_2(\text{ring}))$	1027.85	5.8017	$\omega(-\text{CH}_2(\text{ring})) + \tau(-\text{CH}_2(\text{butyl})) + \omega(-\text{CH}(\text{ring}))$
		1113.73	13.4252	$\tau(-\text{CH}_2(\text{ethyl})) + \tau(-\text{CH}_2(\text{ring})) + \alpha(\text{H}-\text{C}-\text{C}-\text{H}(\text{ring}))$	1084.52	16.9595	$\tau(-\text{CH}_2(\text{butyl})) + \nu(-\text{C}-\text{C}-\text{C}(\text{butyl})) + \tau(-\text{CH}_2(\text{ring})) + \alpha(\text{H}-\text{C}-\text{C}-\text{H}(\text{ring}))$
		1133.68	16.5012	$\rho(-\text{CH}_2(\text{ethyl})) + \tau(-\text{CH}_2(\text{ethyl})) + \omega(\text{H}-\text{C}-\text{C}-\text{H}(\text{ring}))$	1097.81	21.0193	$\rho(-\text{COH}) + \nu(-\text{C}-\text{C}(\text{butyl})) + \tau(-\text{CH}_2(\text{ring})) + \alpha(\text{H}-\text{C}-\text{C}-\text{H}(\text{ring}))$
		1212.35	19.8392	$\delta(-\text{COH}) + \tau(-\text{CH}_2(\text{ethyl})) + \rho(-\text{CH}_2(\text{ring})) + \alpha(\text{H}-\text{C}-\text{C}-\text{H}(\text{ring}))$	1131	4.6931	$\tau(-\text{CH}_2(\text{butyl})) + \rho(\text{H}-\text{C}-\text{C}-\text{H}(\text{ring}))$
		1248.48	134.8336	$\delta(-\text{COH}) + \tau(-\text{CH}_2(\text{ethyl}))$	1200.9	19.9588	$\delta(-\text{COH}) + \tau(-\text{CH}_2(\text{butyl})) + \tau(-\text{CH}_2(\text{ring})) + \alpha(\text{H}-\text{C}-\text{C}-\text{H}(\text{ring}))$
		1316.49	6.768	$\tau(-\text{CH}_2(\text{ethyl})) + \omega(\text{H}-\text{C}-\text{C}-\text{H}(\text{ring}))$	1221.69	8.7772	$\omega(-\text{CH}_2(\text{butyl})) + \rho(\text{H}-\text{C}-\text{C}-\text{H}(\text{ring}))$
		1388.18	8.0457	$\alpha(-\text{COH}) + \omega(-\text{CH}_2(\text{ethyl})) + \omega(\text{H}-\text{C}-\text{C}-\text{H}(\text{ring}))$	1236.99	39.304	$\delta(-\text{COH}) + \omega(-\text{CH}_2(\text{butyl})) + \rho(-\text{CH}_2(\text{ring})) + \tau(-\text{CH}_2(\text{butyl}))$
		1407.94	82.2086	$\alpha(-\text{COH}) + \omega(-\text{CH}_2(\text{ethyl})) + \omega(-\text{CH}(\text{ring})) + \alpha(-\text{CH}_2(\text{ring}))$	1245.82	75.5447	$\alpha(-\text{COH}) + \nu(-\text{O}-\text{C}-\text{C}-) + \tau(-\text{CH}_2(\text{butyl})) + \tau(-\text{CH}_2(\text{ring})) + \omega(-\text{CH}(\text{ring}))$
		1443.33	10.7463	$\alpha(-\text{CH}_2(\text{ethyl}))$	1267.68	25.3533	$\delta(-\text{COH}) + \tau(-\text{CH}_2(\text{butyl})) + \rho(-\text{CH}_2(\text{butyl})) + \tau(-\text{CH}_2(\text{ring})) + \omega(-\text{CH}_2(\text{butyl})) + \omega(-\text{CH}(\text{ring}))$
		1467.85	8.678	$\alpha(-\text{CH}_2(\text{ethyl})) + \alpha(-\text{CH}_2(\text{ring}))$	1410.65	60.6087	$\alpha(-\text{COH}) + \nu(-\text{O}-\text{C}-\text{C}-) + \tau(-\text{CH}_2(\text{butyl})) + \omega(-\text{CH}_2(\text{butyl})) + \alpha(-\text{CH}_2(\text{ring}))$
		1904.45	375.8479	$\nu(\text{C}=\text{O}) + \alpha(-\text{COH}) + \tau(-\text{CH}_2(\text{ethyl}))$	1445.45	12.2097	$\alpha(-\text{CH}_2(\text{butyl}))$
		3051.26	27.6972	$\nu(-\text{CH}_3) + \nu(-\text{CH}_2(\text{ethyl}))$	1480.63	8.3493	$\alpha(-\text{CH}_2(\text{butyl})) + \alpha(-\text{CH}_2(\text{ring}))$
		3060.17	15.2555	$\nu(-\text{CH}_3) + \nu(-\text{CH}_2(\text{ethyl}))$	1904.38	369.6616	$\nu(\text{C}=\text{O}) + \alpha(-\text{COH}) + \tau(-\text{CH}_2(\text{butyl}))$
		3146.15	31.5145	$\nu(-\text{CH}_3) + \nu(-\text{CH}_2(\text{ethyl}))$	3047.91	61.7076	$\nu(-\text{CH}_2(\text{butyl}))$
		3157.28	27.6363	$\nu(-\text{CH}_3) + \nu(-\text{CH}_2(\text{ethyl}))$	3056.98	30.1311	$\nu(-\text{CH}_3)$
		3239.45	8.3971	$\nu(-\text{CH}_2(\text{ring}))$	3073.09	18.1185	$\nu(-\text{CH}_2(\text{butyl}))$
		3782.9	93.6337	$\nu(-\text{OH})$	3095.84	58.6963	$\nu(-\text{CH}_3) + \nu(-\text{CH}_2(\text{butyl}))$

Appendix III Raman track CFA

Functional	Basis set	Ethyl			Butyl		
		Theoretical Wavenumber (cm ⁻¹)			Theoretical Wavenumber (cm ⁻¹)		
		IR (cm ⁻¹)	Intensity	Assignment	IR (cm ⁻¹)	Intensity	Assignment
		SCALING FACTOR	0.933145651		3114.24	26.0717	vass(-CH2(butyl))
					3133.82	43.3852	vass(-CH3) + vass(-CH2(butyl))
					3142.95	31.743	vass(-CH3)
					3152.95	25.5331	v(-CH(ring))
					3237.92	9.5577	vass(-CH2(ring))
					3785.39	94.4516	v(-OH)
					SCALING FACTOR	0.934171285	
	aug-cc-pVDZ	591.91	73.2967	γ (-COOH)	590.82	76.6254	γ (-COOH)
		620.77	62.3724	γ (-COOH) + α (-COO)	620.15	60.6644	γ (-COOH) + α (-COO)
		739.63	20.4423	γ (-COOH) + ρ (-CH2(ethyl))	754.51	23.752	γ (-COOH) + ρ (-CH2(butyl))
		772.21	9.6556	ρ (-CH2(ethyl)) + τ (-CH2(ring))	909.83	6.0156	vs(-C-C-O) + τ (-CH2(butyl)) + τ (-CH2(ring)) + ρ (-CH3)
		911.41	14.2785	vs(-C-C-O) + τ (-CH2(ring)) + α (H-C-C-H (ring))	970.82	9.1392	α (-C-C-C- (ring)) + ω (-CH2(butyl))
		973.05	7.3581	ρ (-CH2(ethyl)) + α (-C-C-C- (ring))	1021.01	12.638	ρ (-CH2(butyl)) + τ (-CH2(butyl)) + ω (-CH2(ring)) + ω (-CH (ring))
		1025.97	12.9501	ω (-CH2(ring)) + ω (-CH2(ethyl)) + ω (H-C-C-H(ring))	1093.9	45.9454	α (-COH) + τ (-CH2(butyl)) + ρ (-CH2(ring)) + ω (-CH (ring))
		1093.9	28.5284	τ (-CH2(ethyl)) + ρ (-CH2(ring))	1123.87	9.5484	τ (-CH2(butyl)) + ω (-CH (ring))
		1110.73	14.1046	τ (-CH2(ethyl)) + τ (-CH2(ring)) + α (H-C-C-H (ring))	1199.92	9.9629	ρ (-CH2(butyl)) + ω (-CH (ring)) + ω (-CH2(butyl))
		1131.34	15.8306	ρ (-CH2(ethyl)) + τ (-CH2(ethyl)) + ω (H-C-C-H (ring))	1231.78	116.1563	δ (-COH) + ρ (-CH2(butyl)) + τ (-CH2(butyl))
		1209.23	28.3859	δ (-COH) + τ (-CH2(ethyl)) + ρ (-CH2(ethyl)) + ω (-CH(ring))	1268.9	25.3122	δ (-COH) + τ (-CH2(butyl)) + ρ (-CH2(butyl)) + τ (-CH2(ring)) + ω (-CH2(butyl))
		1250.64	87.0344	δ (-COH) + ω (-CH2(ethyl))	1347.92	5.2391	ω (-CH2(butyl)) + ω (-CH (ring))
		1316.76	6.0717	τ (-CH2(ethyl)) + ω (H-C-C-H (ring))	1393.9	67.1766	α (-COH) + ω (-CH2(butyl)) + δ (-CH(ring))
		1344.18	5.5888	α (-COH) + ω (-CH2(ethyl)) + ω (-CH(ring))	1459.3	13.7628	α (-CH2(butyl))
		1389.98	54.3981	α (-COH) + α (-CH2(ethyl)) + α (-CH2(ring)) + ω (-CH3)	1476.21	8.2121	α (-CH3)
	1458.44	8.7057	α (-CH2(ethyl))	1485.97	17.2566	α (-CH2(butyl))	

Appendix III Raman track CFA

Functional	Basis set	Ethyl			Butyl		
		Theoretical Wavenumber (cm ⁻¹)			Theoretical Wavenumber (cm ⁻¹)		
		IR (cm ⁻¹)	Intensity	Assignment	IR (cm ⁻¹)	Intensity	Assignment
		1477.74	14.4667	$\alpha(-\text{CH}_2(\text{ethyl})) + \alpha(-\text{CH}_2(\text{ring}))$	1866.01	391.6054	$\nu(\text{C}=\text{O}) + \alpha(-\text{COH}) + \tau(-\text{CH}_2(\text{butyl}))$
		1867.11	402.0688	$\nu(\text{C}=\text{O}) + \alpha(-\text{COH}) + \tau(-\text{CH}_2(\text{ethyl}))$	3056.78	47.3878	$\nu\text{s}(-\text{CH}_3) + \nu\text{s}(-\text{CH}_2(\text{butyl}))$
		3059.53	31.2542	$\nu\text{s}(-\text{CH}_3)$	3099.88	50.1134	$\nu\text{ass}(-\text{CH}_3) + \nu\text{ass}(-\text{CH}_2(\text{butyl}))$
		3093.96	11.746	$\nu\text{ass}(-\text{CH}_3) + \nu\text{ass}(-\text{CH}_2(\text{ethyl}))$	3114.41	34.5346	$\nu\text{ass}(-\text{CH}_2(\text{butyl}))$
		3111.76	9.9836	$\nu\text{ass}(-\text{CH}_2(\text{ethyl})) + \nu(-\text{CH}(\text{ring}))$	3130.23	51.3975	$\nu\text{ass}(-\text{CH}_3) + \nu\text{ass}(-\text{CH}_2(\text{butyl}))$
		3135.63	31.4895	$\nu\text{ass}(-\text{CH}_3) + \nu\text{ass}(-\text{CH}_2(\text{ethyl}))$	3139.34	35.8143	$\nu\text{ass}(-\text{CH}_3)$
		3141.76	33.884	$\nu\text{ass}(-\text{CH}_3) + \nu\text{ass}(-\text{CH}_2(\text{ethyl}))$	3162.01	24.5095	$\nu(-\text{CH}(\text{ring}))$
		3166.68	26.122	$\nu\text{ass}(-\text{CH}_2(\text{ethyl})) + \nu(-\text{CH}(\text{ring}))$	3244.48	10.7667	$\nu\text{ass}(-\text{CH}_2(\text{ring}))$
		3246.86	8.926	$\nu\text{ass}(-\text{CH}_2(\text{ring}))$	3816.11	83.1051	$\nu(-\text{OH})$
		3816.51	92.8748	$\nu(-\text{OH})$	SCALING FACTOR	0.931460557	
		SCALING FACTOR	0.930623331				

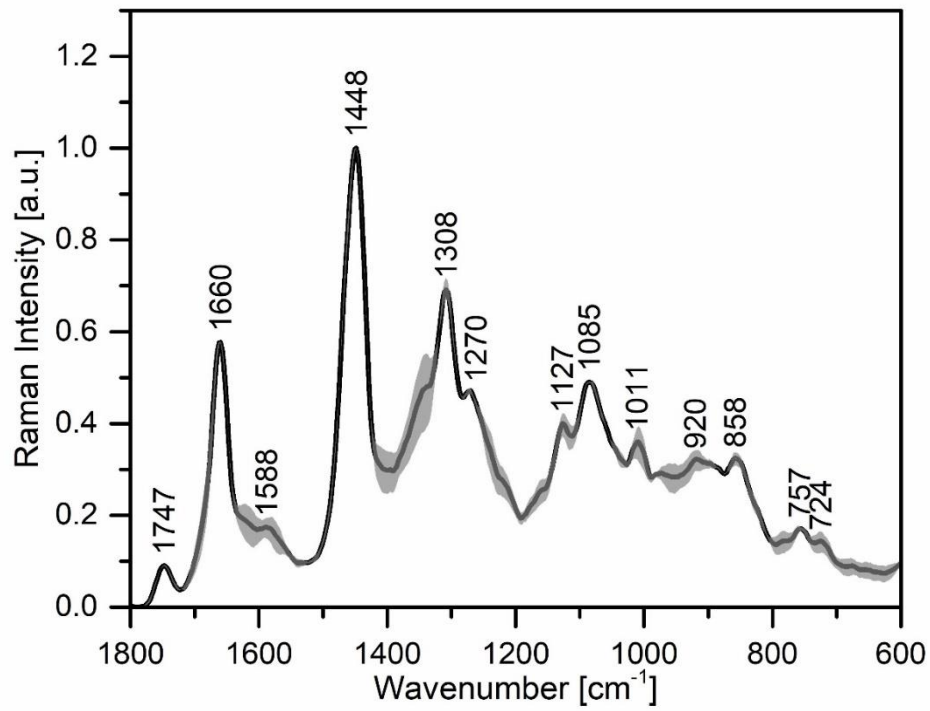


Figure S3. The average Raman spectrum (1800 – 600 cm⁻¹) of LBs from the control cell line (black line) together with standard deviation (grey background), with marked band positions.

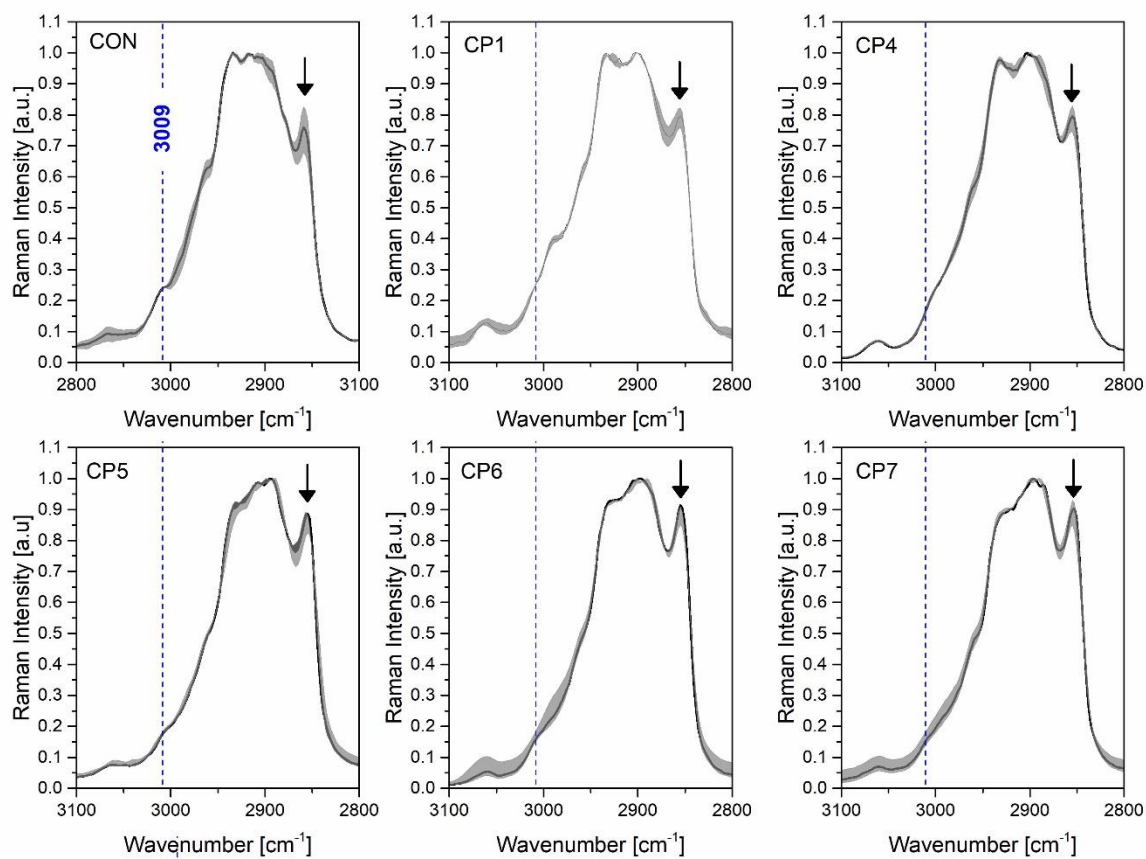


Figure S4. Average Raman spectra (in the range 3100 – 2800 cm⁻¹) of LBs from each cell line (**black line**, in each panel) together with standard deviation (**grey background**, in each panel). Each spectrum was obtained by averaging all average spectra of LBs originating from the selected cell line (more details are given in the ‘Materials and Methods’ section). The **black arrow** marks the position of the band originating from $\nu(\text{CH}_2)$, located at 2855 cm⁻¹. All spectra were normalized. **Blue dashed line** marks the position of the band located at 3009 cm⁻¹ ($\nu(\text{C-H})$), characteristic for UFAs.

Appendix III Raman track CFA

Table S3. Lipid content in the studied cell line obtained *via* GC.

Strain	TCFAs (mg/g DCW)*†	TFAs (mg/g DCW)†	TUFAs(%DCW)**	TSFAs(%DCW)***
CON	0.0	21.3	64.32%	35.68%
CP1	6.7	19.4	24.05%	30.60%
CP4	11.5	35.9	24.41%	34.69%
CP5	11.9	56.1	28.91%	29.89%
CP6	18.3	90.3	19.12%	37.46%
CP7	10.6	70.3	19.35%	31.14%

TFAs – Total Fatty Acids; DCW – Dry Cell Weight; TUFAs – Total Unsaturated Fatty Acids,
TSFAs – Total Saturated Fatty Acids, TCFAs – Total Cyclopropane Fatty Acids

* includes: CycC17, CycC19; ** includes: C16:1, C18:1; ***includes: C16:0, C18:0

†TFAs and TCFAs based on TAG and PL

Table S4. Lipid content of the TAG and PL fractions (Bligh Dyer extraction procedure) obtained *via* GC.

Strain	TAG fraction		PL fraction	
	TAGs (%DCW)	CFAs (%TAGs)	PLs (%DCW)	CAFs (%PLs)
CON	0.6%	0.0%	1.5%	0.0%
CP1	0.7%	42.4%	1.2%	29.9%
CP4	2.2%	27.9%	1.4%	38.4%
CP5	4.3%	17.2%	1.3%	34.4%
CP6	7.4%	16.1%	1.6%	40.0%
CP7	6.2%	12.5%	0.8%	34.2%

TAGs – Triacylglycerols; DCW – Dry Cell Weight; PLs – Phospholipids

